

DUDLEY KNOT, JR.
NAVAL POSTGRADUATE SCHOOL
MONTEREY CALIF 93940

NAVAL POSTGRADUATE SCHOOL

Monterey, California



THESIS

IMPULSIVELY-STARTED FLOW ABOUT
SUBMARINE-SHAPED BODIES

by

Howard Keith Kline

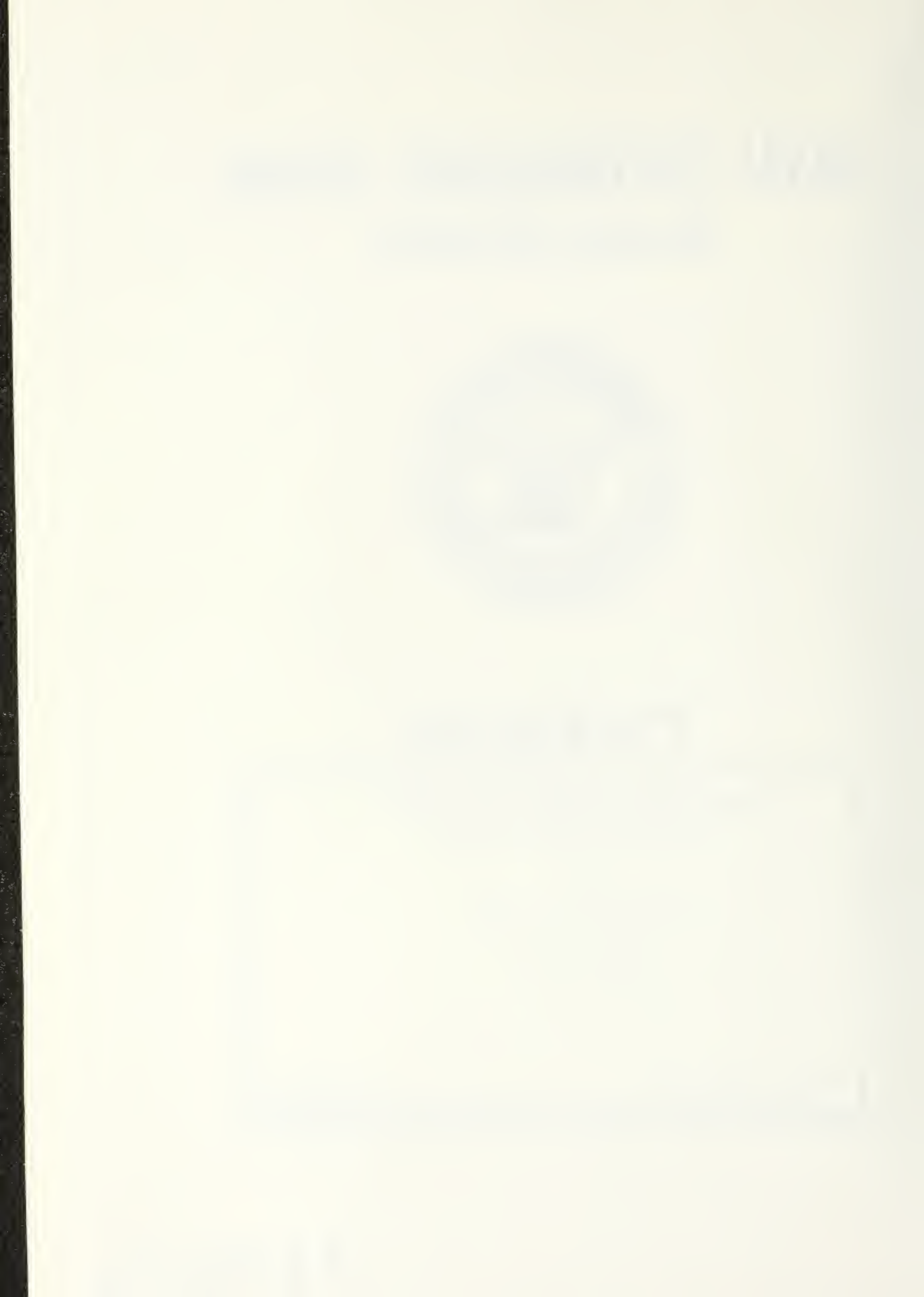
March 1981

Thesis Advisor:

T. Sarpkaya

Approved for public release; distribution unlimited.

T199174



REPORT DOCUMENTATION PAGE		READ INSTRUCTIONS BEFORE COMPLETING FORM
1. REPORT NUMBER	2. GOVT ACCESSION NO.	3. RECIPIENT'S CATALOG NUMBER
4. TITLE (and Subtitle) Impulsively-Started Flow About Submarine-Shaped Bodies		5. TYPE OF REPORT & PERIOD COVERED Master's Thesis March 1981
7. AUTHOR(s) Howard Keith Kline		6. PERFORMING ORG. REPORT NUMBER
9. PERFORMING ORGANIZATION NAME AND ADDRESS Naval Postgraduate School Monterey, California 93940		8. CONTRACT OR GRANT NUMBER(s)
11. CONTROLLING OFFICE NAME AND ADDRESS Naval Postgraduate School Monterey, California 93940		10. PROGRAM ELEMENT, PROJECT, TASK AREA & WORK UNIT NUMBERS
14. MONITORING AGENCY NAME & ADDRESS (if different from Controlling Office)		12. REPORT DATE March 1981
		13. NUMBER OF PAGES 225
		15. SECURITY CLASS. (of this report) Unclassified
		15a. DECLASSIFICATION/DOWNGRADING SCHEDULE
16. DISTRIBUTION STATEMENT (of this Report) Approved for public release; distribution unlimited.		
17. DISTRIBUTION STATEMENT (of the abstract entered in Block 20, if different from Report)		
18. SUPPLEMENTARY NOTES		
19. KEY WORDS (Continue on reverse side if necessary and identify by block number)		
20. ABSTRACT (Continue on reverse side if necessary and identify by block number) Impulsively-started flow about a D-shaped body, a T-shaped body, and a flat plate has been investigated. The forces and moments acting on the bodies have been determined, as a function of the relative displacement of the fluid at a subcritical Reynolds number, for various angles of attack. The results have shown that the shedding of the first two or three vortices and the manner in which they are generated have		

profound effects on all the characteristics of resistance. The evolution of the vortices, and hence the forces, significantly depend on whether the separation points are fixed or mobile, or a combination thereof. The data presented here are expected to form the basis for future numerical analyses of the characteristics of time-dependent flow about bluff bodies. At present, accurate analytical and numerical data, for comparison with those presented herein, do not exist.

Approved for Public Release; Distribution Unlimited

Impulsively-Started Flow About Submarine-Shaped Bodies

by

Howard Keith Kline
Lieutenant Commander, United States Navy
B.S., United States Naval Academy, 1969

Submitted in partial fulfillment of the
requirements for the degree of

MASTER OF SCIENCE IN MECHANICAL ENGINEERING

from the

NAVAL POSTGRADUATE SCHOOL
March 1981

ABSTRACT

Impulsively-started flow about a D-shaped body, a T-shaped body, and a flat plate has been investigated. The forces and moments acting on the bodies have been determined, as a function of the relative displacement of the fluid at a subcritical Reynolds number, for various angles of attack.

The results have shown that the shedding of the first two or three vortices and the manner in which they are generated have profound effects on all the characteristics of resistance. The evolution of the vortices, and hence the forces, significantly depend on whether the separation points are fixed or mobile, or a combination thereof. The data presented here are expected to form the basis for future numerical analyses of the characteristics of time-dependent flow about bluff bodies. At present, accurate analytical and numerical data, for comparison with those presented herein, do not exist.

TABLE OF CONTENTS

I.	INTRODUCTION-----	15
II.	REVIEW OF THE PREVIOUS INVESTIGATIONS-----	20
III.	EXPERIMENTAL EQUIPMENT AND PROCEDURES-----	30
	A. VERTICAL WATER TUNNEL-----	30
	B. VELOCITY, FORCE AND MOMENT MEASUREMENTS-----	36
	C. SUBMARINE-SHAPED TEST BODIES AND TESTING PROCEDURE-----	44
	D. FLOW VISUALIZATION-----	47
IV.	EXPERIMENTAL RESULTS-----	51
	A. PRESENTATION-----	51
	B. DEFINITION OF THE FORCE-TRANSFER COEFFICIENTS--	51
	C. D-SHAPED CYLINDER-----	55
	D. T-SHAPED CYLINDER-----	64
	E. FLAT PLATE-----	83
	F. RECAPITULATORY SYNTHESIS-----	91
V.	CONCLUSIONS-----	95
VI.	RECOMMENDATIONS FOR FURTHER RESEARCH-----	97
	LIST OF REFERENCES-----	99
	APPENDIXES (See the LIST APPENDIXES, p. 6)-----	105
	INITIAL DISTRIBUTION LIST-----	225

LIST OF APPENDIXES

A.	Representative Data for D-Shaped Body at 0 Degrees.	---105
B.	Representative Data for D-Shaped Body at +10 Degrees.	-106
C.	Representative Data for D-Shaped Body at +20 Degrees.	-110
D.	Representative Data for D-Shaped Body at +30 Degrees.	-114
E.	Representative Data for D-Shaped Body at +45 Degrees.	-118
F.	Representative Data for D-Shaped Body at -10 Degrees.	-122
G.	Representative Data for D-Shaped Body at -20 Degrees.	-126
H.	Representative Data for D-Shaped Body at -30 Degrees.	-130
I.	Representative Data for D-Shaped Body at -45 Degrees.	-134
J.	Representative Data for D-Shaped Body at -90 Degrees.	-138
K.	Representative Data for T-Shaped Body at 0 Degrees.	---142
L.	Representative Data for T-Shaped Body at +5 Degrees.	--143
M.	Representative Data for T-Shaped Body at +10 Degrees.	-147
N.	Representative Data for T-Shaped Body at +15 Degrees.	-151
O.	Representative Data for T-Shaped Body at +20 Degrees.	-155
P.	Representative Data for T-Shaped Body at +25 Degrees.	-159
Q.	Representative Data for T-Shaped Body at +30 Degrees.	-163
R.	Representative Data for T-Shaped Body at +45 Degrees.	-167
S.	Representative Data for T-Shaped Body at -5 Degrees.	--171
T.	Representative Data for T-Shaped Body at -10 Degrees.	-175
U.	Representative Data for T-Shaped Body at -15 Degrees.	-179
V.	Representative Data for T-Shaped Body at -20 Degrees.	-183
W.	Representative Data for T-Shaped Body at -25 Degrees.	-187

X.	Representative Data for T-Shaped Body at -30 Degrees.	-191
Y.	Representative Data for T-Shaped Body at -45 Degrees.	-195
Z.	Representative Data for Flat Plate at 90 and 85 Degrees.-----	-199
AA.	Representative Data for Flat Plate at 80 and 75 Degrees-----	-202
AB.	Representative Data for Flat Plate at 70 and 65 Degrees-----	-207
AC.	Representative Data for Flat Plate at 60 and 55 Degrees-----	-212
AD.	Representative Data for Flat Plate at 50 and 45 Degrees-----	-215
AE.	Representative Data for Flat Plate at 40 and 30 Degrees-----	-220

LIST OF FIGURES

1.	Vertical Water Tunnel.-----	31
2.	Mushroom Valve Cross-Section.-----	32
3.	Three-Way Valve Cross-Section.-----	33
4.	Three-Way Valve Piston Cross-Section.-----	35
5.	Analog Record for the D-Shaped Body at 0 deg.-----	37
6.	Drag/Lift Force Transducer Assembly.-----	39
7.	Force Transducer Indicating Plate.-----	40
8.	Moment Transducer Assembly (Connecting Load Gage).--	42
9.	Moment Transducer Assembly (Torque-Beam).-----	43
10.	Geometrical Characteristics of the Test Bodies: (a) D-Shape. (b) T-Shape. (c) Flat Plate.-----	45
11.	Analog Record for the T-Shaped Body at 0 deg.-----	48
12.	Analog Record for the Flat Plate at 45 deg.-----	49
13a.	Definition Sketch for the D-Shaped Body.-----	53
13b.	Definition Sketch for the T-Shaped Body.-----	54
13c.	Definition Sketch for the Flat Plate.-----	56
14.	C_d vs. UT/C for the D-Shaped Body at 0 deg.-----	57
15.	C_l vs. UT/C for the D-Shaped Body at 0 deg.-----	58
16.	C_m vs. UT/C for the D-Shaped Body at 0 deg.-----	59
17.	C_d vs. UT/C for the T-Shaped body at 0 deg.-----	65
18.	C_l vs. UT/C for the T-Shaped Body at 0 deg.-----	66
19.	C_m vs. UT/C for the T-Shaped Body at 0 deg.-----	67
20.	Flow About the T-Shaped Body at 0 deg. and $UT/C = 3.5$.-----	70

21.	Flow About the T-Shaped Body at 0 deg. and UT/C = 4.1.-----	71
22.	Flow About the T-Shaped Body at 0 deg. and UT/C = 5.0.-----	72
23.	Flow About the T-Shaped Body at 0 deg. and UT/C = 5.8.-----	73
24.	Flow About the T-Shaped Body at 0 deg. and UT/C = 6.6.-----	74
25.	Flow About the T-Shaped Body at 0 deg. and UT/C = 7.1.-----	75
26.	Flow About the T-Shaped Body at 0 deg. and UT/C = 7.8.-----	76
27.	Cn vs. UT/B for the Flat Plate at 90 deg.-----	84
28.	Cn vs. UT/B for the Flat Plate at 55 deg. (Indirect Measurement)-----	85
29.	Cn vs. UT/B for the Flat Plate at 55 deg. (Direct Measurement)-----	86
30.	Cn vs. UT/B for the Flat Plate at 55 deg. (Compar- ison of Indirect and Direct Force Measurement).-----	88
31.	X/B vs. UT/B for the Flat Plate at 55 deg.-----	89
32.	Cd vs. UT/C for the D-Shaped Body at +10 deg.-----	107
33.	Cl vs. UT/C for the D-Shaped Body at +10 deg.-----	108
34.	Cm vs. UT/C for the D-Shaped Body at +10 deg.-----	109
35.	Cd vs. UT/C for the D-Shaped Body at +20 deg.-----	111
36.	Cl vs. UT/C for the D-Shaped Body at +20 deg.-----	112
37.	Cm vs. UT/C for the D-Shaped Body at +20 deg.-----	113
38.	Cd vs. UT/C for the D-Shaped Body at +30 deg.-----	115
39.	Cl vs. UT/C for the D-Shaped Body at +30 deg.-----	116
40.	Cm vs. UT/C for the D-Shaped Body at +30 deg.-----	117
41.	Cd vs. UT/C for the D-Shaped Body at +45 deg.-----	119

42.	C1 vs. UT/C for the D-Shaped Body at +45 deg.	-----120
43.	Cm vs. UT/C for the D-Shaped Body at +45 deg.	-----121
44.	Cd vs. UT/C for the D-Shaped Body at -10 deg.	-----123
45.	C1 vs. UT/C for the D-Shaped Body at -10 deg.	-----124
46.	Cm vs. UT/C for the D-Shaped Body at -10 deg.	-----125
47.	Cd vs. UT/C for the D-Shaped Body at -20 deg.	-----127
48.	C1 vs. UT/C for the D-Shaped Body at -20 deg.	-----128
49.	Cm vs. UT/C for the D-Shaped Body at -20 deg.	-----129
50.	Cd vs. UT/C for the D-Shaped Body at -30 deg.	-----131
51.	C1 vs. UT/C for the D-Shaped Body at -30 deg.	-----132
52.	Cm vs. UT/C for the D-Shaped Body at -30 deg.	-----133
53.	Cd vs. UT/C for the D-Shaped Body at -45 deg.	-----135
54.	C1 vs. UT/C for the D-Shaped Body at -45 deg.	-----136
55.	Cm vs. UT/C for the D-Shaped Body at -45 deg.	-----137
56.	Cd vs. UT/C for the D-Shaped Body at -90 deg.	-----139
57.	C1 vs. UT/C for the D-Shaped Body at -90 deg.	-----140
58.	Cm vs. UT/C for the D-Shaped Body at -90 deg.	-----141
59.	Cd vs. UT/C for the T-Shaped Body at +5 deg.	-----144
60.	C1 vs. UT/C for the T-Shaped Body at +5 deg.	-----145
61.	Cm vs. UT/C for the T-Shaped Body at +5 deg.	-----146
62.	Cd vs. UT/C for the T-Shaped Body at +10 deg.	-----148
63.	C1 vs. UT/C for the T-Shaped Body at +10 deg.	-----149
64.	Cm vs. UT/C for the T-Shaped Body at +10 deg.	-----150
65.	Cd vs. UT/C for the T-Shaped Body at +15 deg.	-----151
66.	C1 vs. UT/C for the T-Shaped Body at +15 deg.	-----153
67.	Cm vs. UT/C for the T-Shaped Body at +15 deg.	-----154

68.	Cd vs. UT/C for the T-Shaped Body at +20 deg.	156
69.	C1 vs. UT/C for the T-Shaped Body at +20 deg.	157
70.	Cm vs. UT/C for the T-Shaped Body at +20 deg.	158
71.	Cd vs. UT/C for the T-Shaped Body at +25 deg.	160
72.	C1 vs. UT/C for the T-Shaped Body at +25 deg.	161
73.	Cm vs. UT/C for the T-Shaped Body at +25 deg.	162
74.	Cd vs. UT/C for the T-Shaped Body at +30 deg.	164
75.	C1 vs. UT/C for the T-Shaped Body at +30 deg.	165
76.	Cm vs. UT/C for the T-Shaped Body at +30 deg.	166
77.	Cd vs. UT/C for the T-Shaped Body at +45 deg.	168
78.	C1 vs. UT/C for the T-Shaped Body at +45 deg.	169
79.	Cm vs. UT/C for the T-Shaped Body at +45 deg.	170
80.	Cd vs. UT/C for the T-Shaped Body at -5 deg.	172
81.	C1 vs. UT/C for the T-Shaped Body at -5 deg.	173
82.	Cm vs. UT/C for the T-Shaped Body at -5 deg.	174
83.	Cd vs. UT/C for the T-Shaped Body at -10 deg.	176
84.	C1 vs. UT/C for the T-Shaped Body at -10 deg.	177
85.	Cm vs. UT/C for the T-Shaped Body at -10 deg.	178
86.	Cd vs. UT/C for the T-Shaped Body at -15 deg.	180
87.	C1 vs. UT/C for the T-Shaped Body at -15 deg.	181
88.	Cm vs. UT/C for the T-Shaped Body at -15 deg.	182
89.	Cd vs. UT/C for the T-Shaped Body at -20 deg.	184
90.	C1 vs. UT/C for the T-Shaped Body at -20 deg.	185
91.	Cm vs. UT/C for the T-Shaped Body at -20 deg.	186
92.	Cd vs. UT/C for the T-Shaped Body at -25 deg.	188
93.	C1 vs. UT/C for the T-Shaped Body at -25 deg.	189

94.	Cm vs. UT/C for the T-Shaped Body at -25 deg.	-----190
95.	Cd vs. UT/C for the T-Shaped Body at -30 deg.	-----192
96.	Cl vs. UT/C for the T-Shaped Body at -30 deg.	-----193
97.	Cm vs. UT/C for the T-Shaped Body at -30 deg.	-----194
98.	Cd vs. UT/C for the T-Shaped Body at -45 deg.	-----196
99.	Cl vs. UT/C for the T-Shaped Body at -45 deg.	-----197
100.	Cm vs. UT/C for the T-Shaped Body at -45 deg.	-----198
101.	Cn vs. UT/B for the Flat Plate at 85 deg.	-----200
102.	X/B vs. UT/B for the Flat Plate at 85 deg.	-----201
103.	Cn vs. UT/B for the Flat Plate at 80 deg.	-----203
104.	X/B vs. UT/B for the Flat Plate at 80 deg.	-----204
105.	Cn vs. UT/B for the Flat Plate at 75 deg.	-----205
106.	X/B vs. UT/B for the Flat Plate at 75 deg.	-----206
107.	Cn vs. UT/B for the Flat Plate at 70 deg.	-----208
108.	X/B vs. UT/B for the Flat Plate at 70 deg.	-----209
109.	Cn vs. UT/B for the Flat Plate at 65 deg.	-----210
110.	X/B vs. UT/B for the Flat Plate at 65 deg.	-----211
111.	Cn vs. UT/B for the Flat Plate at 60 deg.	-----213
112.	X/B vs. UT/B for the Flat Plate at 60 deg.	-----214
113.	Cn vs. UT/B for the Flat Plate at 50 deg.	-----216
114.	X/B vs. UT/B for the Flat Plate at 50 deg.	-----217
115.	Cn vs. UT/B for the Flat Plate at 45 deg.	-----218
116.	X/B vs. UT/B for the Flat Plate at 45 deg.	-----219
117.	Cn vs. UT/B for the Flat Plate at 40 deg.	-----221
118.	X/B vs. UT/B for the Flat Plate at 40 deg.	-----222
119.	Cn vs. UT/B for the Flat Plate at 30 deg.	-----223
120.	X/B vs. UT/B for the Flat Plate at 30 deg.	-----224

TABLE OF SYMBOLS AND ABBREVIATIONS

B	One-half of the Width of the Flat Plate
C	Radius of a Cylindrical Body's Base Circle
Cd	Drag Coefficient
Cl	Lift Coefficient
Cm	Moment Coefficient
Cn	Normal Force Coefficient
f	Vortex-Shedding Frequency
Fn	Normal Force
L	Test Body Length
Ma	Mach Number
M+	Moment, Positive Direction
r	Radial Coordinate
s	Relative Displacement
S	Strouhal Number
t	Time
t*	Time of Boundary Layer Separation
T	Time
U	Velocity
x	Coordinate Axis
X	Moment Arm
θ	Test Body Angle of Rotation or Angle of Attack Relative to the Direction of the Ambient Flow
ν	Fluid Viscosity
ρ	Fluid Density

ACKNOWLEDGEMENT

The author is most grateful for the comprehensive support of Distinguished Professor Turgut Sarpkaya, whose patient guidance and astute perception of all facets of the problem at hand has made this research a very meaningful and rewarding experience. A significant note of thanks is extended to Mr. Jack McKay, of the Naval Postgraduate School technical staff, for his skillful and industrious efforts which were essential to the experimental process described herein. The author also is especially appreciative for the love, understanding and support that has been provided by his wife, Ann.

I. INTRODUCTION

The motion of bodies through fluids and fluid motion in or about bodies gave rise to a great number of practical and theoretical studies regarding the determination of resistance in steady and time-dependent flows.

Observations as well as numerical experiments show that the wake of a bluff body is comprised of an alternating vortex street. The character of the vortices immediately behind the body and in the wake further downstream depend, for a steady ambient flow, on the Reynolds number and the intensity and scale of the turbulence present in the ambient flow. For a time-dependent flow, the instantaneous state as well as the past history of the flow play significant roles and it is not possible to give a general set of normalized parameters. Heuristic reasoning, and laboratory and numerical experiments often will have to supplement the information gathered from relatively idealized solutions in order to correctly identify the most important governing parameters.

Even if the fluid is assumed to be inviscid, flow involving separation is beyond the reach of rigorous calculation. In reality, the flow behind a bluff body moving steadily through a fluid (or held stationary in a steadily moving fluid) is accompanied by large scale unsteadiness. Furthermore, any type of disturbance or unsteadiness experienced

by the ambient flow and/or the body introduces additional changes in the characteristics of the flow and in the fluid-structure interaction.

The formation of a wake gives rise not only to a form drag, as would be the case if the motion were steady, but also to significant changes in the inertial forces. The velocity-dependent form drag is not the same as that for steady flow in a viscous fluid; and, the acceleration-dependent inertial resistance is not the same as for unseparated flow in an inviscid fluid. In other words, the drag and inertial forces are interdependent as well as time-dependent. Thus the relationships between the various resistance components must be determined in terms of the unsteadiness of the ambient flow. Also, these relationships must take into consideration the geometry of the body, the degree of upstream turbulence, the roughness of the body, and the past history of the flow.

The hydrodynamics of unsteady flow, in particular those set in motion impulsively from rest, has been most aptly described by Sedov [1]. Birkhoff and Zarantonello [2] have brought together results of nearly a hundred years of research on the motion of jets, wakes and cavities. More recently, revolutionary changes in computers and numerical methods have generated new concepts which are scattered throughout the literature.

As in a great many steady flow problems, where potential flow analysis provides many approximate solutions, real wake behavior using models involving potential theory have been tried. (For example, see Sarpkaya and Shoaff [3].) Some of these approximations may be expected to provide realistic solutions and make it possible to eventually introduce the effects of roughness, viscosity, gravity, turbulence and past history, among other variables.

Favorable comparison between theoretical results and experimental observations may not always occur, but the objective is not always the achievement of a completely favorable comparison. Rather, it is the careful selection of those theoretical predictions found to be reasonably accurate (in their agreement with experiments) that should be regarded as a first step toward further exploration of potential flow methods and then eventually the complete modeling of all phases of the flow phenomena. These efforts logically lead to the reasons why impulsive flows are studied extensively.

As noted earlier, time-dependent flows involve changes in both the drag and inertial forces. The history of the motion may affect significantly the instantaneous value of the resistance and the time it takes to reach a given value. Thus, a general time-dependent flow cannot yet be analyzed numerically and, therefore, does not provide an opportunity for the development and testing of numerical techniques and for the comparison of the results with those obtained

experimentally. However, the impulsively-started flow about a simple bluff body is relatively more manageable and can be analyzed analytically and/or numerically, at least for the early stages of motion, and provides an excellent opportunity for the validation of the methods used through the comparison of the theoretical and experimental results. It is partly because of this reason that the study of impulsively-started flows has attracted a great deal of attention during the past fifty years.

Flow started impulsively from rest are of importance from a practical point of view also. Examples of applications of such flows include the effects upon bodies immersed in a boiling water reactor during a loss-of-cooling-water accident and the understanding of the motion of missiles at high angles of attack. As will be noted later, impulsive flow is analagous to the evolution of separated flow about slender bodies moving at high angles of attack. Underwater vehicles, such as torpedoes and submarines, have impulsive changes imposed upon their motion, particularly during a turn or dive.

Lastly, from a basic research point of view, the evolution of the wake and the formation of the first few vortices are far more important than the subsequent steady state. As the results presented herein show, the most dramatic changes in the force-transfer coefficients take place during the early stages of motion. Understanding of the kinematics and dynamics

of the early stages of the evolution of the wake provides valuable information regarding the growth of shear layers and the distribution of vorticity.

It is in view of its practical and theoretical significance that this investigation of impulsively-started flow about three types of bluff bodies (a D-shaped cylinder, a T-shaped cylinder and a flat plate) has been undertaken.

II. REVIEW OF THE PREVIOUS INVESTIGATIONS

Impulsively-started flow is one of the unsteady flow situations where analytical and numerical solutions exist at least for small times and relatively low Reynolds numbers.

During the early stages of motion the vorticity does not have enough time to diffuse. The boundary layers are very thin, the flow is essentially irrotational and the fluid force acting on the body is primarily inertial. The inertia coefficient is $C_m = 1 + C_a$ where C_a is the added mass coefficient obtained from potential flow theory. For bodies without sharp corners, as in the case of a circular cylinder, separation does not occur immediately. Furthermore, the separation does not necessarily initiate at the downstream stagnation point (as in the case of an elliptic cylinder).

For two-dimensional cylinders, it can be shown that the separation begins, after a time t^* at a place where the absolute value of dU/dx is largest. The relationship between t^* and Du/dt is [4]

$$1 + \left(1 + \frac{4}{3\pi}\right) \frac{dU}{dt} t^* = 0 \quad (1)$$

For a smooth circular cylinder started impulsively from rest to a constant velocity, the distance covered until separation begins is $s = 0.351C$ (C is the radius of the cylinder). Here, the separation does begin at the rear stagnation point. For a uniformly accelerating circular cylinder the corresponding distance traveled is $s = 0.52C$.

For axisymmetric bodies t^* is given by the expression [4]

$$1 + t^* \left[\frac{dU}{dx} \left(1 + \frac{4}{3\pi} \right) + 0.15 \frac{U}{r} \frac{dr}{dx} \right] = 0 \quad (2)$$

For a sphere impulsively set in motion $s = 0.392C$. The distance covered by the sphere until the onset of separation is somewhat larger, as in the case of the cylinder, when the sphere is accelerated uniformly from rest. The rate of acceleration as well as the history of acceleration is important in the calculation of the relative distance covered prior to the occurrence of separation. For bodies with sharp corners separation starts immediately.

Consider an impulsive change superimposed on an already established flow pattern and, with that change, the role played by separation on the added mass. Just prior to the impulsive change the drag coefficient is given by its steady state value at the corresponding Reynolds number. Sears, as reported by Rott [5], has shown that "the initial motion following the impulsive change of the conditions consists of the superposition of the velocity pattern existing just before the change and the inviscid flow velocity pattern due to the impulsive boundary values." In other words, at the initial instants of impulsive change the drag coefficient is equal to its steady state value and $C_m = 1 + C_a$ (C_a again comes from the potential theory; for example, $C_m = 2$ for a circular cylinder). As time progresses, neither C_d nor C_a

remains the same and both change with the evolution of the flow. These changes are affected by the past history of the motion and the features of the current state. Thus, the changes in the added mass coefficient come about not only because of separation but also because of changes in the state of the separated flow, such as the additional movement of separation points and the increase or decrease of the rate of circulation.

Theoretical investigations of impulsively-started motion of a circular cylinder in a fluid otherwise at rest were first conducted in the early 1900's and confined to very small Reynolds numbers. Such a motion was first considered by Blasius [6] in 1908 and his work was later extended by Goldstein and Rosenhead [7] in 1936, Görtler [8,9] in 1944 and 1948, Schuh [10] in 1953, Watson [11] in 1955, and Wundt [12] in 1955. It was found, as noted earlier, that after a certain lapse of time, the boundary layer separates from the surface of the cylinder; the time and location of separation depending on the Reynolds number and the bluntness of the body. The separation points then move rapidly around the cylinder until at some greater time they coincide with the average positions of the points of laminar separation for steady flow.

Finite difference techniques have been employed in the analysis of separated flows by several investigators (Payne [13] in 1958, Hirota and Miyakoda [14] in 1965, Kawaguti

and Jain [15] in 1966, Wang [16] in 1967, Jain and Rao [17] in 1969, Rimon [18] in 1969, Son and Hanratty [19] in 1969, Thoman and Szewczyk [20] in 1969, Honji [21] in 1972, Mehta and Lavan [22] in 1972, Collins and Dennis [23,24] in 1973, Wu and Thompson [25] in 1973, Lugt and Haussling [26] in 1974, Telionis and Tsahalis [27] in 1974, Bar-lev and Yang [28] in 1975, Panniker and Lavan [29] in 1975, and Cebeci [30] in 1979). Among others, Tuann and Olson [31] employed the finite element method in 1976.

Experiments at relatively low Reynolds numbers have been reported by Schwabe [32] in 1935, Taneda and Honji [33] in 1972, Taneda [34] in 1972, and Coutanceau and Bouard [35] in 1977.

Very little experimental data for impulsively-started flow at sufficiently high Reynolds numbers (for Reynolds numbers in the supercritical and post-critical regimes) exists. This is partly because of the experimental difficulties encountered in establishing a vibration-free impulsively-started steady flow and partly because of the instrumentation required to measure the transient quantities involved. In fact, the force that acts on a cylinder in impulsive flow at relatively high Reynolds numbers has been measured directly only by Sarpkaya [36,37] in 1968 and 1978.

Schwabe [32] used a circular cylinder with a radius of $C = 1.7$ inches, and conducted his experiments in an open water channel. The velocity of the cylinder was $U = 0.328$

inches per second at a Reynolds number of about 600. Velocities were determined from the path lengths of particles suspended on the water surface. Other quantities such as the time rate of change of the difference of the square of the velocities, rate of change of the circulation, and the radius of curvature of the streamlines needed to calculate the drag coefficient from the Bernoulli equation were all determined by graphical methods. A careful examination of this work indicates that a considerable amount of experimental error may have existed in the evaluation of the pressures and, therefore, in the resulting drag coefficient. (Schwabe's drag coefficient is about twice the steady-state value and still increasing, when the cylinder has moved about 9 body radii.)

Bingham et al. [38] carried out a number of experiments in a shock tube to observe the influence of Reynolds and Mach number on the impulsive loading of a 0.5 inch cylinder for Reynolds numbers in the range of 31,000 and 77,000 and the Mach number range of 0.15 to 0.4. The pressures were determined from the density fields and the drag coefficients were calculated by an integration of the pressures. The variation of the drag coefficient with UT/C , for a given set of Re and Ma values and from one set of Re , Ma to another, is significant. These variations occur partly because of the growth and shedding of vortices and partly because of different

rates of decay of the initially high pressure on the rear of the cylinder due to passage of the two branches of the original shock.

Friberg [39] quickly immersed a circular cylinder into the steady and uniform free-stream flow field of a water table. Asher and Dosanjh [40] conducted experiments in a shock tube in a manner similar to that done by Bingham et al., and determined the characteristics of the wake. (For example, the position of the vortices, their relative velocities and Strouhal number). Their experiments suffered from the same drawbacks as those of Bingham et al. Other than through numerical simulation, there is no mechanical or traveling shock system which is capable of generating a truly impulsive flow. Efforts to create impulsive or uniformly accelerated flow at high Reynolds numbers or accelerations in a liquid medium may be hampered by the generation of compression and rarefaction waves and regions of intense cavitation. These have been some of the difficulties of experiments with impulsive flows.

Sarpkaya [37] recently repeated his previous work with circular cylinders using a water tunnel with considerably more-sophisticated instrumentation, and simultaneously measured both the drag and lift forces. Sarpkaya and Shoaff [3,4] attempted to numerically simulate the evolution of the early stages of motion through the use of the discrete vortex model.

They have shown that the drag coefficient in the initial stages ($UT/C = 4$) of an impulsively-started flow can exceed its steady value by as much as 30 percent. In the early periods of the flow, vorticity is slow to diffuse and, therefore, accumulates rapidly in the close vicinity of the cylinder. Although the growing vortex soon reaches unstable proportions and separates from its shear layer, the growth of the vortices is so rapid that they become larger than their quasi-steady-state size (at about the same positions) before they separate from their shear layers. This leads to the large drag coefficient observed in the experiments (see Roos and Willmarth [42] for similar observations with spheres). Shortly after the onset of asymmetry, the drag coefficient decreases sharply and the lift coefficient begins to increase. Subsequently, the lift coefficient oscillates with the frequency of the shedding vortices, from the same side of the cylinder.

In the subsonic to moderately supersonic velocity range, the approximate flow similarity between the development of the cross-flow with distance along an inclined body of uniform diameter and the development with time of impulsive flow about a cylinder is known as the "cross-flow analogy." This analogy was first suggested by Allen and Perkins [43] in 1951. It has been subsequently used by many other researchers to calculate the in-plane normal force and the out-of-plane force (side force normal to the plane of flight)

acting on slender bodies moving at high angles of attack. A detailed discussion of the analogy, along with extensive measurements for various nose shapes and body combinations, may be found in Thomson and Morrison [44,45]; Thomson [46]; Bostock [47]; Lamont [48]; Lamont and Hunt [49]; Wardlaw [50]; and Ericsson and Reding [51].

A blunt-nosed cylinder, such as a submarine, at high angles of attack generates a stationary asymmetric vortex array which is similar to the Karman vortex street. Here, the approximate time-space equivalence for the analogy is possible because the vortices have an axial degree of freedom for their lift-off. However, it must be pointed out that the analogy is far from perfect. On a pointed slender body the first asymmetric vortex pair originates at the apex and the analogy no longer applies. Asymmetric vortices give rise to a coupling between longitudinal and lateral degrees of freedom which is often discontinuous and associated with hysteresis effects. Consequently, the phenomenon ceases to be a simple two-dimensional space-time equivalence and becomes a complex three-dimensional fluid structure interaction problem. Additional discussion and references for this and other types of time-dependent flows are presented by Sarpkaya and Isaacson [52].

Because most of the past analytical and experimental studies dealt with a circular cylinder attention herein has been, thus far, primarily directed to impulsive flow about that particular body. Very few studies exist regarding other

bluff bodies. Fage and Johansen [53], in 1927 and 1928, conducted experiments with various bluff bodies, including the evolution of flow about an inclined flat plate. From their ingenious efforts it is known that vorticity is shed from the two sides of an asymmetric body at the same rate and, that the motion in a vortex sheet is steady near the body, except possibly near the inner edge of the shear layers. They have also provided detailed observations regarding the growth and expansion of the shear layers.

In 1975, Sarpkaya [54], presented an inviscid flow model of two-dimensional vortex shedding for an impulsively-started flow over an inclined plate. This work was followed by Fink and Soh [55] with a slightly refined version of the discrete vortex model. Their analysis was confined to the early stages of the vortex development and the calculations were not extended for sufficiently long times to examine the shedding of the vortices from the plate. Belotserkovski and Nisht [56] presented the results of a discrete vortex model of flow over a flat plate at large angles of attack. They did not describe the details of their analysis. Their calculations resulted in unrealistically large oscillations of the drag coefficient. The early stages of the evolution of vortices from a flat plate was studied by Wedemeyer [57]. Subsequently, Pullin [58] extended this work to flow past wedges at various included angles. Telste and Lugt [59] examined the vortex shedding from finned circular cylinders and found that the

force coefficients are very sensitive to the numerical model. However, they have not reported those force coefficients. Kiya and Arie [60] attempted to extend Sarpkaya's work [54] by assuming that the point vortices may be introduced at fixed points near the tips of the plate. Their calculations resulted in large fluctuations in the drag coefficient. This and the conjecture that the nascent vortices are shed from fixed positions prevents realistic assessment of their results.

As noted before, numerous investigations have used the Navier-Stokes equations, together with appropriate finite-difference methods, and modeled the evolution of the wake during the earliest stages of the motion. Unfortunately, such calculations are limited to very small Reynolds numbers (in the order of 100); partly because of problems encountered with numerical instabilities and partly because of the size limitations of the existing computers. Consequently, the results of these studies cannot be compared with those obtained experimentally at larger and practically more significant Reynolds numbers.

The work described herein has been conducted for the purpose of providing data at significant Reynolds numbers for a flat plate and for two cylindrical shapes which have not been analyzed or tested previously. It is hoped that additional numerical work will be undertaken in the future and will be guided by the results presented herein.

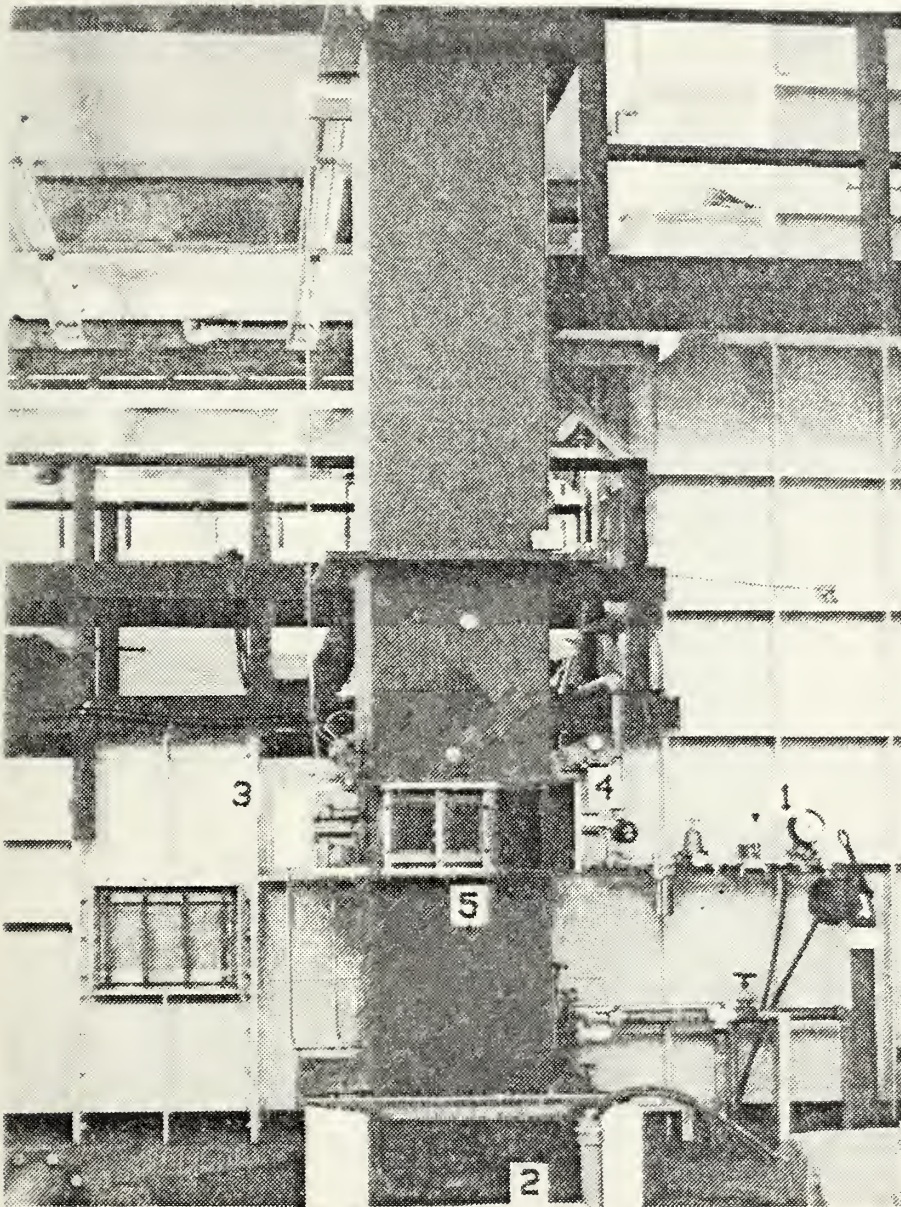
III. EXPERIMENTAL EQUIPMENT AND PROCEDURES

A. VERTICAL WATER TUNNEL

The experiments were conducted in a vertical water tunnel (see Figure 1) which was previously used for the study of impulsive flow about circular cylinders in 1977 [61]. A quick-release valve located at the base of the tunnel is used to create an impulsively-started flow of constant linear velocity. A partial drawing of the mushroom-like seating surface of the quick release valve is shown in Figure 2.

In order to prevent distortion of the force and moment indications, the water-side profile of the mushroom valve has been especially designed to ensure continuous undisturbed flow past the seat while the valve is in any open position. As shown in Figure 2, when the valve is closed, it is in the fully up position. It seats against an 'O' ring inserted on the bottom of the seating surface so that no leakage is present prior to initiating fluid motion.

The vertical position of the mushroom valve is controlled by a three-way valve mounted beneath the tunnel (Figure 3). The stem extends downward from the mushroom valve and is directly coupled to the control valve piston assembly. Compressed air is provided to the two air chambers in the upper part of the valve. A two-way valve in the air supply line provides on-off control of the quick release valve and,



1. Two-Way Air Supply Valve.
2. Quick-Release Valve (Inside the Base).
3. Moment Indicating System.
4. Drag/Lift Force Indicating System.
5. Front Access and Shadow Box.

Figure 1. Vertical Water Tunnel.

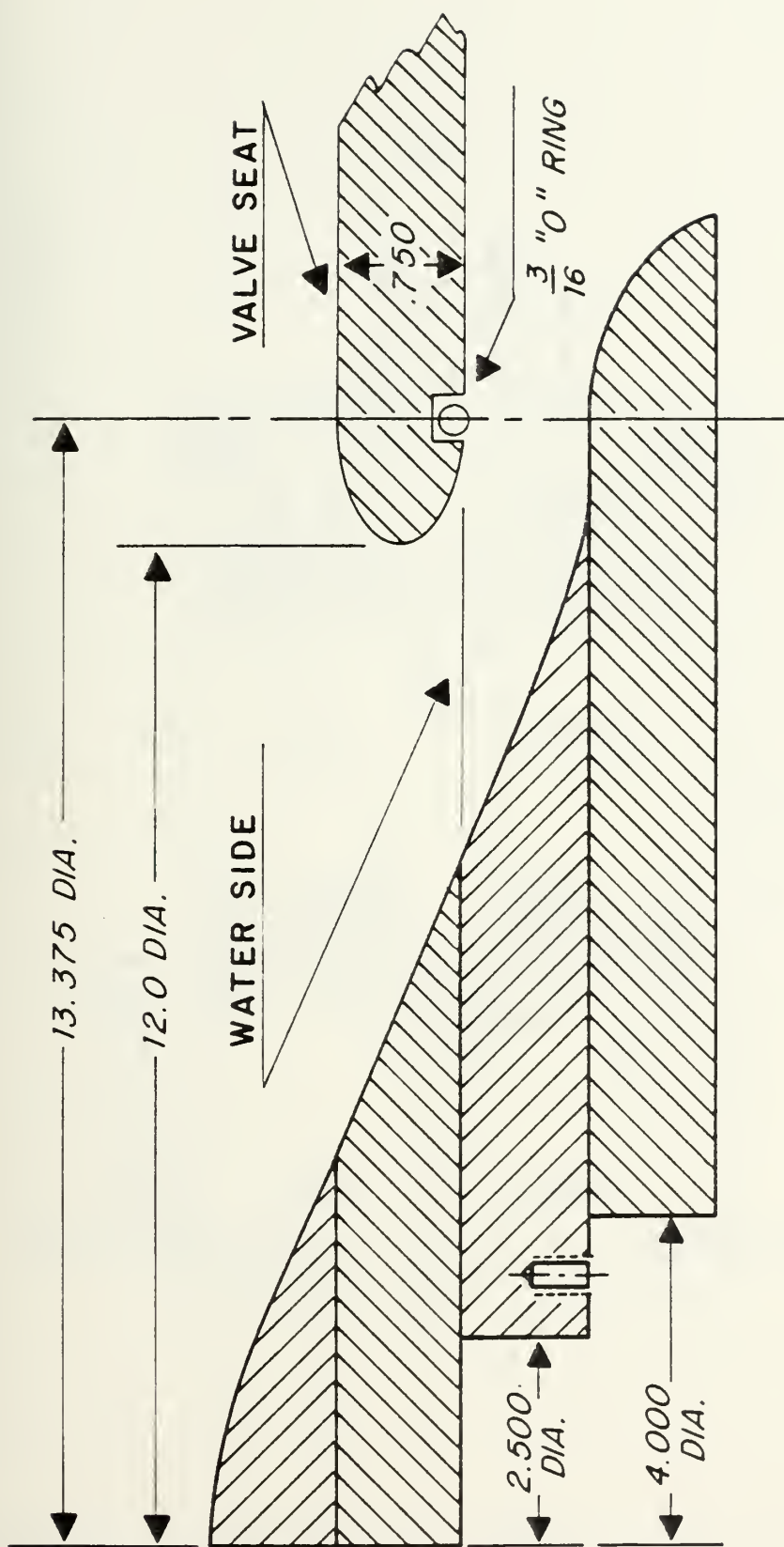


Figure 2. Mushroom Valve Cross-Section (Not to Scale).

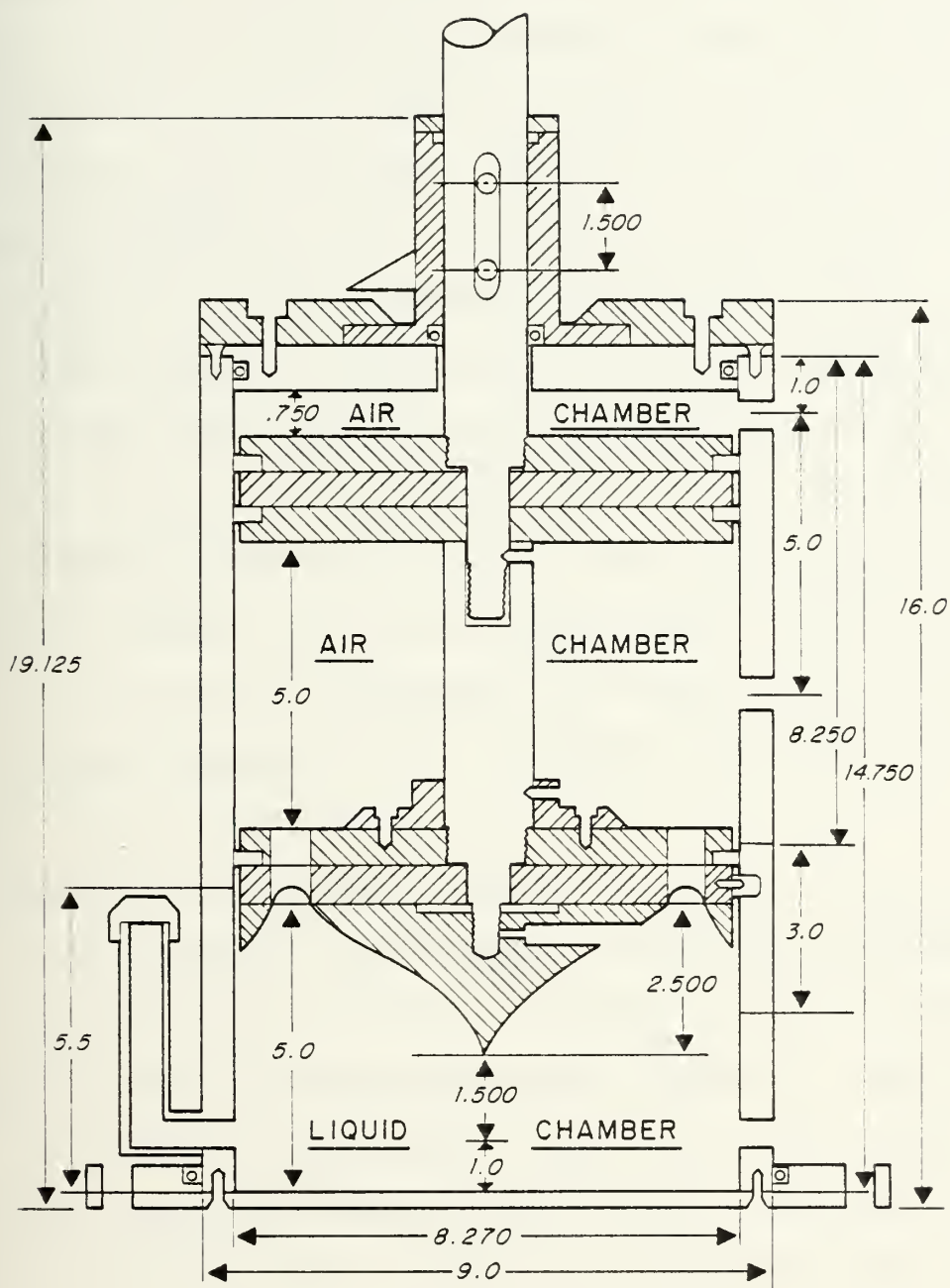


Figure 3. Three-Way Valve Cross-Section (Not to Scale).

therefore, the flow itself. A sight glass provides visual monitoring of the fluid level during an experiment.

Upon opening the two-way air supply valve, the differential pressure between the two air chambers in the upper part of the control valve initiates motion of the piston, rapidly opening the mushroom valve. Thus, flow is initiated and the fluid drains out into a reservoir beneath the tunnel. Subsequent valve motion is regulated by the vertical motion of the piston in the lower part of the control valve and the viscosity of oil in the liquid chamber. The area of the opening (and consequently the amount of resistance which the piston encounters) between the liquid chamber and the upper air chamber can be varied by opening or closing the dual ports in the piston (Figure 4). Oil viscosity and supply air pressure can also be adjusted.

These adjustments allow constant velocities at desired rates to be obtained. Following the rapid initial opening, which accelerates the flow in 0.1 seconds or less, slower further opening of the mushroom valve sustains a controlled drop of the tunnel water level. This controlled slowdown of the rate at which the mushroom valve opens, provided steady flow velocities of about 0.9 feet per second for the experiments described herein. No attempt was made to repeat the experiments at other velocities.

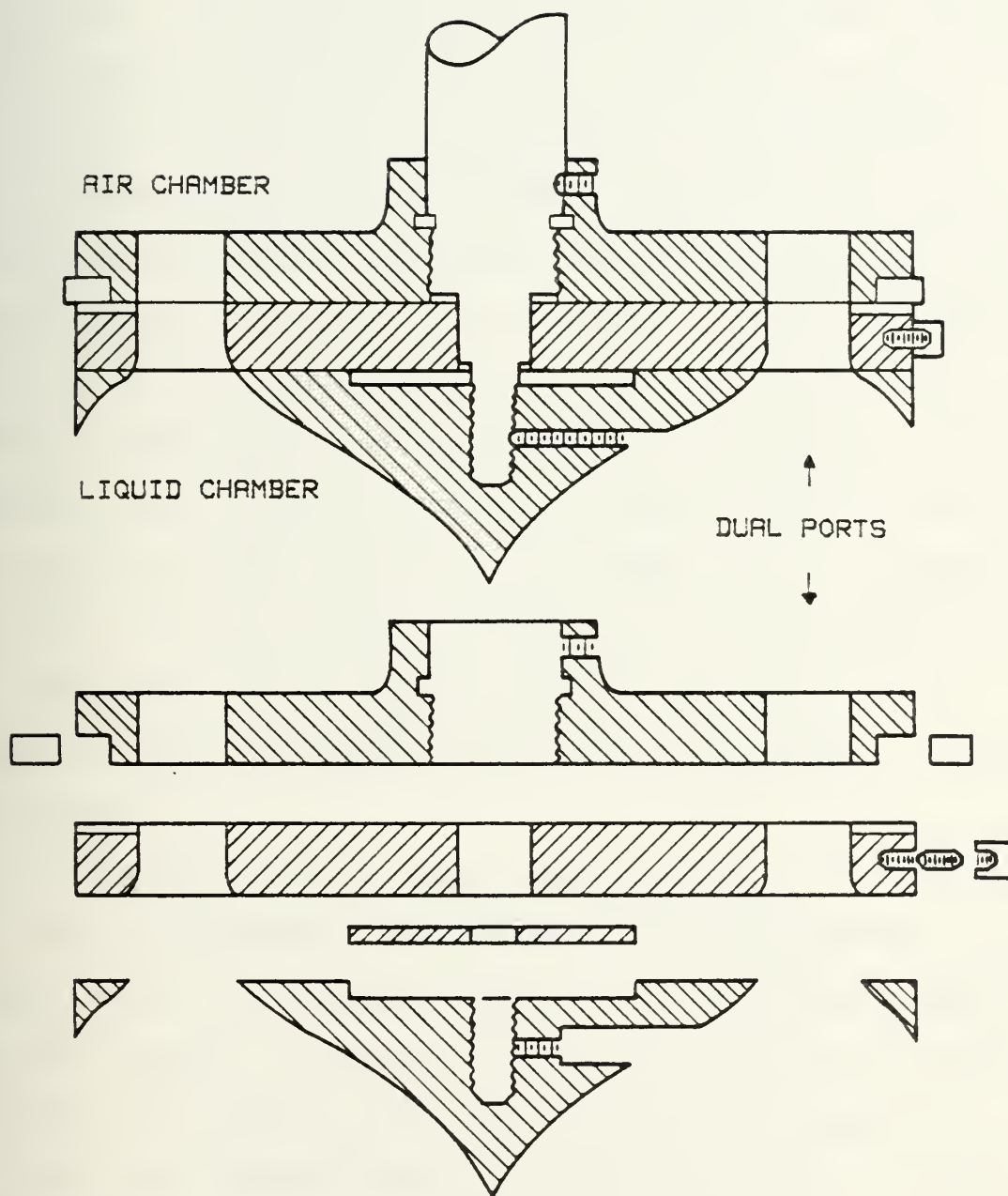


Figure 4. Three-Way Valve Piston Cross-Section (Not to Scale).

B. VELOCITY, FORCE AND MOMENT MEASUREMENTS

Velocity was measured through the use of a variable resistance probe. A five foot long platinum wire, placed vertically in the tunnel and mounted away from the walls, provides tunnel water level indication to an amplifier-recorder assembly. Prior to conducting any experiments, impulsive flow was initiated several times. Adjustments to the quick release valve control system were made, as necessary, to ensure a linear slope on the elevation versus time plot on the recorder. Velocity calibration settings were thereby verified. Additionally, for each run, a consistent water level of three feet above the lower end of the platinum wire was visually set using the installed sight glass. This enabled run to run consistency of the velocity profile to be verified. Figure 5 shows an example of the recorder output for velocity measurement.

BLH Electronics 10 kg load transducers were used to measure the instantaneous lift and drag forces and moment on the bodies tested. Special housings were built for each gage so that they could be mounted on the tunnel at each end of the test body. As shown in the tunnel photograph (Figure 1), the moment was measured from one end of the test body while the lift or drag was simultaneously measured at the other end. The bellows protecting the strain gages were filled with Dow-Corning RTV coating for water proofing and then the ends of the bellows were sealed air tight.

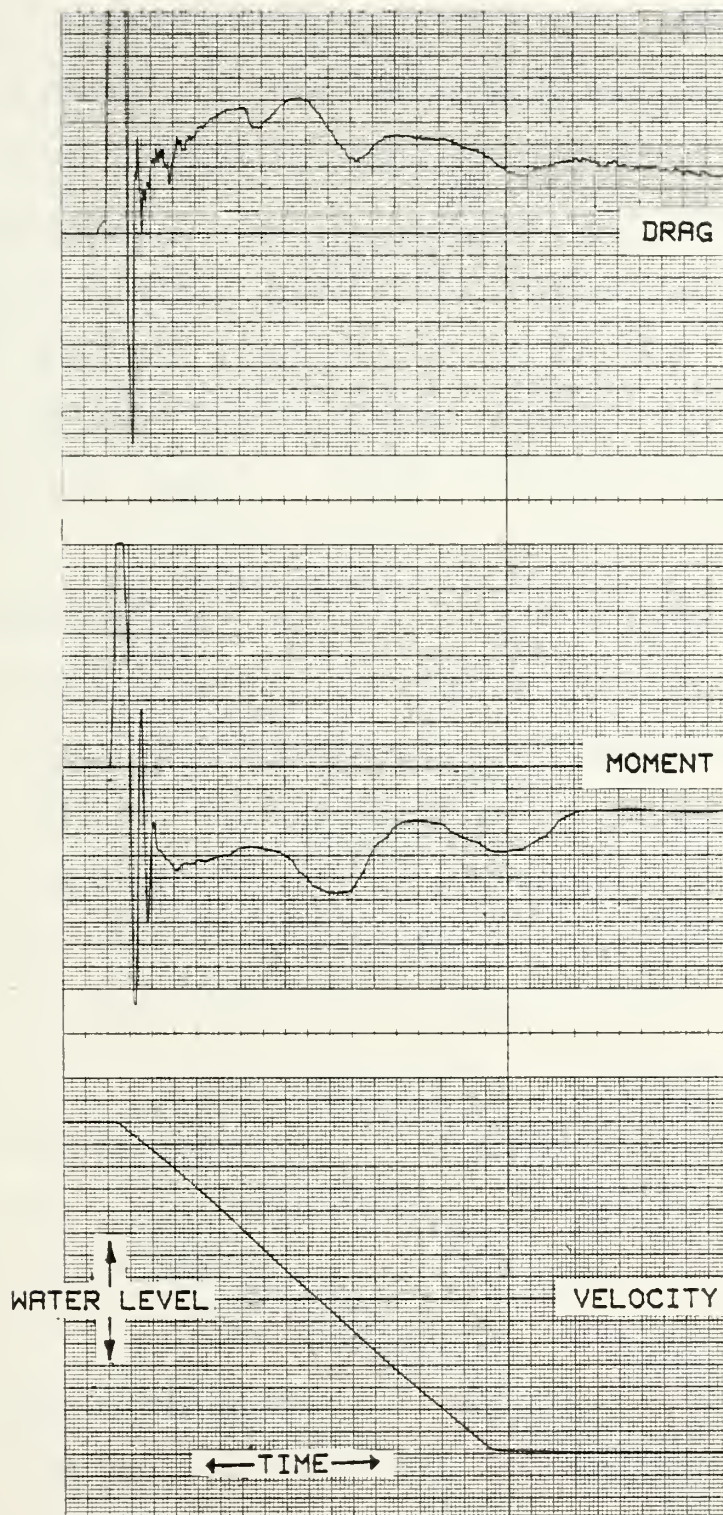


Figure 5. Analog Record for the D-Shaped Body at 0 deg.

In order to measure drag or lift without affecting the moment measurement, the test bodies were mounted in a self-aligning bearing (Figure 6) whose housing was connected to the force transducer. This allowed the test body to be freely mounted (thereby permitting true moment indication at the other end) and accurately aligned. The bearing and housing for the drag and lift gage assembly were also designed to let the gage be rotated to either measure drag or lift.

After mounting the test body, the force gage lift position was determined by rotating the strain gage beam to the vertical position and then hanging different loads from the body. The lift position was fixed when a zero drag force reading was obtained. The final position was marked with an alignment hole, drilled through the indicating plate and housing at the outer end of the assembly, at the top of the vertical axis of the indicating plate (Figure 7). A set pin was then placed in this hole to lock the gage in the lift position. Another alignment hole, marking the drag position, was drilled into the indicating plate exactly 90 degrees from the vertical. Four bolts in the gage housing hold it rigidly in place. Removal of these bolts and the set pin permitted rotation of the gage to either the drag or lift position. Then the pin is placed in the proper location to secure the alignment accurately.

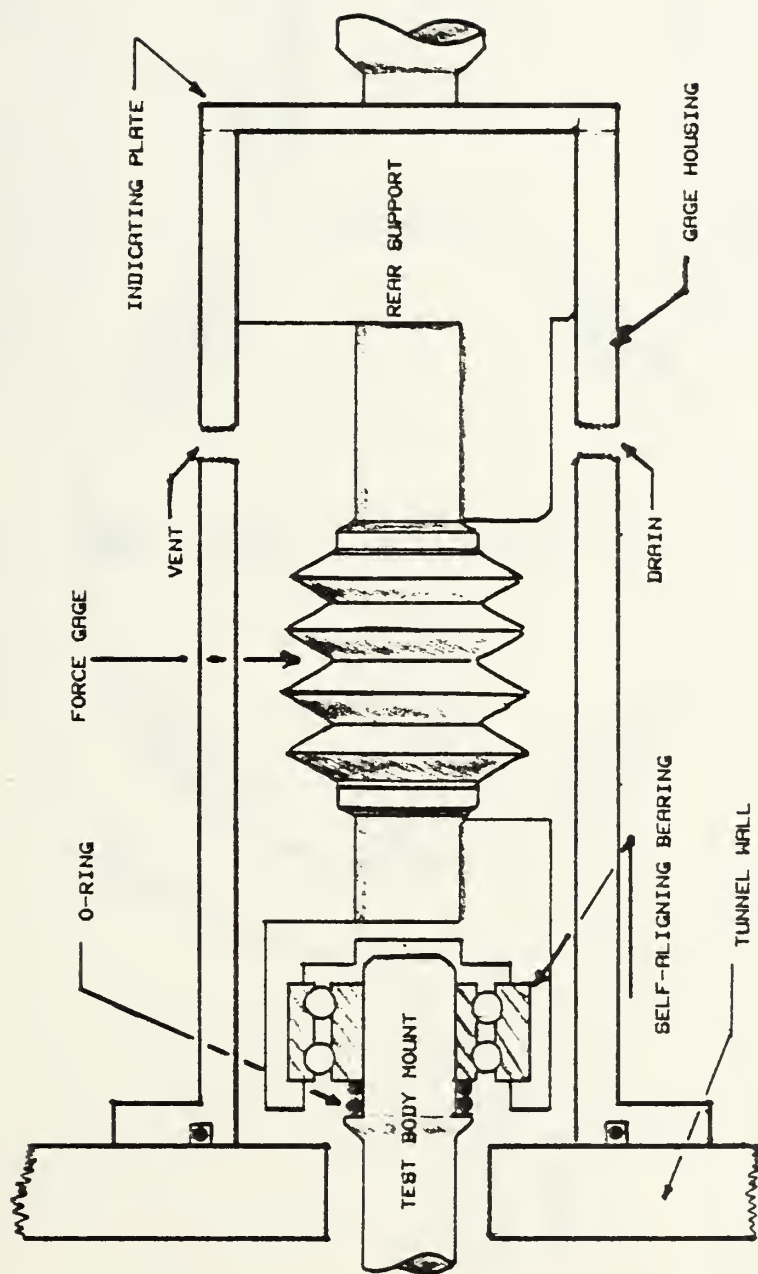


Figure 6. Drag/Lift Force Transducer Assembly (Not to Scale).

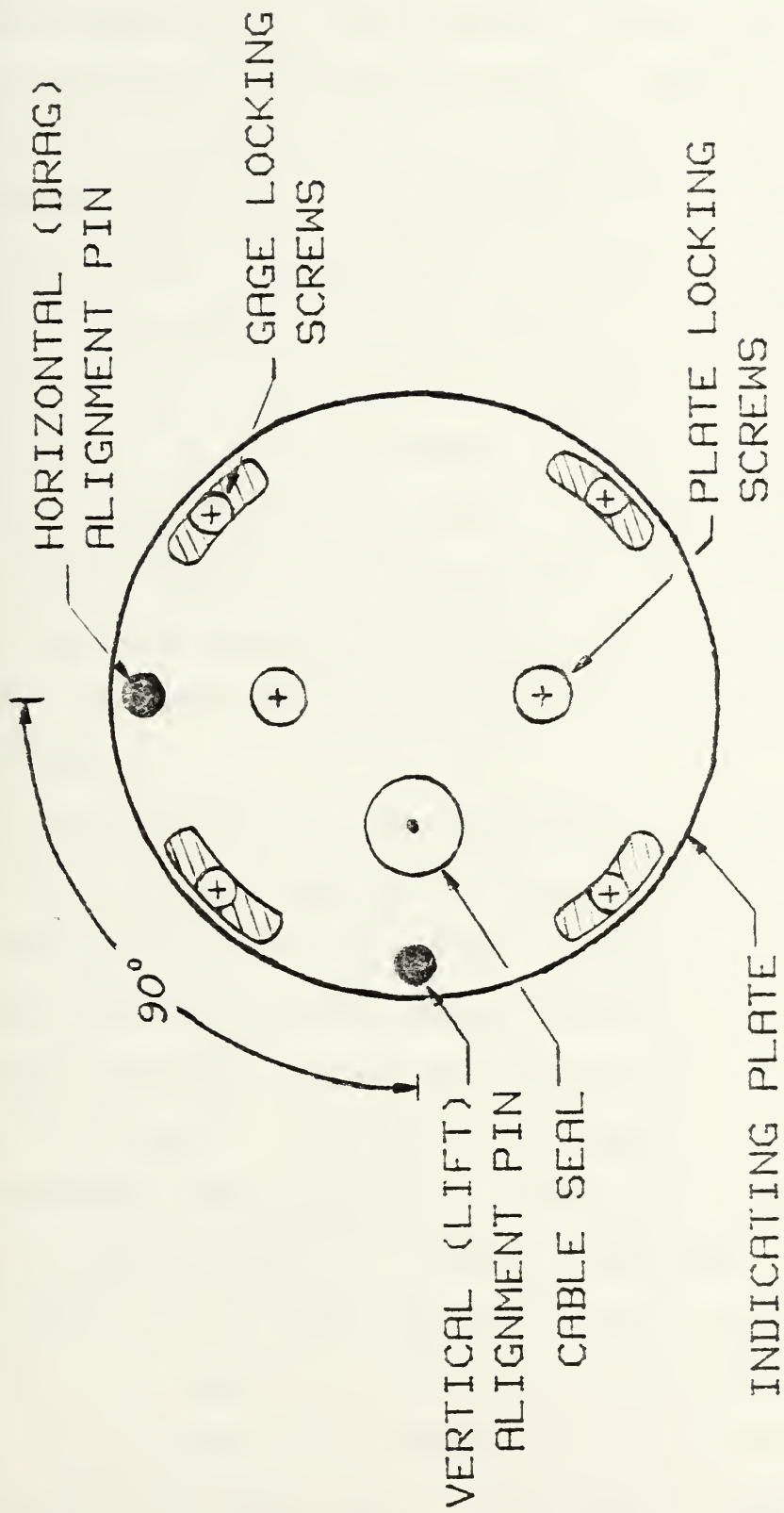


Figure 7. Force Transducer Indicating Plate (Not to Scale).

At the moment side of the tunnel, the test body is connected to another 10 kg load transducer. However, in this case the load transducer acts as a connection to the strain gage (torque-beam) which actually measures and transmits the moment indications. As displayed in Figure 8, the water side (front) of the connecting load transducer is secured to a front mounting where an access hole through the beam housing allows a set pin to lock or release the coupling for the body mounting. This decouples the moment indicating system when the test body's angle of rotation needs to be changed. This set pin, reinstalled prior to testing, locks the test body to the front mount and thus allows twist to be transmitted through from the body.

The rear end of the connecting gage is placed on the torque-beam mount and passes through a roller bearing support. This support permits the connecting load transducer to twist under the moment which may be experienced during the flow tests. The torque-beam mount (Figure 9) serves as the support and reference position for the torque load gage, another 10 kg force transducer which responds to deflections caused by the rotation of the rear end of the connecting gage. While the front support of the torque transducer rests on the beam mount, the rear support is attached to an adjustable support bracket. By shifting the connection position along the support bracket, different orders of magnitude of moment can be compensated for and, therefore, permit more accurate recording and calibration.

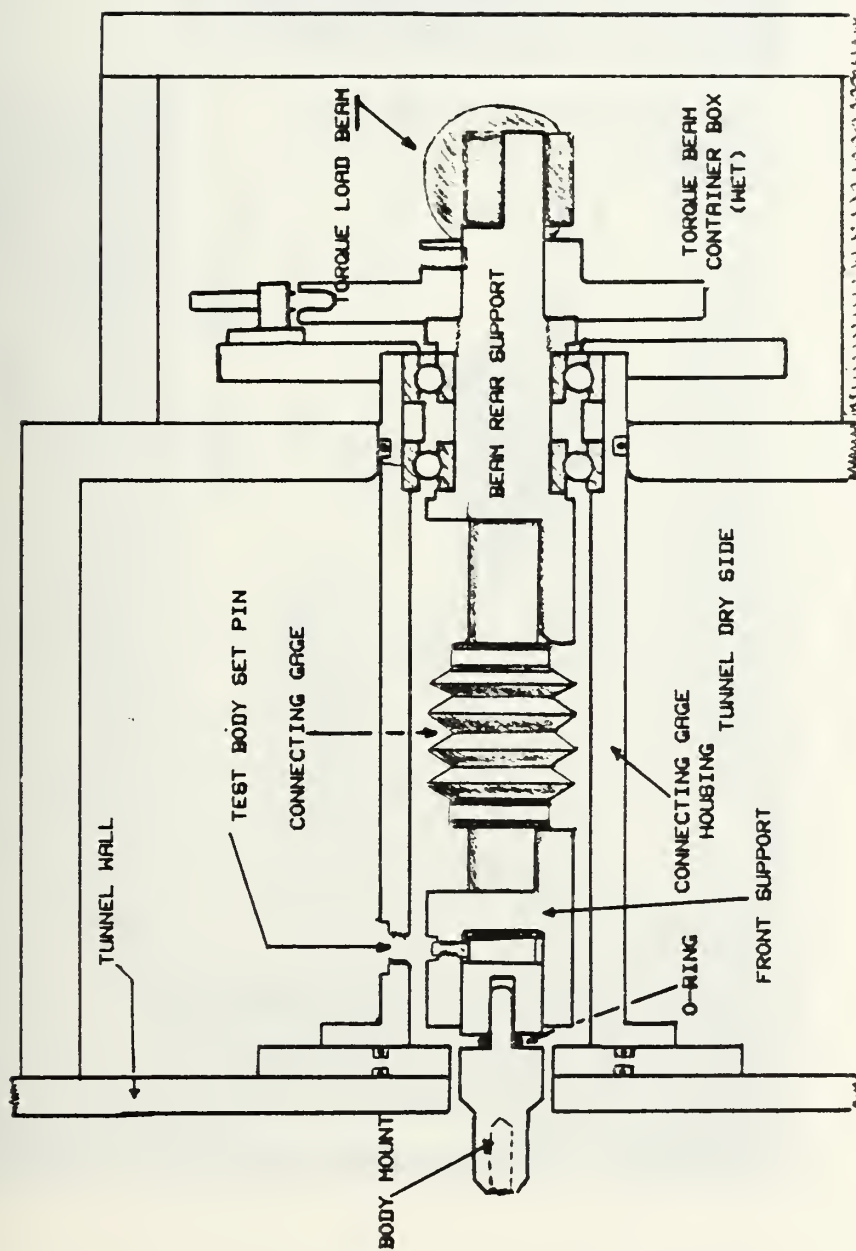
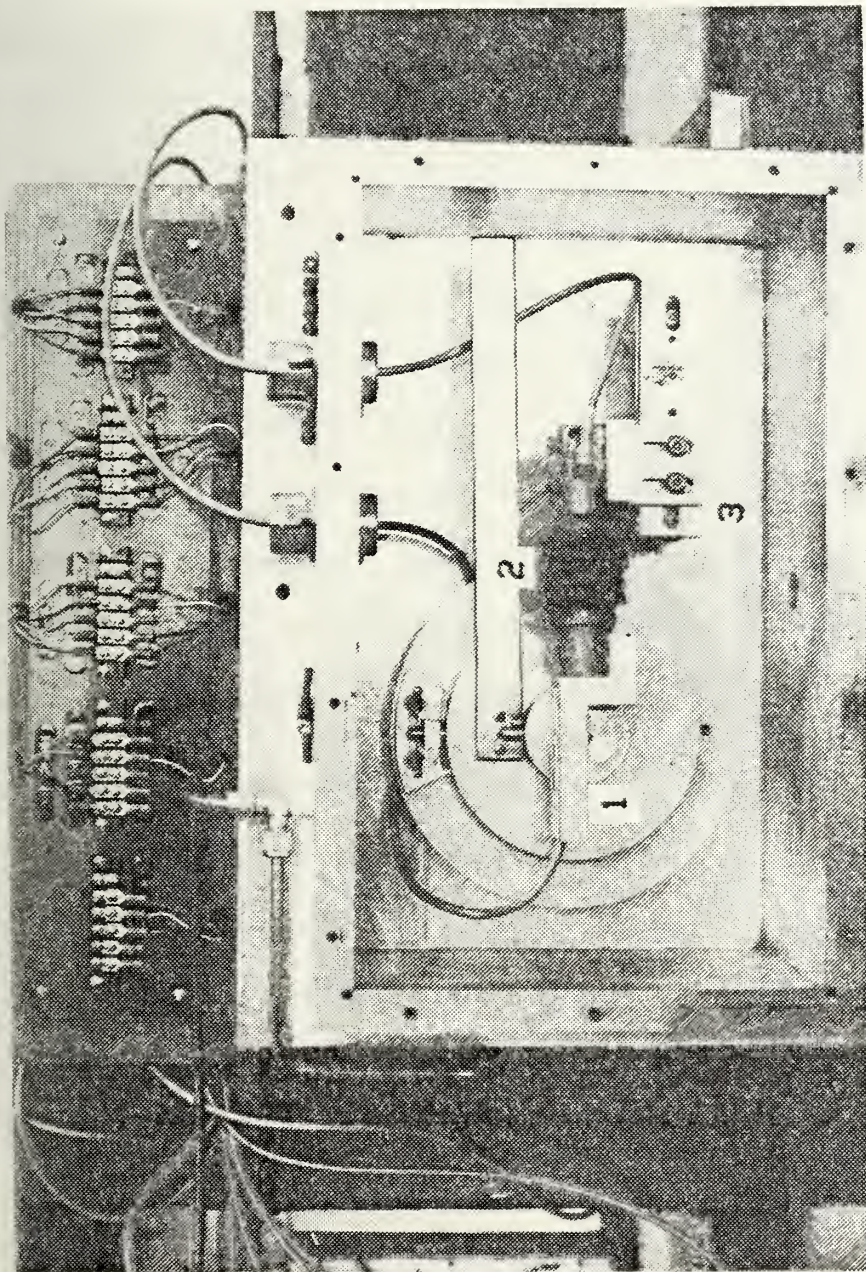


Figure 8. Moment Transducer Assembly (Connecting Load Gage).



1. Torque-Beam Mount.
2. Torque-Load Gage.
3. Adjustable Support Bracket.

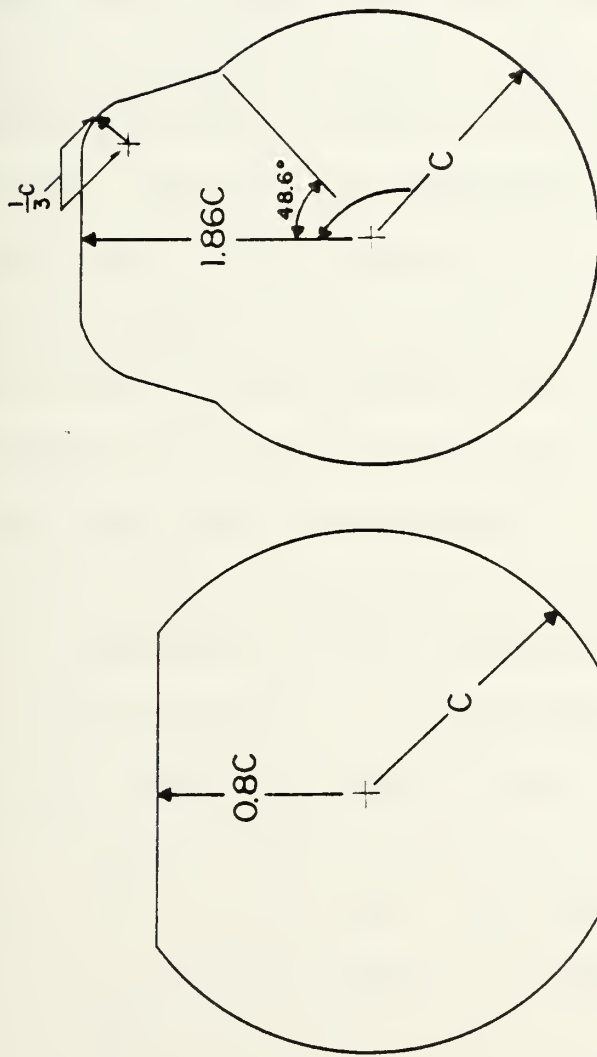
Figure 9. Moment Transducer Assembly (Torque-Beam).

Prior to testing a new body, calibration of the drag and moment transducers was conducted. Known loads of up to 2,000 grams were hung from the midlength of each body with the force gage in the drag position. The amplifier-recorder attenuation settings were adjusted and compared for each different load to ensure consistency.

Similarly, the moment transducer was calibrated by securing a clamp assembly, with a known moment arm, to the midpoint of the test body and then hanging various known loads from the arm to create test moment values. Calibration settings were checked by filling the tunnel with water and recording the signal generated by the buoyant force. This signal was subsequently removed by zeroing the strip chart recorder before an actual flow test was conducted.

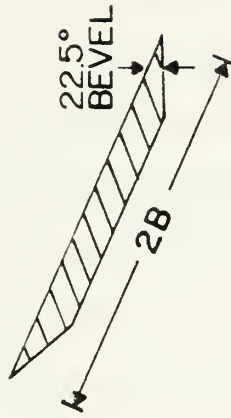
C. SUBMARINE-SHAPED TEST BODIES AND TESTING PROCEDURE

Three shapes, two cylinders and a flat plate, were tested during this research project. All of the bodies were 23.85 in. long. Figures 10a and 10b provide cross-sectional profiles and dimensions for the 'D' and 'T' shapes, respectively. (Note that the letters 'D' and 'T' are used as designations only and do not necessarily define the shape of the cylinder cross-section.) Each of these cylinders was constructed from solid plexiglas, turned on a milling machine and then polished for a smooth finish. The length of each cylinder was cut so that a gap of approximately 0.06 in. was present between the tunnel wall and each end.



$C = 2 \text{ in}$
[a]

$C = 1.75$
[b]



$B = 1.5 \text{ in}$
[c]

Figure 10. Geometrical Characteristics of the Test Bodies:
(a) D-Shape. (b) T-Shape. (c) Flat Plate.

Aluminum mounts were constructed on a lathe and then countersunk and bolted into the cylinder ends so that the surfaces were smooth and flush. The attachment at the drag and lift end of each cylinder is round and compatible with the self-aligning bearing. At the moment end, the cylinder attachment is a flat cantilever beam which is compatible with the connection to the front mounting of the connecting gage for the torque indicating assembly.

The flat plate (Figure 10c) was fashioned from steel plate and polished to a smooth surface. Its attachments are similar to those described above except for slots which hold the plate bolted to them. Each body is prevented from moving laterally toward either wall of the tunnel by 'O' rings attached between the cantilever ends of the cylinder mounts and the force transducer connections. (See Figures 6 and 8.)

By removing the various locking devices previously described each test body can be rotated to various angles of attack. Both of the cylinders have a small pin hole at the top where an indicator fits for aligning the angle of rotation at 5 degree intervals. The indicator was lined up with the appropriate markings placed on the window surrounding the drag and lift gage. The indicator was removed from the cylinder shapes prior to testing. Flat plate angle of rotation was set by using the knife-edge as a reference to the markings on the window.

Each body was tested at various angles of attack for drag, lift and moment measurement. At least three runs were conducted

for drag and lift, respectively, at each reference angle. Therefore, six moment runs were generated at each reference angle. Velocity was indicated by the elevation versus time plot which was generated for every run.

Raw analog data was produced from the force and moment transducers and the variable resistance probe by connecting their outputs to individual Hewlett-Packard 7702B Recorder-Amplifiers and then to a Gould 2600 Strip-Chart Recorder which was operated at a speed of 50 mm per second for each run. Figures 11 and 12 are examples of the strip-chart recorder outputs for the T-shaped cylinder and the flat plate, respectively. Note that for the purposes of presenting these examples, and the example in Figure 5, chart speed was reduced to 25 mm per second. Strip chart data was digitized using a Hewlett-Packard 9874A Digitizer coupled to an HP-9845A desktop computer. This analog data was processed in accordance with the governing equations described in Chapter IV, producing the graphical and tabular presentations of the force-transfer coefficients included there and in the appendixes.

D. FLOW VISUALIZATION

Motion pictures, at film speeds of 32, 48 and 64 frames per second, were taken of the flow past the T-shaped body at the zero reference position. The flow was filmed through the window adjacent to the lift and drag gage housing. A plane of light across the cylinder was provided through slits

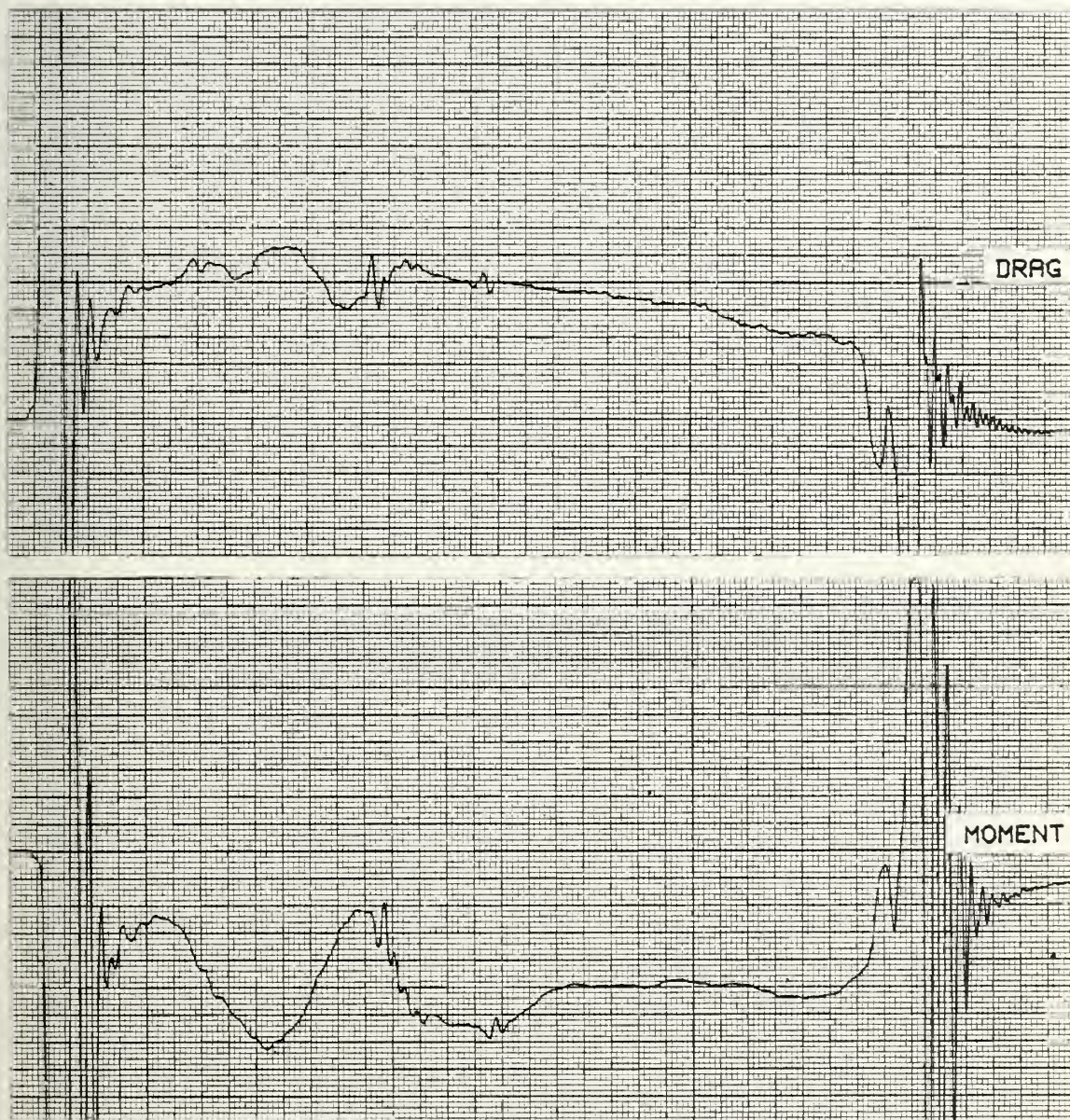


Figure 11. Analog Record for the T-Shaped Body at 0 deg.

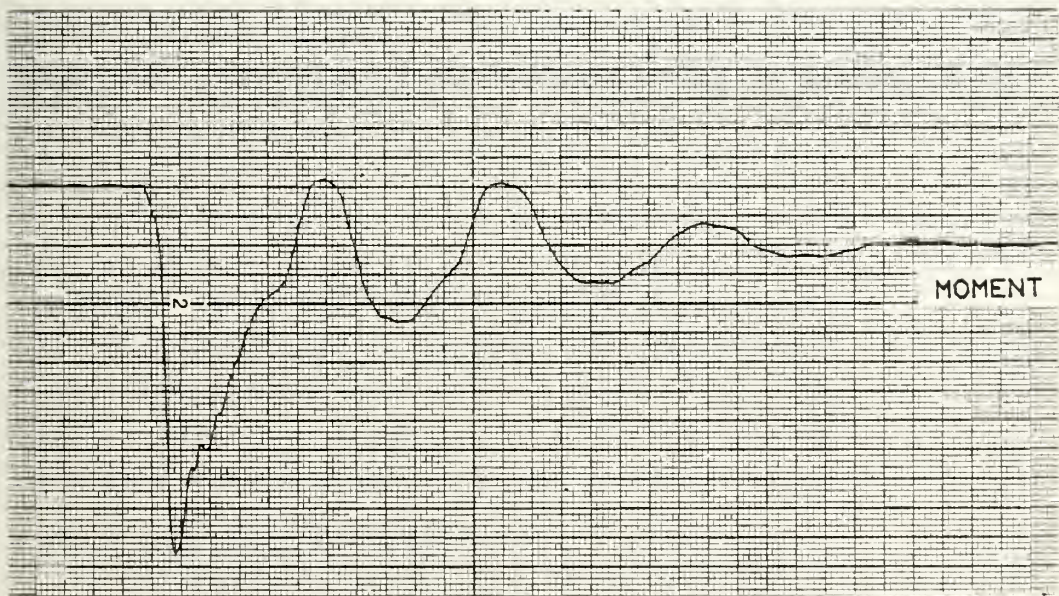
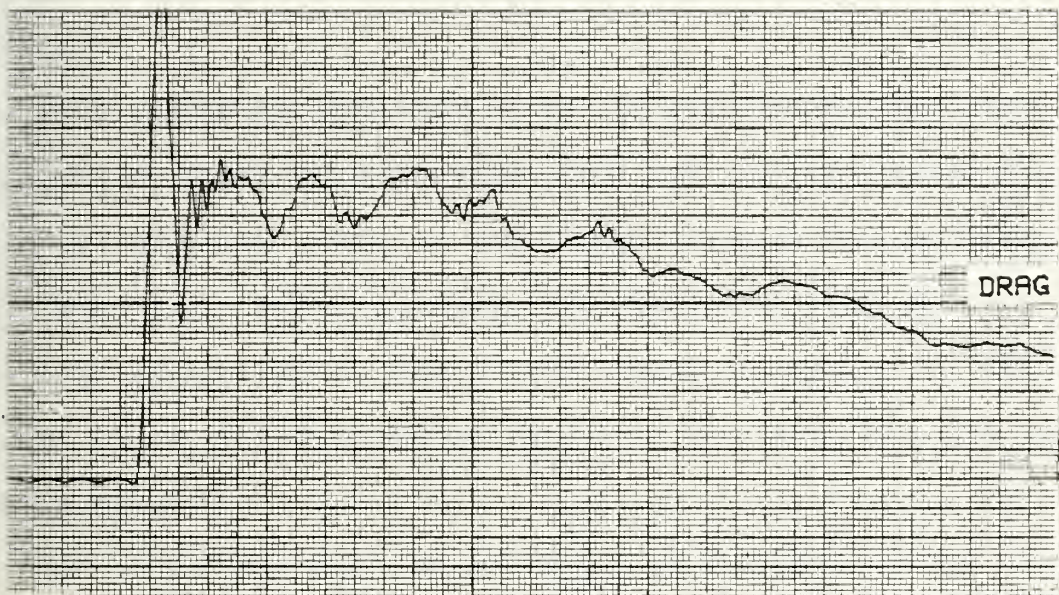


Figure 12. Analog Record for the Flat Plate at 45 deg.

approximately one foot long cut into the front and rear walls of the tunnel. Shadow boxes were attached externally to the tunnel (Figure 1), into which were mounted high intensity lights.

After ensuring that the water in the tunnel was calm, polystyrene beads were dropped into the filled tunnel from directly over the plane of the light through the cylinder cross section. After allowing the beads to sink down to the level of the cylinder, while continuing to add more, the quick release valve was tripped to initiate the flow for the already running camera.

Flow visualization efforts were restricted to the T-shaped body because the view of the other shapes was obstructed by the drag and lift gage housing and due to limited window area.

IV. EXPERIMENTAL RESULTS

A. PRESENTATION

The experimental results (drag, lift and moment coefficients [C_d , C_l , and C_m , respectively] for the D- and T-shaped cylindrical bodies; normal force coefficient [C_n] and the normalized moment arm [X/B] for the flat plate) are presented primarily in graphical form. Plots of the force-transfer coefficients versus an appropriate normalized displacement have been provided. For the purposes of discussion in this chapter, results are addressed, for a given body at a specific angle of attack, with reference to specific figures which display the plotted information. Since not all of the large volume of data are discussed herein, representative data together with the remainder of the graphs have been assembled in the appendixes by body shape and reference angle (angle of attack). (For more specific information refer to the List of Appendixes, p. 6).

With a few exceptions, each plot shows data obtained in three separate experimental runs.

B. DEFINITION OF THE FORCE-TRANSFER COEFFICIENTS

The drag coefficient for the D- and T-shaped bodies is defined as

$$C_d = \frac{\text{DRAG FORCE}}{\rho C L U^2} \quad (3)$$

where C is the radius of the cylinder base circle; U, the velocity of the ambient flow; L, the length of the body; and ρ , the density of the fluid. Similarly, the lift coefficient for these two bodies is defined as

$$C_l = \frac{\text{LIFT FORCE}}{\rho C L U^2} \quad (4)$$

The moment coefficient is defined as

$$C_m = \frac{\text{MOMENT}}{\rho L C^2 U^2} \quad (5)$$

The positive directions of drag, lift and moment, along with the positive direction of angle of attack with respect to the direction of the impulsive flow, are shown in Figures 13a and 13b. The normalized displacement for the D- and T-shaped bodies is UT/C .

For definition of force and moment coefficients for the flat plate, a choice had to be made between separate lift and drag coefficients and a single, normal force coefficient. Since current literature on flow about flat plates often refers to the normal force and the use of one coefficient permits calculation of the lift or drag through the angle of attack, it was decided to present the normal force coefficient as

$$C_n = \frac{\text{FORCE NORMAL TO PLATE}}{\rho B L U^2} \quad (6)$$

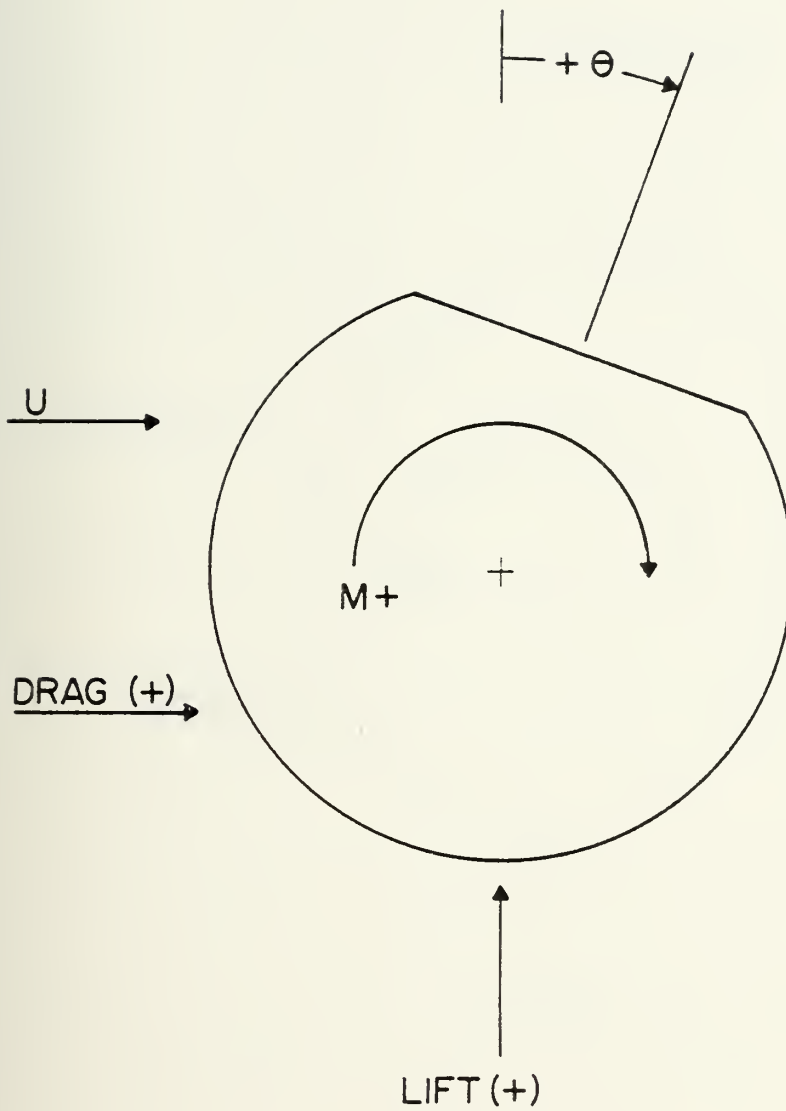


Figure 13a. Definition Sketch for the D-Shaped Body.

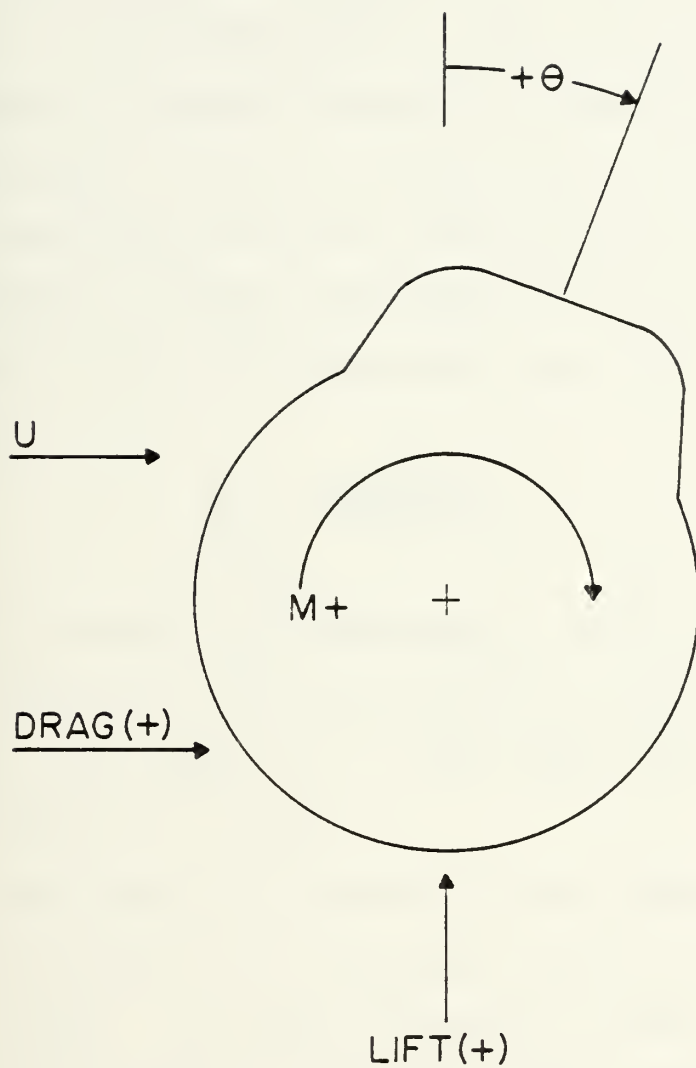


Figure 13b. Definition Sketch for the T-Shaped Body.

where B is one-half of the plate width (see Figure 13c). For each angle of attack the lift and drag forces were separately measured and vectorially combined to yield the normal force, F_n , at the corresponding times. Only for $\theta = 55$ degrees, the normal force was measured directly, by suitably rotating the force transducer in order to compare the direct and indirect (vector combination) methods of evaluating the normal force.

Information regarding the moment acting on the plate is presented in terms of a normalized moment arm, X/B , which is defined by

$$\frac{X}{B} = \frac{\text{MOMENT}/F_n}{B} \quad (7)$$

MOMENT/F_n represents the distance, X , from the centerline axis of the plate to the point where the resultant normal force acts (see Figure 13c). The normalized displacement for the flat plate is UT/B .

Note that "angle of attack" is used synonymously with "angle of rotation" as a reference position for the two cylindrical bodies. As shown in Figures 13a and 13b, this should not be confused with the angle of attack routinely associated with an airfoil.

C. D-SHAPED CYLINDER

This body was tested at angles of attack of 0, ± 10 , ± 20 , ± 30 , ± 45 and, -90 degrees. The drag, lift and moment coefficients for the zero degree angle of attack are shown in Figures 14 through 16, respectively, as a function of UT/C , the

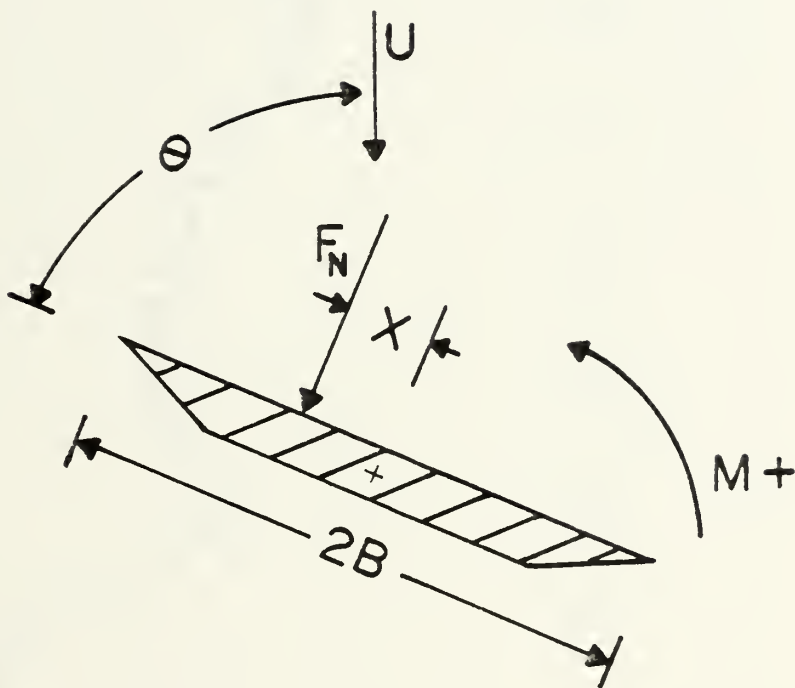


Figure 13c. Definition Sketch for the Flat Plate.

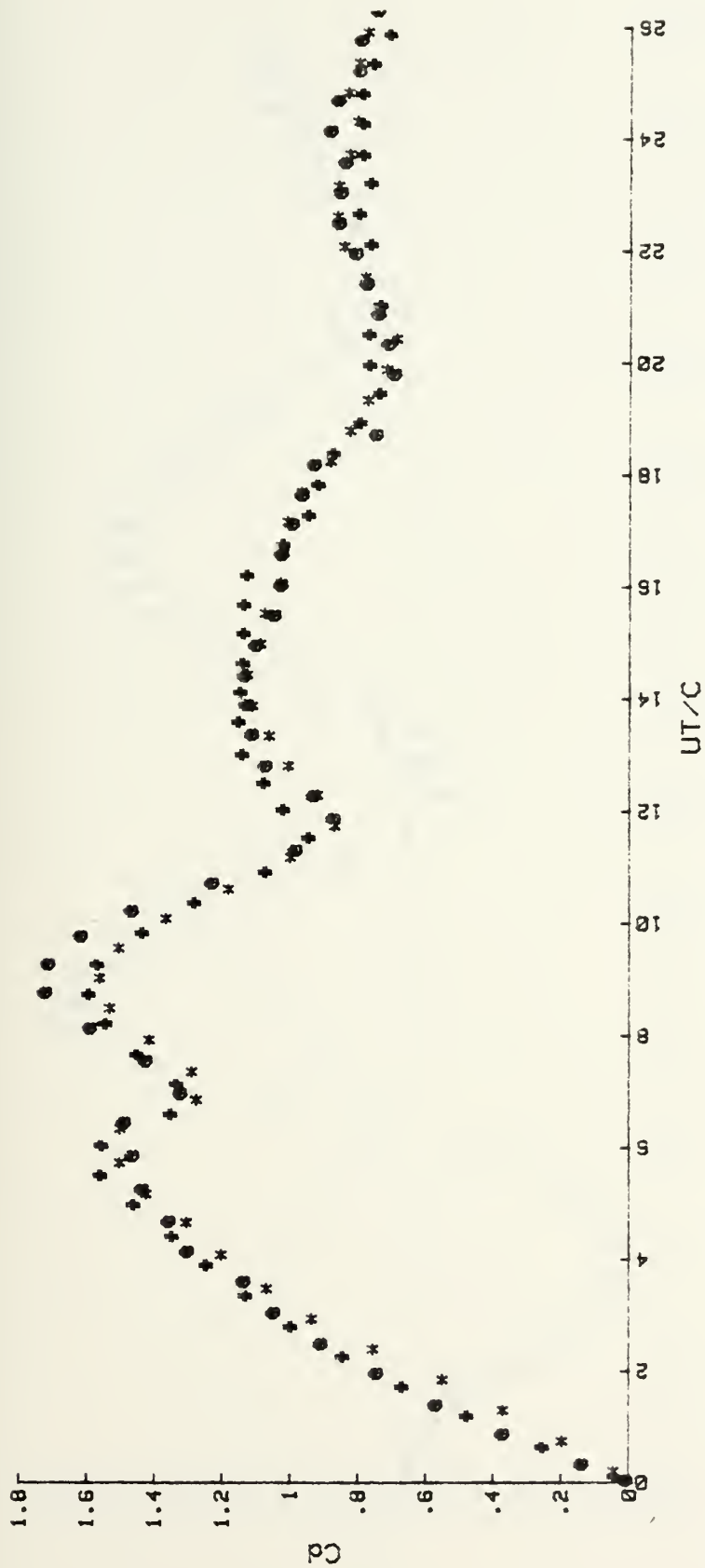


Figure 14. C_d vs. U_T/C for the D-Shaped Body at 0 deg.

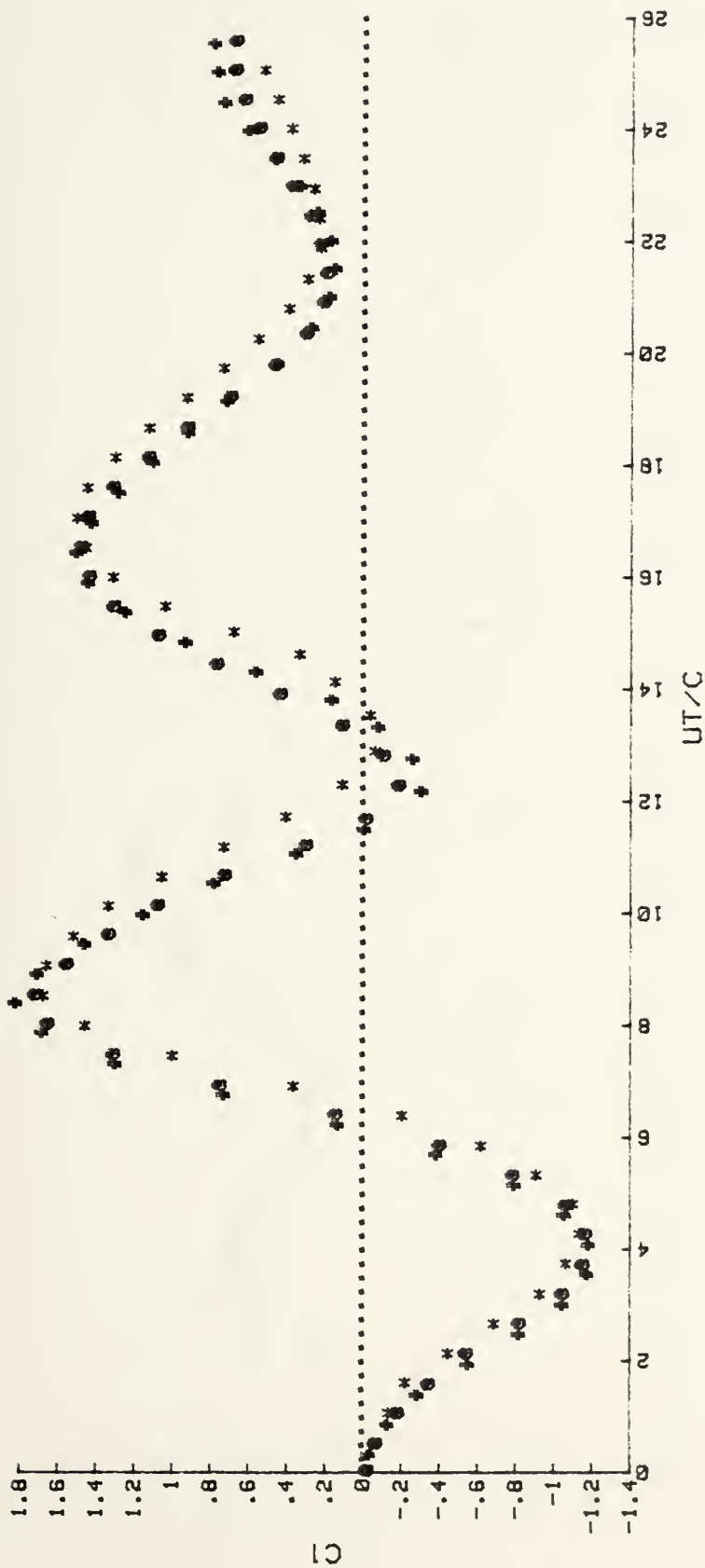


Figure 15. $C1$ vs. UT/C for the D-Shaped Body at 0° .

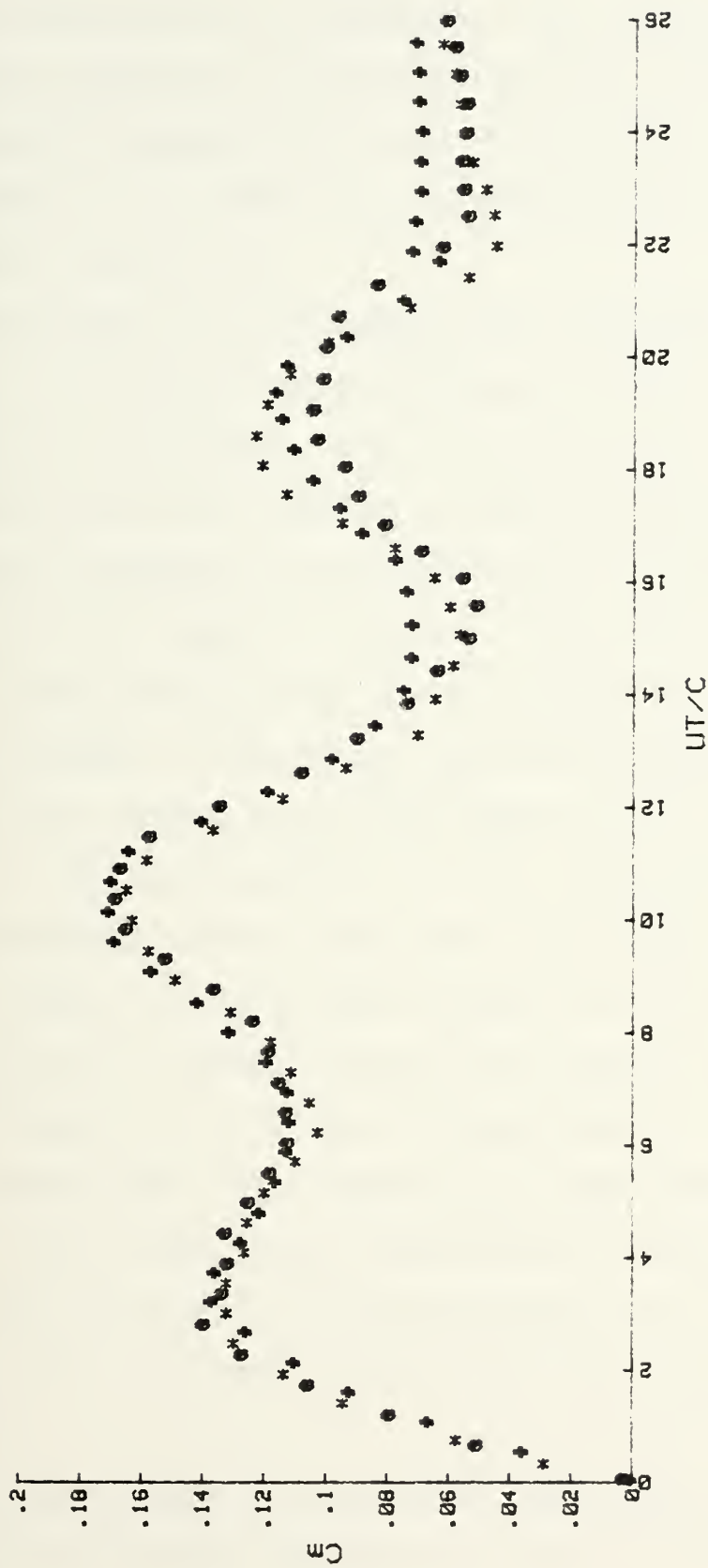


Figure 16. C_m vs. UT/C for the D-Shaped Body at 0 deg.

normalized displacement of the fluid. By carefully controlling the flow mechanism in the vertical water tunnel, repeatable and nearly constant velocities were maintained. The Reynolds number, $Re = 2Uc/\nu$, was, therefore, kept nearly constant at $Re = 27830 \pm 270$.

Dramatic effects are associated with the growth of the first three or four vortices shed from the body following the initiation of the impulsive flow. At the start of the motion, the vortices grow rapidly and at a rate of growth such that the vorticity accumulates to an amount far in excess of that found in the later stages of motion. This excess vorticity reduces the base pressure and causes a large drag overshoot. As shown in Figure 14, the drag coefficient reaches a value of slightly more than 1.6 with dual peaks in the region of overshoot, extending from $UT/C = 6$ to 9. Following the shedding of the second vortex (which can be estimated by studying the plot of the lift coefficient, Figure 15), C_d drops rapidly and asymptotically reaches a mean value close to that of a circular cylinder (in this case, C_d approaches a value of 0.8 for UT/C greater than 20). Although the experiments were not extended to UT/C values larger than about 26, the indications from the data in all cases are that beyond $UT/C = 25$ the drag coefficient will not change further beyond the asymptotic values.

For positive angles of attack the drag overshoot is also present with C_d reaching values of 1.7 to 1.8. At negative

angles of attack, however, the drag coefficient increases further, to as high as 2.3 for $\theta = -20$ degrees. Note that at negative angles of attack, the flat face of the body is rotated toward the flow, presenting a sharp edge from which immediate separation can occur. The higher C_d values at negative angles of attack are, therefore, indicative of a more significant accumulation of excess vorticity in the early stages of motion (UT/C less than a value of about 11). (See Appendixes B through J). Asymptotic values of the drag coefficient for UT/C greater than 25 generally ranged from 0.8 to 1.4.

Figure 15 shows the variation of the transverse force as a function of UT/C . At the start of the fluid motion the lift force is directed toward the flat surface of the D-shaped body. (In this case C_l is negative by the definition adopted here and so is the lift force; see Figure 13a). Consequently, a D-shaped submarine with the flat surface horizontal (i.e., a level keel) is subjected to a negative lift force when pushed downward and a positive lift force when lifted toward the free surface. As displayed in Figure 15, the initial lift force resulting from the impulsive fluid motion is negative. A submarine turning (to the right or left) would thus be subjected to a vertical force which tends to submerge the body for a lateral displacement of UT/C less than about 6.

With reference to Figure 13a, the reasons for this behavior may be explained as follows. At the start of motion the flow

separates immediately at the sharp front edge of the flat surface. A vortex forms and grows rapidly. On the round face of the D-shaped (bottom side of the submarine), however, the separation is not as immediate as on the top. Studies of impulsively-started flows about circular cylinders have shown that separation does not start until the relative displacement (UT/C) reaches a value of about 0.35 [4,62]. A circulation is imposed on the flow about the body which is of equal strength and opposite sign for each shed vortex. Therefore, a vortex shed with a clockwise circulation from the top of the D-shaped body (Figure 13a) imposes a counter-clockwise circulation on the flow. As a result, the velocity increases and the pressure decreases on the round face relative to the other side where the vortex is first formed. The differential pressure creates a transverse force directed from the flat face (top) toward the center of the body. In other words, the lift force always acts on a body in a direction away from the last shed vortex and normal to the direction of the ambient flow.

The subsequent shedding of vortices results in an alternating transverse force as shown in Figure 15. For the zero degree angle of attack, the lift force acting on the D-shaped body fluctuates about a positive mean value. For all other angles of attack the value of the mean lift force is slightly smaller than that corresponding to the zero-degree angle of attack (see Appendixes B through J).

The phenomenon of vortex shedding is non-stationary in the early stages of impulsive motion and consequently a single vortex shedding frequency does not exist. An estimate of the frequency was made from plots similar to Figure 15. Time intervals between consecutive peaks of the lift coefficient curves were used to derive a Strouhal number in terms of the period defined by those time intervals. Analysis of Figure 15 shows that the first two vortices shed from the D-shaped body, at zero degrees angle of attack, correspond to a Strouhal number, $S = 2fC/U$, of approximately 0.23. For other angles of attack, the Strouhal numbers ranged from 0.19 to 0.24 with no particular correlation to the specific direction or magnitude of the angle of attack.

It should not be inferred from the foregoing discussion that the initial right or left turn of a D-shaped cylindrical body will necessarily and always result in a force which will tend to generate a diving motion. Other body- and control-surface generated vortices will interact with the first vortex resulting from the impulsive motion of the submarine's turn. Although it was not the purpose of this investigation, analysis of the lift coefficient data presented herein indicates that the turn of a submarine may result in a diving or rising motion due in part to the impulsive cross-flow, the interaction of all vortices in the flow surrounding the body, and partly due to the heel of the submarine during the turn. Emphasis in this discussion has been placed on the separate effects of impulsive motion on the underwater body.

Figure 16 shows that the D-shaped body at zero degrees angle of attack is subjected to a positive moment as defined in Figure 13a. The direction of the moment could have been inferred from the vectorial sum of the lift and drag forces. Moment resulting from the impulsive flow tends to bank the submarine in a direction opposite to the direction of heel that normally occurs during the initial phase of the turn (a submarine rolls inboard during a turn [64]). In other words, that portion of the moment acting on the body which is created by the impulsive cross-flow of the turn helps to stabilize the heeling position of the body. It is important to emphasize that the qualitative as well as quantitative understanding of the forces resulting from the impulsive motion is valuable in deriving a better overall understanding of all the forces which determine the resultant motion of the body.

D. T-SHAPED CYLINDER

Figures 17, 18 and 19 are the plots of drag, lift and moment coefficients, respectively, for the T-shaped body at zero degrees angle of attack. Force and moment directions and other geometrical details are provided in Figure 13b. The Reynolds number, $Re = 2UC/\nu$, for the T-shaped cylinder was kept within a range of $Re = 24380 \pm 240$.

As in the case of the D-shaped body, the first vortex develops on the side where geometrical symmetry is disturbed, i.e., at the side of the protrusion. In the case of the D-shaped cylinder, the disturbance is the flat face (at the top

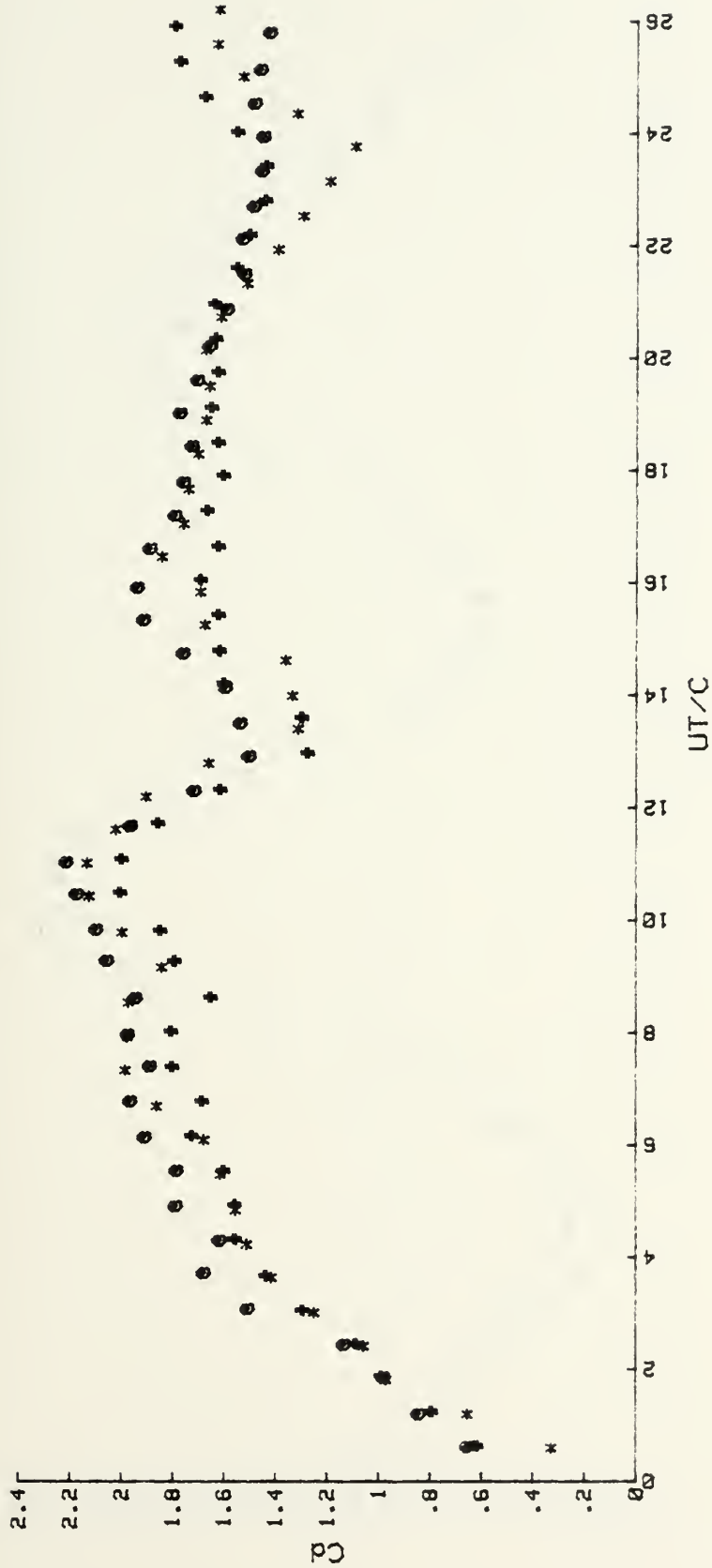


Figure 17. C_d vs. UT/C for the T-Shaped Body at 0 deg.

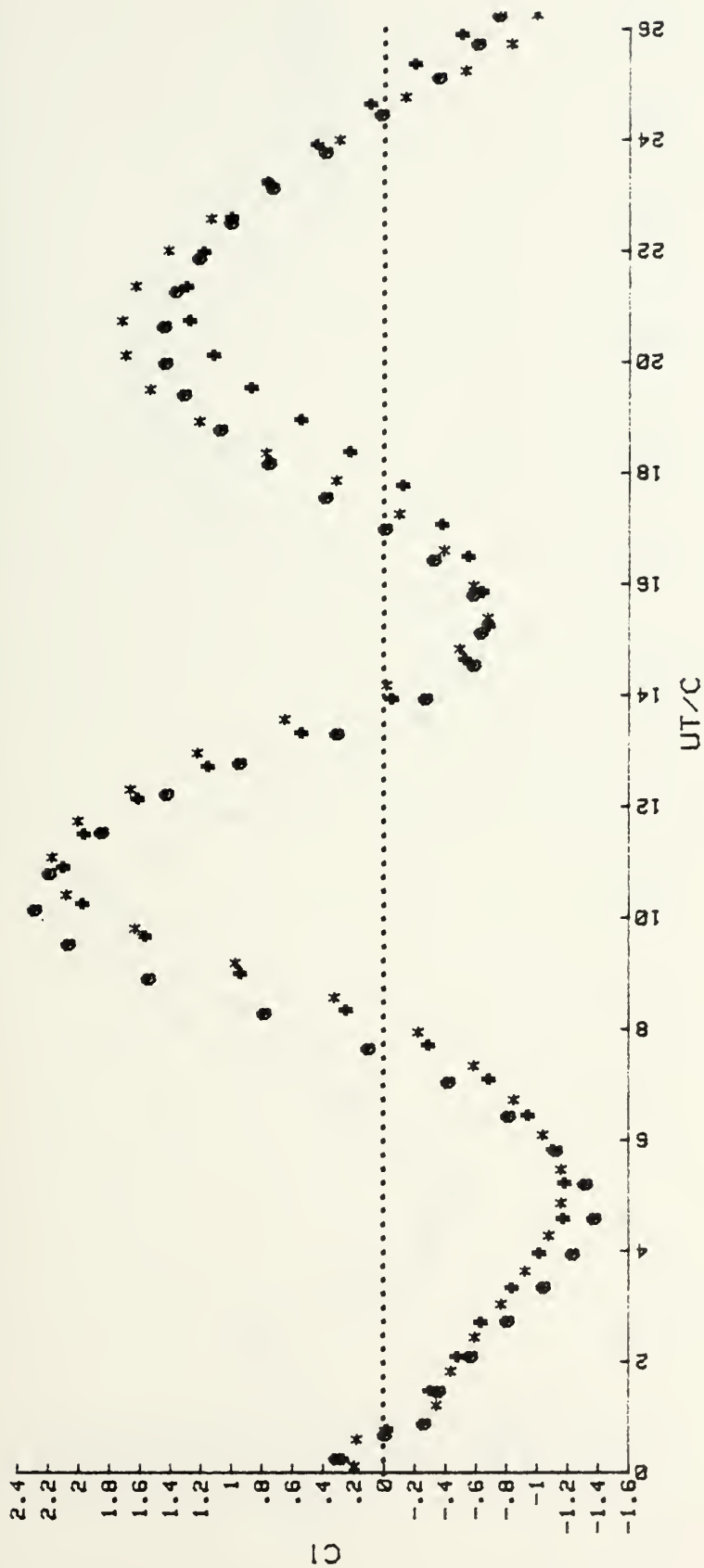


Figure 18. CI vs. UT/C for the T-Shaped Body at 0 deg.

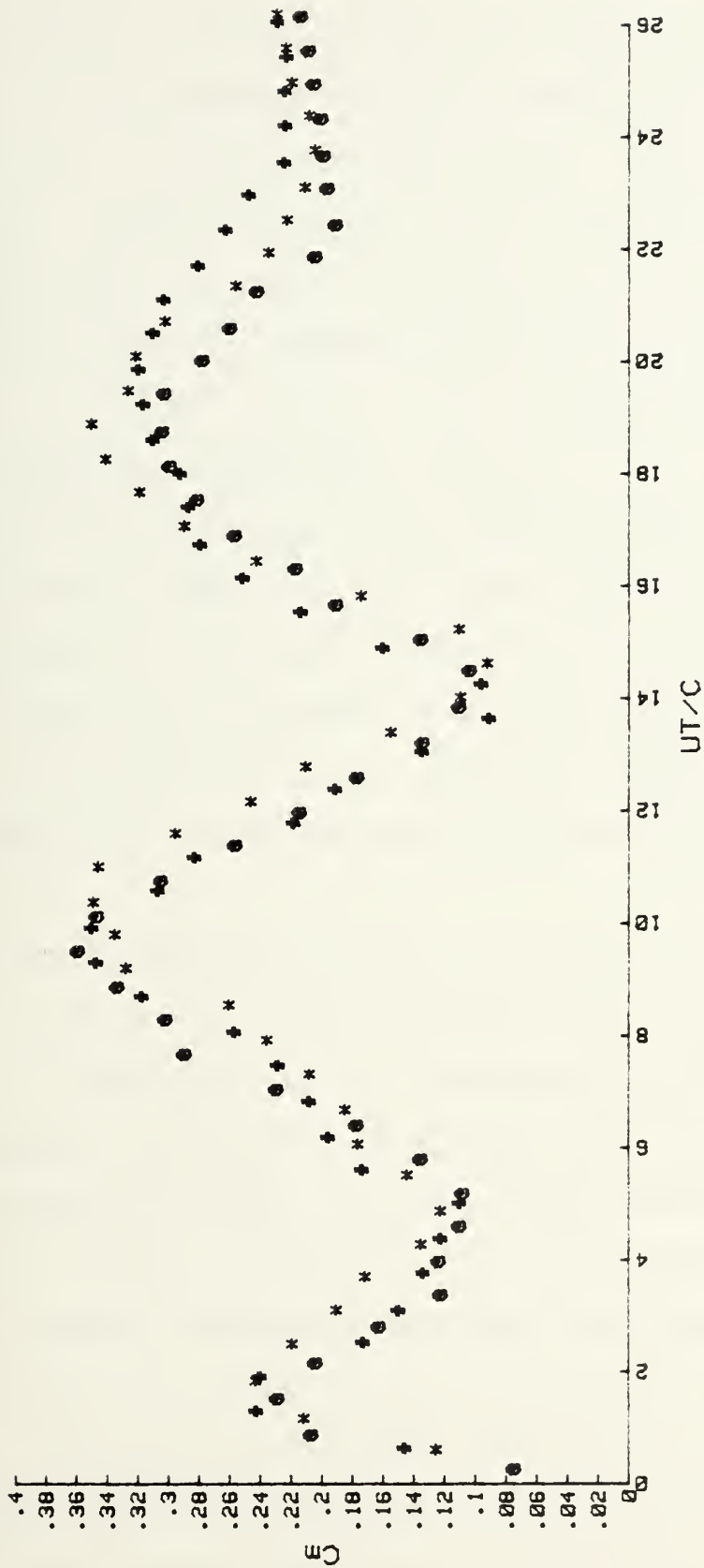


Figure 19. C_m vs. UT/C for the T-Shaped Body at 0 deg.

of the cylinder). On the T-shaped body geometric symmetry is unbalanced by the presence of a flat-topped protrusion from the top of the cylinder (see Figure 13b). Rapid accumulation of vorticity (referring to the case of the T-shaped body at zero degrees angle of attack) results in a large drag coefficient over a relatively long time period or relative displacement ($C_d = 2.2$ at $UT/C = 10.5$). The terminal value of C_d in Figure 17 appears to approach a value of 1.5. Comparison of Figures 17 and 18 shows that the shedding of the second vortex brings an abrupt reduction in the drag coefficient at $UT/C = 11$. The development of the third vortex from the protruding side of the cylinder again increases the drag coefficient to a relatively smaller second maximum. Subsequent shedding of vortices may be expected to result in smaller fluctuations in the drag coefficient.

For increasing values of positive angles of attack (as defined by Figure 13b), the asymptotic values of C_d are equal to about 1.9 until the angle is increased to ± 45 degrees where the asymptotic value (for UT/C greater than 25) drops to 1.4. (see Appendixes K through Y for the force-transfer coefficient data at other angles of attack). It is interesting to note that the secondary maximum of the drag curve persists for all positive angles of attack and that for positive angles greater than zero the drag force resulting from the development of the third vortex (at UT/C of about 14 to 15) is greater than the maximum reached during development of the first vortex.

Assymptotic values of the drag coefficient for negative angles of attack up to -45 degrees are all in the range of $C_d = 1.2$. For $\theta = -15$ degrees and below, the large drag overshoot of the secondary maximum (third vortex development) persists as it did for positive angles of rotation. This secondary maximum disappears for negative angles of attack greater than or equal to -20 degrees and, the drag coefficient characteristics closely approximate those of a circular cylinder.

For zero degrees angle of attack, the initial lift force direction is from the protrusion toward the axis of the cylinder (negative lift) during the development and shedding of the first vortex. This is a characteristic which is similarly exhibited by the D-shaped cylinder. This phenomenon is clarified through the study of the photographs depicting the evolution of the first two vortices (see Figures 20-26). Note that each photograph sequentially displays the formation and shedding of the vortices for corresponding relative displacements. As seen in Figures 20 through 24, the first vortex, emanating from the protrusion on the T-shaped body, grows rapidly and then the second vortex begins to grow on the opposite side of the cylinder. Gradually the second vortex moves toward the downstream stagnation point. The first lift maximum occurs at about $UT/C = 5$, which corresponds to Figure 22. This is the instant at which the first vortex is still attached to (and about to be separated from) its shear layer and, the second vortex has not yet grown sufficiently.

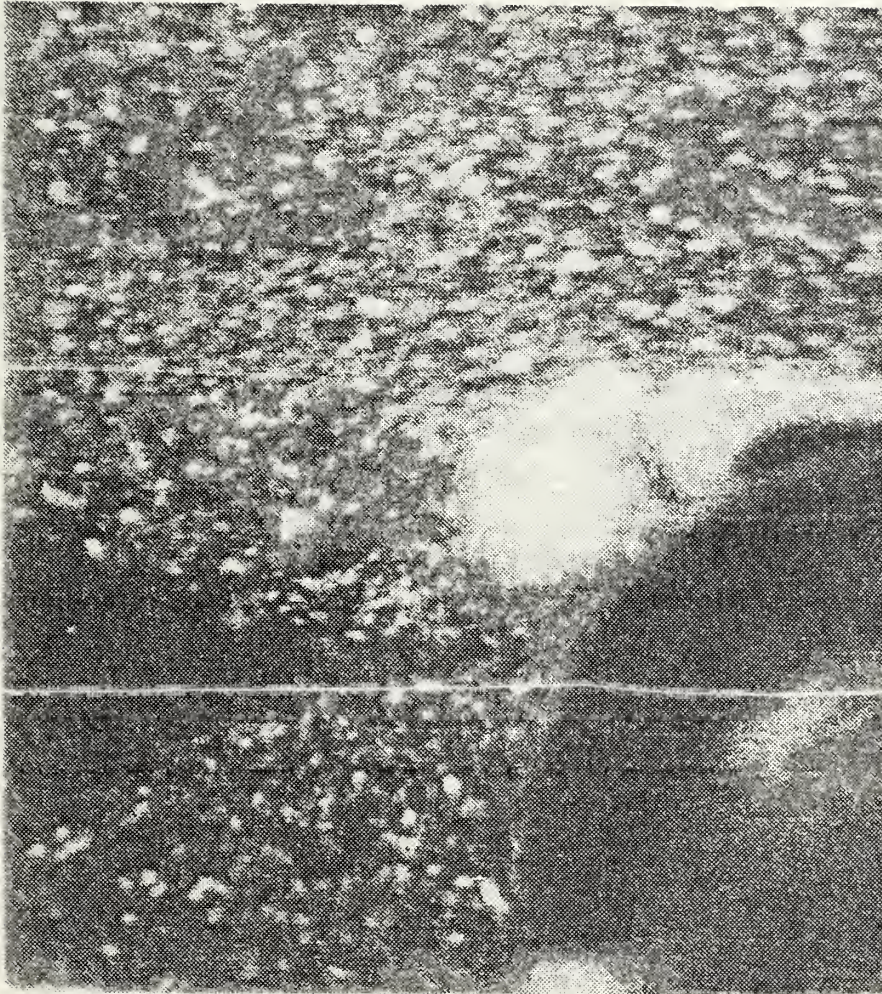


Figure 20. Flow About the T-Shaped Body at 0 deg. and $UT/C = 3.5$.

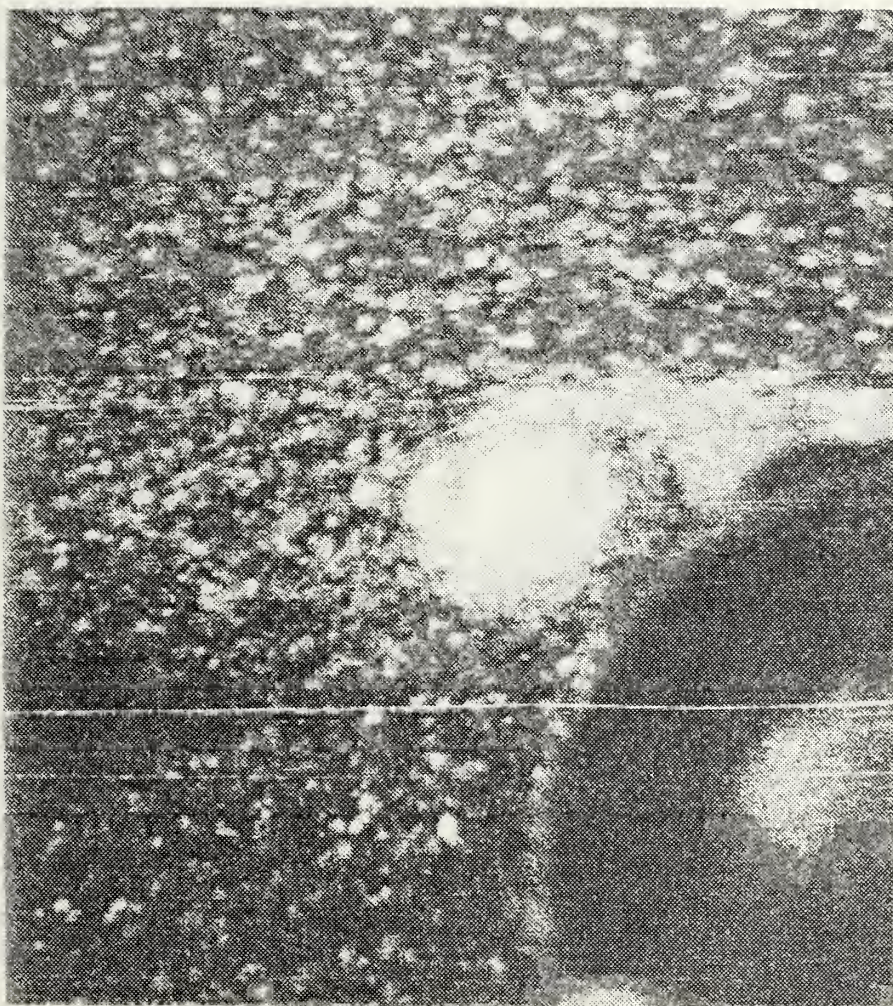


Figure 21. Flow About the T-Shaped Body at 0° deg. and $UT/C = 4.1$.

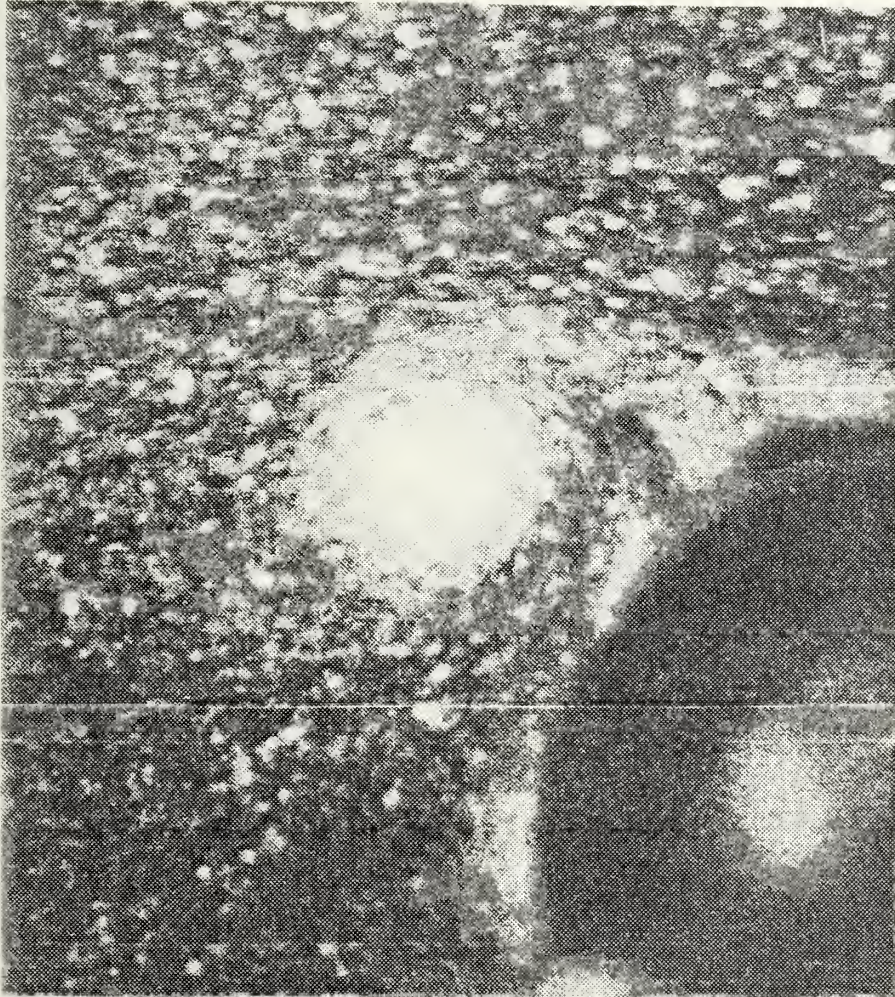


Figure 22. Flow About the T-Shaped Body at 0 deg. and $UT/C = 5.0$.

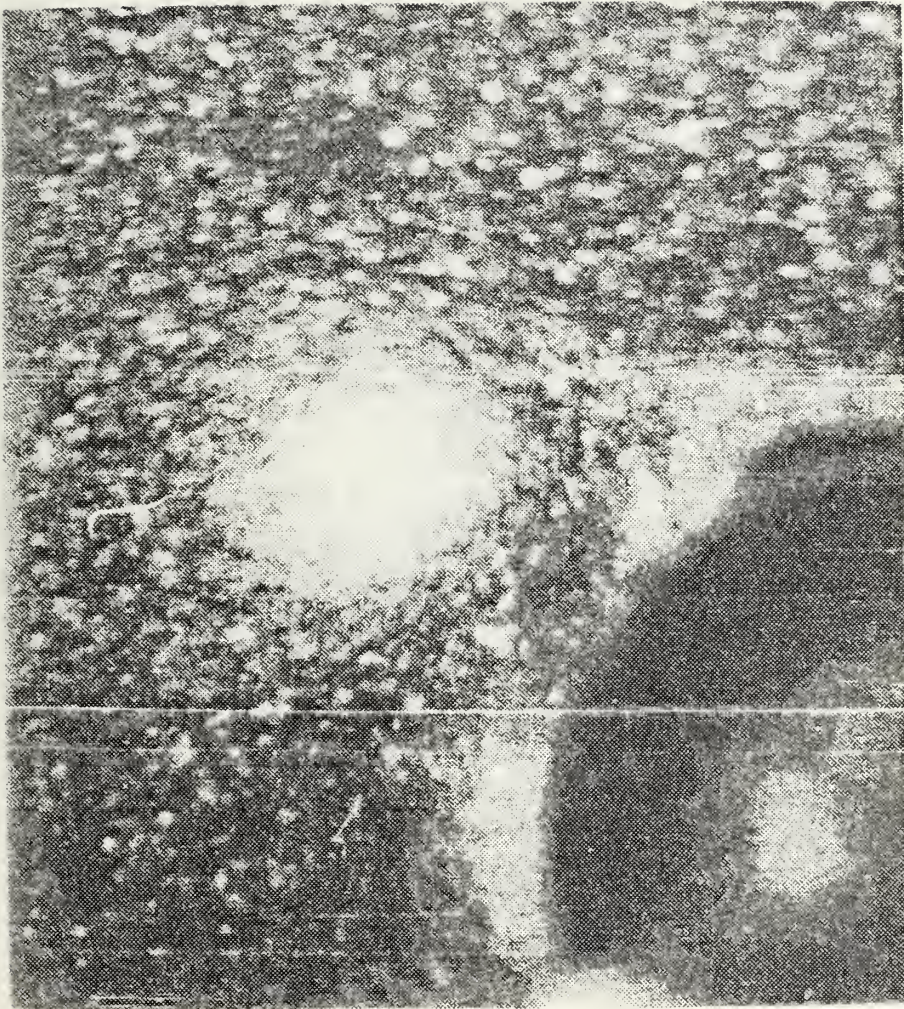


Figure 23. Flow About the T-Shaped Body at 0 deg. and $UT/C = 5.8$.

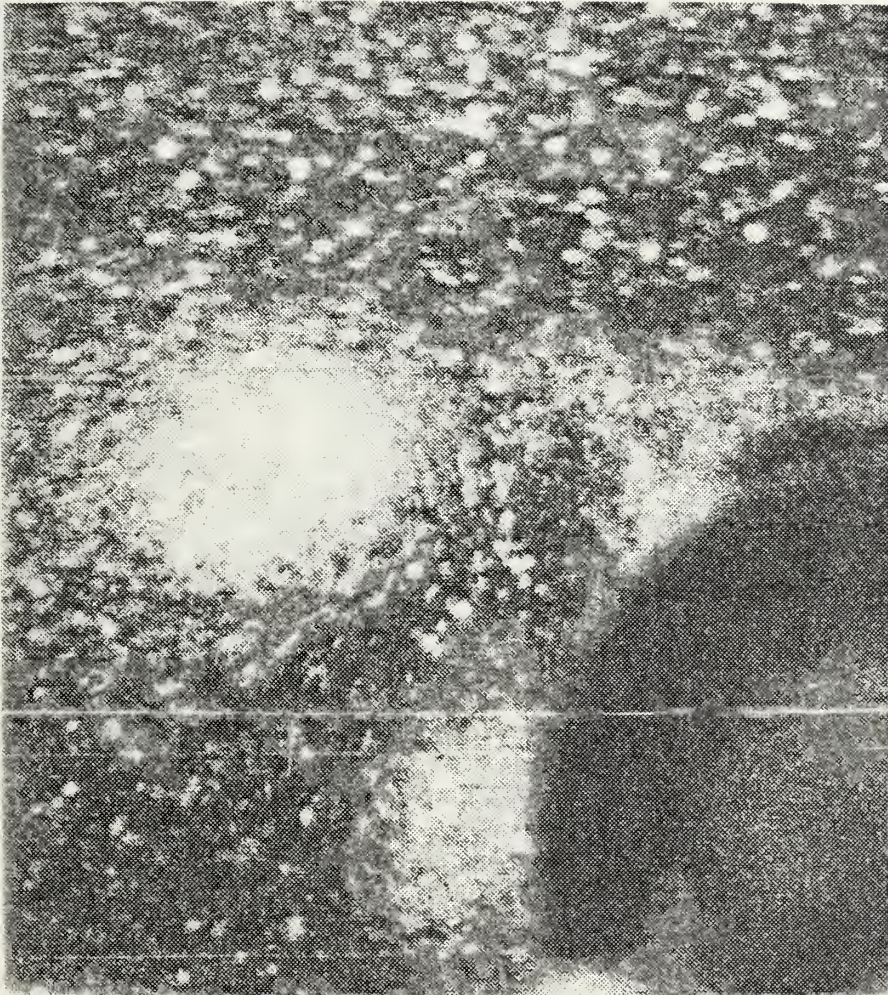


Figure 24. Flow About the T-Shaped Body at 0 deg. and $UT/C = 6.6$.

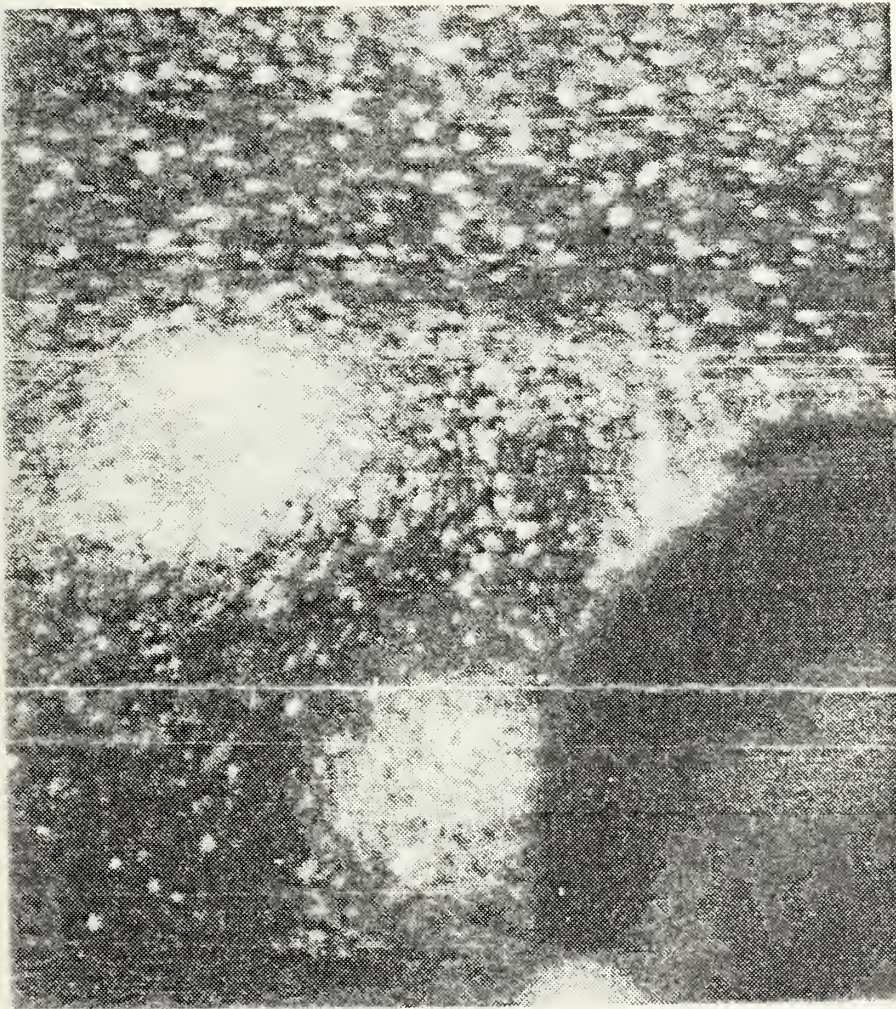


Figure 25. Flow About the T-Shaped Body at 8° deg. and $UT/C = 7.1$.

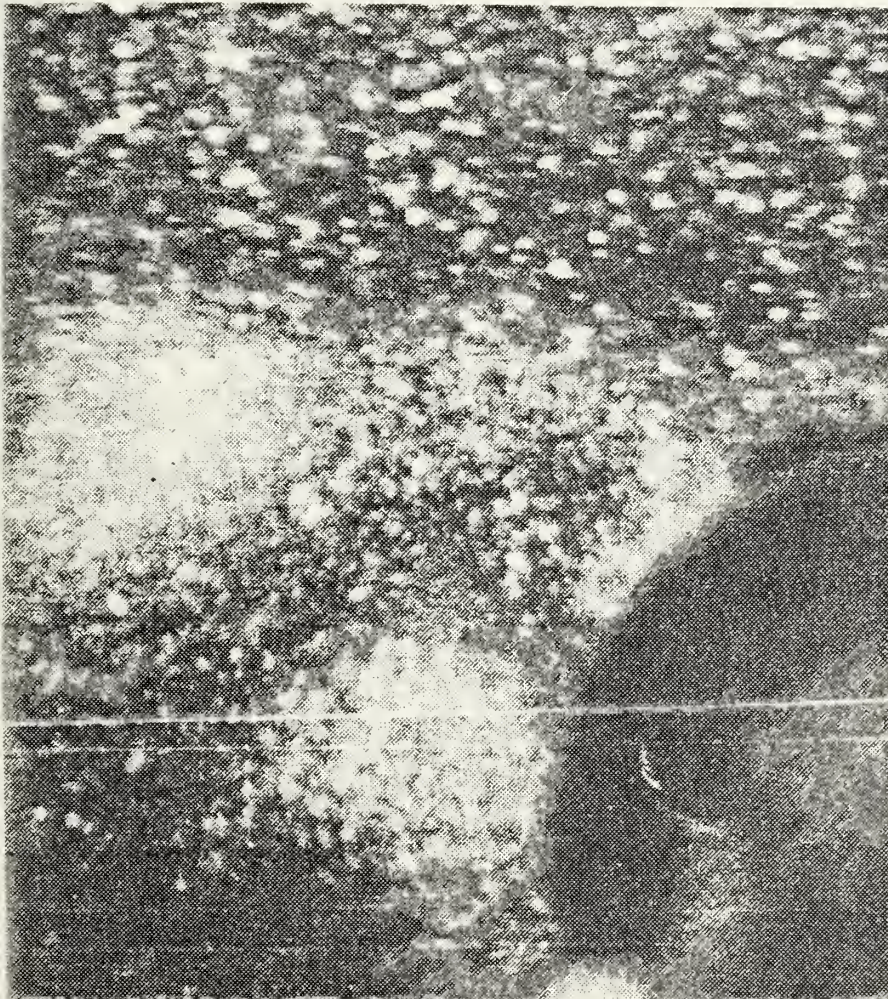


Figure 26. Flow About the T-Shaped Body at 0° and $UT/C = 7.8$.

In Figure 23, the first vortex begins to extend from the shear layer as the separation bubble of the second vortex (shed from the bottom of the body) has started to form. As time or the relative displacement of the fluid progresses, the second vortex grows and the lift coefficient passes through $C_l = 0$ at $UT/C = 8$, as seen in Figure 26 (where the first vortex is almost completely shed). At this point the circulation contributed by the developed vortices is nearly in equilibrium. Study of the subsequent frames of the motion pictures (not provided herein) has shown that the second vortex reaches full strength at $UT/C = 10.3$ and then the third vortex begins to develop from the protruding side of the body (where the first vortex was initiated).

As discussed in detail in connection with the D-shaped cylinder at zero degrees angle of attack, the growth and motion of the first vortex sets up a circulation about the body which is equal in magnitude and opposite in direction to that of the first vortex. This, in turn, results in a negative lift force (directed from the protrusion or the flat surface toward the axis of the body). The same result is evident for the T-shaped body at zero degrees angle of attack (see Figure 18) for the early stages of motion up to about $UT/C = 10$.

The foregoing statements regarding the initial lift characteristics were true for all angles of rotation of the D-shaped body. This does not imply that the same holds true for the T-shaped body. A detailed analysis of the lift

coefficient data presented herein provides a more complex lift force action with exceptions to the general characteristics previously discussed, which are dependent upon the angle of attack.

Unlike the D-shaped cylinder, analog data from the force transducer for the T-shaped body evidenced a brief but significant period of dynamic change of lift direction within the immediate moments of the beginning of fluid motion. This period is indicated by the first few data points for UT/C less than 1 in Figure 18. Referring to Figure 13b and the remaining lift coefficient plots in the appendixes, this brief perturbation in the lift data involves that time when the flow is attached and nearly irrotational. For positive angles of rotation less than +10 degrees and through all negative angles of attack, the initial lift force at the very earliest instants of fluid motion is positive. In these cases, the attached flow on the side of the protrusion must have larger velocities, hence lower pressures relative to the other side, and a small positive lift force of brief duration results. At positive angles of attack greater than +10 degrees, the initiation of fluid motion results in a small negative lift force for about the same relative displacement just described. Significant rotation of the protrusion past the vertical and closer to the approximate position of the downstream stagnation point apparently changes the initial velocity characteristics so that the higher velocity shifts to the bottom of the body and the brief duration of potential flow is characterized by negative lift.

While the presence of the protrusion on the body provides a consistent reference for the asymmetrical disturbance of the ambient flow, the direction and magnitude of the angle of attack can also change the lift characteristics occurring during the period when the first vortex is shed (relative displacements of UT/C between 1 and 12). For all positive angles of attack, the lift force, relative to the shedding of the first vortex, begins with negative values (force directed from the side of the protrusion toward the cylinder axis), indicating that separation on the side of the protrusion dominates the early stages of motion and the accumulation of vorticity. At negative angles of rotation, however, where the protrusion is rotated toward the flow, the reasons for strong, rapid generation of the first vortex on that side appear to be lessened and the lift force changes direction. This is most evident as the negative angle of rotation is increased beyond $\theta = -20$ degrees (see Appendixes W, X and Y). A careful examination of the information provided by the plots of drag, lift and moment coefficients for these angles gives some insight into the possible reasons for this change. A relatively steep increase of the drag coefficient is evident, in each case, which is directly related to the onset of asymmetry and separation. The lift force is negative for UT/C smaller than about 10 during which time the first vortex grows at the side of the protrusion. When the T-shaped cylinder was rotated from -20 to -25 degrees angle of attack, the lift force became positive

after separation. The change in lift direction during the early stages of motion was more evident when the angle was increased from -30 to -45 degrees. Without further investigation through the use of flow visualization it is not possible to confirm where separation first occurs. However, the effects of circulation applied to the flow about the body as a result of the shed vortices, as previously discussed, imply that a clockwise circulation is present when the angle of attack is about -25 degrees. This would lead to the tentative conclusion that the vortex shed from the bottom (round face) of the body is dominant at these angles of rotation for values of UT/C up to about 10 or 12.

Two additional comments regarding the foregoing description of the lift force characteristics of the T-shaped body with respect to the angle of rotation are appropriate. First, the initial positive lift force generated at the onset of fluid motion is very small and of such short duration that it would have negligible effects upon the motion of an underwater body, with this cross-section, undergoing an impulsive turn. The discussion regarding this particular experimental observation is presented here because it provides further experimental information relevant to the applications of potential flow theory. Second, the explanation of the shift in direction of the initial lift force as a function of increasing negative angles of attack is somewhat conjectural and requires further experimental investigation, with detailed flow visualization, for its substantiation.

Unlike the D-shaped body, the shedding of the vortices causes significant changes in the moment acting on the T-shaped body (see Figure 19). This is due primarily to the fact that the protrusion increases the available moment arm whereas, with the D-shaped body, the flat face decreases the moment arm. Consequently, underwater bodies with protrusions are more likely to undergo larger amplitudes of moment fluctuations as a result of an impulsive motion. This may give rise to greater stability problems. Representative tabulated data and plots of the force-transfer coefficients are presented in Appendixes K through Y.

Vortex shedding frequencies and the corresponding Strouhal numbers for the T-shaped body have been examined in a manner similar to that for the D-shaped body. It was found that $S = 0.21$ for zero degrees angle of attack. The Strouhal number for all other angles of rotation varied from 0.13 to 0.21. Decreasing Strouhal numbers, relative to the D-shaped body, are in conformity with the general rule that the Strouhal number decreases with the increasing degree of bluntness of the body.

A summary observation is in order regarding the description of the characteristics of the forces acting on and the vortices shedding from the D-shaped and T-shaped bodies. First, the asymmetry of the body relative to the direction of the flow removes the randomness from the position of the growth of the first vortex. In the case of a circular

cylinder the first vortex may form from either side, at random. The introduction of a geometric deformity to the otherwise axisymmetrical shape of the cylinder (such as a flat face or a protrusion) fixes the direction of the lift force and the position of the first vortex, in the early stages of the motion (as evidenced by the data and their repeatability for multiple runs). Second, an enlargement rather than a reduction of the otherwise circular cross section increases the moment and accentuates the fluctuations of the moment due to the vortex shedding. Furthermore, an increase in the bluffness of the body, by the addition of a protrusion, decreases the Strouhal number and hence the vortex shedding frequency. Lastly, the interaction of the body and the vortices in the early stages of the impulsive motion is such that a satisfactory analytical model requires both the representation of the shear layers by discrete vortices and, the evolution of the time-dependent boundary layer. Future analytical efforts should find the data presented herein useful for their evolution and calibration. Although the results presented here were obtained at nearly constant and relatively low subcritical Reynolds numbers, the observations and conclusions are not expected to differ significantly from those cited above even at much higher subcritical Reynolds numbers. One must add that the upper limit of the supercritical range is not known for non-circular bodies and can be determined only through painstakingly difficult experiments.

E. FLAT PLATE

The geometrical characteristics of the flat plate and the direction of the forces and moment acting on it are shown in Figure 13c. The Reynolds number for this body was kept at a nearly constant value of $Re = 2UB/\nu = 20750 \pm 260$. The results are discussed with respect to two representative angles of attack ($\theta = 90$ and 55 degrees), in order to accentuate the differences brought about by the shedding of the vortices on the normal force coefficient (C_n) and the position of the resultant force as defined by the normalized moment arm (X/B).

Figure 27 shows the normal force coefficient data for $\theta = 90$ degrees. As anticipated, the symmetric growth of the vortices causes a large normal force coefficient to develop during the early stages of the fluid motion. For UT/B larger than about 12, C_n reaches a nearly constant value of about 2.2. With the plate positioned normal to the ambient flow, the shedding of the vortices does not cause large fluctuations in C_n .

Figures 28 and 29 are the plots of the normal force coefficient for $\theta = 55$ degrees. The results shown in Figure 28 were obtained by summing vectorially the lift and drag forces. Data plotted in Figure 29 were obtained by measuring the normal force directly, as described in Chapter 3. A quick review of the two figures shows that they are nearly identical. Thus the indirect method (vector sum) of evaluating C_n is free from experimental errors within acceptable limits. This fact

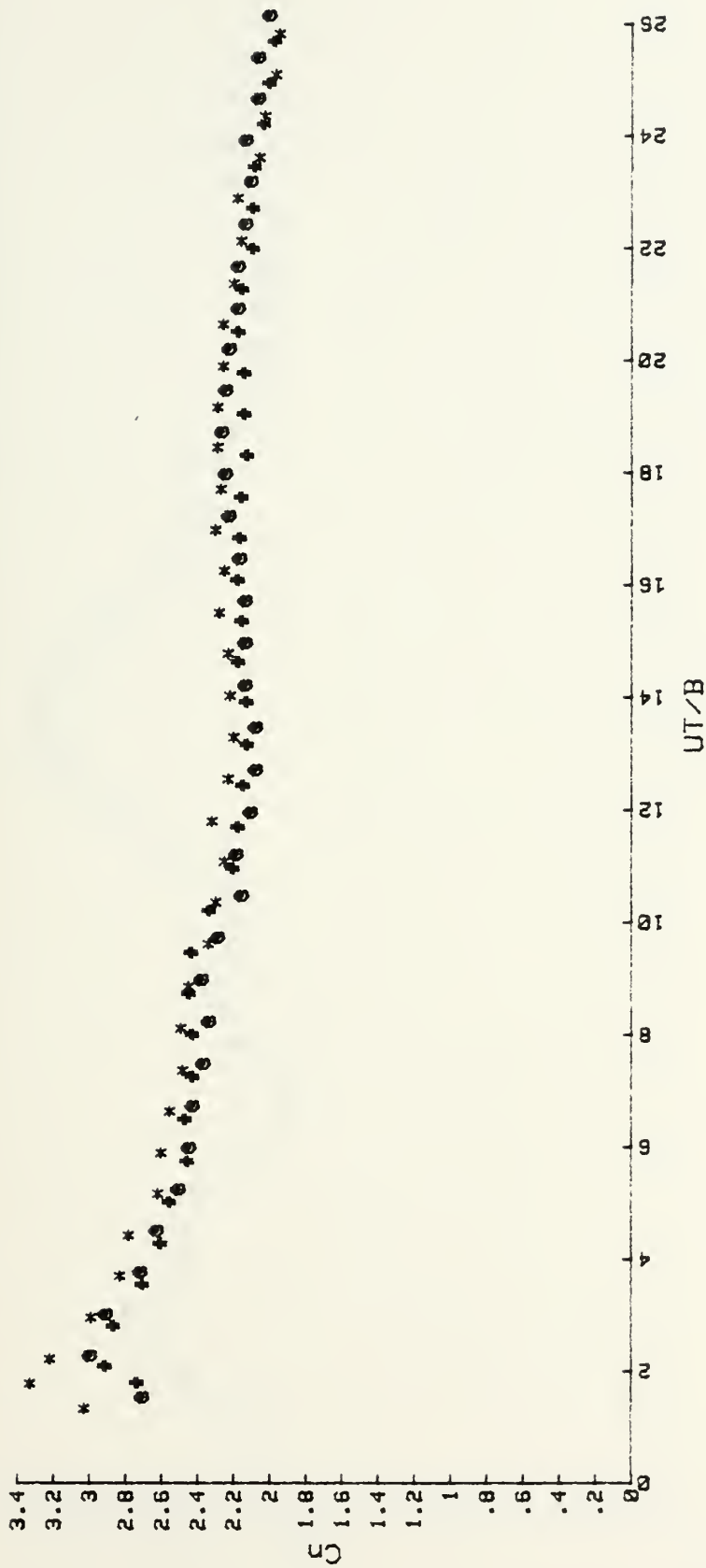


Figure 27. C_n vs. UT/B for the Flat Plate at 90° deg.

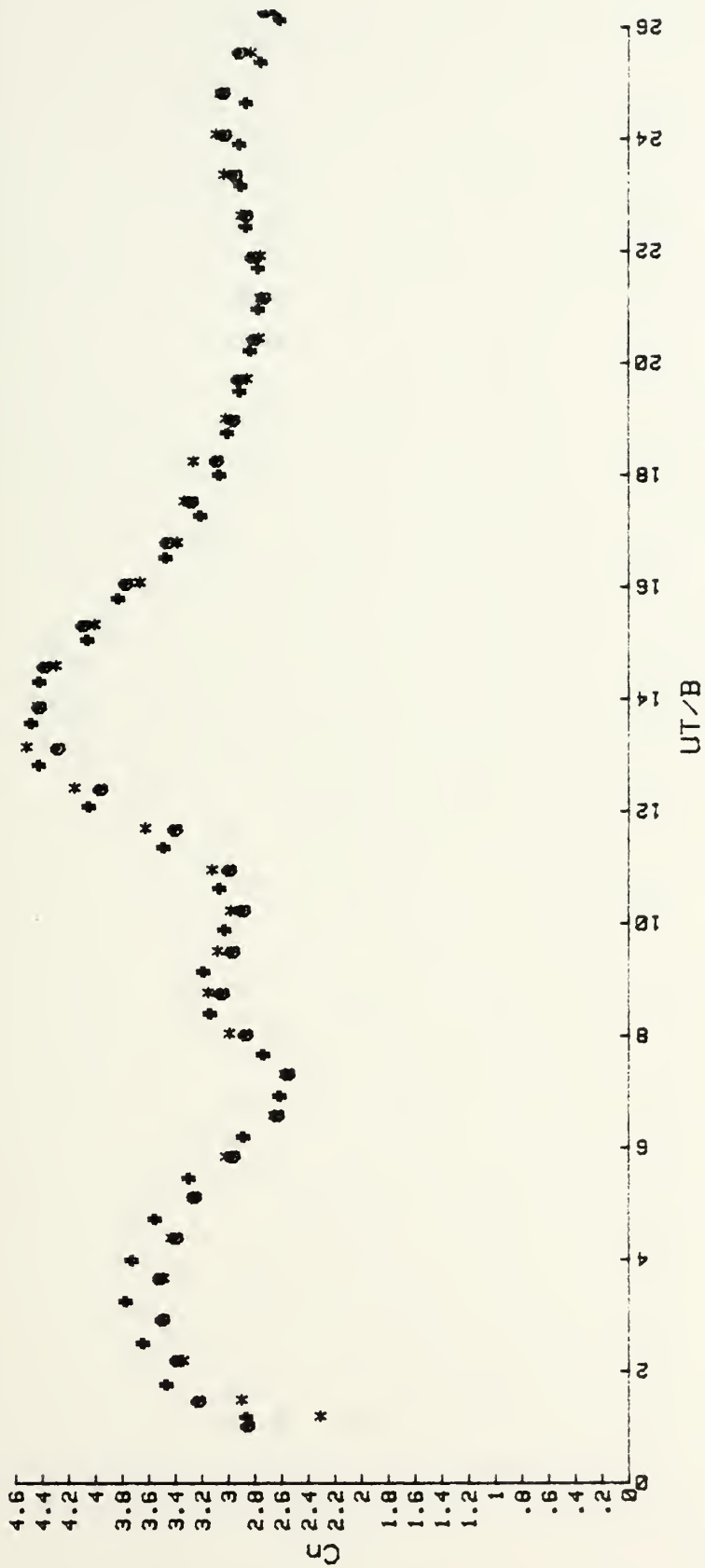


Figure 28. C_n vs. UT/B for the Flat Plate at 55 deg. (Indirect Measurement).

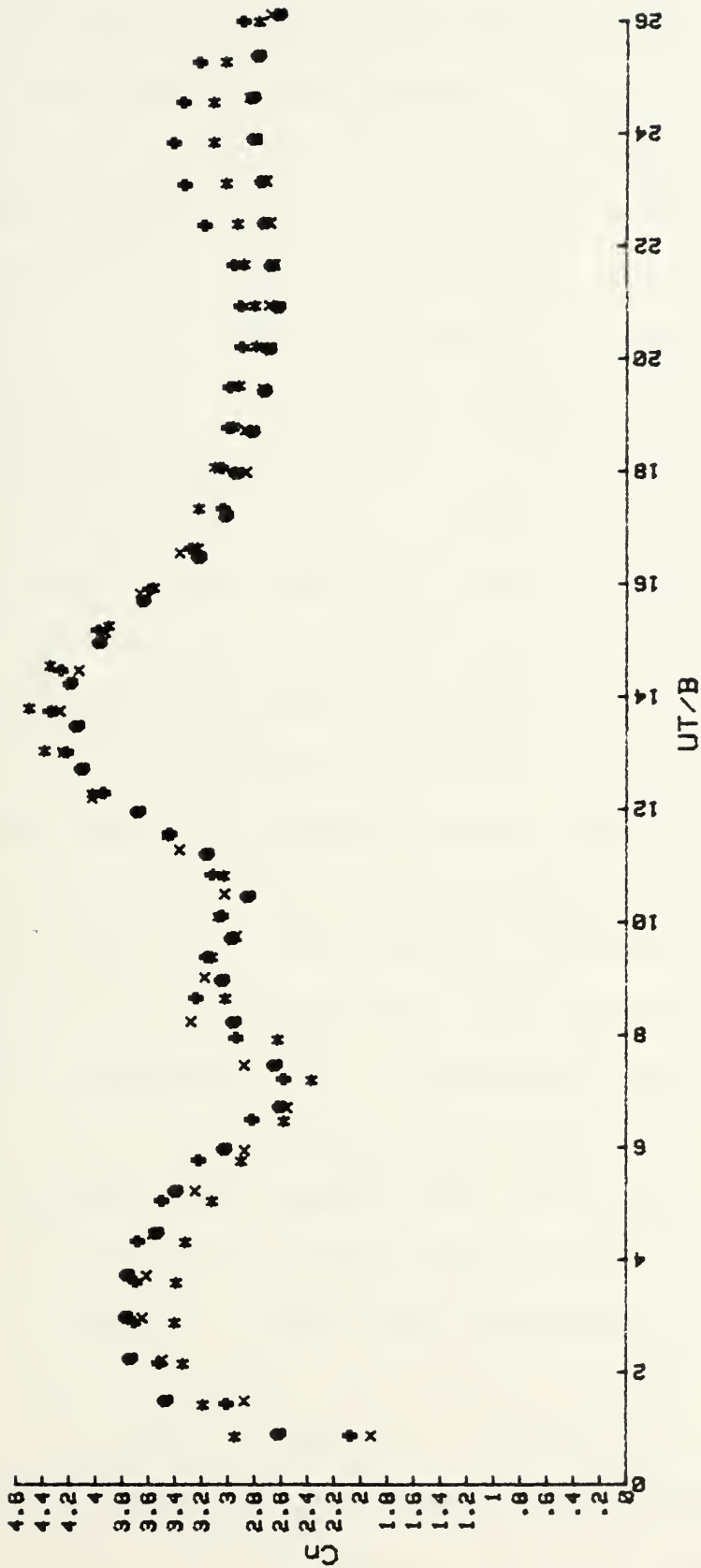


Figure 29. C_n vs. UT/B for the Flat Plate at 55 deg. (Direct Measurement, 4 runs).

is further evidenced by Figure 30 where the results of two representative runs for each method are superimposed.

Referring to Figure 30, at the early stages of fluid motion C_n increases dramatically to values never before noted in the relevant literature. The shedding of the first vortex at about $UT/B = 9$ (also refer to Figure 31) brings about an abrupt change in C_n . A subsequent maximum in the normal force coefficient occurs at $UT/B = 14$, as a result of the shedding of the second vortex. In fact, a flat plate at all angles of attack, other than those where the plate is nearly normal to the flow ($\theta = 80$ and 85 degrees, see Appendixes Z and AA) exhibited the largest C_n value at about $UT/B = 14$.

Within the range of relative displacement encountered during these tests, C_n exhibits smaller fluctuations and reaches nearly constant values for relative displacements greater than $UT/B = 14$. The results of discrete vortex analysis [54] for $\theta = 50$ degrees, show normal force coefficients with a maximum of 2.5. Contrasted with a value of 4, encountered at the corresponding angle of attack for these experiments (see Appendix AD), the present experimental evidence implies that the predictions of the discrete vortex model are in need of further fine-tuning and correction.

The normalized moment arm (X/B) for an angle of attack of 55 degrees is shown in Figure 31. Clearly the fluctuations of the moment arm are directly related to the shedding of the vortices. Generally, the maximum absolute change in the

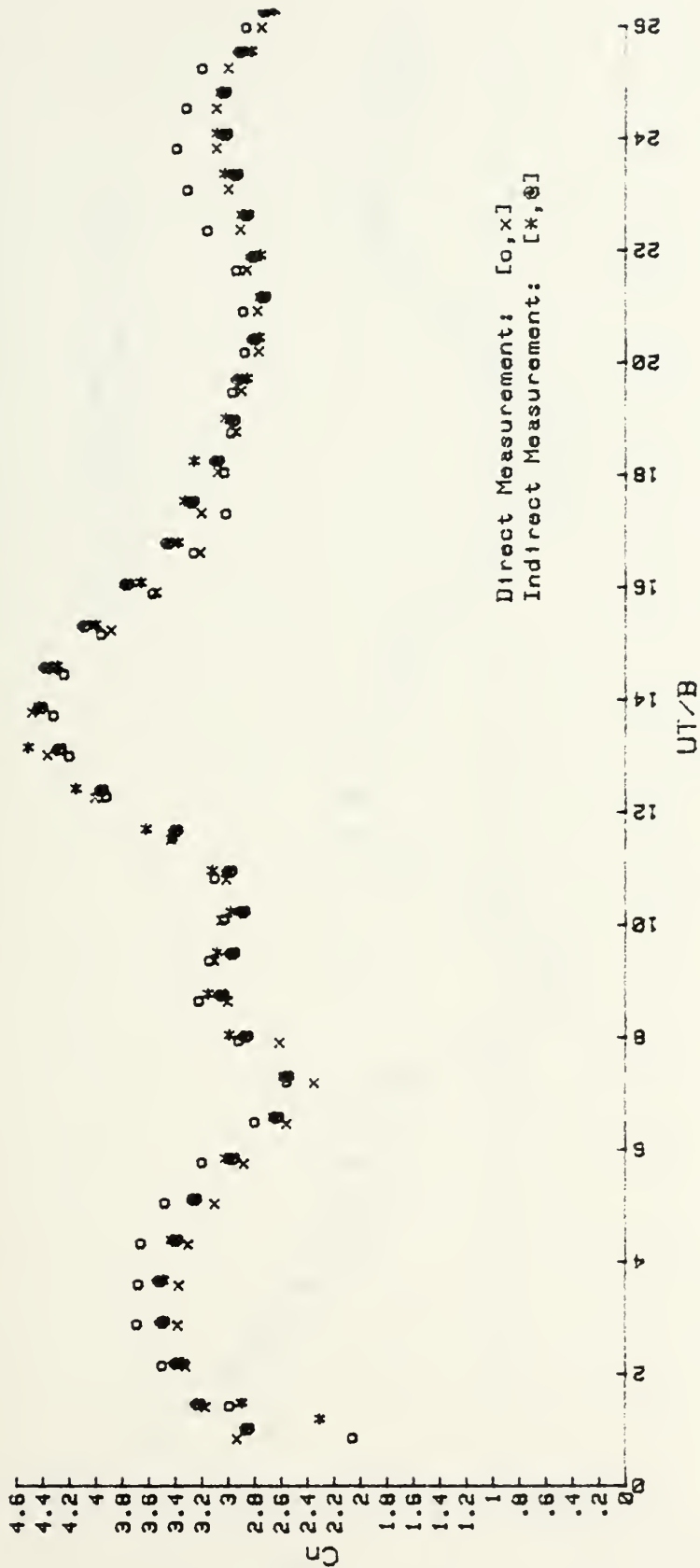


Figure 30. Cn vs. UT/B for the Flat Plate at 55 deg. (Comparison of Indirect and Direct Force Measurement).

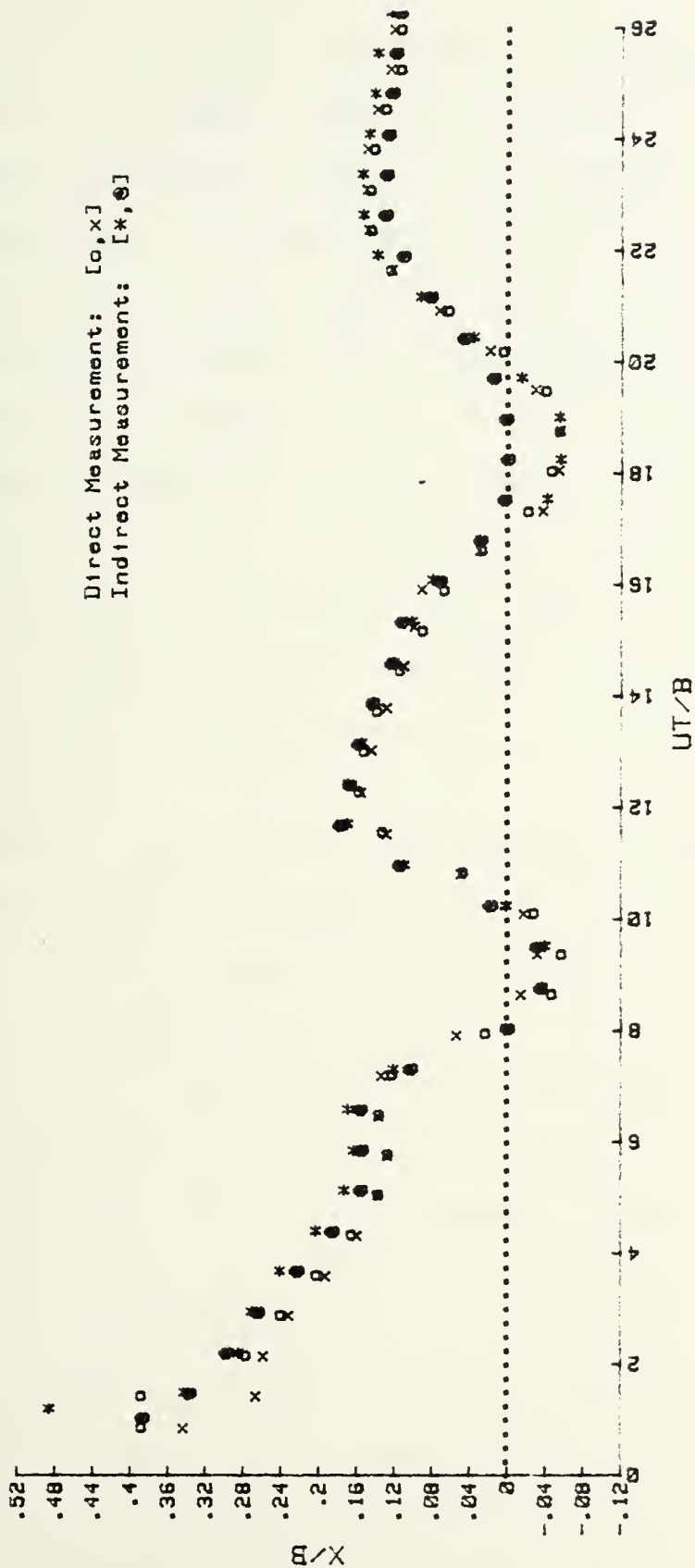


Figure 31. X/B vs. UT/B for the Flat Plate at 55 deg.

moment arm decreases with a decrease in the angle of attack. When the plate is nearly normal to the flow ($\theta = 85$ degrees or more) the moment arm is reduced and remains closer to the plate centerline. As evidenced by the data presented in Appendix Z, at very large angles of attack, the normalized moment arm and the normal force coefficient are noticeably more sensitive to changes in the ambient flow conditions than at smaller angles of attack. When the angle of attack is reduced to less than 40 degrees the normalized moment arm remains positive throughout the range of relative displacement encountered herein and there is a significant reduction in the fluctuations of X/B in response to the vortex-shedding.

The analog traces of the lift force and moment and the plots of the normalized moment arm were sufficient to identify the vortex shedding times and to estimate the Strouhal number, $S = 2fB/U$, for most angles of attack. For $\theta = 55$ degrees (Figure 31) the Strouhal number was about 0.22. The Strouhal number ranged from 0.14 at $\theta = 85$ degrees to 0.25 at $\theta = 40$ degrees. Clearly, the Strouhal number decreases as the bluffness of the body is increased, by increasing the angle of attack. It is also important to note that the fluctuations in moment acting on the flat plate are much more dramatic than for either the D- or T-shaped bodies. This is partly due to the fact that the vortex strength for a flat plate is larger and partly because the sharp edges of the plate

fix the separation points and increase the spanwise coherence along the plate. For bodies without sharp edges, the separation points are mobile and there are often significant phase shifts in pressure at the corresponding points along the plate. This leads to a reduction in the spanwise coherence of the vortices and hence to a reduction in lift forces.

F. RECAPITULATORY SYNTHESIS

The hydrodynamical behavior of the three bodies under consideration may be compared relative to each other, relative to that of a circular cylinder and, relative to analytical or numerical results.

An extensive literature search and the perusal of the most relevant works have shown that the analytical or numerical methods are not yet in a position to describe the behavior of the large scale motion in the wake of bluff bodies subjected impulsively started flow. Solutions based on the Navier-Stokes equations are limited to extremely small Reynolds numbers and to relatively small displacements. Solutions based on the discrete vortex method, or on its variations, suffer from the problems associated with the introduction of the nascent vortices, vortex excursions, shear-layer instabilities, inaccurate representation of viscous and turbulent dissipation of vorticity, and numerous other numerical instabilities. The assumption of an inviscid fluid imposes an unrealistically large number of

conditions on the simulation of the behavior of a viscous flow. It does not, therefore, appear that the numerical methods applied either directly or indirectly (through the use of one or more conformal transformations) are in a position to predict the force, moment and vortex-shedding characteristics of bluff bodies in time-dependent flows even for the most manageable impulsively-started flow. Experiments must be carried out to delineate the most important features of such flows partly for practical purposes and partly, and perhaps more importantly, for the purpose of providing physical insight toward the development of analytical methods.

Of the three bodies, the T-shaped body had mobile separation points, the flat plate had clearly fixed separation points, and the D-shaped body had at times only mobile separation points and at times both mobile and fixed separations, depending on the angle of attack. In any case, however, the D-shaped cylinder had at least two and as much as three separation points. It was for the purposes of accentuating the effects of these three types of separations that these three particular body shapes were chosen.

The results have shown that the fixing of the separation point has numerous and yet incalculable consequences. The vortex strengths are larger (as evidenced by the magnitude of the force fluctuations), the spanwise coherence is increased out of necessity, and the Strouhal number is reduced partly because of the increase of the strength of the vortices

and partly because of the bluntness of the body. On the other hand, a body with mobile separation points, with a preferred position of initial separation (T-shaped cylinder), exhibits relatively smaller drag overshoots and fluctuations of forces and moment. The magnitude of the moment obviously depends on the amount of protrusion relative to the base circle of the cylinder shapes. The protrusion also fixes the direction of the lift force in the initial stages of the motion. This then is the basic difference between the impulsive flow on a circular cylinder and on a T-shaped cylinder, both of which have mobile separation points. On a circular cylinder the side from which the first vortex sheds is random and determined primarily by small disturbances in the ambient flow. Furthermore, the circular cylinder experiences little or no moment. On a geometrically deformed cross section, as in the case of the T-shaped body, the randomness is removed from the shedding of the first vortex, the direction of the lift is fixed and a moment is created. At large angles of attack (e.g., -25 degrees) the T-shaped body may exhibit three mobile separation points. This may lead to a change in the direction of the initial lift force, but still does not introduce randomness into the evolution of the lift force.

For a body with mixed separation points, as in the case of the D-shaped cylinder, the angle of attack plays a relatively more important role in determining the flow characteristics.

Once again the position of the first vortex and the direction of the initial lift force are fixed on the side of the body where the separation is fixed. A closer examination of this and other bodies shows that any geometrical deformity which precipitates the occurrence of separation necessarily leads to a preferential shedding of the first vortex and to the determination of all other features of the flow. On a circular cylinder the separation does not start immediately, but at a fixed perturbation in the otherwise smooth circular cross-section, separation of the flow takes place immediately. Consequently, any physical disturbance imposed on the body, be it a sharp edge, a rounded protrusion or a flat surface, precipitates separation either relative to a circular cylinder or relative to the undisturbed side of the body, and fixes the rest of the history of the motion by removing any degree of randomness.

V. CONCLUSIONS

The experimental investigations of the impulsively-started flow about a D-shaped cylinder, a T-shaped cylinder and a flat plate resulted in the following conclusions:

1. Shedding of the first two or three vortices from the D- and T-shaped cylinders produced a significant drag overshoot of as much as fifty percent.
2. Drag coefficients for the D-shaped cylinder asymptotically approached values in the range of 0.8 to 1.4 for UT/C greater than about 20. For the T-shaped body, asymptotic values of C_d ranged from 1.4 to 1.9. There were no significant fluctuations in the drag coefficients for these bodies at relative displacements beyond $UT/C = 20$.
3. Higher C_d values occur, for the D-shaped body, at negative angles of rotation.
4. For the D-shaped cylinder the lift force direction is negative during the early stages of motion, for all angles of attack investigated here.
5. For the T-shaped body, at most angles of attack, C_d reached a secondary maximum due to the development and subsequent shedding of the third vortex. This secondary maximum is larger than that occurring during the earlier stages of the motion.

6. The lift force direction during the early stages of impulsive motion about the T-shaped body is dependent upon the angle of rotation relative to the ambient flow.

7. Asymmetry of a body relative to the direction of the impulsive flow removes the randomness from the position of initiation of the first vortex and fixes the initial direction of the lift force acting on the body.

8. Asymmetric enlargement of an otherwise circular cross-section increases the magnitude of the moment experienced by the body and accentuates the fluctuations in that moment. Moment fluctuations for the flat plate are more dramatic than for either of the cylindrical bodies.

9. The maximum normal force coefficients for the flat plate are significantly greater in magnitude, and in the amplitude of fluctuations, than those predicted by the discrete vortex model.

10. Strouhal numbers ranged from 0.19 to 0.24 for the D-shaped cylinder, from 0.13 to 0.21 for the T-shaped cylinder, and from 0.14 to 0.25 for the flat plate.

11. There are, at present, no reliable analytical techniques which accurately predict the behavior of the impulsive flow about bluff bodies. Those available have proven to be deficient in one or more ways. Experimental measurements and observations still form the basis for a comprehensive understanding of the behavior of impulsively-started flow about bluff bodies.

VI. RECOMMENDATIONS FOR FURTHER RESEARCH

It is recommended that additional research on impulsively-started flow about bluff bodies be conducted in the following area:

1. Impulsive flow tests of the three bodies presented herein should be conducted at significantly different, and preferably higher, Reynolds numbers.

2. Attempts should be made to determine the velocities and vortex strength either through visualization or through the use of a laser velocimeter.

3. The pressure distribution about the circumference of the bodies should be measured and evaluated as a function of time from the start of the fluid motion.

4. Extensive flow visualization photographs of the tests on these bodies should be conducted with attempts to monitor the flow for UT/C values of 100 or more. Accurate correlation of the time-sequence of the photographs with the analog traces of the forces and moments should be an important part of this effort.

5. The present results should be extended to larger UT/C values (in connection with the recommendation above) in order to verify the asymptotic behavior of the drag coefficients and to calculate the Strouhal numbers for larger times.

6. The present study should be extended to different cross-sections. Rectangular cylinders present the possibility of multiple separations and reattachments of the flow.

7. The T-shaped body should be tested with its axis at different angles of pitch to determine the effects of the body vortices and the interaction of all vortices shed when the body's axis is inclined other than normal to the flow.

8. These investigations should be expanded to cover general three-dimensional bluff bodies, on which there is very little or no research, save for the sphere.

9. The effect of ambient flow turbulence on the impulsively-started flow should be investigated in order to understand the initiation of vortex asymmetry on axisymmetric bodies.

10. The foregoing investigations should be extended to relatively more complex time-dependent flows where the velocity varies as a known function of time or displacement in order to understand the effect of the local acceleration of the ambient flow on the vortex development and on the time-dependent resistance.

LIST OF REFERENCES

1. Sedov, L. I., Two-Dimensional Problems in Hydrodynamics and Aerodynamics. Translated from Russian and edited by C. K. Chu et al., Interscience Publishers, 1965.
2. Birkhoff, G. and Zarantonello, E. H., Jets, Wakes and Cavities, Academic Press, 1957.
3. Sarpkaya, T. and Shoaff, R. L., "Inviscid Model of Two-Dimensional Vortex Shedding by a Circular Cylinder," AIAA Journal, Vol. 17, No. 11, pp.1193-1200, 1979.
4. Schlichting, H., Boundary-Layer Theory, McGraw-Hill Book Co. 1968.
5. Rott, N., Theory of Laminar Flows, F. K. Moore (ed.), Princeton University Press, pp. 395-438, 1964.
6. Blasius, H., "Grenzschichter in Flussigkeiten mit Kleiner Reibung," Z. Math u. Phys., Vol. 56, pp. 1-6, 1908.
7. Goldstein, S. and Rosenhead, L., "Boundary Layer Growth," Proceedings of the Cambridge Philosophical Society, Vol. 32, pp. 392-401, 1936.
8. Görtler, H., "Verdrängungswirkung der Laminaren Grenzschicht und Druckwiderstand," Ing.-Arch., Vol. 14, pp. 286-305, 1944.
9. Görtler, H., "Grenzschichtentstehung an Zylindern bei Anfahrt aus der Ruhe," Arch. d. Math., Vol. 1, pp. 138-147, 1948.
10. Schuh, H., "Calculation of Unsteady Boundary Layers in Two-Dimensional Laminar Flow," Zeitschrift für Flugwissenschaften, Vol. 1, pp. 122-131, 1953.
11. Watson, E. J., "Boundary Layer Growth," Proceedings of the Royal Society of London, Vol. 231, pp. 104-116, 1955.
12. Wundt, H., "Wachstum der Laminaren Grenzschicht an schrag angestromten Zylindren bei Anfahrt aus der Ruhe," Ing.-Arch., Vol. 23, pp. 212-230, 1955.
13. Payne, R. B., "Calculations of Unsteady Viscous Flow Past a Circular Cylinder," Journal of Fluid Mechanics, Vol. 4, pp. 81-87, 1955.

14. Hirota, I. and Miyakoda, K., "Numerical Solution of Karman Vortex Street Behind a Circular Cylinder," J. Met. Soc. Japan, Vol. 43, p. 30, 1965.
15. Kawaguti, M. and Jain, P. C., "Numerical Study of a Viscous Fluid Flow Past a Circular Cylinder," Journal of the Physical Society of Japan, Vol. 21, No. 10, p. 2055, 1966.
16. Wang, C. Y., "The Flow Past a Circular Cylinder which is Started Impulsively From Rest," Journal of Mathematical Physics, Vol. 46, p. 195, 1967.
17. Jain, P. C. and Rao, K. S., "Numerical Solution of Unsteady Viscous Incompressible Fluid Flow Past a Circular Cylinder," Physics of Fluids Supplement, Vol. 12, pp. 11-57, 1969.
18. Rimon, Y., "Numerical Solution of the Incompressible Time-Dependent Viscous Flow Past a Thin Oblate Spheroid," Physics of Fluids Supplement, Vol. 12, p. II-65, 1969.
19. Son, J. S. and Hanratty, T. H., "Numerical Solution for the Flow Around a Cylinder at Reynolds Numbers of 40, 200 and 500," Journal of Fluid Mechanics, Vol. 35, pp. 369-375, 1969.
20. Thoman, D. C. and Szewczyk, A. A., "Time-Dependent Viscous Flow Over a Circular Cylinder," Physics of Fluids Supplement, Vol. 12, pp. II-76 - II-80, 1969.
21. Honji, H., "Starting Flows Past Spheres and Elliptic Cylinders," Rep. Res. Inst. Appl. Mech., Kyushu University, Vol. 19, p. 271, 1972.
22. Mehta, U. B. and Lavan Z., "Starting Vortex, Separation Bubbles and Stall - A Numerical Study of Laminar Unsteady Flow Around an Airfoil," AFOSR Technical Report TR-73-0640, 1972.
23. Collins, W. M. and Dennis, S. C. R., "The Initial Flow Past an Impulsively Started Circular Cylinder," Quarterly Journal Mech. Appl. Math., Vol. 26, pp. 53-75, 1973.
24. Collins, W. M. and Dennis, S. C. R., "Flow Past an Impulsively-Started Circular Cylinder," Journal of Fluid Mechanics, Vol. 60, pp. 105-110, 1973.
25. Wu, Y. T. and Thompson, J. F., "Numerical Solution of Time-Dependent Incompressible Navier-Stokes Equations Using an Integro-Differential Formulation," Computers and Fluids, Vol. 1, p. 197, 1973.

26. Lugt, H. J. and Haussling, H. J., "Laminar Flow Past an Abruptly Accelerated Elliptic Cylinder at 45 Degrees Incidence," Journal of Fluid Mechanics, Vol. 65, pt. 4, pp. 711-734, 1974.
27. Telionis, D. P. and Tsahalis, D. T., "Unsteady Laminar Separation over a Cylinder Started Impulsively From Rest," Acta Astronautica, Vol. I, p. 1487, 1974.
28. Bar-lev, M. and Yang, H. T., "Initial Flow Field over an Impulsively-Started Circular Cylinder," Journal of Fluid Mechanics, Vol. 72, pp. 625-647, 1975.
29. Panniker, P. K. G. and Lavan, Z., "Flow Past Impulsively-Started Bodies Using Green's Functions," Journal of Computational Physics, Vol. 18, pp. 46-52, 1975.
30. Cebeci, T., "The Laminar Boundary Layer on a Circular Cylinder Started Impulsively from Rest," Journal of Computational Physics, Vol. 31, pp. 153-172, 1979.
31. Tuann, S. Y. and Olson, M. D., "Numerical Studies of the Flow Around a Circular Cylinder by the Finite Element Method," Structural Research Series Report No. 16, ISSN 0318-3378, University of British Columbia, Vancouver, B. C., Canada, 1976.
32. Schwabe, M., "Über Druchermittlung in der Instationären ebenen Stromung," Ing.-Arch., Vol. 6, pp. 34-50, 1935.
(Also, see NACA TM 1039)
33. Taneda, S. and Honji, H., "Unsteady Flow Past a Flat Plate Normal to the Direction of Motion," Journal of the Physical Society of Japan, Vol. 30, No. 1, pp. 262-272, 1971.
34. Taneda, S., "The Development of the Lift of an Impulsively-Started Elliptic Cylinder at Incidence," Journal of the Physical Society of Japan, Vol. 33, No. 6, pp. 1706-1711, 1972.
35. Contanceau, M. and Bouard, R., "Experimental Determination of the Main Features of the Viscous Flow in the Wake of a Circular Cylinder in Uniform Translation. Part I: Steady Flow; Part II: Unsteady Flow," Journal of Fluid Mechanics, Vol. 79, pt. 2, pp. 231-256 and 257-272, 1977.
36. Sarpkaya, T., "An Analytical Study of Separated Flow About Circular Cylinders," Journal of Basic Engineering, Vol. 90, Series D, No. 4, pp. 511-520, 1968.

37. Sarpkaya, T., "Impulsive Flow About a Circular Cylinder," Naval Postgraduate School Technical Report No. NPS-69SL78-008, Monterey, California, 1978.
38. Bingham, H. H., Werner, D. K. and Griffith, W., "The Cylinder and Semi-Cylinder in Subsonic Flow," Princeton University Department of Physics Technical Report 11-13, 1952.
39. Friberg, E. G., "Measurements of Vortex Separation, Part I: Two-Dimensional Circular and Elliptic Bodies," MIT Aerophysics Lab Technical Report 114, 1965.
40. Asher, J. A. and Dosanjh, D. S., "An Experimental Investigation of the Formation and Flow Characteristics of an Impulsively-Generated Vortex Street," Journal of Basic Engineering, Vol. 90, pp. 596-606, 1968.
41. Sarpkaya, T. and Shoaff, R. L., "A Discrete Vortex Analysis of Flow About Stationary and Transverse Oscillating Circular Cylinders," Naval Postgraduate School Technical Report No. NPS-69 SL79011, Monterey, California, 1979.
42. Roos, F. W. and Willmarth, W. W., "Some Experimental Results on Sphere and Disk Drag," AIAA Journal, Vol. 9, No. 2, pp. 285-291, 1971.
43. Allen H. J. and Perkins, E. W., "A Study of Effects of Viscosity on Flow over Slender Inclined Bodies of Revolution," NACA Technical Report No. 1048, 1951.
44. Thomson, K. D. and Morrison, D. F., "The Spacing, Position and Strength of Vortices in the Wake of Slender Cylindrical Bodies at Large Incidence," Australian Dept. of Supply, WRE, HSA 25, 1969.
45. Thomson, K. D. and Morrison, D. F., "The Spacing, Position and Strength of Vortices in the Wake of Slender Cylindrical Bodies at Large Incidence," Journal of Fluid Mechanics, Vol. 50, pt. 4, pp. 751-783, 1971.
46. Thomson, K. D., "The Estimation of Viscous Normal Force, Pitching Moment Side Force and Yaw Moment on Bodies of Revolution of Incidences Up to 90 Degrees," WRE Rep. 782 (WR & D), Australian Defense Scientific Service, Melbourne, Australia, 1972.
47. Bostock, B. R., Slender Bodies of Revolution at Incidence Ph.D. Thesis, University of Cambridge, 1972.

48. Lamont, P. J., The Out-of Plane Force on an Ogive-Nosed Cylinder at Large Angles of Inclination to a Uniform Stream, Ph.D. Thesis, University of Bristol, England, 1973.
49. Lamont, D. J. and Hundt, B. L., "Pressure and Force Distribution on a Sharp-Nosed Circular Cylinder at Large Angles of Inclination to a Uniform Stream," Journal of Fluid Mechanics, Vol. 76, pt. 3, pp. 519-559, 1976.
50. Wardlaw, A. D., Jr., "Prediction of Yawing Force at High Angles of Attack," AIAA Journal, Vol. 12, No. 8, pp. 1142-1144, 1974.
51. Ericsson, L. E. and Reding, J. P., "Vortex-Induced Asymmetric Loads on Slender Vehicles," Lockheed Missiles and Space Company, Inc., Report No. LMSC-D630807, 1979.
52. Sarpkaya, T. and Isaacson, M., Mechanics of Wave Forces on Offshore Structures, Van Nostrand Reinhold, New York, 1981.
53. Fage, A. and Johansen, F. C., "On the Flow of Air Behind an Inclined Flat Plate of Infinite Span," Proceedings of the Royal Society, London, Series A, p. 170, 1927.
54. Sarpkaya, T., "An Inviscid Model of Two-Dimensional Vortex Shedding for Transient and Asymptotically Steady Separated Flow over an Inclined Plate," Journal of Fluid Mechanics, Vol. 68, pt. 1, pp. 109-128, 1975.
55. Fink, P. T. and Soh, W. K., "Calculation of Vortex Sheets in Unsteady Flow and Applications in Ship Hydrodynamics," Tenth Symposium of Naval Hydrodynamics, Cambridge, Mass., 1974.
56. Belotserkovski, S. M. and Nisht, M. I., "Investigation of Special Features of Flow Over a Flat Plate at Large Angles of Attack," Fluid Dynamics, 1973.
57. Wedemeyer, E., "Ausbildung eines Wirbelpaares an den Kanten einer Platte," Ing.-Arch., 1961.
58. Pullin, D. I., "The Large-Scale Structure of Unsteady Self-Similar Rolled-Up Vortex Sheets," Journal of Fluid Mechanics, Vol. 88, p. 401, 1978.
59. Telste, J. G. and Lugt, H. J., "Vortex Shedding from Finned Circular Cylinders," DTNSRDC-80/124, November, 1980.

60. Kiya, M. and Arie, M., "A Contribution to an Inviscid Vortex Shedding Model for an Inclined Flat Plate in Uniform Flow," Journal of Fluid Mechanics, Vol. 82, pt. 2, pp. -23-240, 1977.
61. Bruns, W. M. S., Impulsive Flow About a Circular Cylinder M.S.M.E. Thesis, U.S. Naval Postgraduate School, Monterey, Ca., 1977.
62. Sarpkaya, T., "Separated Flow About Lifting Bodies and Impulsive Flow About Cylinders," AIAA Journal, Vol. 4, pp. 414-420, 1966.
63. Mandel, P., "Ship Maneuvering and Control," Principles of Naval Architecture, SNAME, Chapt. 8, Sect. 7, pp. 487-488, 1977.

APPENDIX A: REPRESENTATIVE DATA FOR D-SHAPED BODY AT 0 DEGREES

<u>UT/C</u>	<u>Cd</u>	<u>UT/C</u>	<u>Cl</u>	<u>UT/C</u>	<u>Cm</u>
.03	.01	.04	-.01	.03	0
.11	.05	.32	-.03	.54	.04
.63	.26	.85	-.12	1.07	.07
1.2	.48	1.39	-.28	1.61	.09
1.72	.67	1.93	-.55	2.13	.11
2.25	.85	2.47	-.81	2.68	.13
2.8	1	3	-1.04	3.21	.14
3.35	1.13	3.54	-1.17	3.73	.14
3.89	1.25	4.07	-1.18	4.26	.13
4.41	1.35	4.61	-1.05	4.8	.12
4.98	1.46	5.15	-.79	5.34	.12
5.5	1.56	5.69	-.38	5.88	.11
6.04	1.56	6.22	.14	6.41	.11
6.6	1.35	6.76	.74	6.93	.11
7.13	1.34	7.31	1.3	7.48	.12
7.66	1.45	7.87	1.69	8	.13
8.21	1.55	8.4	1.83	8.53	.14
8.74	1.6	8.91	1.71	9.08	.16
9.27	1.57	9.45	1.47	9.61	.17
9.83	1.44	9.98	1.16	10.13	.17
10.37	1.28	10.53	.79	10.67	.17
10.92	1.07	11.06	.35	11.21	.16
11.53	.95	11.49	0	11.74	.14
12.02	1.02	12.18	-.3	12.27	.12
12.5	1.08	12.75	-.25	12.85	.1
13.01	1.14	13.31	-.07	13.45	.08
13.59	1.15	13.8	.17	14.06	.08
14.11	1.15	14.31	.57	14.65	.07
14.63	1.14	14.83	.94	15.23	.07
15.16	1.14	15.36	1.25	15.83	.07
15.68	1.14	15.88	1.45	16.39	.08
16.2	1.13	16.43	1.51	16.85	.09
16.75	1.02	16.95	1.43	17.31	.1
17.28	.95	17.5	1.29	17.8	.1
17.82	.92	18.04	1.11	18.35	.11
18.38	.88	18.57	.93	18.88	.11
18.93	.8	19.13	.72	19.36	.12
19.45	.74	19.8	.46	19.84	.11
19.96	.77	20.45	.28	20.35	.09
20.52	.77	21	.19	21	.08
21.03	.74	21.5	.16	21.69	.06
22.11	.77	22.01	.18	21.86	.07
22.66	.8	22.51	.25	22.4	.07
23.21	.77	22.98	.34	22.94	.07
23.71	.79	23.46	.47	23.47	.07
24.27	.79	23.97	.61	24	.07
24.81	.79	24.47	.74	24.53	.07
25.34	.76	25.02	.78	25.06	.07
25.87	.71	25.53	.8	25.58	.07

APPENDIX B: REPRESENTATIVE DATA FOR D-SHAPED BODY AT +10 DEGREES

<u>UT/C</u>	<u>Cd</u>	<u>UT/C</u>	<u>C1</u>	<u>UT/C</u>	<u>Cm</u>
.11	.06	.06	-.03	.08	0
.54	.35	.33	-.08	.56	.1
1.09	.57	.86	-.18	1.1	.15
1.59	.71	1.38	-.32	1.65	.16
2.15	.95	1.92	-.52	2.16	.16
2.7	.87	2.45	-.72	2.71	.17
3.23	1	2.97	-.84	3.22	.14
3.78	1.17	3.5	-.84	3.79	.11
4.34	1.32	4.04	-.73	4.34	.07
4.9	1.44	4.58	-.47	4.88	.04
5.46	1.55	5.12	-.1	5.48	.02
6	1.69	5.63	.26	6.04	.02
6.53	1.66	6.19	.7	6.58	.03
7.09	1.49	6.71	1.13	7.09	.05
7.64	1.57	7.26	1.52	7.66	.06
8.17	1.65	7.79	1.81	8.21	.06
8.74	1.82	8.32	1.93	8.76	.06
9.31	1.73	8.86	1.88	9.3	.06
9.83	1.67	9.38	1.69	9.81	.05
10.36	1.64	9.92	1.36	10.37	.04
10.89	1.62	10.46	.95	10.94	.03
11.44	1.64	10.98	.4	11.48	.02
11.95	1.66	11.5	-.29	12.02	.02
12.52	1.73	12.03	-.94	12.53	.01
13.06	1.7	12.56	-1.36	13.09	.01
13.57	1.67	13.1	-1.5	13.62	.02
14.13	1.62	13.62	-1.4	14.17	.02
14.69	1.53	14.17	-1.1	14.7	.02
15.23	1.44	14.72	-.67	15.24	.02
15.77	1.37	15.28	-.1	15.77	.03
16.28	1.34	15.79	.5	16.28	.03
16.8	1.31	16.33	1.03	16.81	.04
17.34	1.32	16.88	1.35	17.32	.06
17.87	1.27	17.42	1.52	18.35	.07
18.41	1.22	17.95	1.55	17.84	.07
18.94	1.19	18.5	1.49	18.91	.07
19.48	1.18	19.01	1.36	19.44	.07
20.03	1.13	19.53	1.22	20.01	.07
20.53	1.16	20.06	.98	20.52	.05
21.11	1.17	20.61	.69	21.08	.03
21.65	1.19	21.2	.4	21.69	.02
22.18	1.21	21.78	.14	22.24	.01
22.71	1.19	22.29	-.15	22.77	.01
23.27	1.17	22.82	-.39	23.33	.01
23.81	1.1	23.34	-.57	23.85	.02
24.35	1	23.89	-.68	24.41	.02

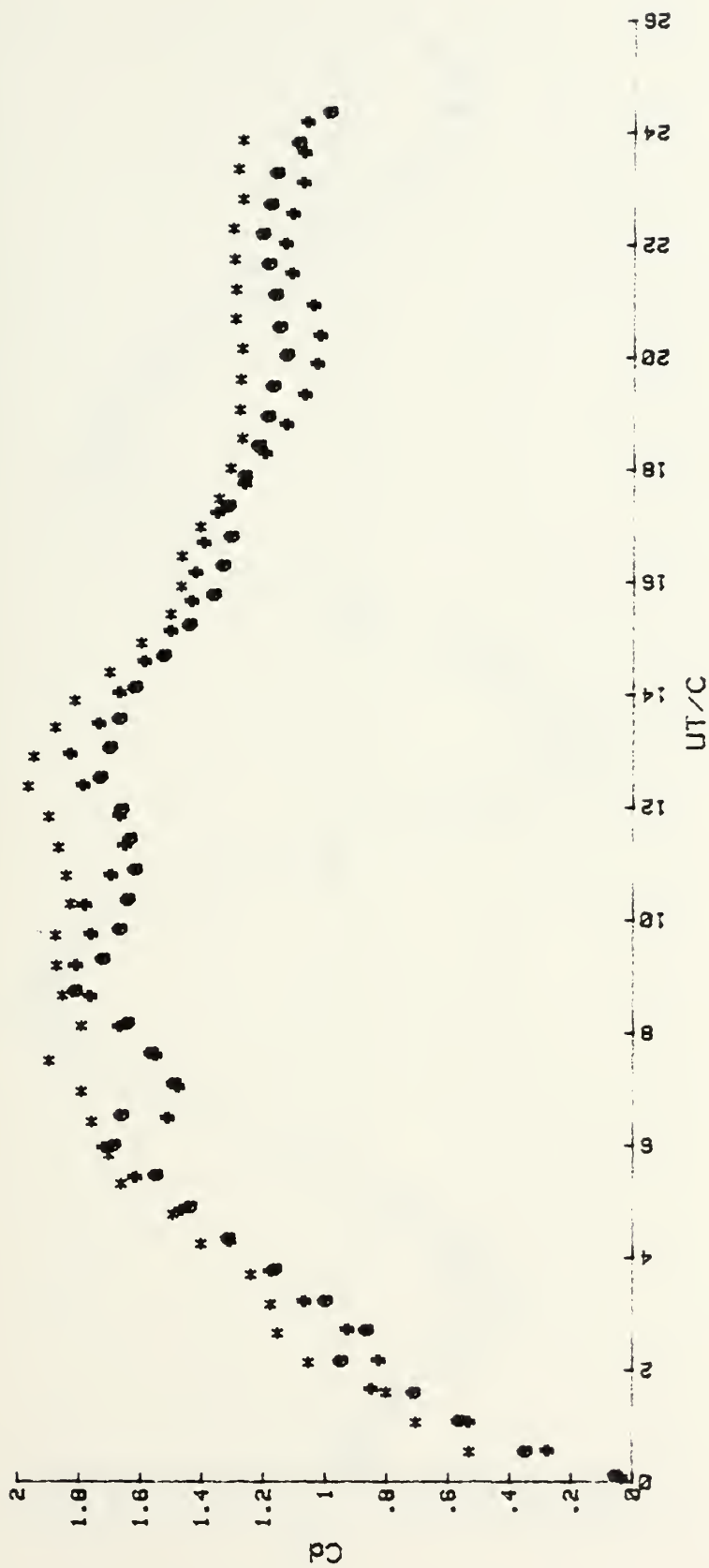


Figure 32. C_d vs. UT/C for the D-Shaped Body at +10 deg.

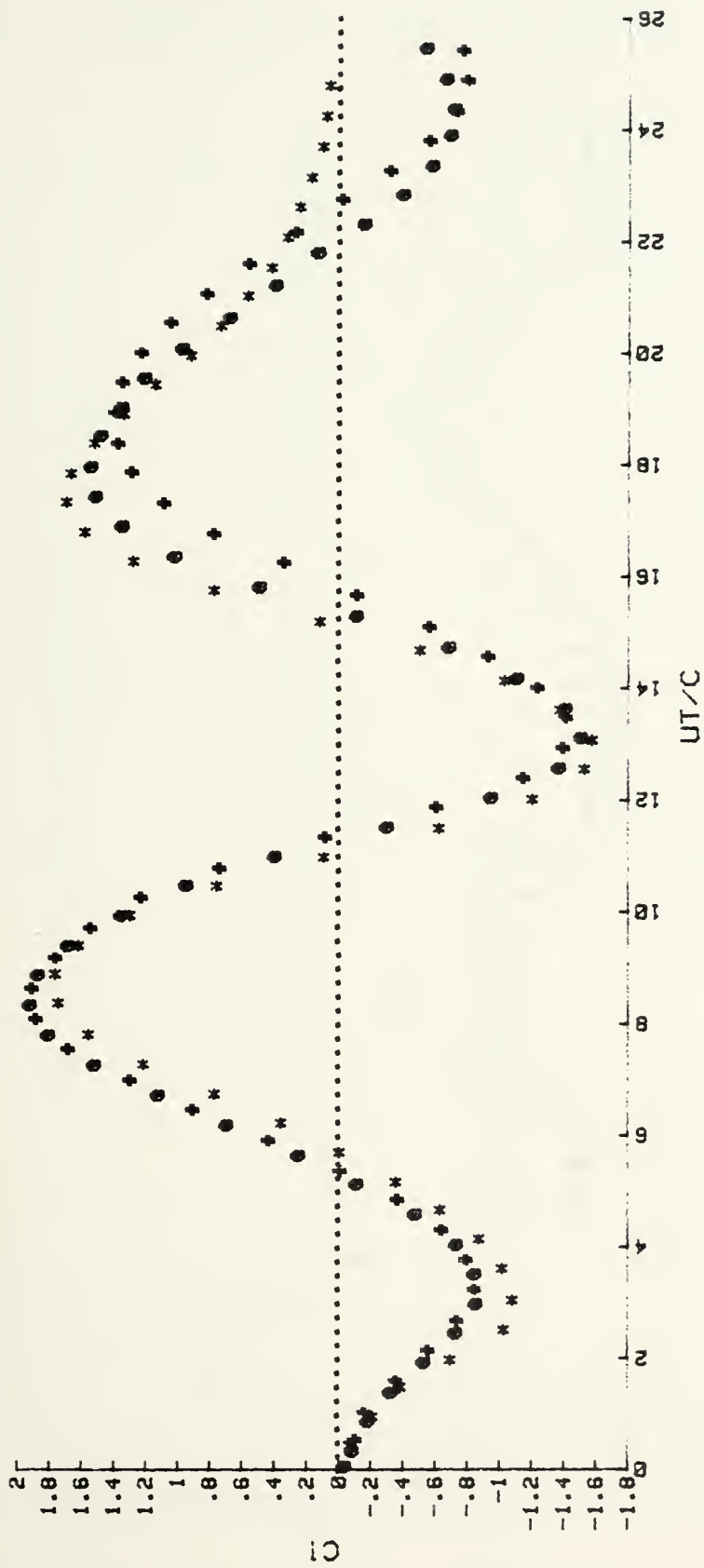


Figure 33. $C1$ vs. UT/C for the D-Shaped Body at $+10^\circ$.

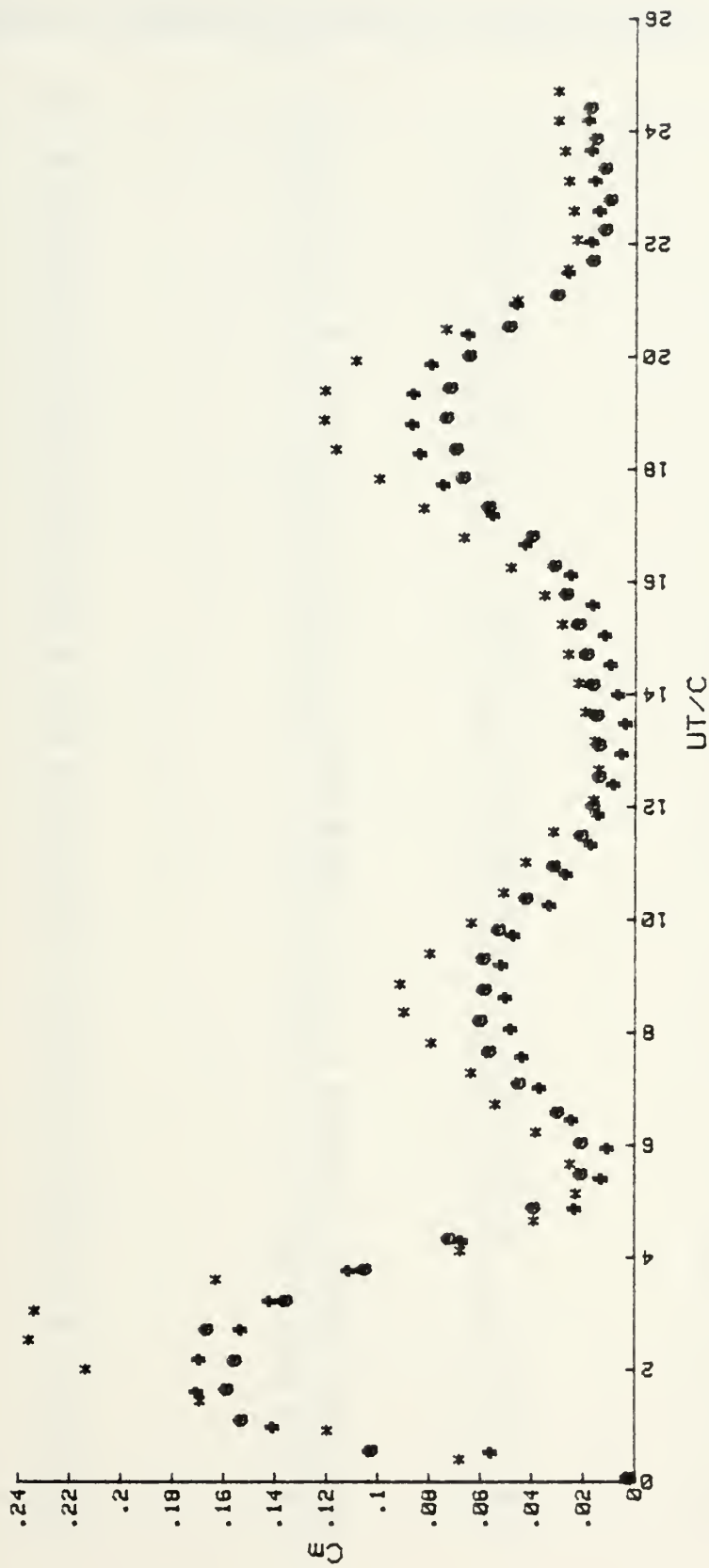


Figure 34. C_m vs. UT/C for the D-shaped Body at +10 deg.

APPENDIX C: REPRESENTATIVE DATA FOR D-SHAPED BODY AT +20 DEGREES

<u>UT/C</u>	<u>Cd</u>	<u>UT/C</u>	<u>C1</u>	<u>UT/C</u>	<u>Cm</u>
.07	.04	.06	-.02	.05	0
.23	.12	.65	-.14	.53	.11
.76	.36	1.19	-.22	1.1	.18
1.3	.61	1.73	-.35	1.66	.21
1.84	.82	2.26	-.44	2.19	.2
2.4	.94	2.79	-.49	2.73	.15
2.93	1.07	3.34	-.47	3.27	.09
3.48	1.18	3.88	-.34	3.83	.02
4.04	1.41	4.41	-.21	4.37	-.03
4.59	1.62	4.95	-.04	4.99	-.05
5.16	1.72	5.48	.14	5.56	-.05
5.74	1.74	6.01	.34	6.07	-.04
6.26	1.68	6.55	.55	6.58	0
6.74	1.39	7.09	.77	7.16	.02
7.28	1.34	7.62	1	7.69	.03
7.83	1.44	8.16	1.16	8.24	.03
8.35	1.58	8.69	1.26	8.77	.03
8.9	1.67	9.23	1.25	9.31	.03
9.43	1.7	9.77	1.15	9.87	.03
9.97	1.68	10.31	.93	10.39	.02
10.51	1.59	10.83	.61	10.95	.02
11.03	1.51	11.38	.18	11.5	.02
11.56	1.47	11.88	-.28	12.04	.01
12.1	1.53	12.49	-.74	12.57	.01
12.66	1.64	13.06	-1.03	13.11	0
13.22	1.69	13.58	-1.12	13.67	0
13.74	1.64	14.14	-1.03	14.22	0
14.27	1.57	14.71	-.84	14.77	0
14.8	1.5	15.24	-.55	15.31	.01
15.34	1.43	15.69	-.17	15.85	.02
15.87	1.38	16.21	.26	16.4	.02
16.4	1.36	16.74	.69	16.95	.02
16.95	1.36	17.28	1.01	17.49	.03
17.49	1.34	17.83	1.23	18.02	.03
18.02	1.34	18.37	1.32	18.59	.03
18.56	1.33	18.89	1.32	19.12	.03
19.1	1.36	19.44	1.22	19.65	.03
19.64	1.37	19.96	1.04	20.22	.02
20.18	1.34	20.48	.8	20.77	.02
20.72	1.29	21.03	.52	21.32	.01
21.26	1.24	21.57	.21	21.85	.01
21.78	1.19	22.15	-.12	22.39	.01
22.33	1.19	22.73	-.41	22.94	.01
22.88	1.21	23.22	-.66	23.5	.01
23.45	1.21	23.74	-.85	24.03	.01
24.05	1.21	24.26	-.9	24.58	.01
24.58	1.18	24.81	-.88	25.12	.01
25.14	1.16	25.35	-.79	25.68	.01

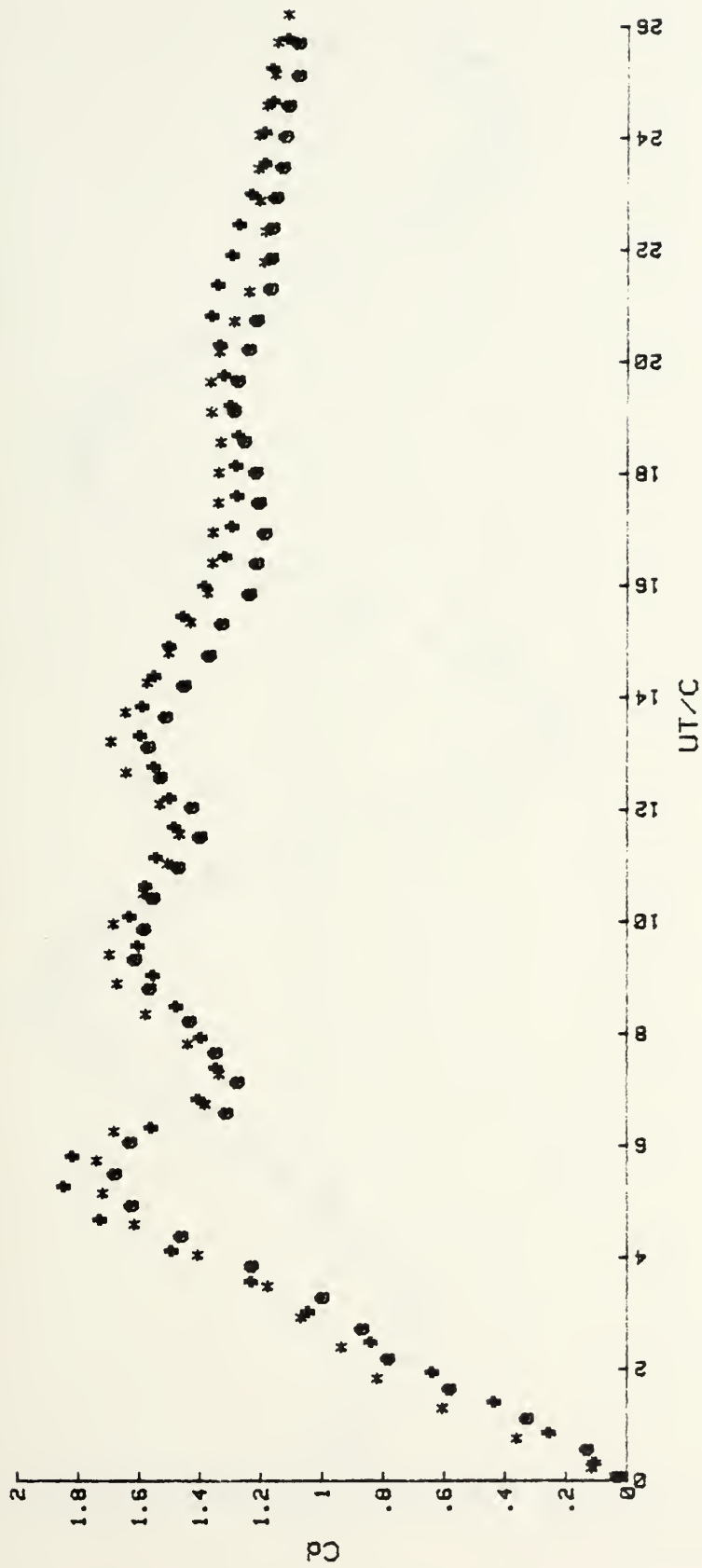


Figure 35. C_d vs. UT/C for the D-Shaped Body at $+20^\circ$ deg.

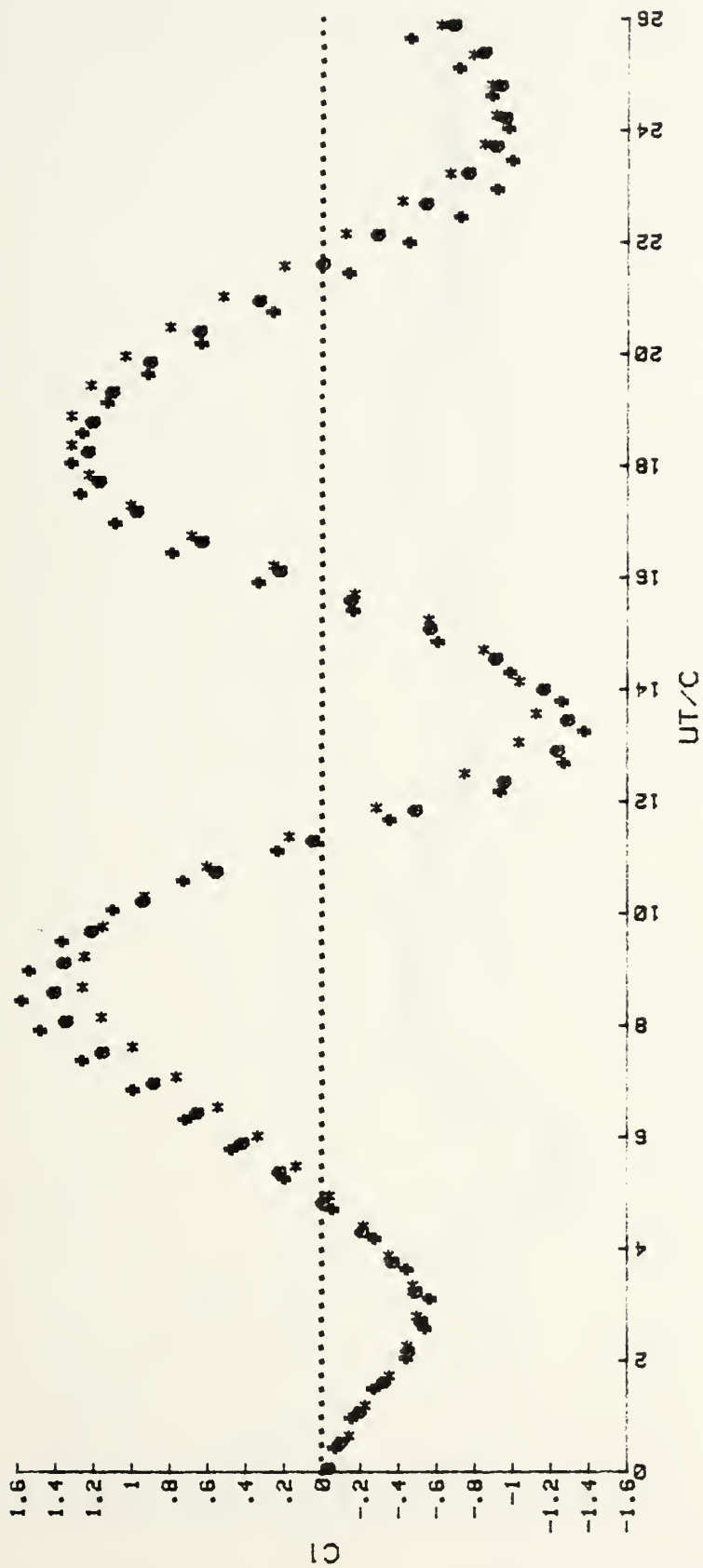


Figure 36. $C1$ vs. UT/C for the D-Shaped Body at $+20^\circ$ deg.

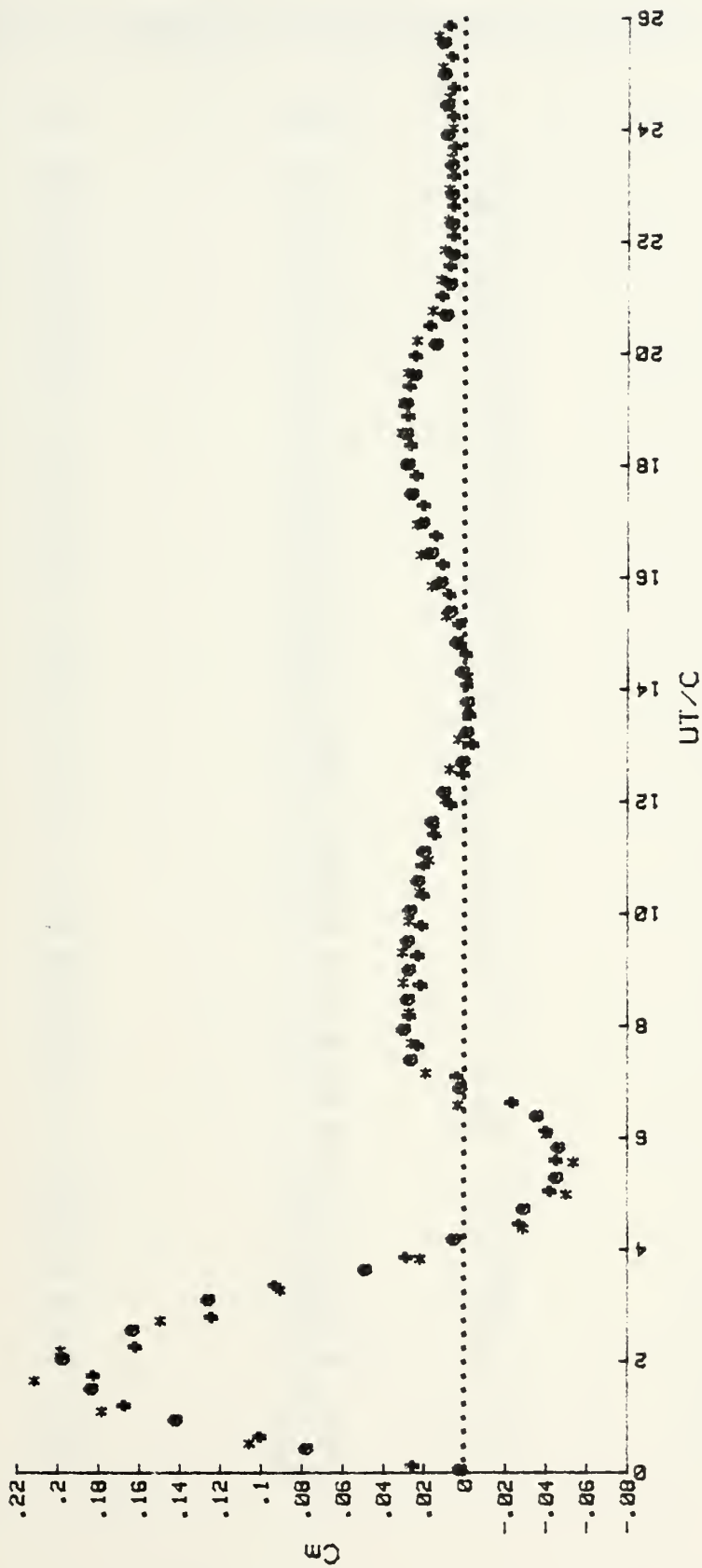


Figure 37. Cm vs. UT/C for the D-Shaped Body at +20 deg.

APPENDIX D: REPRESENTATIVE DATA FOR D-SHAPED BODY AT +30 DEGREES

<u>UT/C</u>	<u>Cd</u>	<u>UT/C</u>	<u>Ci</u>	<u>UT/C</u>	<u>Cm</u>
.05	.03	.06	-.03	.32	.09
.82	.57	.53	-.09	.55	.2
1.42	.77	1.06	-.18	1.08	.23
1.74	.89	1.61	-.23	1.64	.21
2.24	.81	2.15	-.34	2.16	.18
2.81	1.03	2.66	-.36	2.66	.12
3.35	1.31	3.2	-.37	3.21	.04
3.88	1.53	3.72	-.37	3.76	-.02
4.43	1.7	4.25	-.36	4.29	-.04
4.97	1.74	4.81	-.39	4.83	-.04
5.51	1.64	5.33	-.45	5.38	-.04
6.04	1.57	5.88	-.52	5.89	-.02
6.58	1.31	6.39	-.55	6.44	0
7.12	1.23	6.92	-.58	6.98	.01
7.66	1.23	7.45	-.59	7.5	.01
8.21	1.2	7.99	-.58	8.04	.01
8.74	1.15	8.53	-.55	8.59	.01
9.29	1.08	9.06	-.49	9.13	.01
9.82	1.13	9.5	-.36	9.67	.01
10.35	1.12	10.12	-.23	10.2	.01
10.9	1.12	10.66	-.07	10.73	.01
11.44	1.13	11.21	.1	11.26	.01
11.96	1.12	11.73	.21	11.81	.01
13.08	1.11	12.26	.3	12.34	.01
12.54	1.11	12.82	.36	12.86	.01
13.57	1.11	13.32	.39	13.41	.01
14.14	1.09	13.86	.38	13.97	.01
14.68	1.06	14.4	.33	14.49	.01
15.21	1.05	14.94	.26	15.04	.01
15.74	1.05	15.45	.19	15.55	.01
16.3	1.05	15.99	.14	16.11	.01
16.85	1.08	16.52	.06	16.64	.01
17.37	1.11	17.06	0	17.19	.01
17.94	1.11	17.59	-.05	17.71	.01
18.46	1.1	18.16	-.1	18.26	.01
18.99	1.07	18.66	-.13	18.77	.02
19.53	1.05	19.24	-.14	19.31	.02
20.08	1.01	19.74	-.12	19.85	.02
20.6	.99	20.27	-.09	20.39	.02
21.16	.97	20.8	-.05	20.94	.02
21.7	.97	21.34	.02	21.45	.02
22.23	.99	21.88	.08	21.99	.02
22.77	1	22.4	.14	22.54	.02
23.3	1.01	22.94	.21	23.06	.02
23.85	1.01	23.46	.26	23.59	.02
24.39	1	24.01	.3	24.14	.02

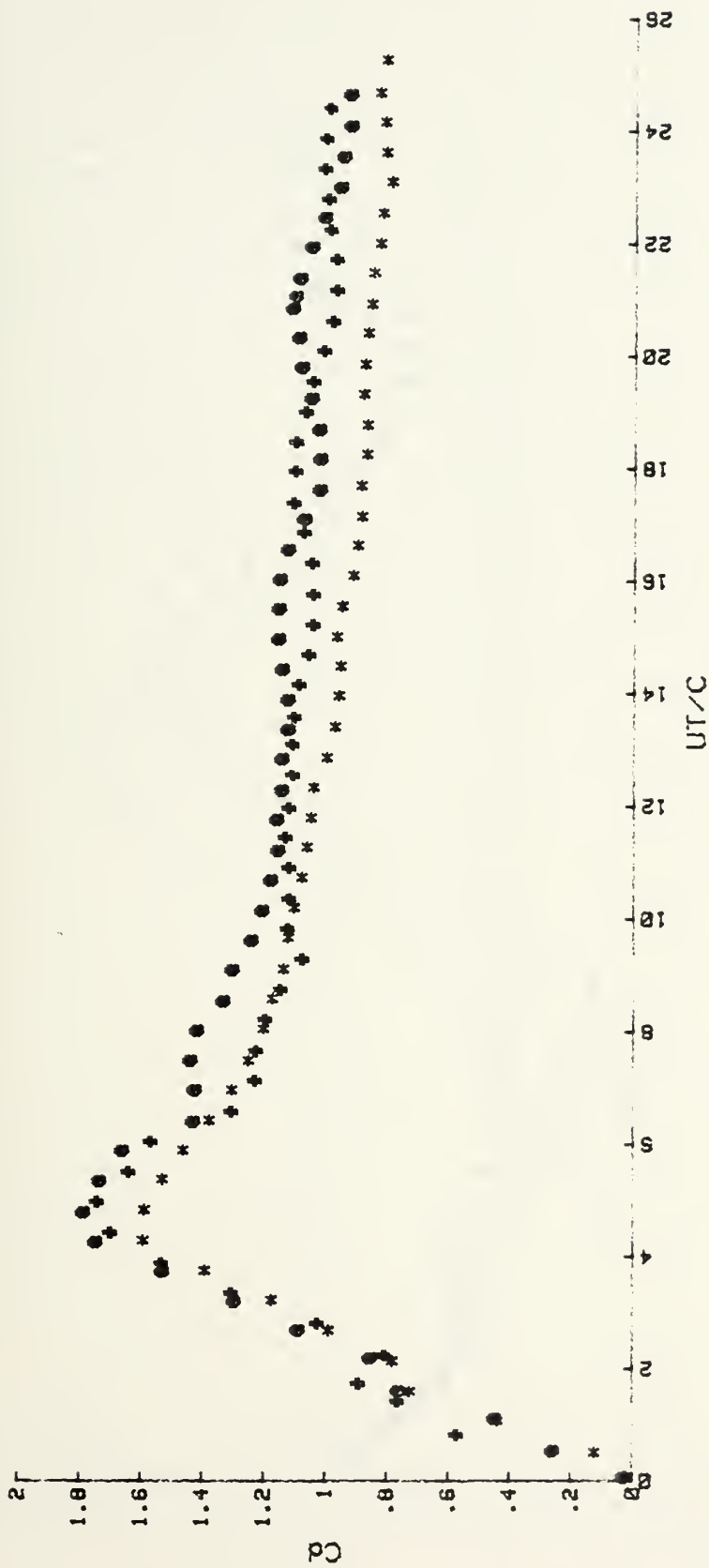


Figure 38. C_d vs. UT/C for the D-Shaped Body at +30 deg.

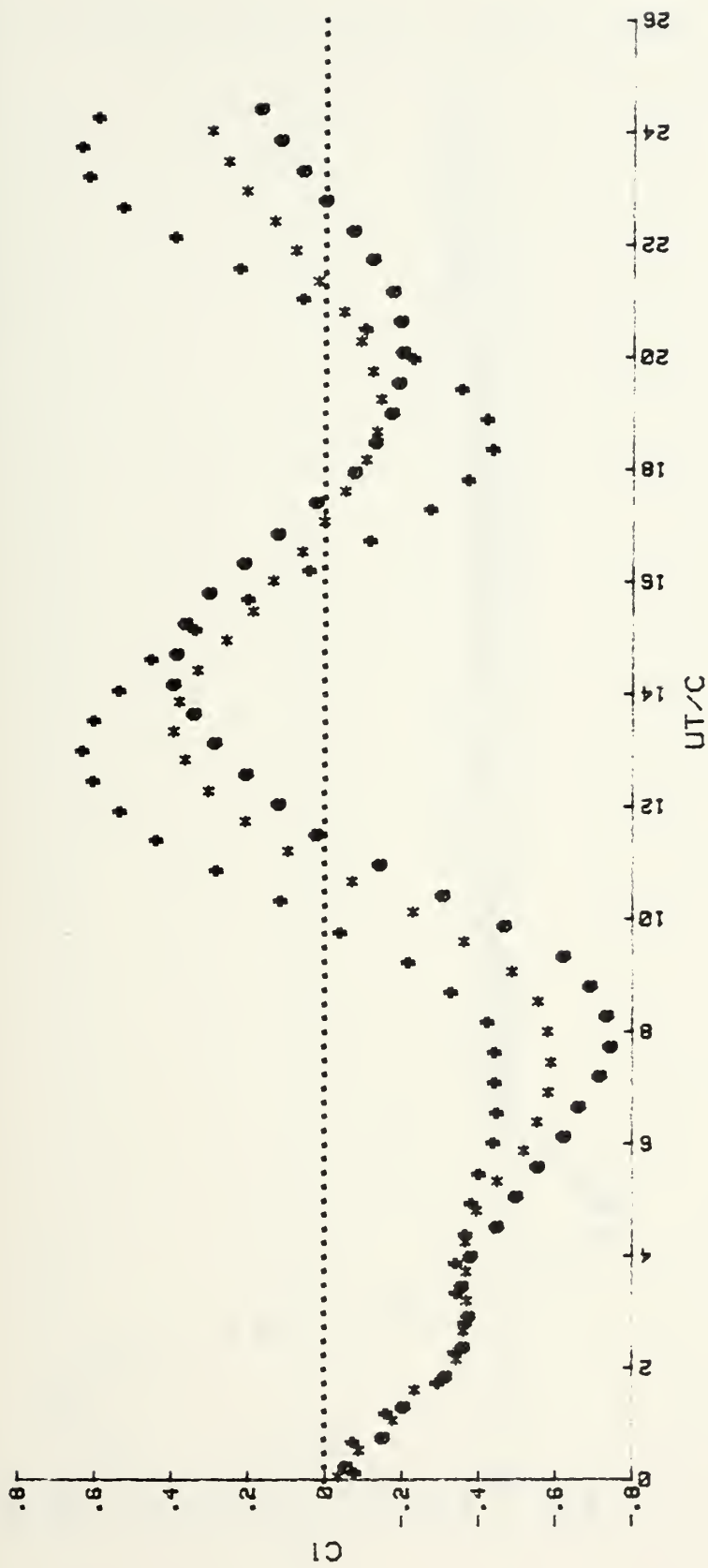


Figure 39. CI vs. UT/C for the D-Shaped Body at +30 deg.

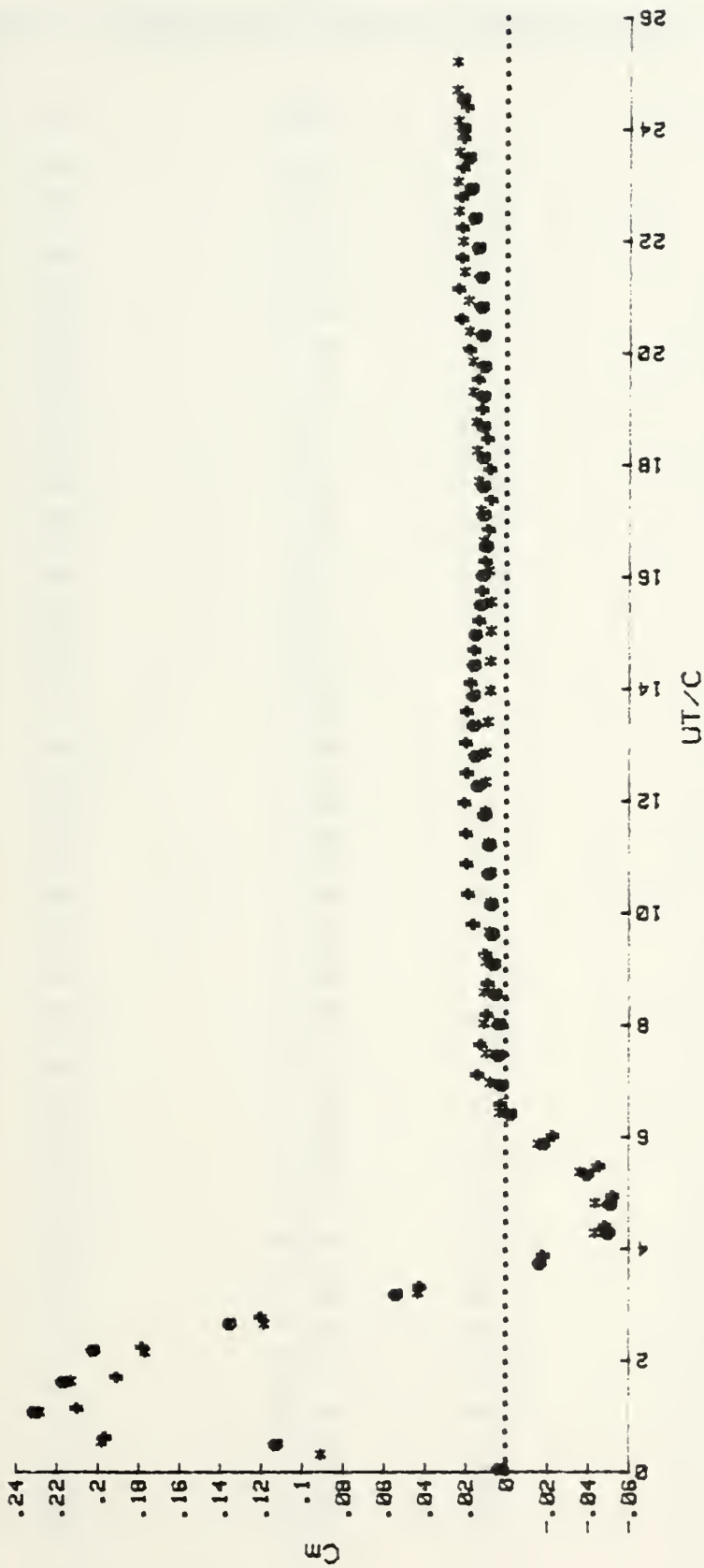


Figure 40. Cm vs. UT/C for the D-Shaped Body at +30 deg.

APPENDIX E: REPRESENTATIVE DATA FOR D-SHAPED BODY AT +45 DEGREES

<u>UT/C</u>	<u>Cd</u>	<u>UT/C</u>	<u>C1</u>	<u>UT/C</u>	<u>Cm</u>
.06	.04	.33	.19	.22	.06
.53	.23	.88	-.15	.77	.19
1.06	.4	1.43	-.19	1.33	.22
1.59	.58	1.95	-.29	1.81	.2
2.15	.89	2.5	-.36	2.37	.16
2.7	1.14	3.04	-.48	2.89	.1
3.23	1.38	3.58	-.63	3.32	.06
3.76	1.62	4.14	-.8	3.98	0
4.31	1.72	4.7	-1.01	4.52	-.02
4.88	1.69	5.24	-1.26	5.07	-.02
5.41	1.63	5.8	-1.49	5.62	-.01
5.93	1.69	6.37	-1.68	6.16	-.01
6.5	1.63	6.95	-1.75	6.73	-.01
7.04	1.61	7.51	-1.69	7.26	-.02
7.62	1.66	8.03	-1.52	7.84	-.02
8.14	1.69	8.55	-1.27	8.37	-.03
8.71	1.67	9.05	-.92	8.9	-.03
9.25	1.58	9.57	-.4	9.41	-.02
9.78	1.57	10.13	.25	9.95	.01
10.32	1.41	10.66	.89	10.46	.03
10.9	1.42	11.22	1.2	10.99	.03
11.41	1.48	11.77	1.3	11.53	.03
11.93	1.52	12.32	1.2	12.06	.03
12.47	1.65	12.88	.99	12.59	.03
12.99	1.68	13.42	.69	13.14	.02
13.54	1.66	13.94	.32	13.69	.01
14.06	1.59	14.51	-.12	14.28	0
14.6	1.51	15.03	-.53	14.79	-.01
15.13	1.42	15.56	-.87	15.31	-.01
15.67	1.35	16.08	-1.02	15.84	-.01
16.21	1.34	16.63	-1.03	16.37	0
16.76	1.35	17.2	-.92	16.9	0
17.28	1.38	17.75	-.72	17.43	0
17.82	1.38	18.31	-.47	17.96	0
18.35	1.37	18.85	-.21	18.5	0
18.89	1.34	19.37	.08	19.04	.01
19.46	1.31	19.87	.34	19.56	.02
20.01	1.26	20.42	.59	20.09	.02
20.54	1.22	20.98	.78	20.62	.03
21.07	1.2	21.49	.87	21.15	.03
21.61	1.18	22.05	.89	21.71	.02
22.13	1.17	22.61	.85	22.25	.01
22.69	1.19	23.14	.76	22.77	.01
23.24	1.19	23.69	.62	23.33	0
23.78	1.18	24.24	.48	23.86	0
24.32	1.15	24.79	.33	24.41	0
24.86	1.12	25.32	.16	24.92	0
25.38	1.07	25.89	-.02	25.47	0

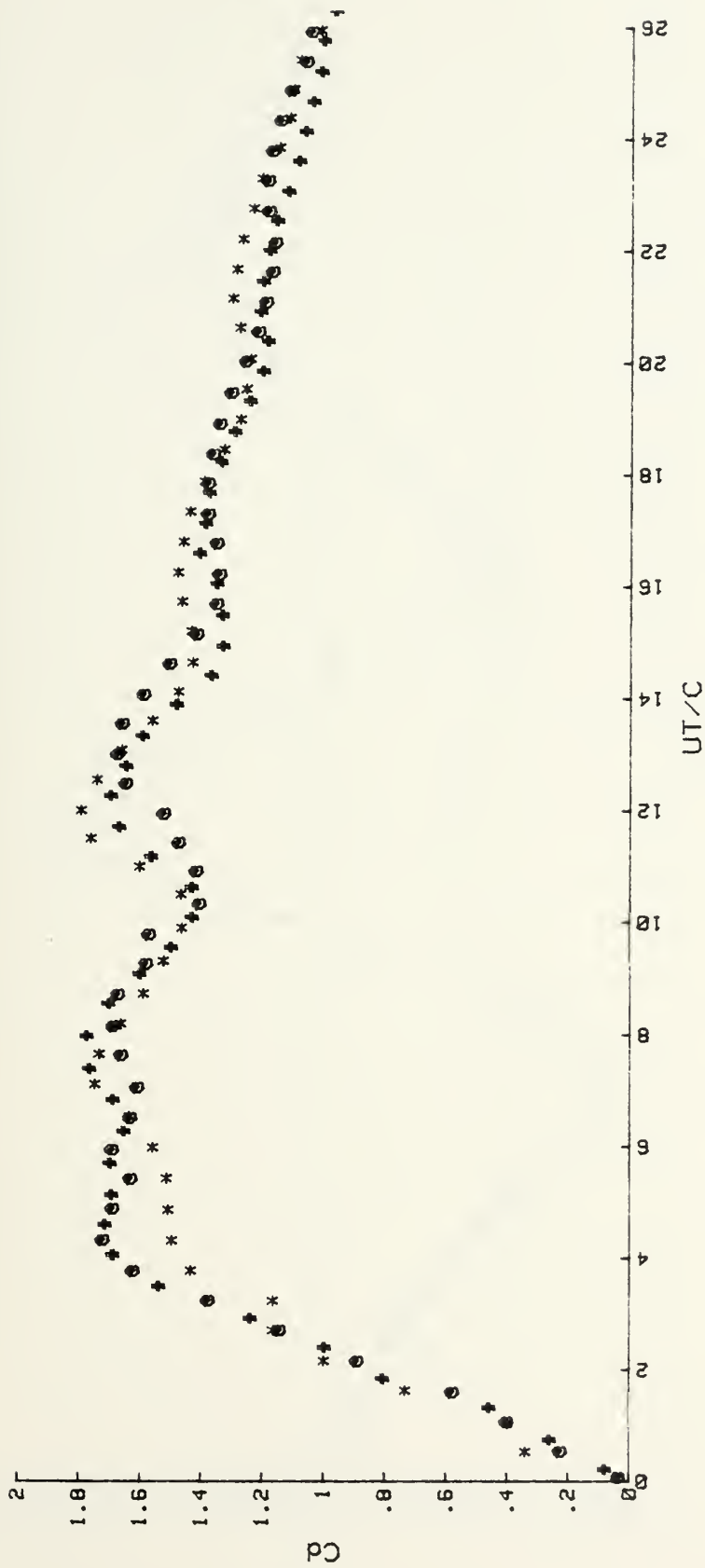


Figure 41. C_d vs. UT/C for the D-Shaped Body at +45 deg.

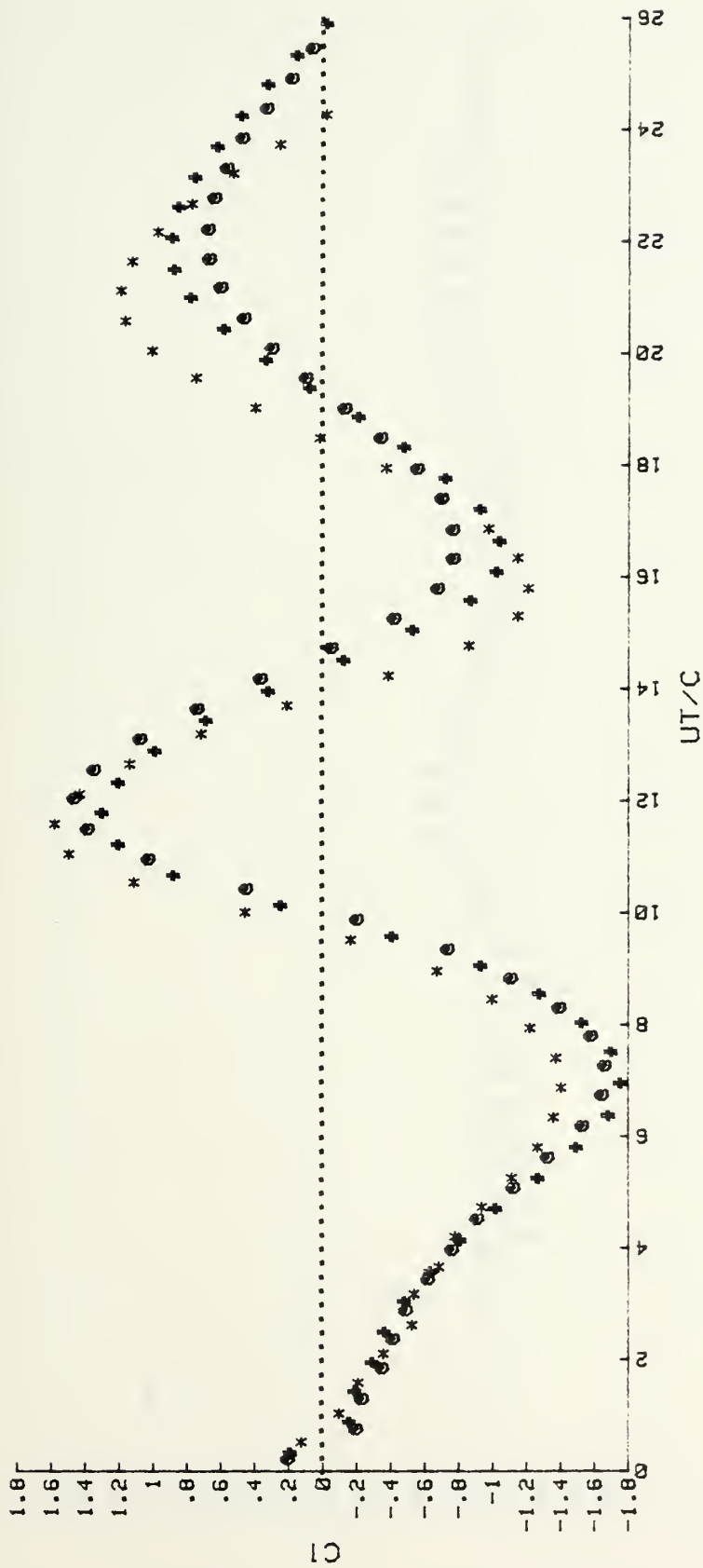


Figure 42. $C1$ vs. UT/C for the D-Shaped Body at +45 deg.

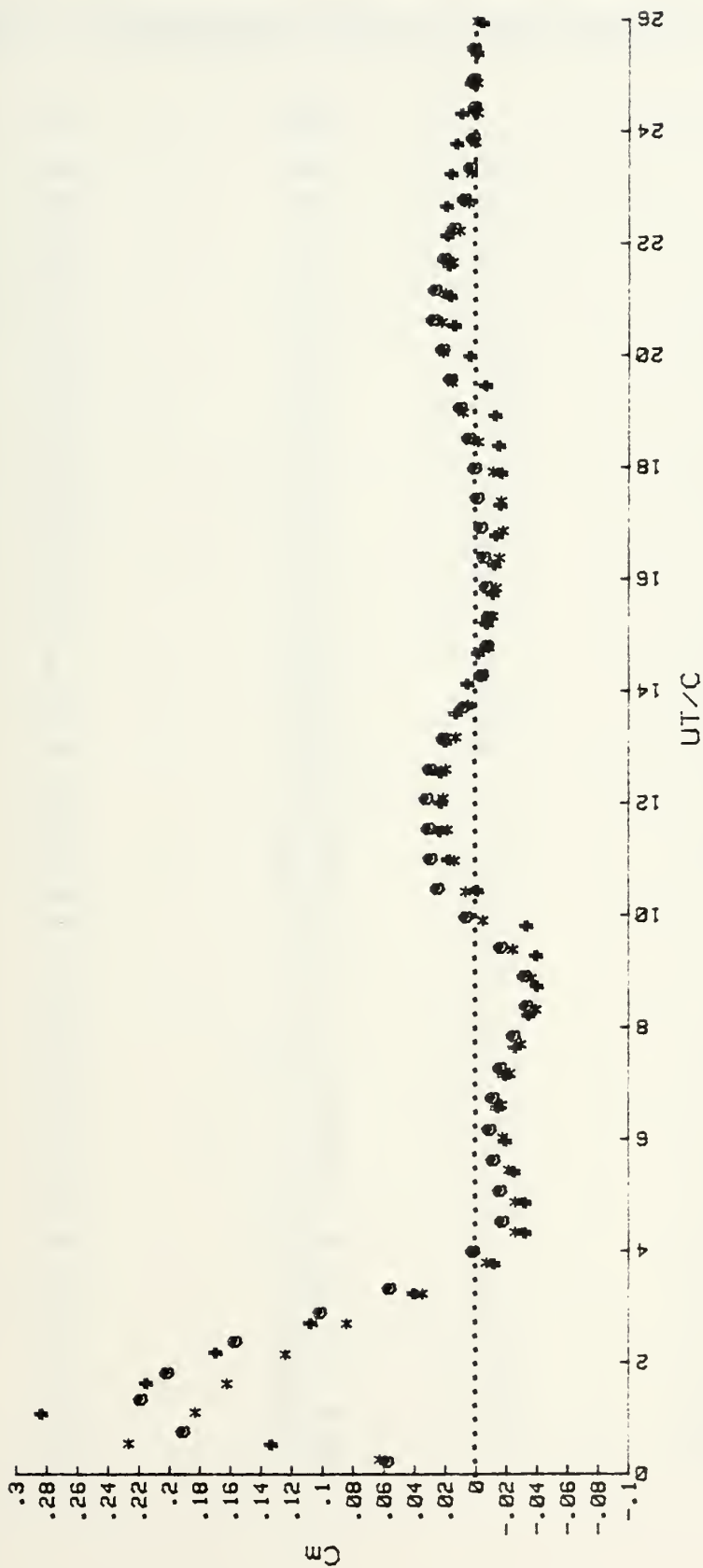


Figure 43. C_m vs. UT/C for the D-Shaped Body at +45 deg.

APPENDIX F: REPRESENTATIVE DATA FOR D-SHAPED BODY AT -10 DEGREES

<u>U/C</u>	<u>Cd</u>	<u>U/C</u>	<u>C1</u>	<u>U/C</u>	<u>Cm</u>
.21	.29	.25	-.23	.26	0
.75	.12	.55	-.26	.31	.02
1.27	.59	1.1	-.19	.91	.03
1.81	.96	1.64	-.38	1.39	.24
2.34	1.16	2.17	-.6	1.92	.26
2.85	1.11	2.71	-.89	2.46	.37
3.4	1.3	3.27	-1.16	2.99	.28
3.97	1.34	3.8	-1.35	3.51	.07
4.46	1.36	4.34	-1.48	4.05	.37
5.01	1.42	4.89	-1.49	4.59	.27
5.54	1.48	5.43	-1.34	5.13	.27
6.07	1.5	5.97	-1.05	5.66	.27
6.62	1.32	6.55	-.59	6.21	.27
7.14	1.32	7.06	-.31	6.73	.06
7.68	1.47	7.59	.68	7.25	.26
8.24	1.72	8.11	1.18	7.82	.27
8.76	1.91	8.64	1.43	8.33	.27
9.28	2	9.19	1.4	9.38	.08
9.82	1.92	9.72	1.26	9.93	.1
10.38	1.75	10.27	1.08	10.46	.1
10.9	1.49	10.8	.83	10.98	.11
11.44	1.2	11.33	.5	11.52	.11
11.97	1.08	11.88	.24	12.05	.11
12.49	1.17	12.43	-.49	12.59	.11
13.01	1.25	12.95	-.84	13.12	.11
13.55	1.24	13.51	-.86	13.66	.1
14.26	1.21	14.27	-.68	14.19	.29
14.61	1.2	14.64	-.33	14.74	.08
15.14	1.2	15.18	.12	15.28	.28
15.68	1.23	15.7	.58	15.8	.27
16.22	1.28	16.21	.98	16.33	.37
16.73	1.34	16.75	1.22	16.87	.28
17.28	1.37	17.26	1.28	17.4	.28
17.8	1.37	17.83	1.24	17.96	.08
18.33	1.27	18.38	1.13	18.49	.09
18.86	1.2	18.92	.96	19.01	.29
19.4	1.08	19.44	.75	19.58	.1
19.94	.96	19.99	.54	20.09	.1
20.47	.81	20.54	.31	20.63	.1
21.01	.81	21.1	.29	21.14	.1
21.54	.78	21.65	-.07	21.96	.1
22.35	.77	22.21	-.18	22.2	.1
22.59	.78	22.78	-.26	22.72	.1
23.13	.75	23.32	-.23	23.25	.09
23.68	.72	23.85	-.14	23.79	.09
24.19	.69	24.41	0	24.33	.29

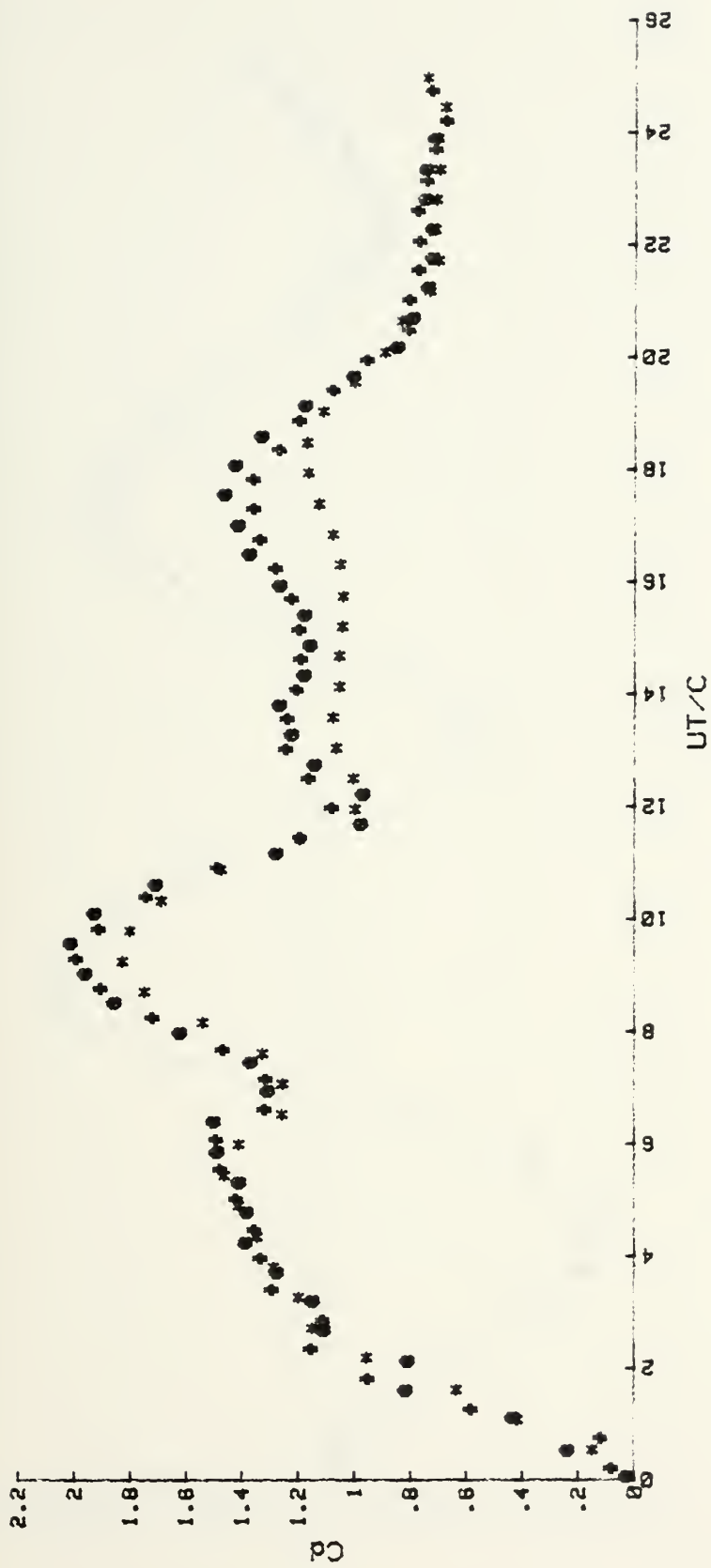


Figure 44. C_d vs. UT/C for the D-Shaped Body at -10° .

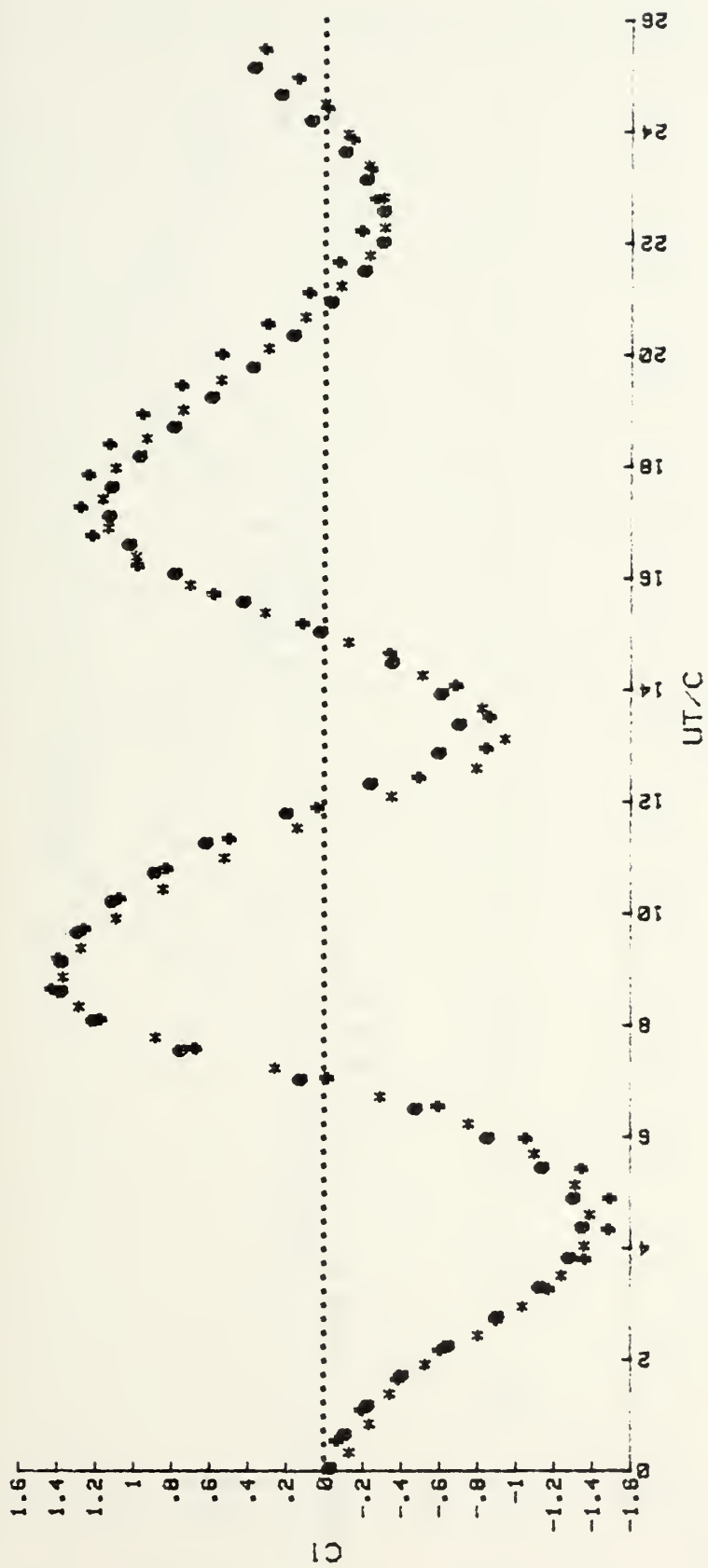


Figure 45. CI vs. UT/C for the D-Shaped Body at -10° deg.

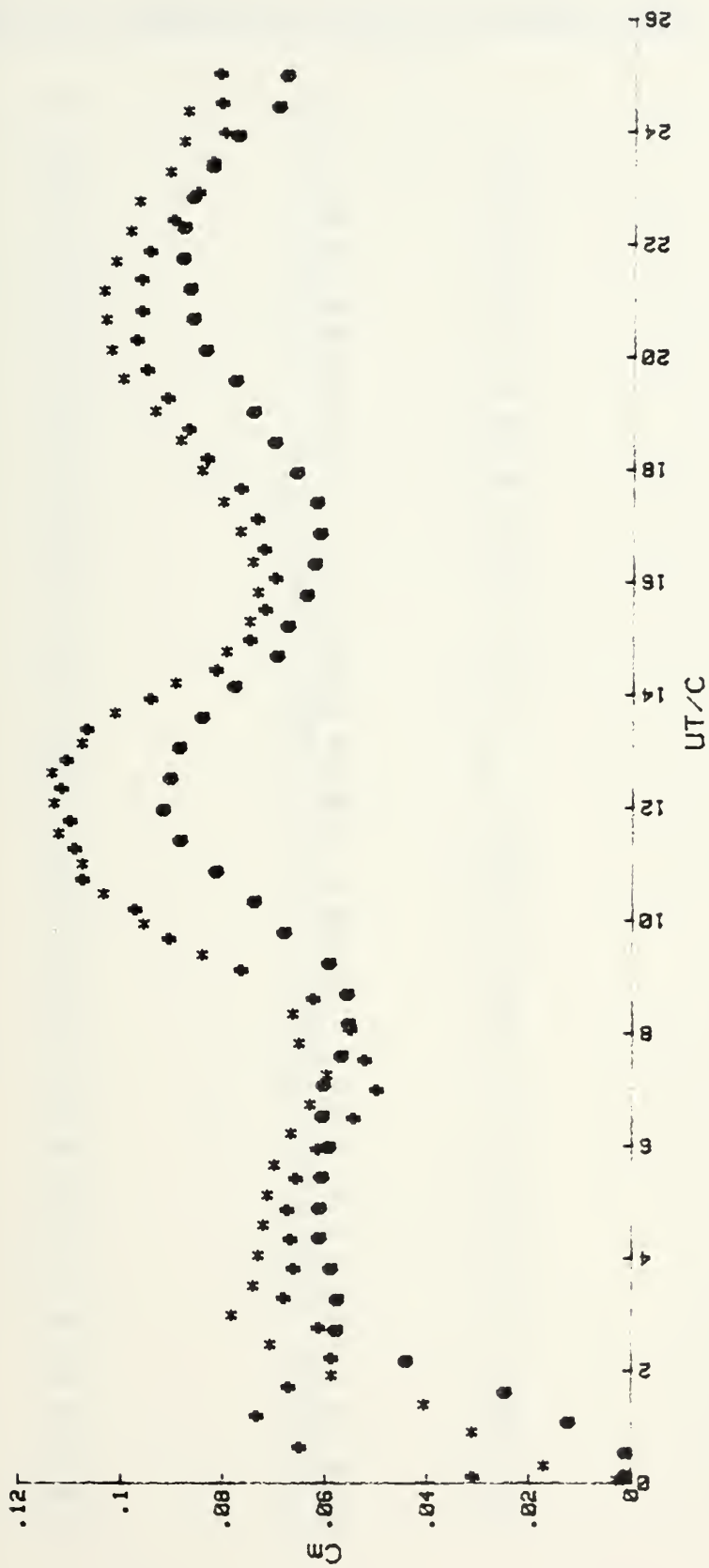


Figure 46. C_m vs. UT/C for the D-Shaped Body at -10° .

APPENDIX G: REPRESENTATIVE DATA FOR D-SHAPED BODY AT -20 DEGREES

<u>UT/C</u>	<u>Cd</u>	<u>UT/C</u>	<u>C1</u>	<u>UT/C</u>	<u>Cm</u>
.05	.04	.07	-.01	.07	0
.54	.23	.54	-.05	.55	-.01
1.07	.47	1.06	-.13	1.09	-.02
1.62	.73	1.63	-.26	1.63	-.02
2.19	1.19	2.15	-.44	2.18	-.02
2.74	1.41	2.68	-.67	2.71	-.01
3.22	1.53	3.25	-.96	3.26	.01
3.82	1.51	3.79	-1.24	3.79	.01
4.38	1.54	4.39	-1.41	4.32	.01
4.94	1.59	4.99	-1.53	4.84	.01
5.6	1.67	5.55	-1.56	5.4	.01
6.2	1.6	6.11	-1.46	5.94	.01
6.73	1.58	6.61	-1.24	6.5	.01
7.27	1.48	7.11	-.89	7.05	.01
7.83	1.39	7.59	-.46	7.56	.01
8.51	1.54	8.1	.14	8.11	0
9.18	1.8	8.65	.74	8.65	0
9.77	2.12	9.19	1.17	9.21	0
10.45	2.26	9.69	1.29	9.74	0
11.04	2.3	10.26	1.17	10.28	0
11.58	2.26	10.8	.91	10.8	.01
12.01	2.08	11.31	.54	11.35	.02
12.37	1.71	11.88	.08	11.87	.03
12.86	1.4	12.46	-.47	12.41	.03
13.38	1.28	13	-1.03	12.95	.03
13.87	1.37	13.54	-1.38	13.49	.03
14.39	1.44	14.02	-1.51	14.02	.03
14.91	1.42	14.62	-1.41	14.59	.03
15.49	1.37	15.16	-1.18	15.13	.02
16.05	1.36	15.76	-.86	15.66	.01
16.59	1.38	16.3	-.47	16.19	.01
17.13	1.44	16.78	.03	16.73	0
17.68	1.52	17.29	.5	17.27	-.01
18.25	1.58	17.82	.84	17.81	-.01
18.79	1.62	18.36	1.05	18.35	-.01
19.36	1.67	18.9	1.14	18.9	0
19.84	1.59	19.45	1.12	19.44	0
20.31	1.48	19.97	1.02	19.97	.01
20.83	1.31	20.51	.84	20.5	.02
21.37	1.14	21.04	.63	21.03	.02
21.88	1.04	21.59	.43	21.59	.03
22.44	.96	22.17	.16	22.11	.03
22.99	.94	22.74	-.14	22.67	.03
23.53	.92	23.34	-.35	23.2	.04
24.08	.9	23.9	-.52	23.75	.04
24.61	.89	24.42	-.61	24.29	.04
25.19	.87	24.92	-.64	24.82	.04
25.7	.82	25.55	-.6	25.37	.04

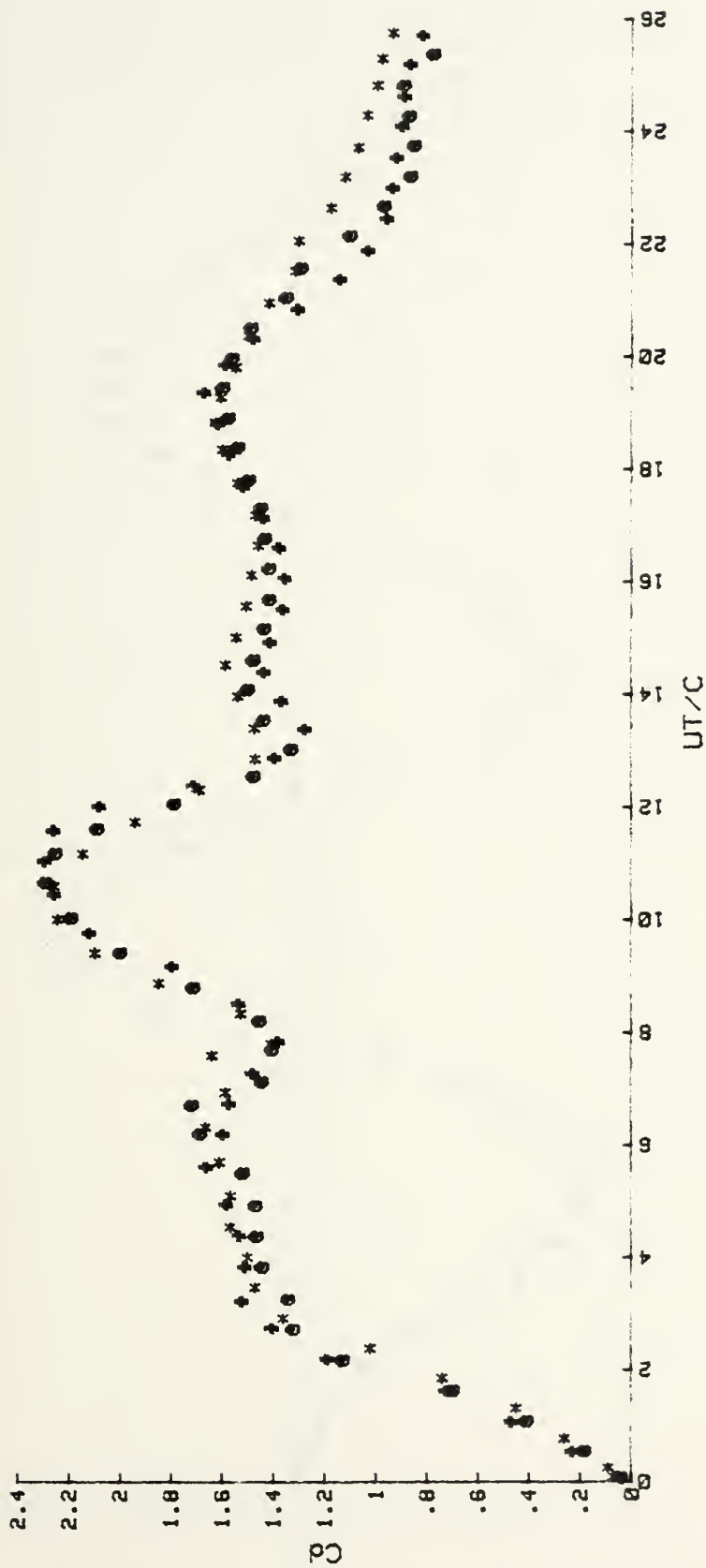


Figure 47. C_d vs. U_T/C for the D-Shaped Body at -20° deg.

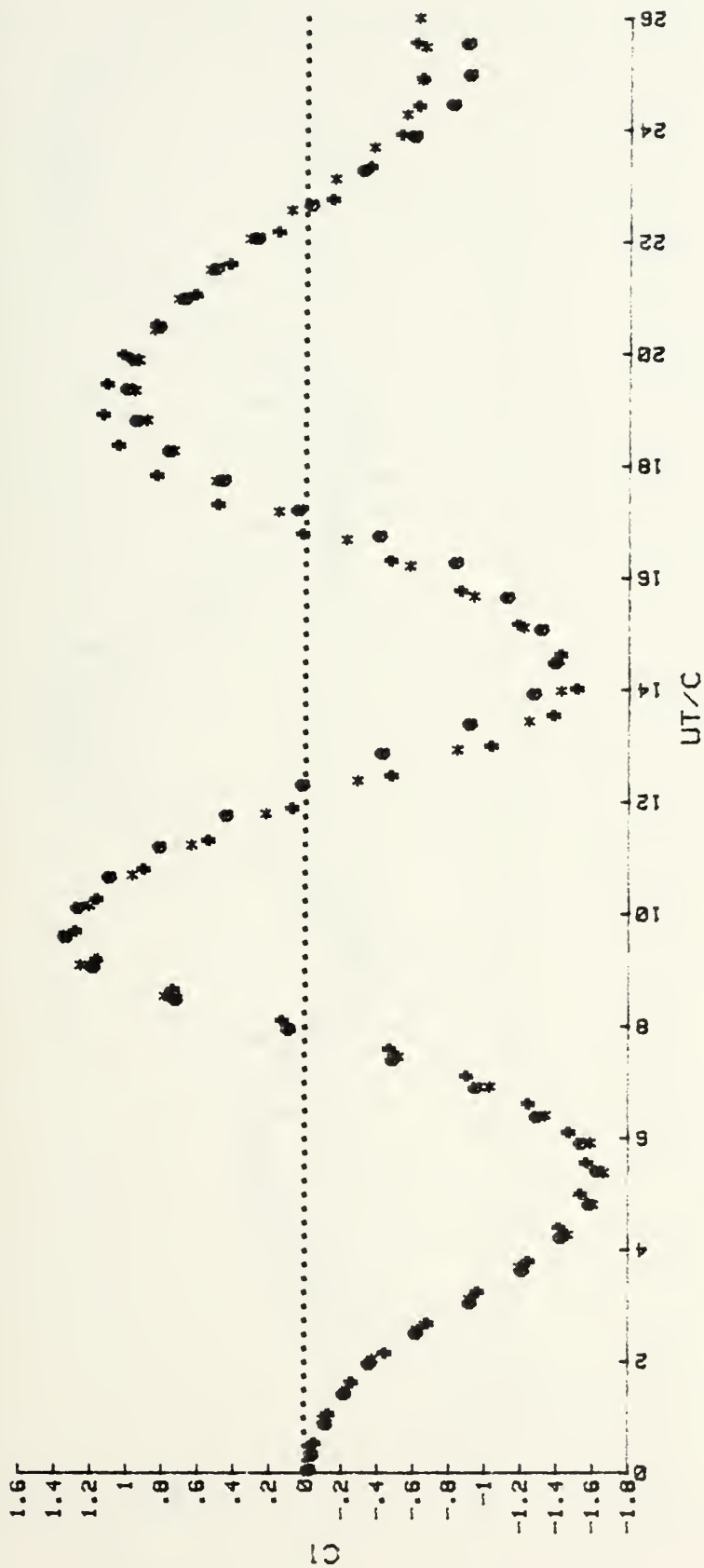


Figure 48. $C1$ vs. UT/C for the D-Shaped Body at -20° .



Figure 49. C_m vs. UT/C for the D-Shaped Body at -20° .

APPENDIX H: REPRESENTATIVE DATA FOR D-SHAPED BODY AT -30 DEGREES

<u>UT/C</u>	<u>Cd</u>	<u>UT/C</u>	<u>C1</u>	<u>UT/C</u>	<u>Cm</u>
.37	.83	.86	-.24	.85	0
.53	.13	.56	-.1	.4	-.28
1.25	.24	1.11	-.14	.75	-.28
1.65	.61	1.64	-.18	1.12	-.29
2.17	1.06	2.18	-.35	1.63	-.27
2.71	1.2	2.7	-.51	2.18	-.26
3.24	1.68	3.24	-.77	2.71	-.25
3.79	1.83	3.8	-1.04	3.22	-.24
4.31	1.78	4.35	-1.29	3.79	-.24
4.86	1.67	4.88	-1.52	4.31	-.24
5.39	1.7	5.42	-1.7	4.86	-.24
5.94	1.71	5.97	-1.78	5.4	-.24
6.48	1.81	6.52	-1.79	5.96	-.24
7.02	1.6	7.05	-1.64	6.48	-.24
7.56	1.61	7.58	-1.37	7.02	-.24
8.1	1.62	8.14	-.96	7.56	-.24
8.63	1.48	8.69	-.44	8.13	-.24
9.19	1.37	9.22	.17	8.65	-.24
9.7	1.52	9.77	.73	9.22	-.25
10.27	1.8	10.3	1.01	9.76	-.25
10.77	2.01	10.86	1.06	10.27	-.25
11.33	2.14	11.41	.9	10.8	-.25
11.88	2.15	11.91	.66	11.34	-.26
12.4	2.09	12.46	.36	11.89	-.25
12.95	1.97	13.02	.01	12.43	-.25
13.49	1.75	13.58	-.43	12.96	-.24
14.03	1.59	14.11	-.84	13.5	-.24
14.55	1.5	14.66	-1.23	14.04	-.23
15.13	1.54	15.17	-1.48	14.56	-.22
15.65	1.57	15.72	-1.6	15.11	-.22
16.19	1.53	16.25	-1.54	15.67	-.22
16.72	1.48	16.83	-1.32	16.19	-.22
17.27	1.47	17.36	-1.03	16.74	-.23
17.82	1.46	17.94	-.62	17.29	-.23
18.35	1.48	18.47	-.25	17.84	-.23
18.88	1.5	19.01	.13	18.36	-.24
19.47	1.53	19.54	.41	18.91	-.25
19.97	1.59	20.08	.58	19.46	-.25
20.51	1.64	20.62	.67	20.01	-.25
21.04	1.67	21.14	.67	20.53	-.25
21.6	1.7	21.69	.65	21.06	-.25
22.14	1.64	22.25	.56	21.59	-.25

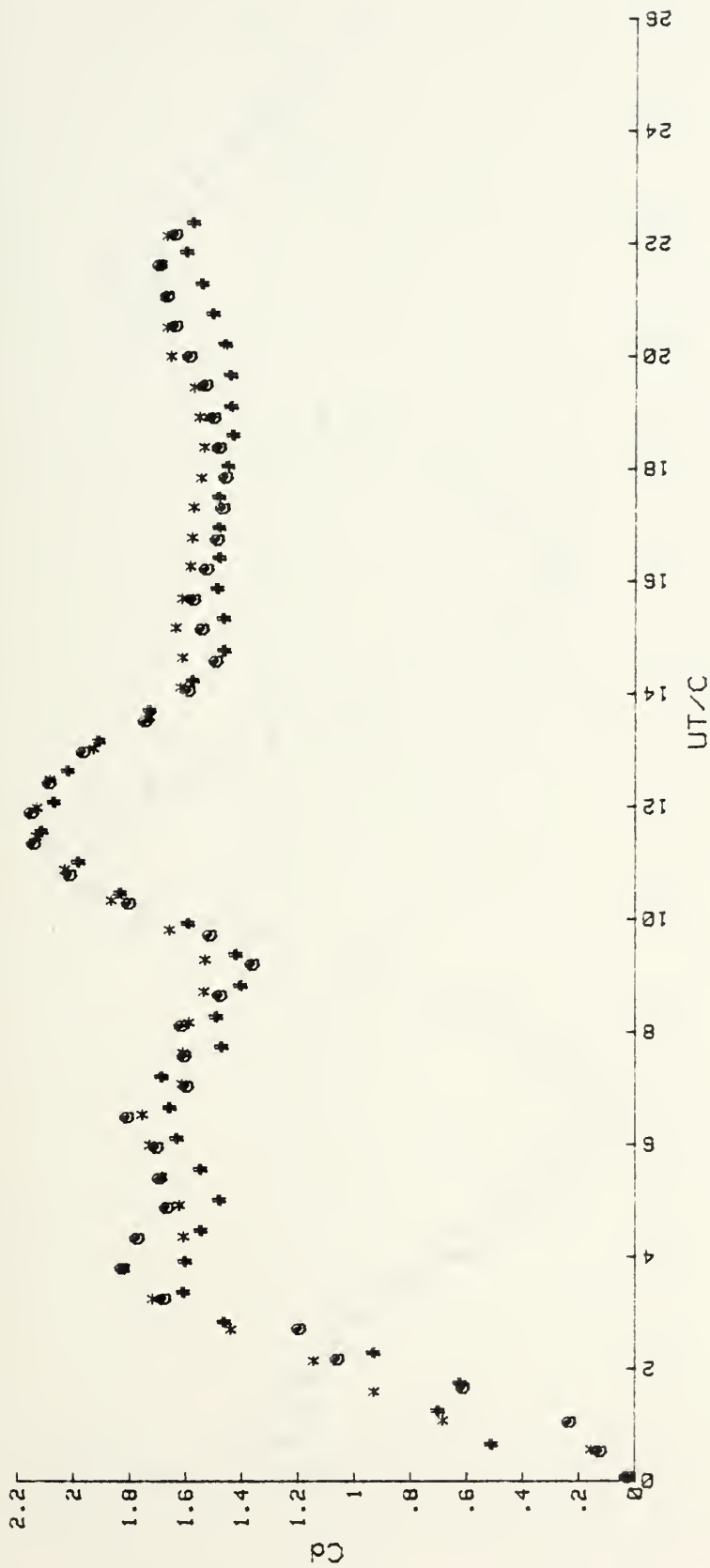


Figure 50. C_d vs. UT/C for the D-Shaped Body at -30° .

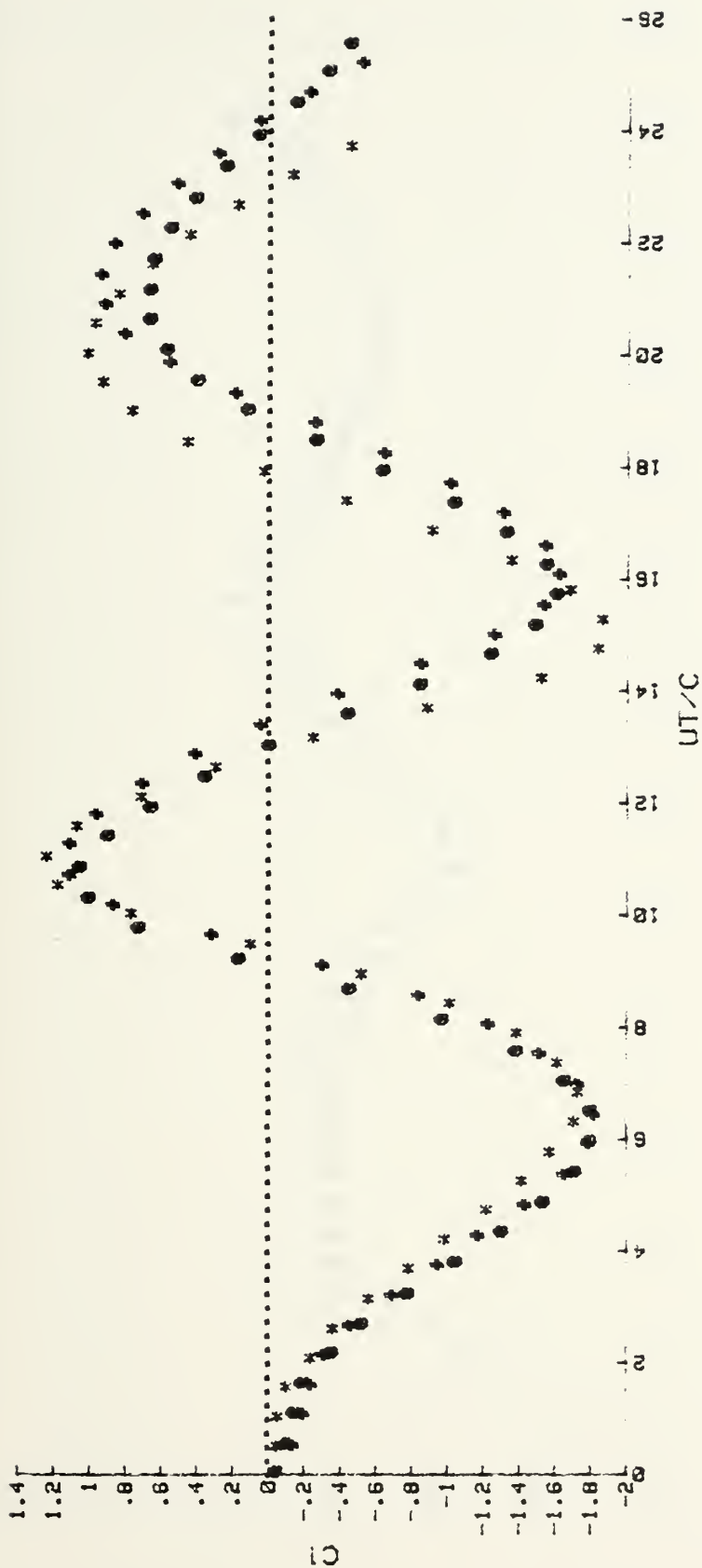


Figure 51. CI vs. UT/C for the D-Shaped Body at -30 deg.



Figure 52. Cm vs. UT/C for the D-Shaped Body at -30 deg.

APPENDIX I: REPRESENTATIVE DATA FOR D-SHAPED BODY AT -45 DEGREES

<u>UT/C</u>	<u>Cd</u>	<u>UT/C</u>	<u>Cl</u>	<u>UT/C</u>	<u>Cm</u>
.05	.04	.06	-.03	.42	-.13
.51	.24	.53	-.04	.98	-.14
1.06	.49	1.09	-.07	1.49	-.15
1.56	.9	1.61	-.09	2.02	-.15
2.11	.74	2.13	-.18	2.61	-.15
2.63	.72	2.66	-.31	3.15	-.14
3.18	1.21	3.17	-.44	3.68	-.14
3.71	1.4	3.68	-.55	4.25	-.14
4.25	1.51	4.22	-.63	4.79	-.13
4.8	1.7	4.78	-.73	5.32	-.13
5.36	1.97	5.38	-.9	5.9	-.12
5.92	2.06	5.98	-1.13	6.46	-.12
6.49	2.01	6.58	-1.37	7.02	-.11
7.03	2	7.19	-1.54	7.57	-.11
7.59	1.81	7.72	-1.68	8.15	-.1
8.12	1.83	8.21	-1.68	8.72	-.1
8.69	1.82	8.74	-1.58	9.24	-.1
9.29	1.75	9.34	-1.41	9.84	-.1
9.78	1.69	9.92	-1.15	10.46	-.1
10.29	1.69	10.31	-.79	11.01	-.1
10.88	1.68	10.76	-.4	11.46	-.1
11.44	1.68	11.25	.02	11.98	-.11
11.92	1.67	11.75	.41	12.53	-.11
12.41	1.67	12.25	.7	13.11	-.11
12.94	1.73	12.77	.86	13.72	-.11
13.48	1.76	13.3	.84	14.24	-.11
14.01	1.79	13.82	.7	14.77	-.11
14.53	1.83	14.37	.45	15.36	-.11
15.05	1.82	15.02	.11	15.9	-.11
15.58	1.76	15.67	-.28	16.4	-.11
16.07	1.67	16.25	-.68	16.93	-.11
16.59	1.6	16.69	-1.12	17.47	-.1
17.08	1.55	17.12	-1.44	17.94	-.1
17.61	1.52	17.61	-1.6	18.45	-.1
18.15	1.47	18.14	-1.59	18.99	-.09
18.69	1.44	18.7	-1.46	19.49	-.09
19.19	1.42	19.25	-1.26	20	-.09
19.72	1.39	19.81	-.94	20.53	-.09
20.31	1.37	20.34	-.55	21.1	-.08
20.84	1.35	20.88	-.13	21.66	-.08
21.4	1.35	21.38	.18	22.2	-.08
22	1.35	21.86	.43	22.7	-.08
22.56	1.33	22.37	.63	23.26	-.09
23.07	1.34	22.84	.75	23.81	-.09
23.62	1.36	23.36	.79	24.29	-.09
24.19	1.38	23.9	.78	24.75	-.09
24.69	1.37	24.44	.68	25.29	-.09

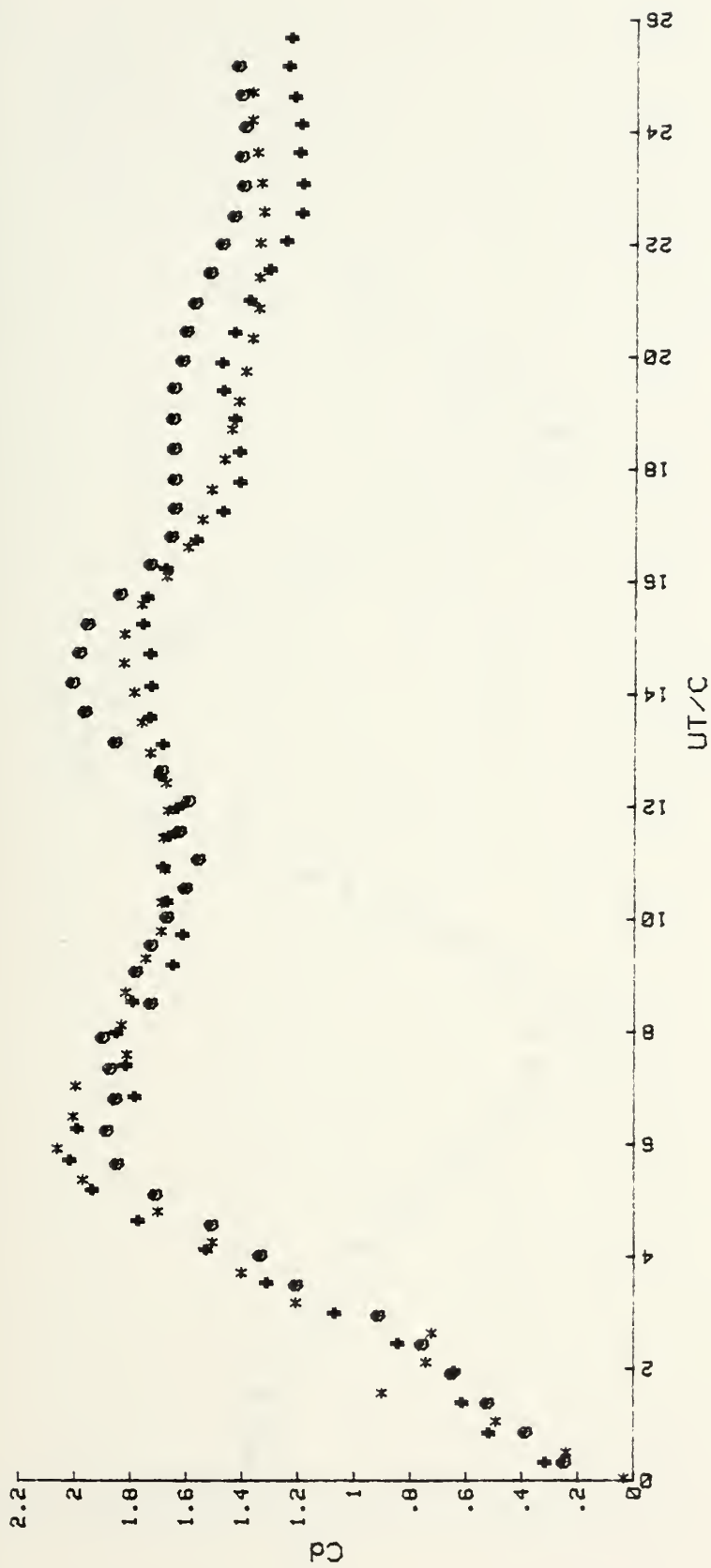


Figure 53. C_d vs. UT/C for the D-Shaped Body at -45° .

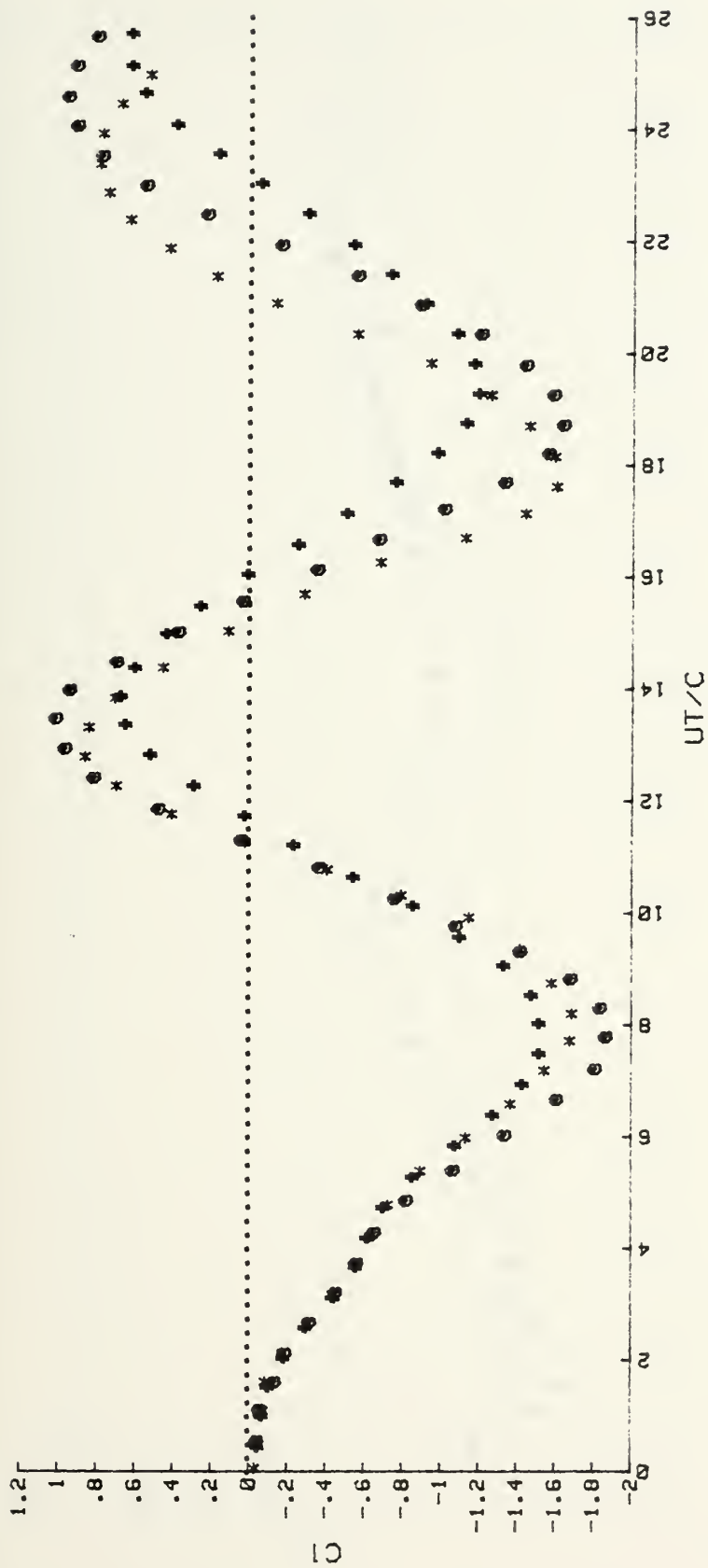


Figure 54. C_1 vs. UT/C for the D-Shaped Body at -45° .

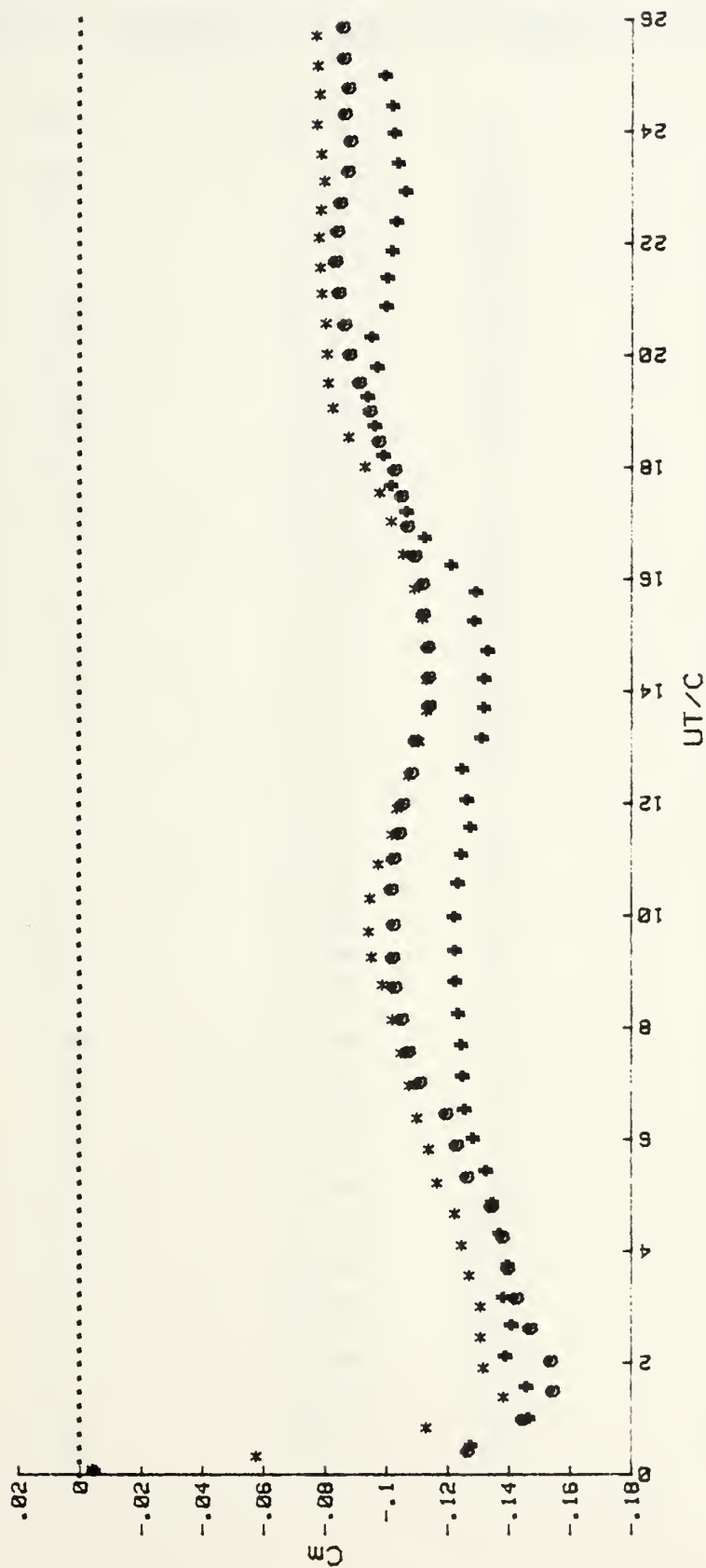


Figure 55. C_m vs. UT/C for the D-Shaped Body at -45° .

APPENDIX J: REPRESENTATIVE DATA FOR D-SHAPED BODY AT -90 DEGREES

<u>UT/C</u>	<u>Cd</u>	<u>UT/C</u>	<u>C1</u>	<u>UT/C</u>	<u>Cm</u>
.06	.01	.07	-.02	.07	0
.85	.19	.55	-.02	.52	0
1.39	.31	1.06	-.02	1.08	0
1.93	.4	1.62	-.01	1.59	0
2.45	.73	2.14	-.02	2.12	0
3	1.02	2.67	-.03	2.64	.01
3.53	1.29	3.2	-.05	3.19	.01
4.04	1.58	3.73	-.07	3.7	.01
4.59	1.66	4.25	-.06	4.24	.01
5.13	1.57	4.79	-.08	4.79	.01
5.67	1.44	5.33	-.11	5.29	0
6.21	1.36	5.84	-.13	5.81	.01
6.76	1.13	6.39	-.18	6.34	.01
7.29	1.14	6.93	-.24	6.89	.01
7.84	1.12	7.45	-.29	7.43	.01
8.36	1.13	7.99	-.32	7.94	.01
8.9	1.07	8.52	-.36	8.48	.01
9.42	1.03	9.07	-.38	9.02	.01
9.96	1.03	9.58	-.35	9.54	.01
10.49	1.03	10.12	-.29	10.06	.01
11.04	.99	10.65	-.23	10.62	.01
11.57	.98	11.2	-.16	11.12	.01
12.13	.96	11.71	-.1	11.66	.02
12.67	.96	12.26	-.01	12.18	.02
13.19	.94	12.79	.09	12.72	.01
13.73	.92	13.32	.18	13.27	.01
14.26	.89	13.85	.29	13.78	.01
14.82	.86	14.39	.36	14.28	.01
15.36	.87	14.92	.41	14.83	.01
15.87	.85	15.45	.41	15.37	0
16.41	.85	15.98	.39	15.88	0
16.95	.83	16.53	.34	16.42	0
17.48	.8	17.05	.27	16.95	0
18.02	.78	17.6	.2	17.47	.01
18.55	.77	18.13	.11	18.01	.01
19.09	.75	18.65	.03	18.55	.01
19.62	.74	19.19	-.06	19.08	.01
20.17	.74	19.72	-.15	19.61	.01
20.7	.72	20.24	-.21	20.13	.01
21.25	.71	20.77	-.24	20.68	.01
21.76	.69	21.31	-.25	21.19	.01
22.3	.7	21.85	-.23	21.72	.01
22.84	.67	22.39	-.17	22.27	.01
23.4	.64	22.91	-.1	22.78	.01
23.93	.62	23.43	-.01	23.32	.01

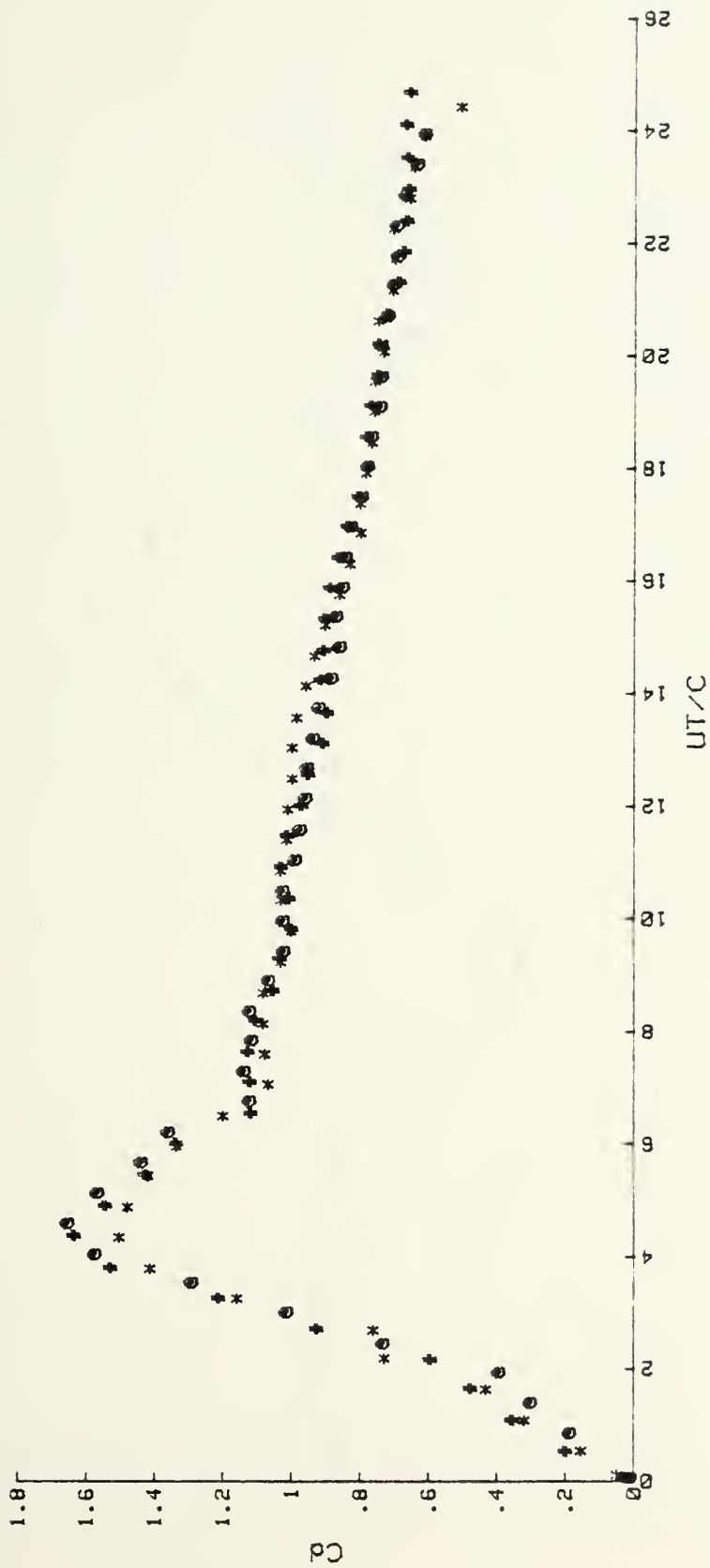


Figure 56. Cd vs. UT/C for the D-Shaped Body at -90 deg.

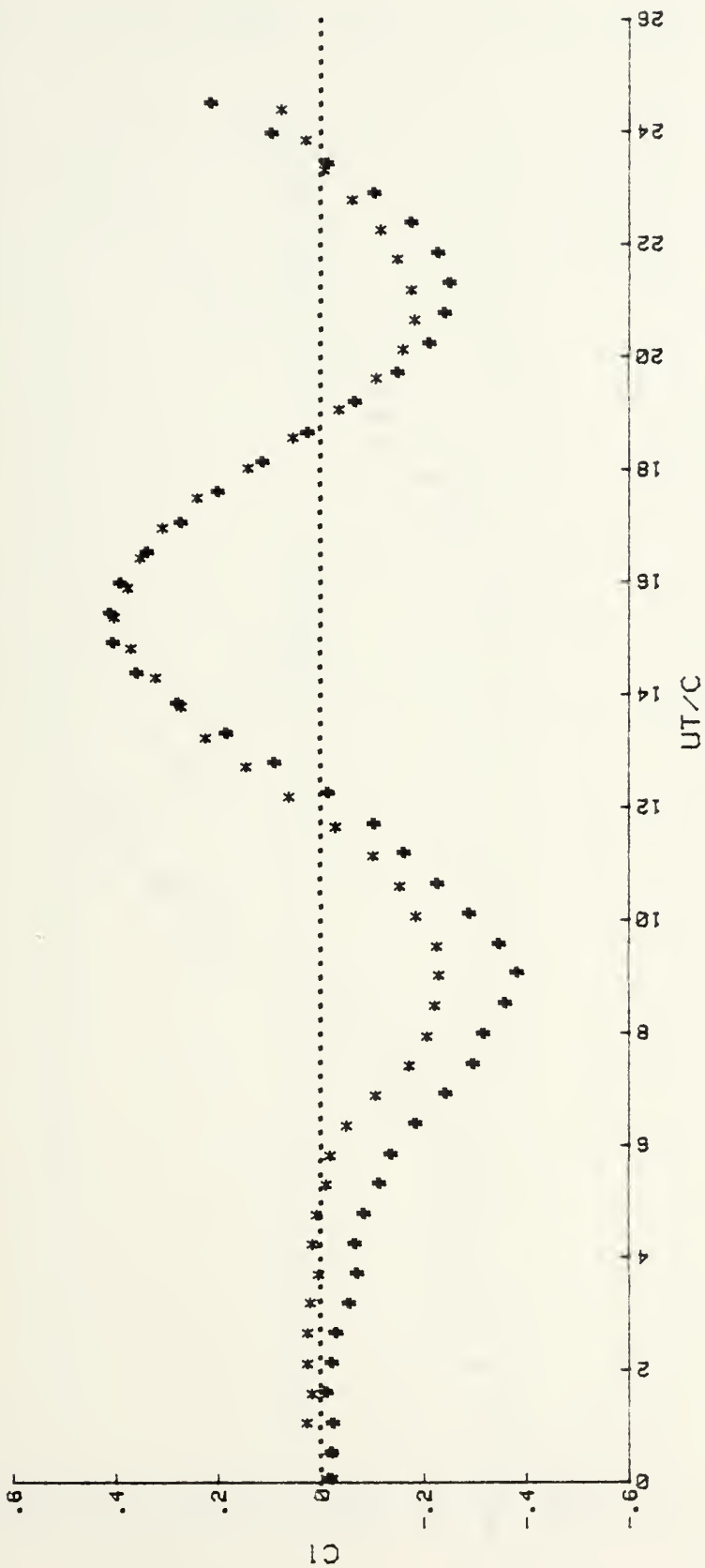


Figure 57. C1 vs. UT/C for the D-Shaped Body at -90° .

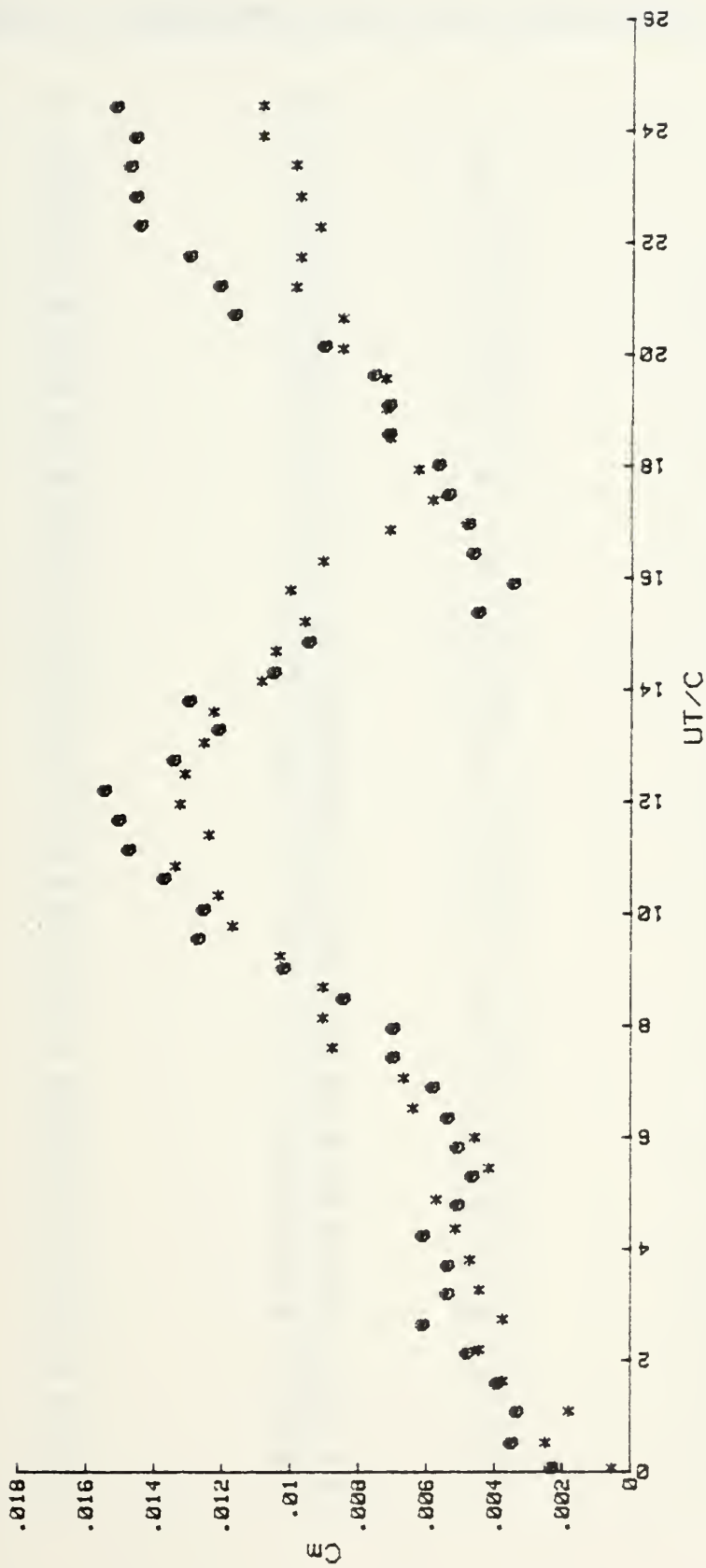


Figure 58. C_m vs. UT/C for the D-Shaped Body at -90° .

APPENDIX K: REPRESENTATIVE DATA FOR T-SHAPED BODY AT 0 DEGREES

<u>UT/C</u>	<u>Cd</u>	<u>UT/C</u>	<u>Cl</u>	<u>UT/C</u>	<u>Cm</u>
.61	.86	.24	.32	.61	.13
1.2	.85	.67	0	.61	.13
1.85	.98	.87	-.26	1.18	.21
2.44	1.14	1.46	-.35	1.84	.24
3.08	1.51	2.09	-.56	2.51	.22
3.71	1.68	2.72	-.8	3.11	.19
4.29	1.62	3.34	-1.04	3.71	.17
4.92	1.79	3.93	-1.23	4.28	.14
5.54	1.79	4.57	-1.37	4.88	.12
6.14	1.91	5.2	-1.31	5.52	.14
6.77	1.97	5.8	-1.12	6.07	.18
7.4	1.89	6.42	-.81	6.7	.19
7.96	1.98	7.03	-.41	7.32	.21
8.61	1.95	7.64	.11	7.93	.24
9.27	2.06	8.27	.79	8.56	.26
9.83	2.1	8.89	1.55	9.2	.33
10.46	2.17	9.51	2.07	9.82	.33
11.03	2.22	10.13	2.29	10.37	.35
11.67	1.97	10.78	2.19	11.01	.35
12.29	1.72	11.52	1.85	11.6	.3
12.9	1.51	12.21	1.43	12.17	.25
13.49	1.54	12.76	.95	12.79	.21
14.13	1.6	13.29	.32	13.41	.16
14.74	1.76	13.91	-.26	14.02	.11
15.33	1.92	14.52	-.58	14.62	.09
15.91	1.94	15.1	-.63	15.24	.11
16.6	1.89	15.79	-.58	15.82	.17
17.18	1.79	16.42	-.32	16.44	.24
17.78	1.76	16.97	0	17.07	.29
18.42	1.73	17.54	.39	17.68	.32
19.01	1.78	18.15	.76	18.26	.34
19.59	1.71	18.76	1.08	18.89	.35
20.21	1.68	19.39	1.31	19.48	.33
20.85	1.59	19.96	1.44	20.1	.32
21.48	1.53	20.62	1.45	20.72	.3
22.11	1.53	21.25	1.37	21.35	.28
22.68	1.49	21.85	1.22	21.95	.23
23.32	1.46	22.48	1.01	22.52	.22
23.93	1.45	23.11	.74	23.11	.21
24.52	1.49	23.75	.39	23.77	.2
25.13	1.47	24.43	.03	24.38	.21
25.79	1.43	25.1	-.35	24.97	.22
26.38	1.41	25.7	-.6	25.59	.22
27	1.43	26.22	-.74	26.2	.23
27.59	1.41	26.79	-.8	26.82	.24
28.25	1.35	27.44	-.77	27.43	.24
28.85	1.44	28.08	-.69	27.99	.24

APPENDIX L: REPRESENTATIVE DATA FOR T-SHAPED BODY AT +5 DEGREES

<u>UT/C</u>	<u>Cd</u>	<u>UT/C</u>	<u>Cl</u>	<u>UT/C</u>	<u>Cd</u>
.89	.44	.14	.08	.88	.22
1.53	.84	.61	-.05	1.62	.16
2.05	1.01	1.22	-.4	2.24	.12
2.74	1.28	1.88	-.8	2.85	.08
3.32	1.43	2.45	-.81	3.46	.05
3.93	1.55	3.1	-.96	4.03	.04
4.58	1.72	3.69	-1.09	4.63	.06
5.21	1.86	4.33	-1.13	5.25	.13
5.82	2.07	4.97	-1.11	5.86	.22
6.48	2.22	5.58	-.98	6.48	.28
7.06	2.22	6.15	-.87	7.11	.29
7.67	2.11	6.81	-.68	7.69	.29
8.29	1.99	7.41	-.43	8.35	.32
8.9	1.97	8.04	0	8.92	.34
9.54	1.96	8.65	.5	9.54	.35
10.2	2.09	9.24	1.01	10.16	.35
10.77	2.35	9.9	1.54	10.82	.35
11.39	2.58	10.48	1.87	11.41	.33
12.03	2.64	11.09	1.96	11.94	.33
12.66	2.69	11.71	1.82	12.64	.32
13.29	2.58	12.35	1.45	13.16	.32
13.91	2.44	12.97	.81	13.82	.31
14.5	2.36	13.59	0	14.43	.29
15.12	2.33	14.18	-.96	15.03	.26
15.73	2.35	14.78	-1.73	15.65	.26
16.34	2.41	15.4	-2.2	16.23	.25
16.98	2.32	15.93	-2.32	16.84	.25
17.6	2.3	16.66	-2.12	17.46	.26
18.23	2.21	17.27	-1.72	18.07	.28
18.85	2.11	17.91	-1.19	18.69	.28
19.49	2.02	18.49	-.67	19.28	.28
20.1	1.9	19.11	-.12	19.91	.3
20.72	1.8	19.74	.42	20.53	.32
21.34	1.74	20.34	.87	21.16	.32
21.98	1.71	20.94	1.28	21.76	.3
22.59	1.65	21.62	1.83	22.35	.27
23.19	1.61	22.23	1.8	22.95	.26
23.83	1.59	22.8	1.84	23.56	.24
24.48	1.55	23.45	1.76	24.19	.23
25.05	1.53	24.09	1.55	24.81	.23
25.69	1.51	24.65	1.27	25.42	.24
26.3	1.52	25.26	.91	26	.25
26.93	1.52	25.9	.44	26.62	.25
27.58	1.53	26.47	-.03	27.22	.24
28.17	1.54	27.1	-.45	27.84	.22

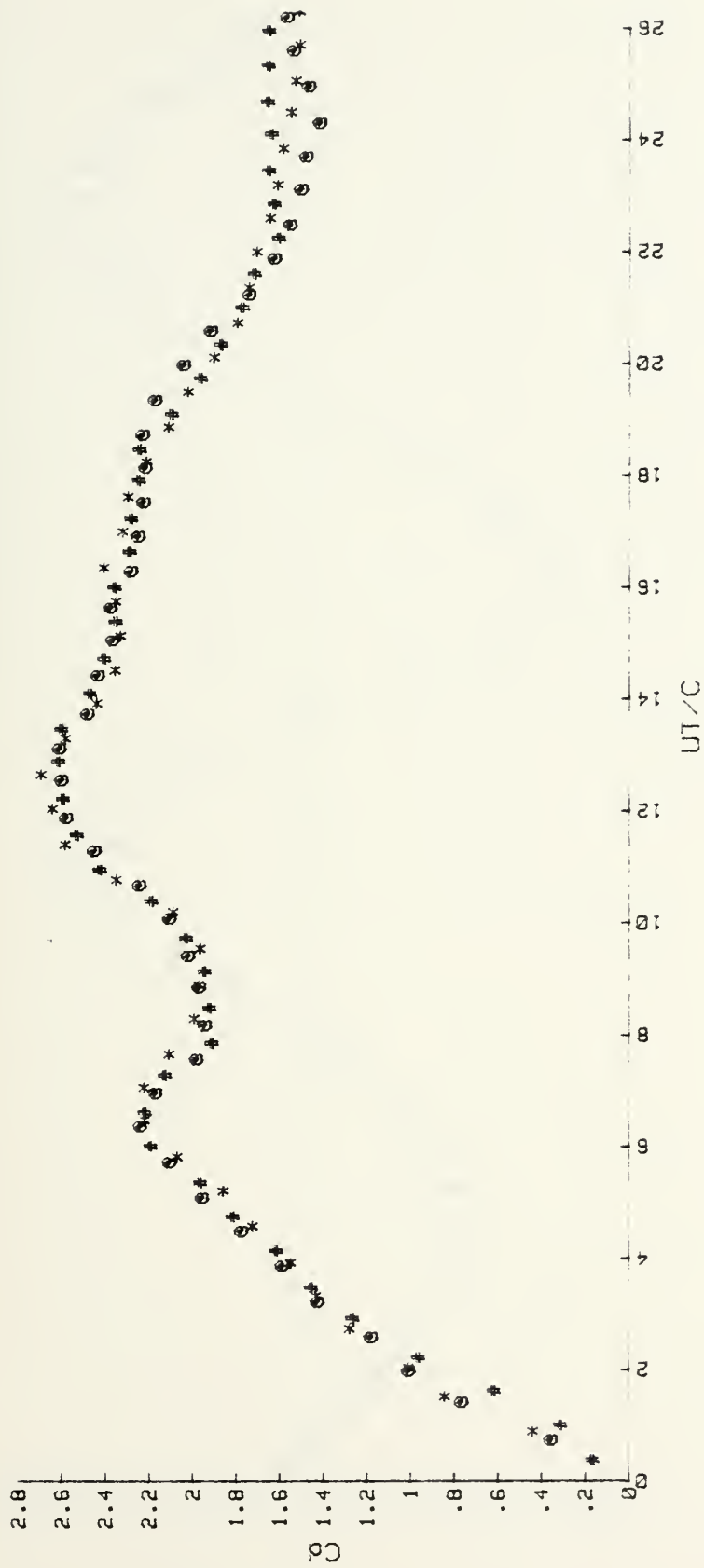


Figure 59. C_d vs. U_T/C for the T-Shaped Body at +5 deg.



Figure 60. $C1$ vs. UT/C for the T-Shaped Body at $+5^\circ$.

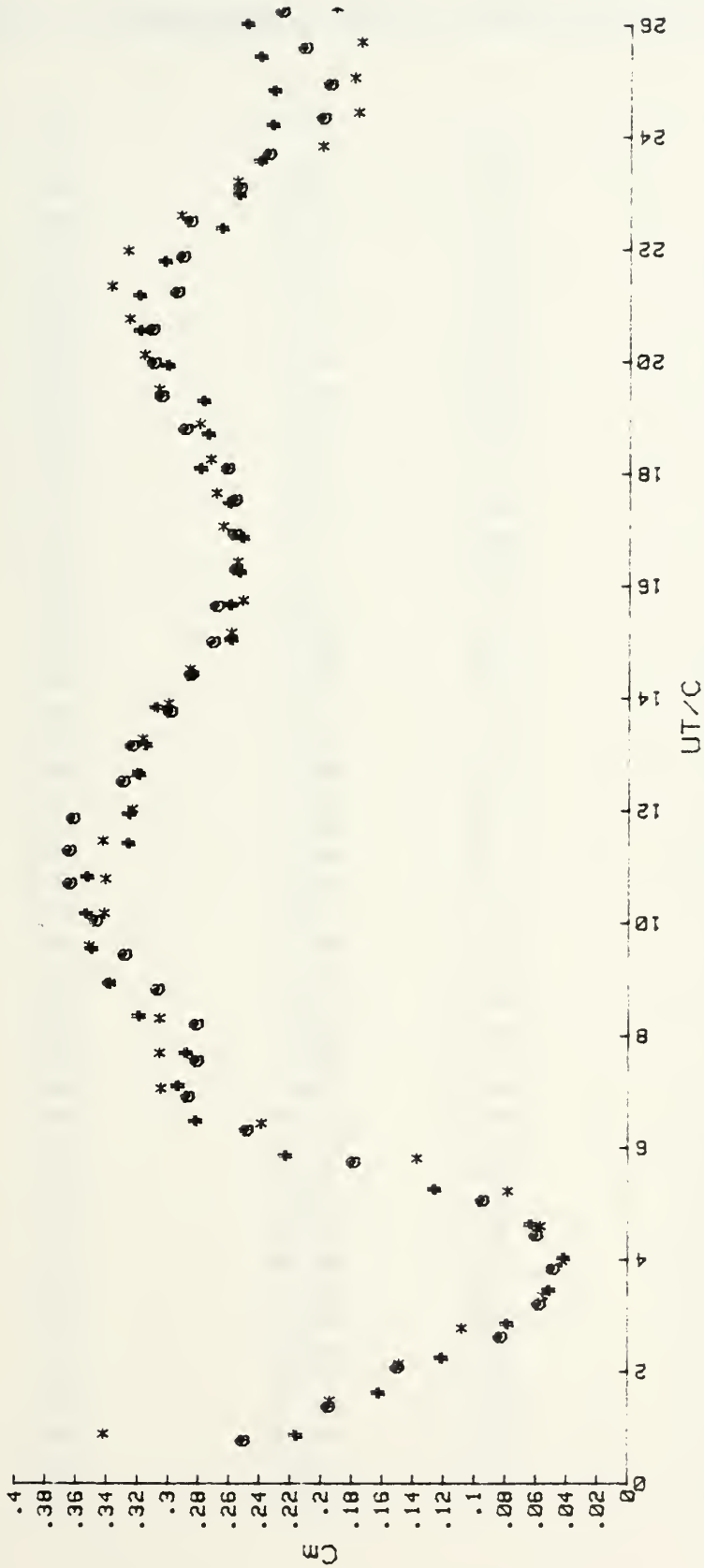


Figure 61. C_m vs. UT/C for the T-Shaped Body at +5 deg.

APPENDIX M: REPRESENTATIVE DATA FOR T-SHAPED BODY AT +12 DEGREES

<u>UT/C</u>	<u>Cd</u>	<u>UT/C</u>	<u>Cl</u>	<u>UT/C</u>	<u>Cm</u>
.62	.17	.24	-.06	.39	.04
1.27	.22	.86	-.18	1	.05
1.87	.82	1.48	-.51	1.63	.07
2.48	1.17	2.1	-.61	2.23	.08
3.07	1.33	2.74	-.77	2.85	-.01
3.69	1.62	3.36	-.87	3.45	-.03
4.36	2.05	4	-.98	4.09	-.03
5.02	2.37	4.62	-1.14	4.66	.03
5.77	2.42	5.28	-1.38	5.29	.15
6.42	2.35	5.97	-1.62	5.92	.24
7.09	2.41	6.69	-1.73	6.54	.24
7.76	2.38	7.3	-1.7	7.11	.23
8.25	2.1	7.86	-1.53	7.72	.22
8.87	2.24	8.4	-1.35	8.36	.24
9.42	2.12	9	-1.09	9.01	.25
9.97	1.98	9.61	-.74	9.6	.25
10.54	1.91	10.24	-.33	10.2	.27
11.14	1.87	10.85	.06	10.83	.27
11.78	1.88	11.49	.43	11.42	.28
12.4	1.91	12.11	.73	12.03	.29
13.03	2.01	12.75	.93	12.72	.29
13.62	2.08	13.34	1.03	13.31	.29
14.25	2.13	13.97	.99	13.85	.29
14.9	2.16	14.62	.86	14.51	.29
15.48	2.13	15.24	.61	15.11	.28
16.09	2.07	15.86	.31	15.72	.28
16.71	1.99	16.5	-.04	16.34	.27
17.29	1.87	17.19	-.41	16.93	.25
17.88	1.84	17.88	-.75	17.57	.24
18.52	1.83	18.59	-1.04	18.15	.23
19.13	1.84	19.19	-1.28	18.76	.22
19.73	1.88	19.82	-1.4	19.4	.22
20.35	1.88	20.5	-1.44	19.98	.23
21.01	1.86	21.13	-1.38	20.61	.23
21.62	1.8	21.71	-1.18	21.22	.24
22.21	1.68	22.2	-.91	21.83	.24
22.84	1.6	22.76	-.66	22.45	.23
23.45	1.59	23.36	-.33	23.05	.24
24.04	1.6	23.99	.02	23.67	.24
24.73	1.63	24.61	.35	24.27	.24
25.3	1.65	25.24	.65	24.89	.25
25.93	1.71	25.83	.88	25.5	.26
26.56	1.78	26.47	1.03	26.1	.26
27.2	1.82	27.09	1.08	26.71	.26
27.83	1.83	27.74	1.03	27.33	.27
28.48	1.84	28.39	.85	27.95	.27
29.14	1.81	28.98	.66	28.56	.25

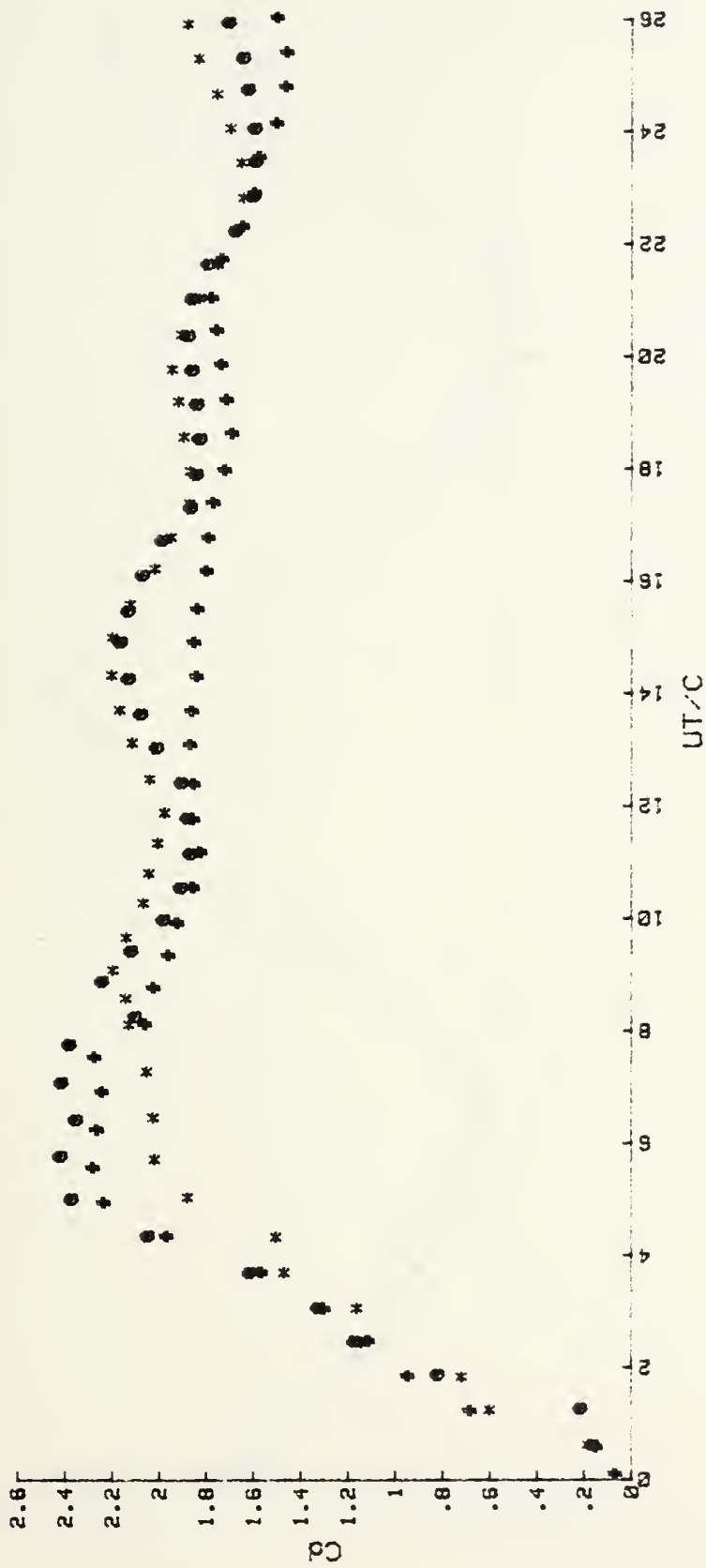


Figure 62. Cd vs. UT/C for the T-Shaped Body at +10 deg.



Figure 63. CI vs. UT/C for the T-Shaped Body at +10 deg.

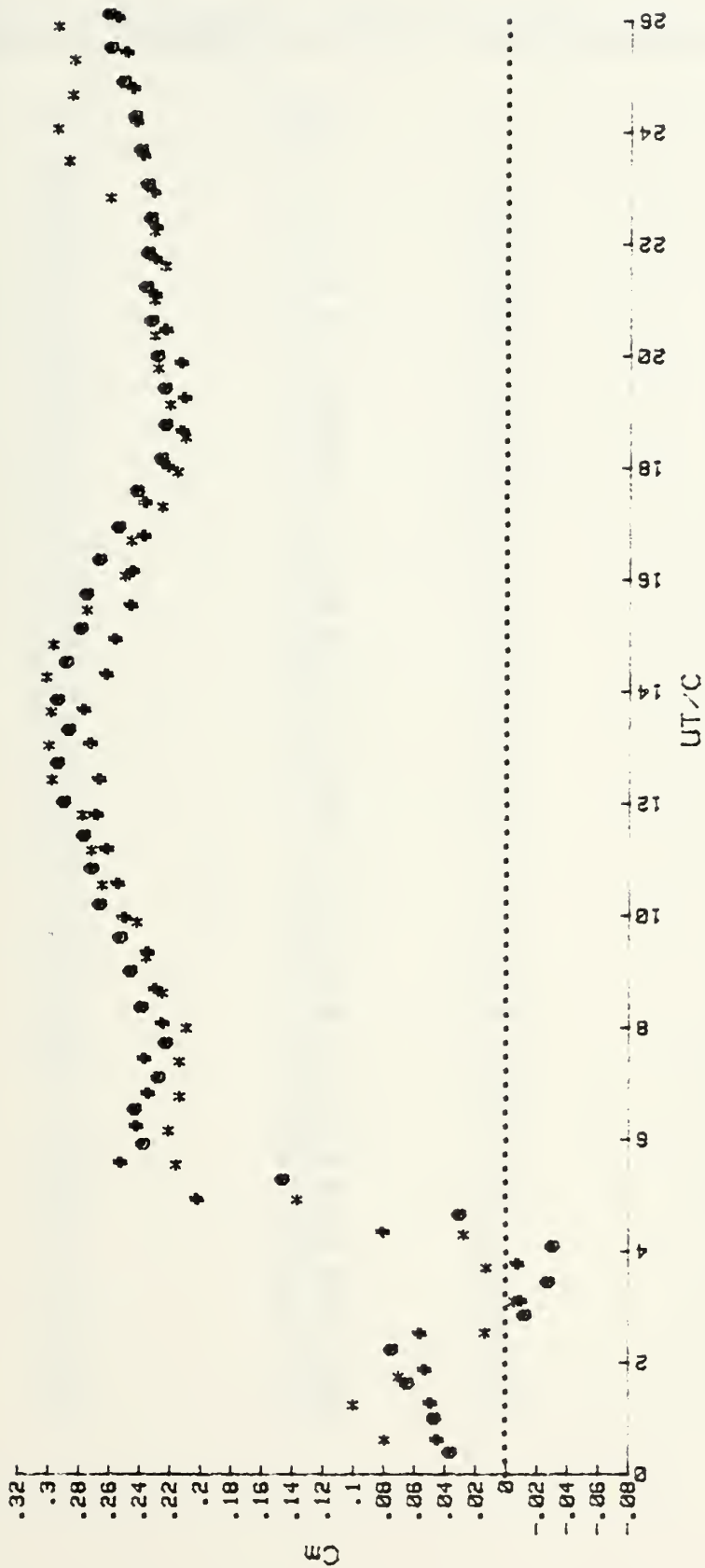


Figure 64. Cm vs. UT/C for the T-Shaped Body at +10 deg.

APPENDIX N: REPRESENTATIVE DATA FOR T-SHAPED BODY AT +15 DEGREES

<u>UT/C</u>	<u>Cd</u>	<u>UT/C</u>	<u>C1</u>	<u>UT/C</u>	<u>Cm</u>
.91	.33	.13	-.17	1.85	-.25
1.26	.55	.61	-.22	2.48	-.24
1.88	1.24	1.21	-.27	3.87	-.25
2.44	1.23	1.83	-.58	3.7	-.25
3.22	1.51	2.44	-.83	4.32	.25
3.62	1.77	3.88	-.98	4.93	.17
4.24	2.12	3.71	-1.11	5.57	.2
4.85	2.52	4.33	-1.27	6.2	.19
5.46	2.54	4.96	-1.48	6.9	.19
6.12	2.46	5.61	-1.63	7.39	.19
6.68	2.42	6.16	-1.65	7.97	.19
7.3	2.44	6.8	-1.53	9.23	.2
7.85	2.31	7.41	-1.41	8.64	.2
8.51	2.25	8.83	-1.17	9.89	.21
9.16	2.19	8.65	-.9	10.52	.21
9.75	2.24	9.26	-.57	11.14	.23
10.36	2.25	9.86	-.22	11.73	.28
11	2.22	10.51	.16	12.31	.29
11.6	2.28	11.13	.31	12.96	.27
12.19	2.2	11.71	.69	13.56	.27
12.8	2.33	12.32	.79	14.18	.28
13.42	2.39	12.98	.77	14.81	.26
14.03	2.43	13.59	.58	15.45	.25
14.61	2.42	14.17	.37	16.82	.22
15.26	2.33	14.79	.1	16.61	.2
15.85	2.24	15.43	-.2	17.28	.2
16.45	2.11	16.81	-.51	17.89	.2
17.05	2.24	16.67	-.84	18.53	.21
17.68	2.23	17.27	-1.12	19.15	.21
18.3	2.21	17.85	-1.26	19.72	.21
18.91	2.25	18.52	-1.27	20.35	.22
19.54	2.22	19.1	-1.15	20.97	.22
20.11	2	19.73	-.98	21.58	.22
20.69	1.98	20.36	-.74	22.19	.21
21.32	1.93	20.99	-.48	22.82	.2
21.94	1.88	21.61	-.22	23.43	.2
22.52	1.84	22.2	.25	24.03	.22
23.11	1.8	22.84	.31	24.64	.23
23.8	1.74	23.46	.5	25.29	.24
24.37	1.75	24.07	.64	25.88	.25
24.99	1.78	24.67	.68	26.55	.25
25.63	1.83	25.31	.84	27.16	.24
26.2	1.86	25.93	.53	27.78	.23
26.78	1.88	26.52	.36	28.39	.23

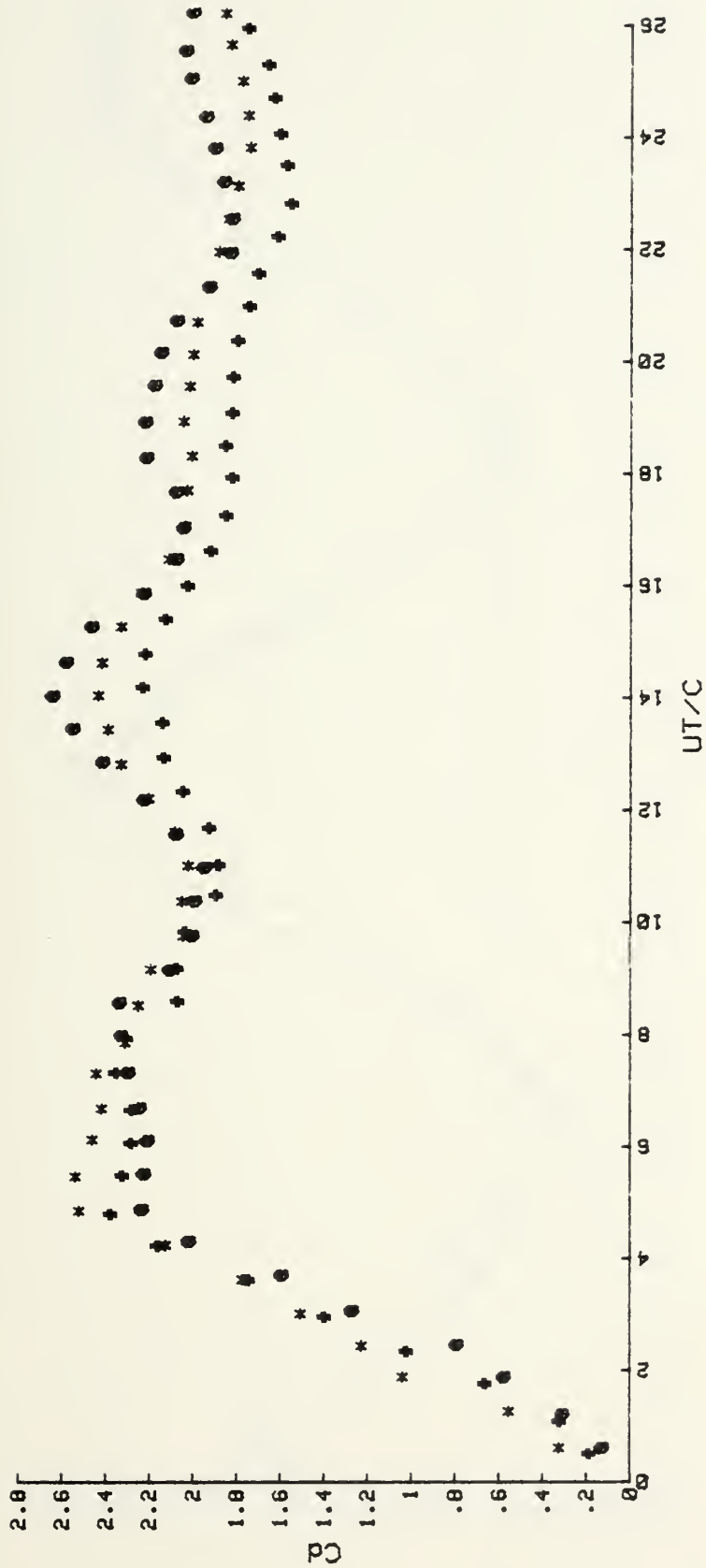


Figure 65. C_d vs. UT/C for the T-Shaped Body at +15 deg.



Figure 66. CI vs. UT/C for the T-Shaped Body at +15 deg.

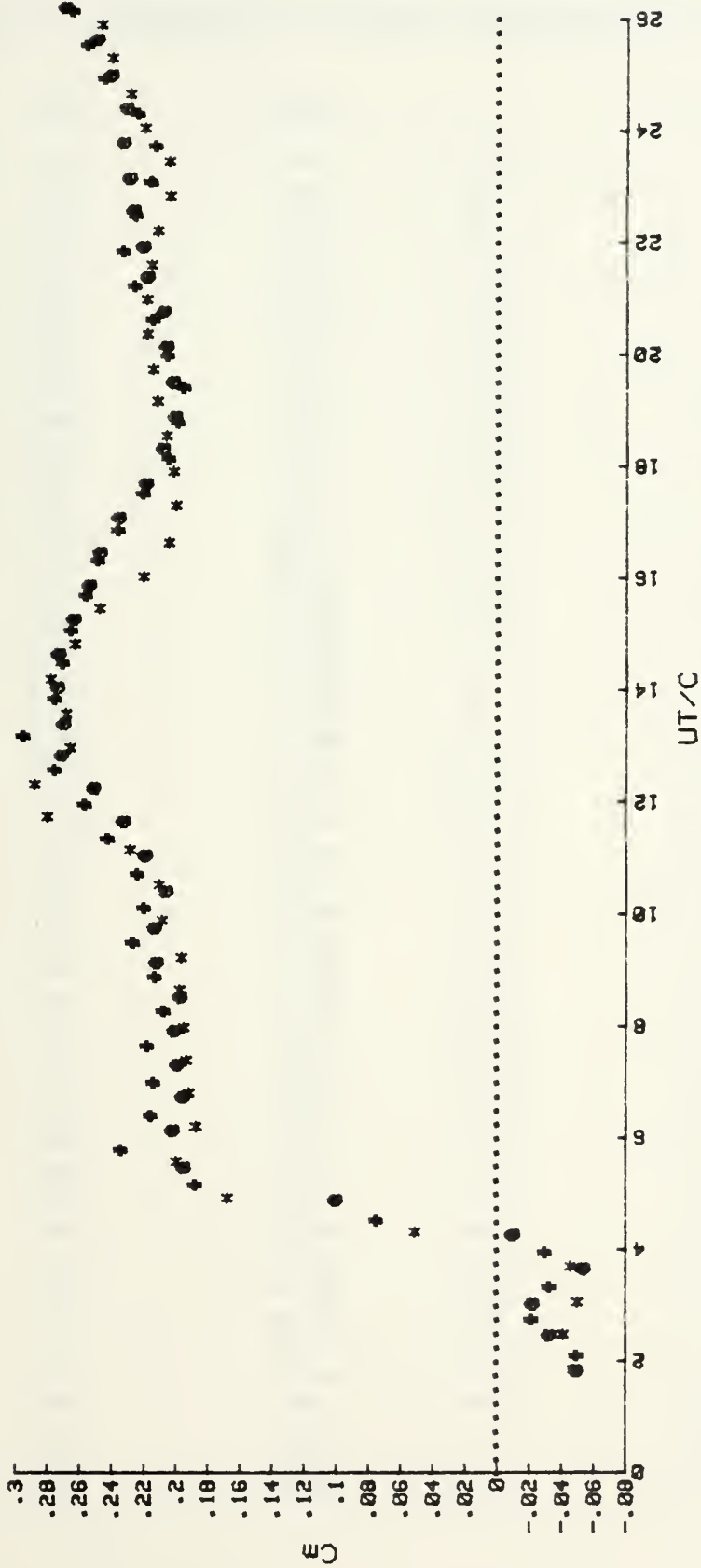


Figure 67. C_m vs. UT/C for the T-Shaped Body at +15 deg.

APPENDIX 0: REPRESENTATIVE DATA FOR T-SHAPED BODY AT +20 DEGREES

<u>UT/C</u>	<u>Cd</u>	<u>UT/C</u>	<u>Ci</u>	<u>UT/C</u>	<u>Cm</u>
.48	.14	.12	-.24	.47	-.08
1.87	.4	.62	-.21	1.87	-.15
1.87	.77	1.28	0	1.7	-.08
2.3	.96	1.89	-.42	2.34	-.07
2.88	1.41	2.52	-.46	2.9	-.07
3.5	1.57	3.09	-.59	3.52	-.07
4.15	2.01	3.79	-.82	4.09	.03
4.73	2.25	4.37	-1.13	4.68	.14
5.41	2.31	5.02	-1.49	5.31	.17
6.03	2.29	5.67	-1.81	5.93	.18
6.64	2.34	6.29	-2.03	6.55	.15
7.32	2.5	6.9	-2.18	7.13	.17
7.95	2.56	7.56	-2.2	7.74	.19
8.58	2.6	8.17	-2.11	8.35	.21
9.15	2.39	8.85	-1.8	8.98	.21
9.58	2.14	9.53	-1.28	9.61	.2
10.28	2.08	10.03	-.75	10.18	.19
10.87	2.05	10.67	-.17	10.77	.17
11.46	2.04	11.29	.44	11.35	.19
12.1	2.24	11.92	.92	11.99	.25
12.79	2.48	12.55	1.27	12.62	.3
13.45	2.62	13.18	1.38	13.21	.3
14.16	2.74	13.78	1.27	13.83	.31
14.77	2.75	14.44	.91	14.43	.3
15.35	2.67	15.07	.45	15.02	.29
15.92	2.45	15.71	-.15	15.62	.27
16.4	2.26	16.33	-.85	16.23	.23
17.03	2.24	16.98	-1.51	16.83	.22
17.65	2.29	17.59	-1.95	17.42	.22
18.19	2.24	18.18	-2.13	18.03	.23
18.77	2.17	18.85	-2.12	18.64	.24
19.35	2.17	19.5	-1.93	19.25	.25
19.93	2.15	20.21	-1.64	19.87	.26
20.5	2.13	20.81	-1.22	20.47	.26
21.13	2.08	21.37	-.74	21.08	.25
21.7	1.93	21.98	-.21	21.7	.23
22.28	1.87	22.61	.34	22.28	.21
22.9	1.86	23.23	.82	22.91	.22
23.52	1.9	23.84	1.14	23.48	.25
24.1	1.97	24.48	1.35	24.08	.27
24.7	1.98	25.11	1.39	24.7	.28
25.28	2	25.79	1.33	25.29	.27
25.94	2.01	26.39	1.11	25.94	.28
26.51	1.97	27	.82	26.51	.28
27.14	1.78	27.65	.49	27.12	.28
27.73	1.65	28.3	.1	27.75	.24
28.39	1.51	28.99	-.35	28.32	.21

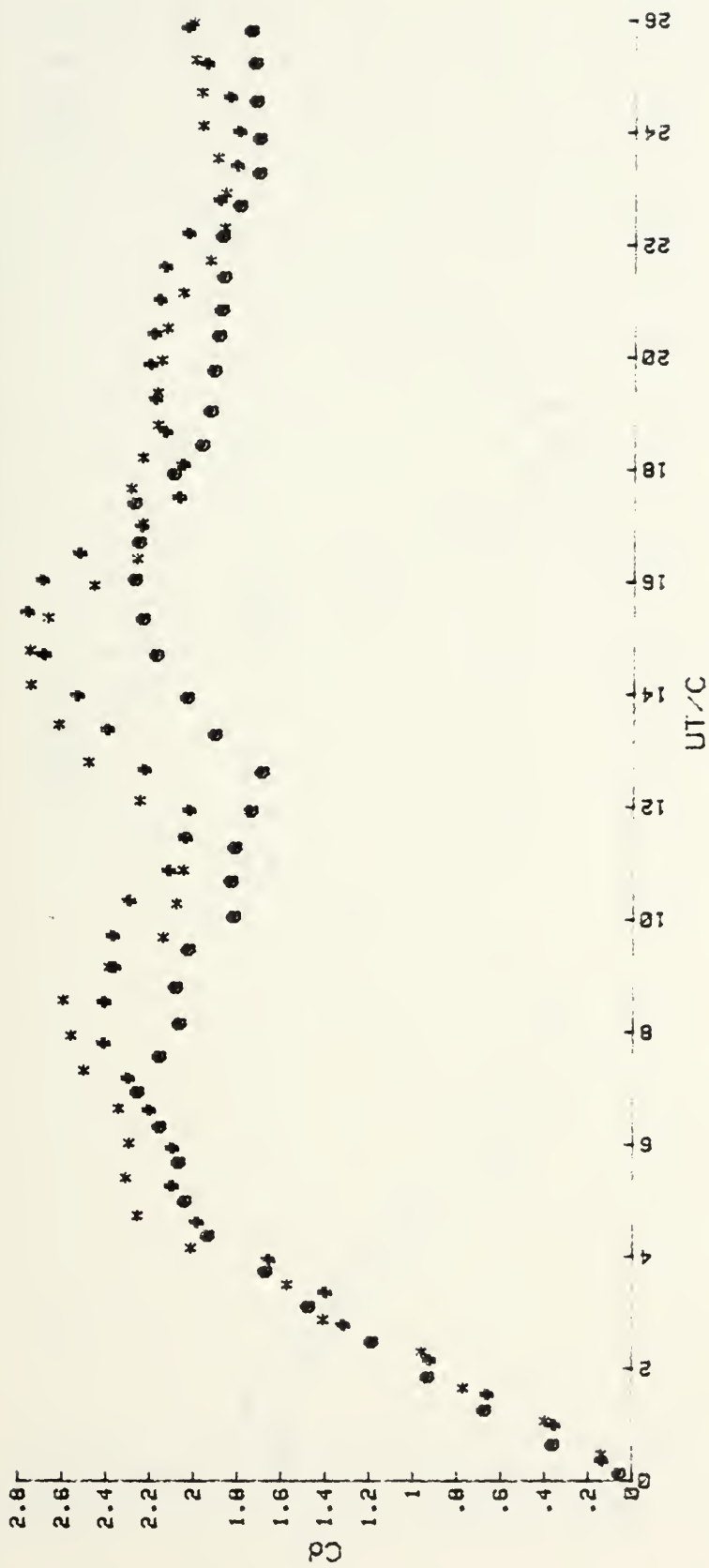


Figure 68. C_d vs. UT/C for the T-Shaped Body at +20 deg.

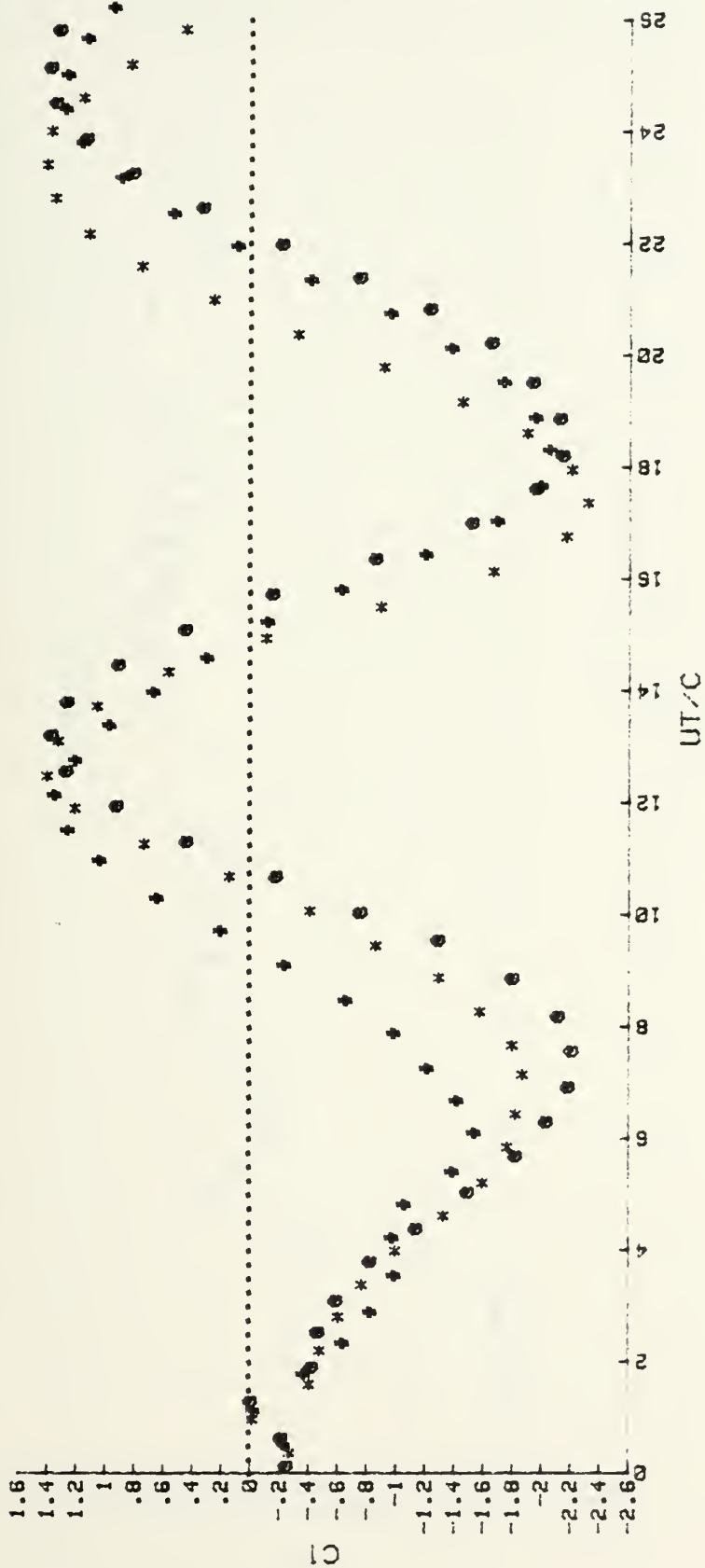


Figure 69. $C1$ vs. UT/C for the T-Shaped Body at +20 deg.

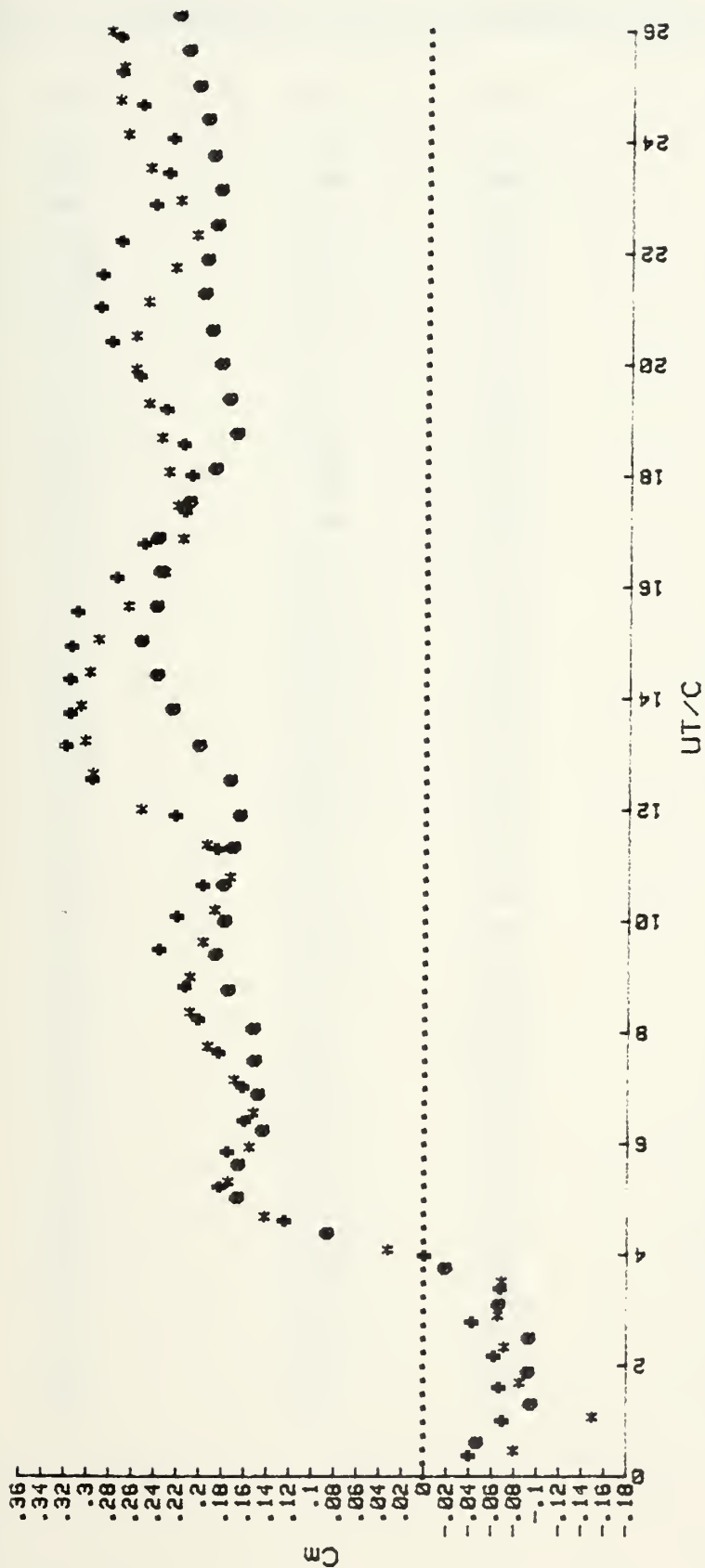


Figure 70. C_m vs. UT/C for the T-Shaped Body at +20 deg.

APPENDIX P: REPRESENTATIVE DATA FOR T-SHAPED BODY AT +25 DEGREES

<u>UT/C</u>	<u>Cd</u>	<u>UT/C</u>	<u>Cl</u>	<u>UT/C</u>	<u>Cm</u>
.63	.26	.13	-.46	.81	.2
1.28	.39	.48	-.38	.92	-.23
1.89	.88	1.03	.21	1.1	-.45
2.42	1.28	1.73	-.25	1.65	-.38
3.03	1.63	2.34	-.31	2.31	-.18
3.65	2.08	2.94	-.42	2.93	-.15
4.28	2.24	3.52	-.6	3.53	-.04
4.31	2.1	4.15	-.31	4.13	.09
5.5	2.05	4.77	-1.2	4.77	.15
6.12	2.14	5.37	-1.39	5.34	.1
6.76	2.22	6.03	-1.55	5.94	.1
7.36	2.28	6.65	-1.73	6.58	.14
7.96	2.24	7.39	-1.91	7.16	.17
8.54	2.06	8.08	-1.98	7.81	.2
9.19	2.05	8.61	-1.79	8.4	.22
9.8	2	9.11	-1.44	9	.25
10.41	1.91	9.64	-1.84	9.63	.24
11.02	1.88	10.27	-.55	10.27	.18
11.65	2.11	10.85	.01	10.8	.15
12.24	2.27	11.46	.62	11.43	.17
12.89	2.42	12.07	1.08	12.04	.24
13.51	2.49	12.67	1.3	12.68	.29
14.12	2.49	13.29	1.27	13.27	.31
14.72	2.37	13.88	1.03	13.89	.31
15.35	2.16	14.5	.67	14.51	.31
15.91	2.08	15.13	.21	15.14	.31
16.55	2.09	15.75	-.29	15.69	.28
17.19	2.18	16.39	-.89	16.34	.23
17.8	2.25	16.98	-1.5	16.94	.19
18.39	2.26	17.56	-1.99	17.52	.21
19.01	2.28	18.17	-2.22	18.17	.23
19.6	2.25	18.8	-2.23	18.76	.26
20.23	2.17	19.42	-1.98	19.37	.29
20.81	2.06	20.03	-1.6	19.97	.31
21.42	1.97	20.63	-1.07	20.58	.31
22.07	1.93	21.22	-.5	21.22	.28
22.66	1.86	21.83	.12	21.8	.23
23.32	1.86	22.46	.69	22.39	.21
23.91	1.88	23.08	1.07	23.04	.23
24.52	1.88	23.65	1.28	23.64	.26
25.13	1.86	24.28	1.34	24.31	.27
25.76	1.85	24.86	1.24	24.89	.29
26.36	1.91	25.51	.97	25.5	.31
26.96	1.88	26.11	.71	26.06	.31
27.57	1.72	26.72	.36	26.68	.3

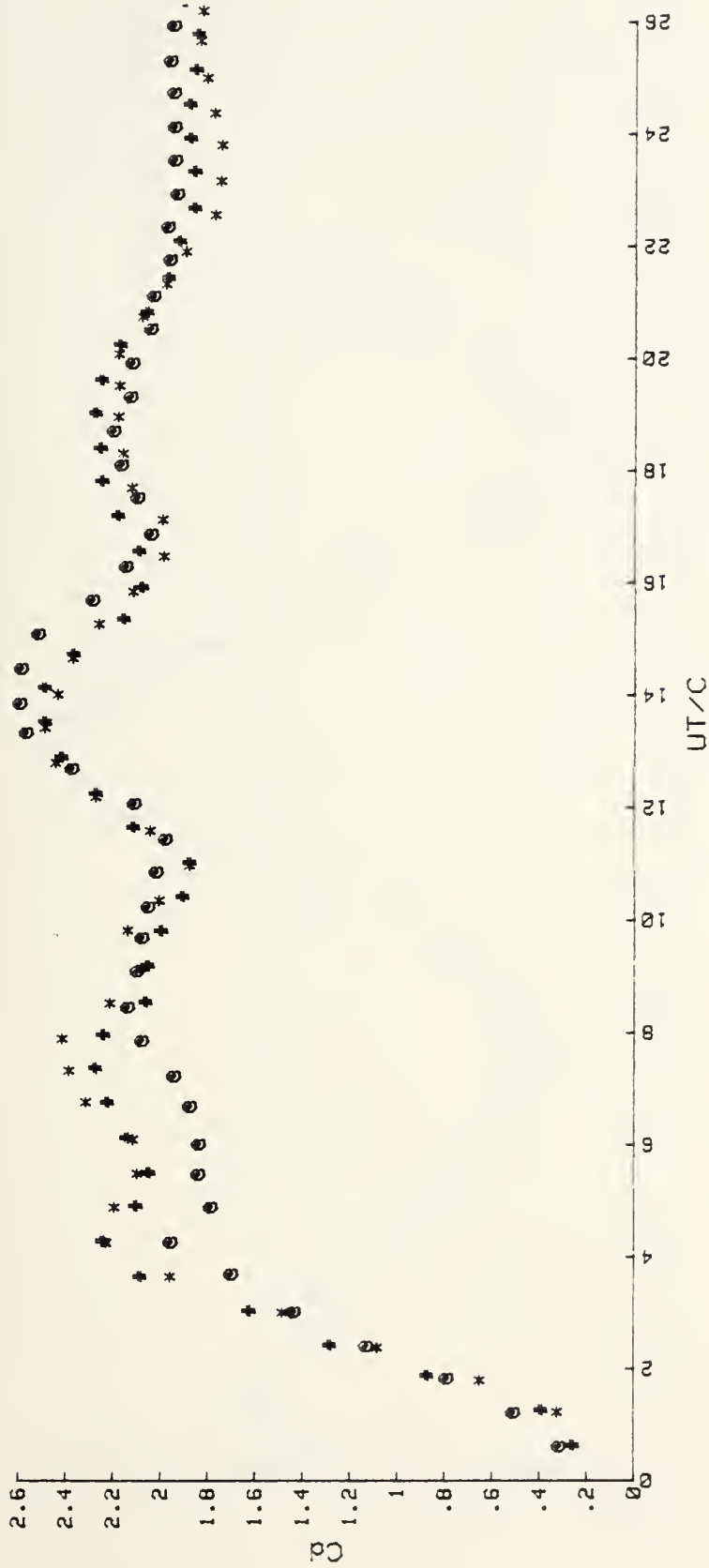


Figure 71. C_d vs. UT/C for the T-Shaped Body at +25 deg.

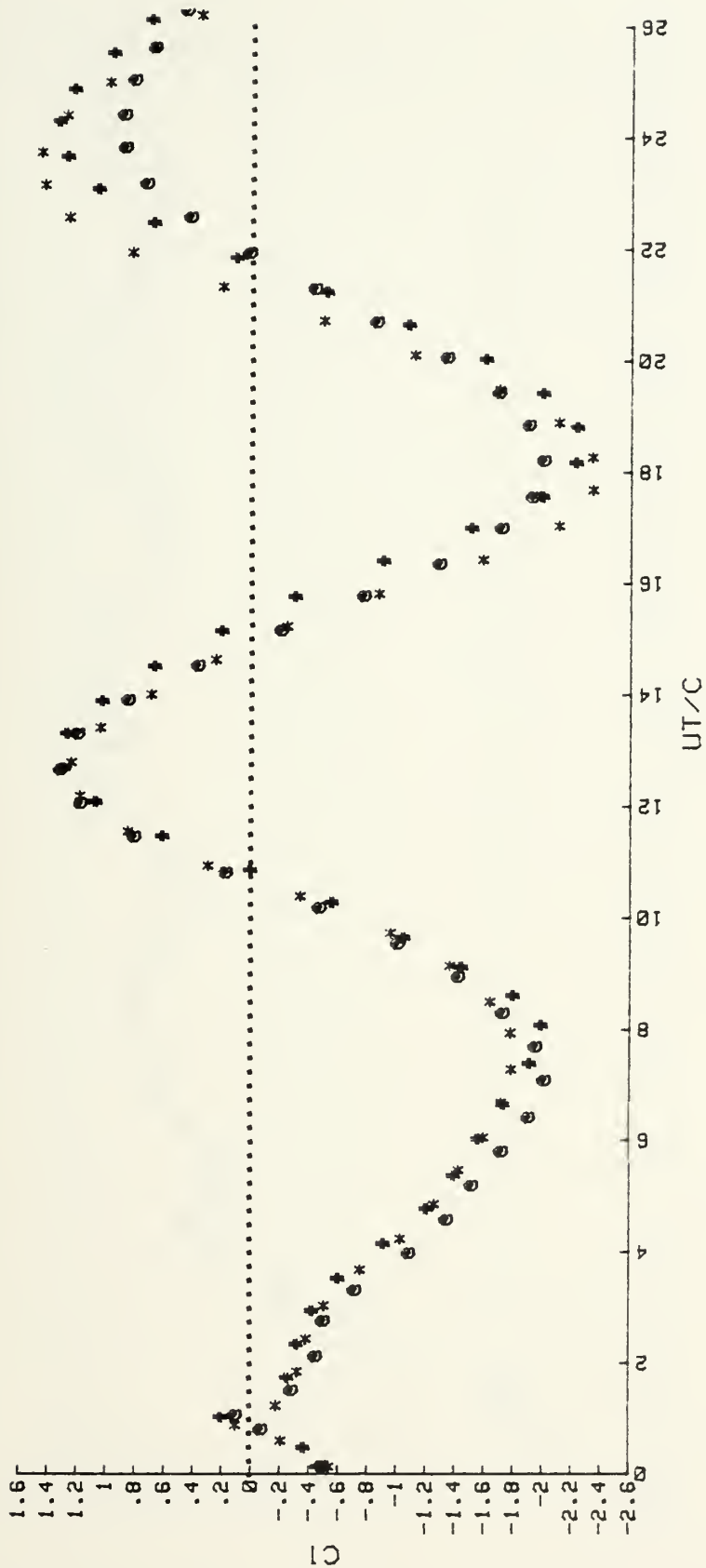


Figure 72. $C1$ vs. UT/C for the T-Shaped Body at +25 deg.



Figure 73. C_m vs. UT/C for the T-Shaped Body at +25 deg.

APPENDIX Q: REPRESENTATIVE DATA FOR T-SHAPED BODY AT +30 DEGREES

<u>UT/C</u>	<u>Cd</u>	<u>UT/C</u>	<u>Cl</u>	<u>UT/C</u>	<u>Cm</u>
.39	.18	.12	-.6	.99	-.43
1	.3	.66	-.28	1.65	-.42
1.61	.58	.95	.27	2.29	-.22
2.23	1.11	1.25	-.14	2.93	-.18
2.84	1.36	1.88	-.34	3.47	-.07
3.49	1.86	2.48	-.37	4.1	.06
4.08	2.2	3.04	-.44	4.74	.1
4.78	2.24	3.67	-.63	5.36	.09
5.43	2.14	4.27	-.92	5.97	.1
6.06	2.18	4.88	-1.15	6.56	.14
6.69	2.36	5.47	-1.29	7.22	.21
7.33	2.45	6.09	-1.47	7.86	.25
7.95	2.42	6.72	-1.62	8.47	.25
8.44	2.24	7.38	-1.69	9.09	.24
9.05	2.13	7.94	-1.66	9.69	.16
9.69	1.94	8.55	-1.55	10.29	.1
10.31	1.91	9.14	-1.34	10.93	.12
10.92	2.12	9.74	-1	11.53	.21
11.52	2.4	10.39	-.45	12.14	.24
12.14	2.58	10.98	.2	12.81	.25
12.79	2.71	11.59	.75	13.42	.26
13.43	2.7	12.19	.99	14.03	.24
14.02	2.48	12.81	1.03	14.65	.24
14.63	2.3	13.41	.88	15.26	.2
15.24	2.08	14.01	.59	15.9	.17
15.86	1.95	14.64	.19	16.53	.17
16.49	2	15.24	-.23	17.14	.22
17.13	2.1	15.84	-.76	17.77	.29
17.74	2.22	16.49	-1.3	18.42	.33
18.35	2.23	17.05	-1.75	19.08	.36
18.99	2.22	17.68	-1.99	19.68	.36
19.58	2.15	18.3	-1.99	20.26	.31
20.18	2.06	18.9	-1.81	20.85	.22
20.82	1.98	19.51	-1.48	21.46	.16
21.46	1.91	20.13	-1	22.09	.15
22.07	1.96	20.73	-.41	22.73	.15
22.67	2.03	21.32	.18	23.31	.17
23.31	2.1	21.93	.73	23.93	.19
23.9	2.17	22.58	1.12	24.6	.24
24.54	2.26	23.14	1.23	25.22	.27
25.14	2.21	23.8	1.21	25.83	.26
25.78	2.01	24.37	1.06	26.44	.22
26.38	1.83	24.97	.81	27.04	.19
27	1.71	25.61	.53	27.66	.17
27.65	1.59	26.21	.24	28.33	.18

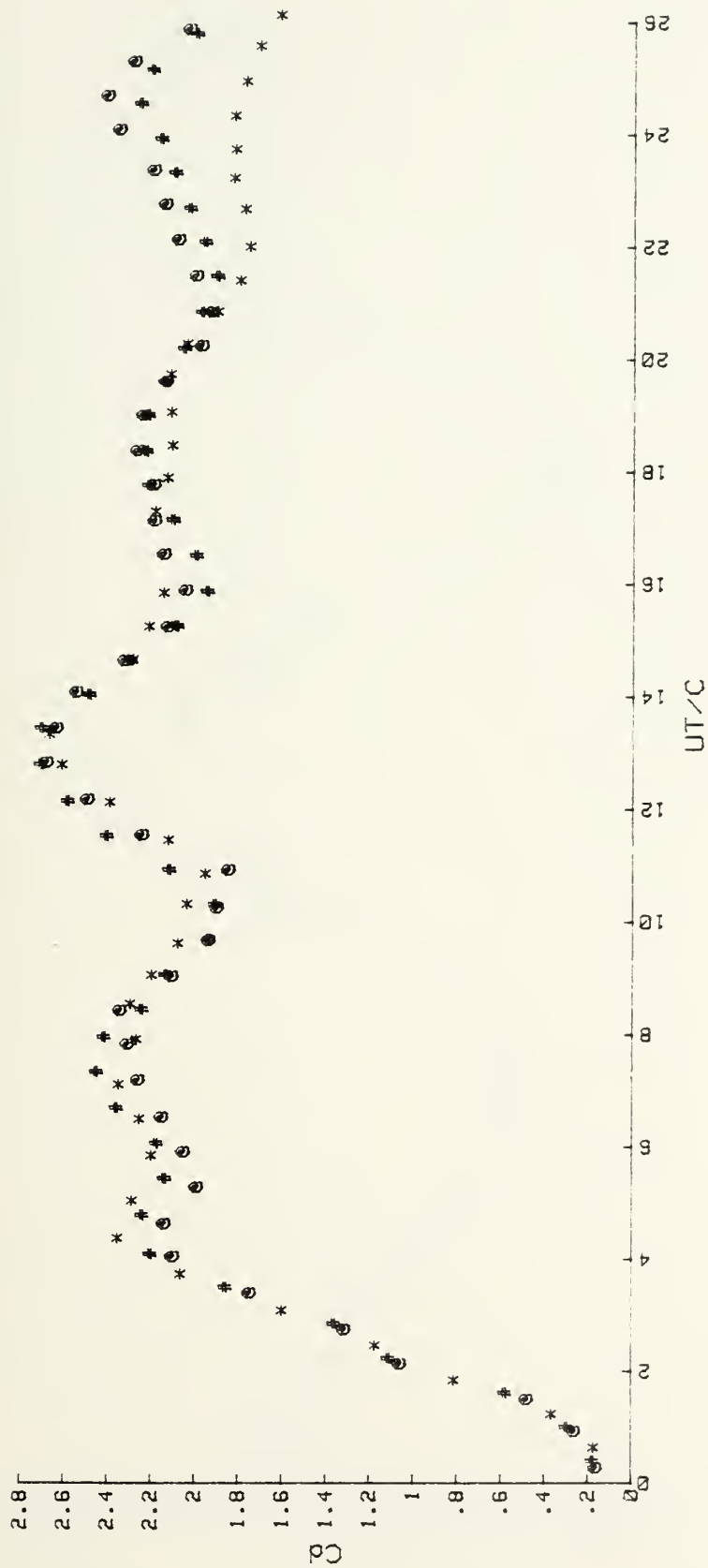


Figure 74. C_d vs. UT/C for the T-Shaped Body at +30 deg.



Figure 75. $C1$ vs. UT/C for the T-Shaped Body at $+30^\circ$ deg.

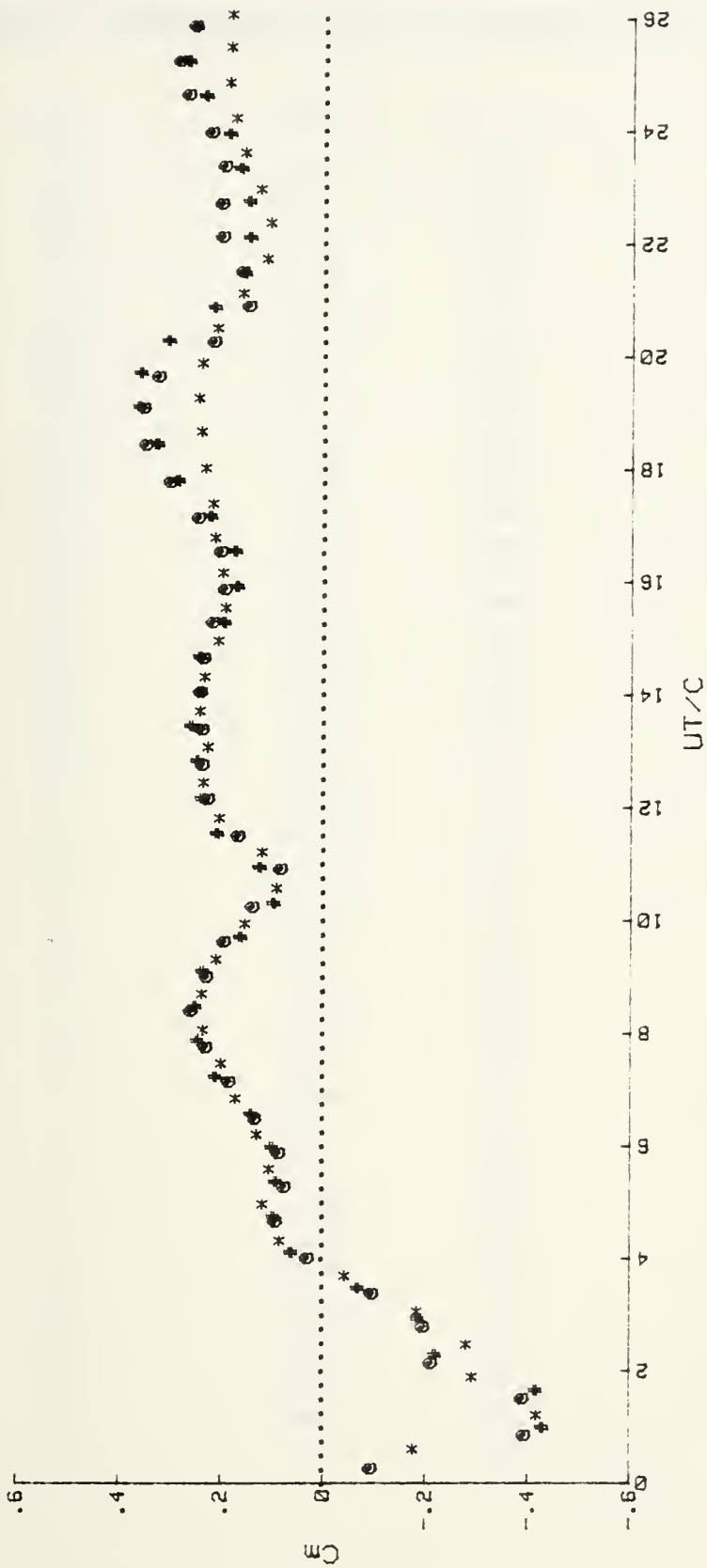


Figure 76. C_m vs. UT/C for the T-Shaped Body at +30 deg.

APPENDIX R: REPRESENTATIVE DATA FOR T-SHAPED BODY AT +45 DEGREES

<u>UT/C</u>	<u>Cd</u>	<u>UT/C</u>	<u>Cl</u>	<u>UT/C</u>	<u>Cm</u>
.4	.14	.26	-.69	.66	-.29
1.02	.29	.63	-.53	1.26	-.41
1.67	.53	1.07	.36	1.84	-.24
2.27	1.25	1.86	-.35	2.5	-.15
2.88	1.5	2.48	-.5	3.12	-.23
3.48	1.72	3.1	-.77	3.76	.09
4.15	1.86	3.73	-1.07	4.4	.17
4.78	1.83	4.38	-1.39	5.01	.24
5.4	1.87	5	-1.64	5.64	.29
5.99	1.97	5.62	-1.79	6.27	.38
6.68	2.13	6.25	-1.87	6.91	.46
7.27	2.21	6.86	-1.84	7.52	.48
7.88	2.11	7.46	-1.68	8.18	.38
8.49	1.94	8.07	-1.38	8.76	.22
9.12	1.93	8.69	-.87	9.41	.06
9.77	2.31	9.33	-.09	9.86	.05
10.48	2.61	9.93	.77	10.33	.14
11.1	2.72	10.59	1.43	10.93	.18
11.74	2.63	11.19	1.58	11.32	.21
12.37	2.36	11.79	1.34	11.94	.24
12.9	1.95	12.42	.94	12.59	.24
13.51	1.69	13.05	.45	13.17	.18
14.14	1.71	13.65	-.11	13.8	.18
14.74	1.85	14.26	-.79	14.41	.22
15.38	1.83	14.9	-1.45	15.04	.23
15.98	1.81	15.52	-1.9	15.65	.26
16.62	1.81	16.13	-2.04	16.35	.28
17.26	1.82	16.75	-1.93	16.92	.29
17.85	1.8	17.41	-1.63	17.59	.26
18.49	1.74	17.98	-1.18	18.26	.21
19.09	1.71	18.61	-.56	18.82	.14
19.75	1.73	19.24	.17	19.44	.09
20.36	1.78	19.87	.87	20.08	.07
20.99	1.8	20.5	1.3	20.71	.06
21.61	1.8	21.1	1.44	21.35	.06
22.2	1.72	21.74	1.35	21.99	.08
22.84	1.6	22.39	1.12	22.65	.11
23.46	1.53	22.99	.88	23.22	.11
24.1	1.37	23.59	.59	23.87	.12
24.72	1.28	24.24	.2	24.5	.12
25.32	1.24	24.86	-.22	25.12	.12
25.98	1.23	25.47	-.63	25.75	.13
26.61	1.24	26.09	-.99	26.37	.15
27.2	1.24	26.7	-1.21	27.01	.17
27.84	1.25	27.34	-1.28	27.59	.18

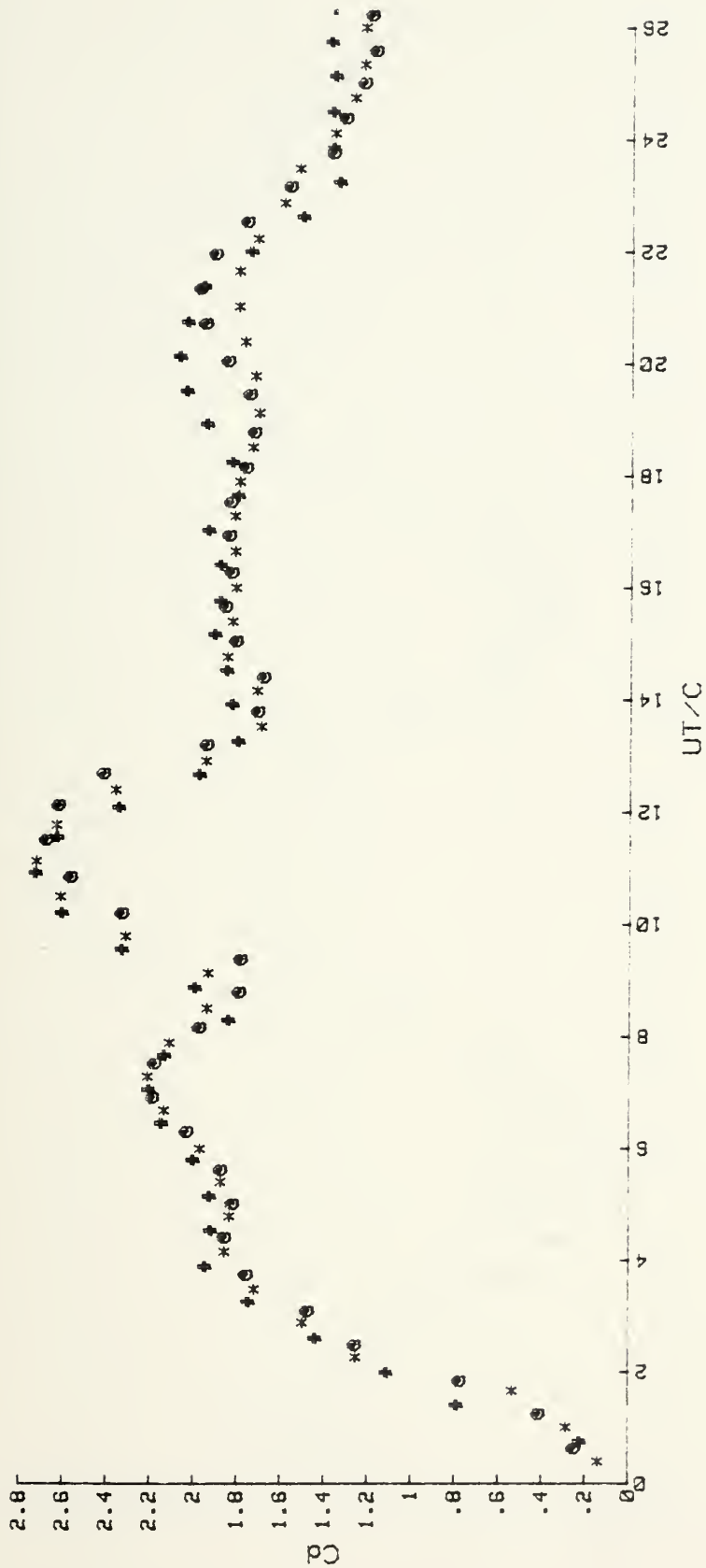


Figure 77. C_d vs. UT/C for the T-Shaped Body at +45 deg.

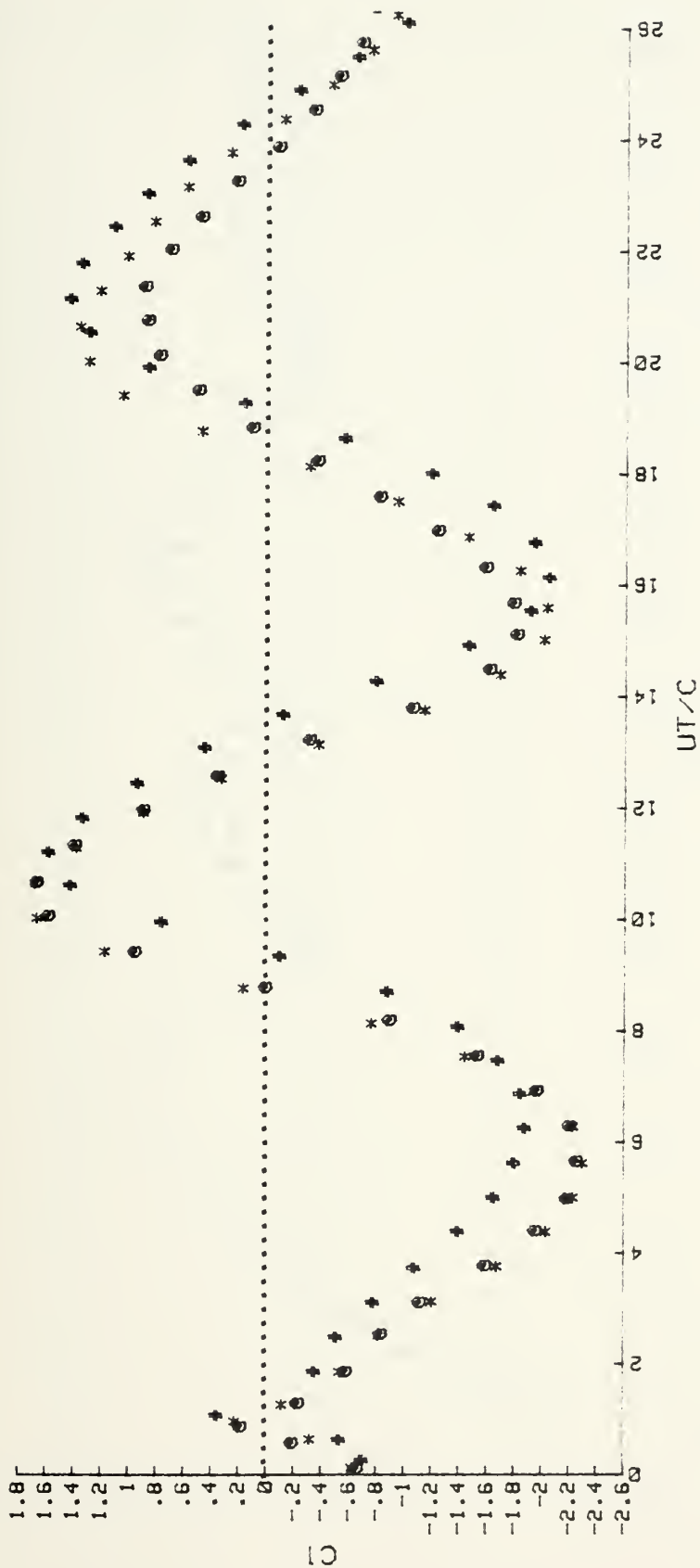


Figure 78. $C1$ vs. UT/C for the T-Shaped Body at +45 deg.

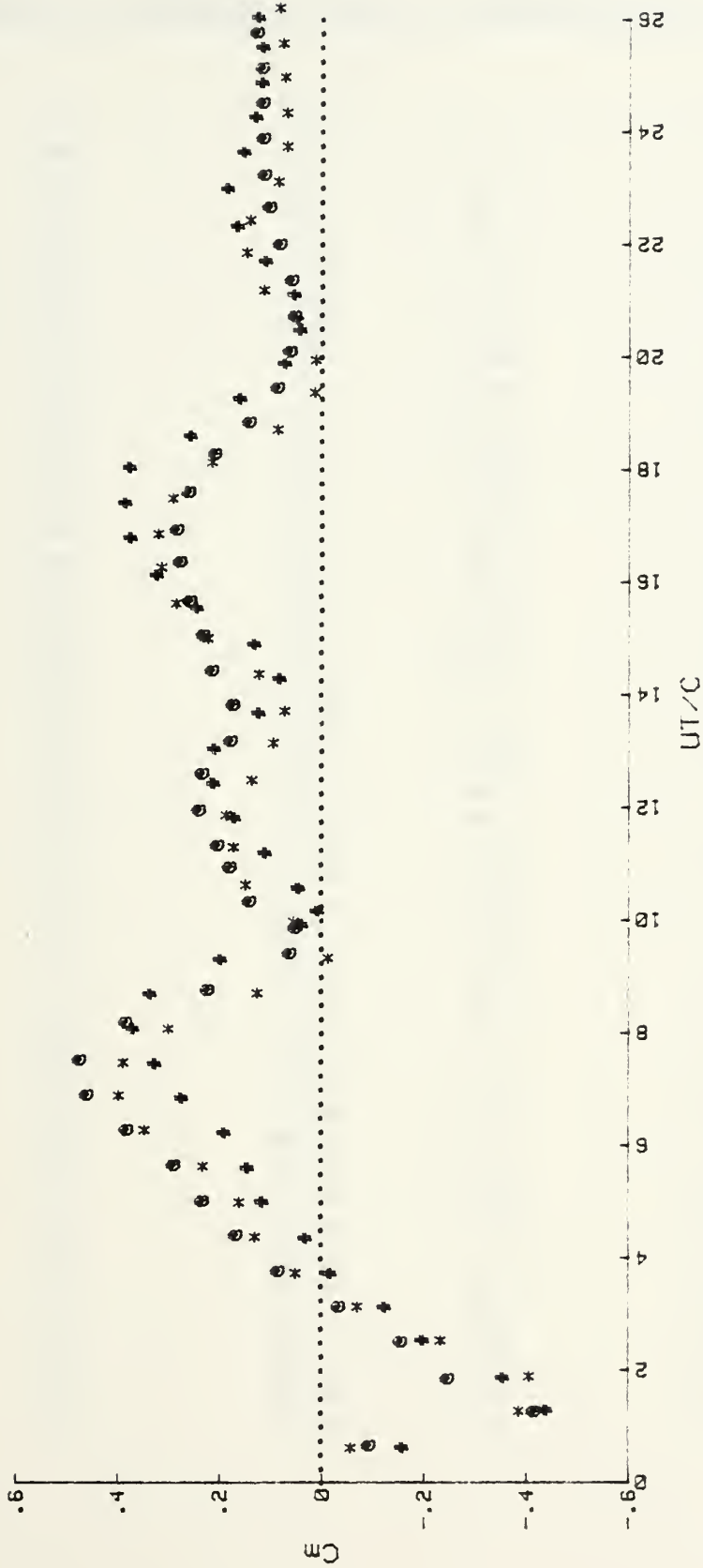


Figure 79. Cm vs. UT/C for the T-Shaped Body at +45 deg.

APPENDIX S: REPRESENTATIVE DATA FOR T-SHAPED BODY AT -5 DEGREES

<u>UT/C</u>	<u>Cd</u>	<u>UT/C</u>	<u>C1</u>	<u>UT/C</u>	<u>Cm</u>
.63	.29	.13	.4	.37	.19
1.25	.59	.39	.48	.97	.32
1.81	.97	.84	.84	1.67	.31
2.47	1.31	1.02	-.41	2.26	.26
3.13	1.56	1.59	-.47	2.83	.23
3.73	1.75	2.23	-.61	3.47	.2
4.35	1.79	2.86	-.83	4.1	.17
4.97	1.77	3.52	-1.09	4.76	.16
5.57	1.74	4.13	-1.29	5.4	.16
6.21	1.81	4.74	-1.41	5.98	.17
6.77	1.84	5.36	-1.36	6.57	.19
7.41	1.72	5.98	-1.19	7.24	.24
8.05	1.72	6.6	-.88	7.85	.27
8.68	1.69	7.24	-.46	8.49	.33
9.31	1.92	7.87	.29	9.11	.39
9.94	2.07	8.5	.83	9.75	.42
10.52	2.2	9.12	1.56	10.36	.43
11.11	2.22	9.74	2.01	10.96	.41
11.8	1.98	10.36	2.13	11.6	.34
12.41	1.78	10.98	2	12.24	.28
13.04	1.62	11.62	1.65	12.86	.24
13.65	1.48	12.24	1.26	13.46	.2
14.26	1.53	12.85	.82	14.08	.15
14.93	1.67	13.46	.27	14.68	.14
15.52	1.79	14.09	-.32	15.34	.17
16.07	1.74	14.71	-.65	15.98	.2
16.75	1.74	15.35	-.68	16.57	.22
17.42	1.69	15.94	-.49	17.25	.26
17.99	1.6	16.53	-.09	17.84	.3
18.58	1.57	17.2	.32	18.46	.32
19.21	1.56	17.84	.79	19.12	.34
19.84	1.58	18.44	1.2	19.71	.34
20.46	1.57	19.07	1.6	20.34	.34
21.03	1.49	19.68	1.84	20.96	.32
21.7	1.36	20.32	1.9	21.59	.29
22.34	1.22	20.95	1.81	22.23	.24
22.94	1.11	21.58	1.56	22.84	.21
23.59	1.07	22.18	1.26	23.47	.18
24.18	1.05	22.82	.9	24.1	.16
24.79	1.08	23.48	.53	24.72	.15
25.43	1.17	24.11	.16	25.33	.16
26.08	1.25	24.73	-.08	25.94	.17
26.62	1.27	25.31	-.18	26.57	.19
27.29	1.26	25.86	-.2	27.19	.21
27.9	1.24	26.55	-.12	27.85	.22

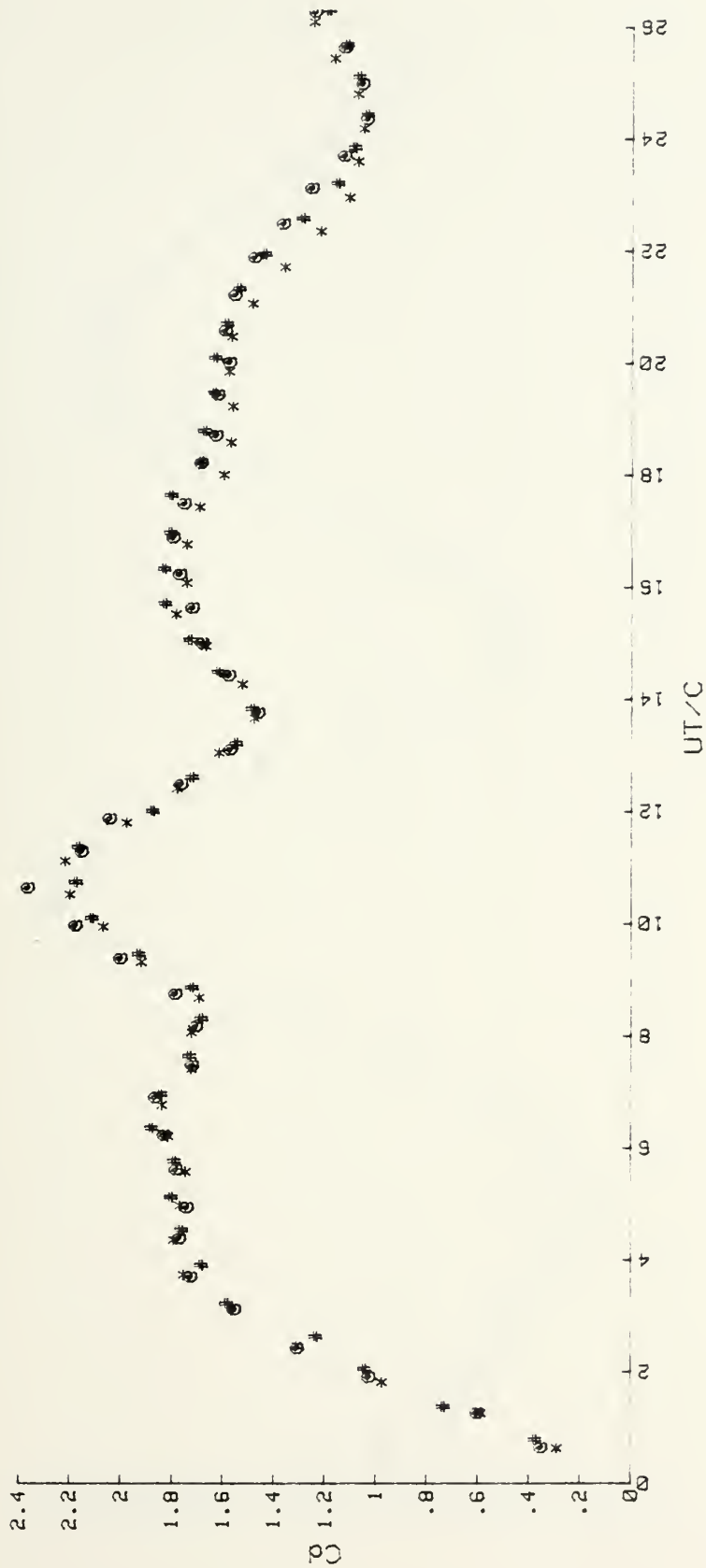


Figure 80. Cd vs. UT/C for the T-Shaped Body at -5 deg.

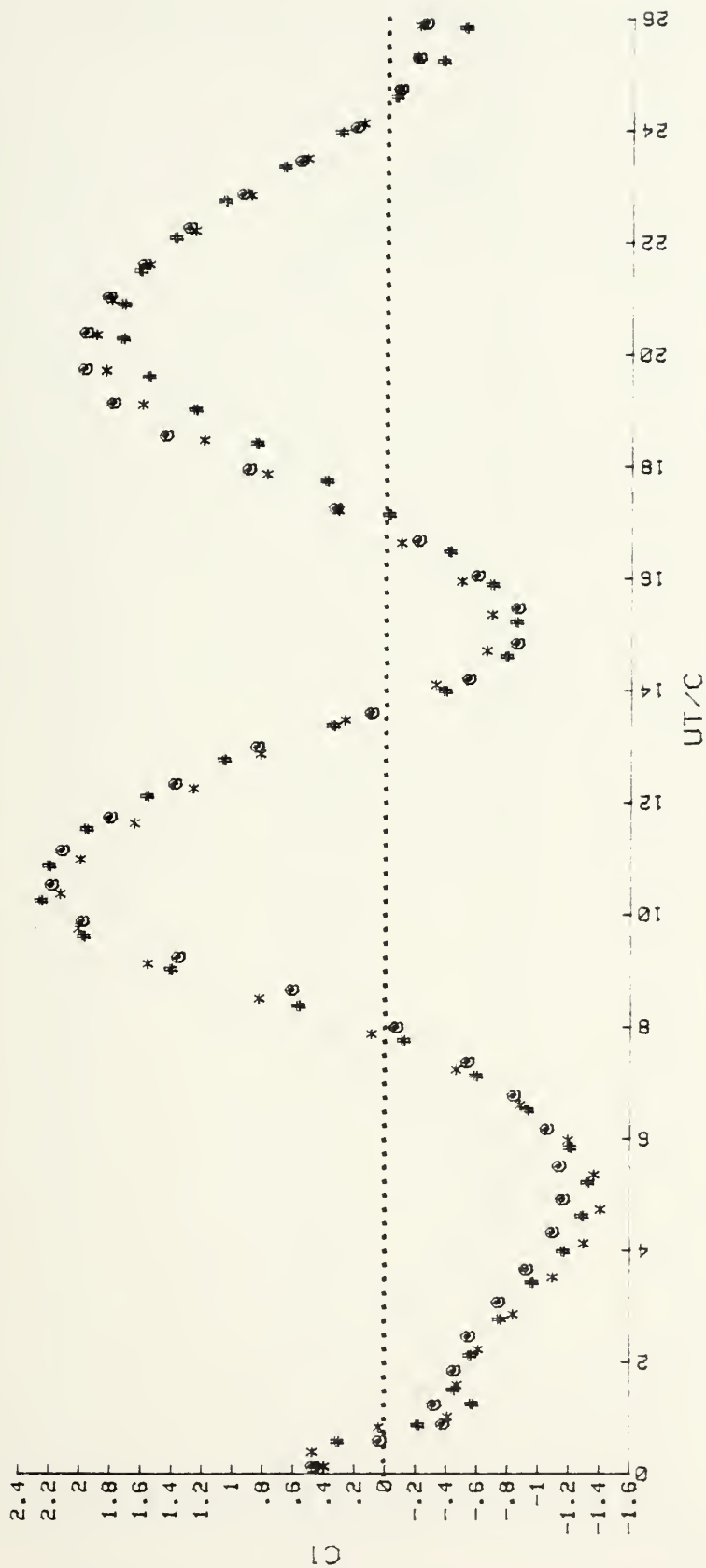


Figure 81. CI vs. UT/C for the T-Shaped Body at -5° .



Figure 82. Cm vs. UT/C for the T-Shaped Body at -5 deg.

APPENDIX T: REPRESENTATIVE DATA FOR T-SHAPED BODY AT -18 DEGREES

<u>UT/C</u>	<u>Cd</u>	<u>UT/C</u>	<u>Cl</u>	<u>UT/C</u>	<u>Cm</u>
.24	.33	.23	.52	.26	.18
.84	.65	.67	.33	.86	.35
1.43	.75	1.19	-.23	1.53	.37
2.07	1.08	1.8	-.39	2.09	.37
2.7	1.2	2.4	-.57	2.71	.33
3.29	1.41	3.02	-.84	3.3	.3
3.9	1.44	3.6	-.92	3.91	.25
4.5	1.54	4.21	-.97	4.5	.24
5.09	1.42	4.79	-1.07	5.12	.21
5.71	1.47	5.42	-1.11	5.71	.21
6.32	1.47	5.99	-1.28	6.33	.22
6.95	1.57	6.61	-.99	6.93	.23
7.56	1.59	7.2	-.82	7.57	.24
8.2	1.67	7.81	-.6	8.2	.27
8.79	1.67	8.43	-.25	8.77	.3
9.37	1.64	9.05	.32	9.39	.38
9.98	1.85	9.66	1	9.99	.46
10.6	1.95	10.26	1.59	10.61	.49
11.24	2.18	10.87	2.02	11.23	.5
11.82	2.31	11.47	2.15	11.83	.48
12.44	2.24	12.07	2.14	12.44	.43
13.05	2.19	12.65	2.02	13.06	.4
13.63	1.83	13.25	1.76	13.67	.33
14.22	1.64	13.84	1.37	14.25	.3
14.91	1.37	14.44	.81	14.91	.21
15.48	1.49	15.11	.2	15.49	.2
16.09	1.65	15.67	-.35	16.12	.2
16.7	1.71	16.26	-.71	16.74	.21
17.31	1.72	16.84	-.78	17.33	.25
17.93	1.65	17.46	-.6	17.92	.3
18.53	1.65	18.08	-.3	18.54	.36
19.13	1.64	18.68	.18	19.11	.42
19.77	1.73	19.27	.72	19.71	.48
20.37	1.76	19.89	1.25	20.35	.49
20.94	1.78	20.46	1.7	20.97	.49
21.6	1.79	21.07	1.98	21.56	.47
22.19	1.83	21.67	1.99	22.19	.42
22.79	1.72	22.29	1.89	22.81	.37
23.39	1.64	22.88	1.7	23.42	.33
24.01	1.44	23.48	1.44	24.04	.29
24.63	1.29	24.1	1.05	24.66	.26
25.24	1.13	24.67	.64	25.27	.23
25.8	1.05	25.32	.27	25.87	.21
26.43	1.04	25.91	.03	26.5	.19
27.06	1.08	26.52	-.11	27.11	.2
27.65	1.11	27.16	-.2	27.7	.2

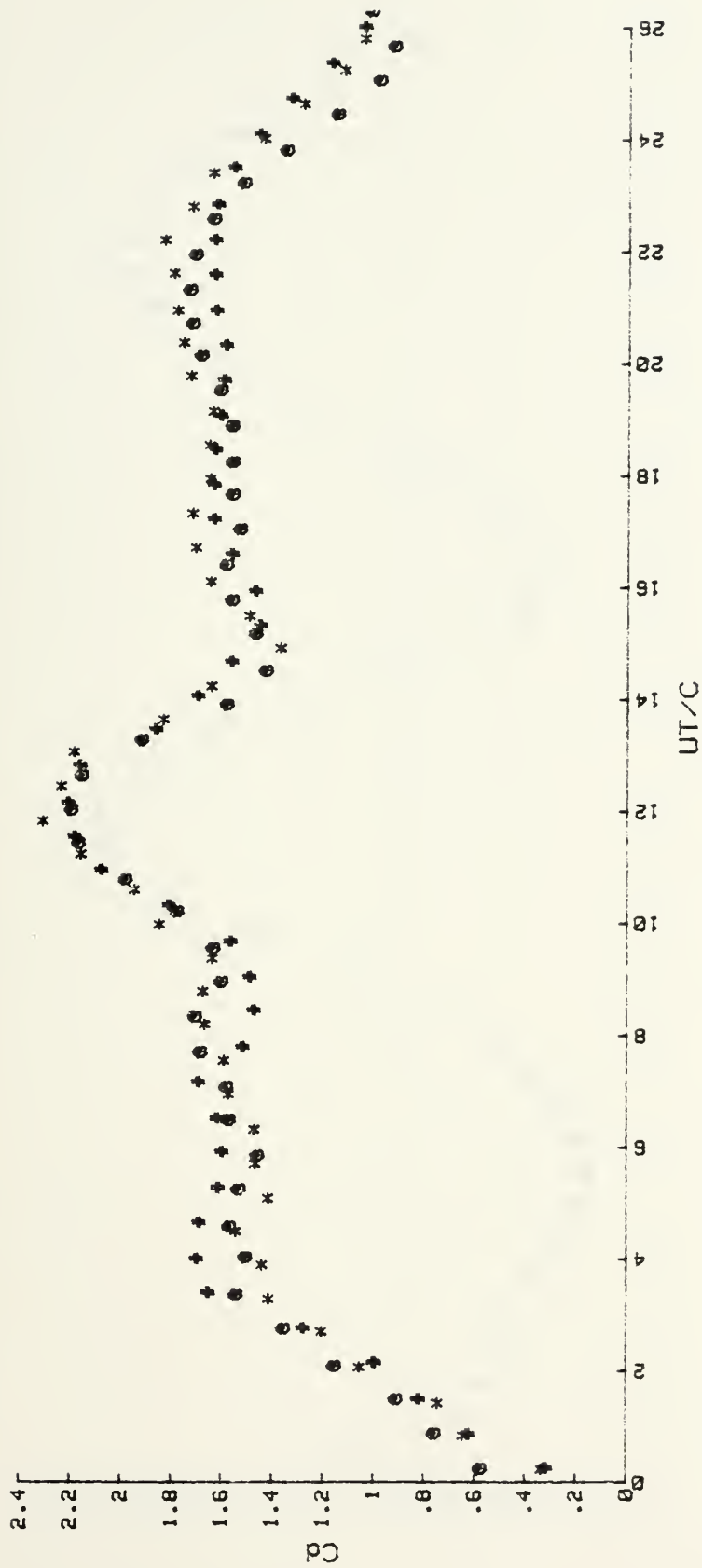


Figure 83. C_d vs. UT/C for the T-Shaped Body at -10° .

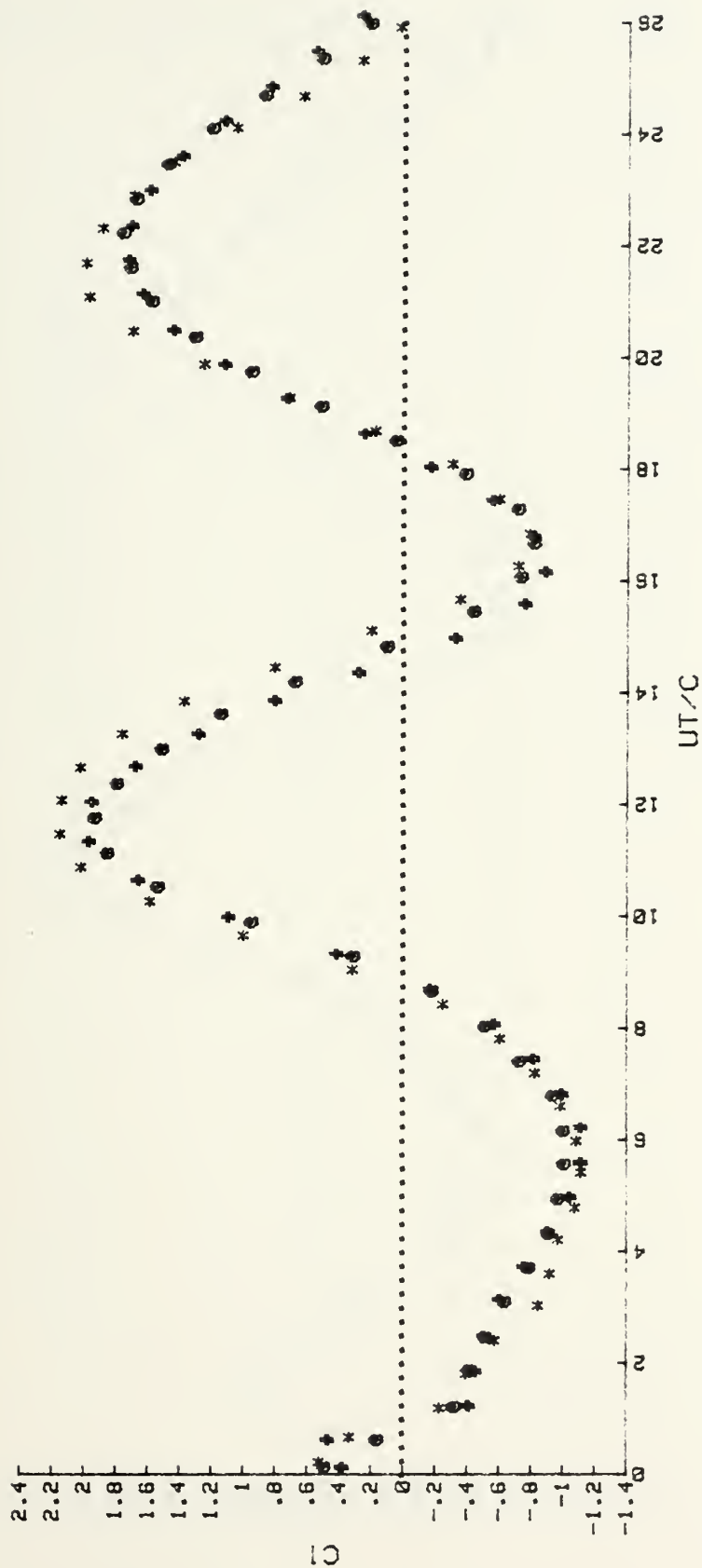


Figure 84. $C1$ vs. UT/C for the T-Shaped Body at -10° deg.

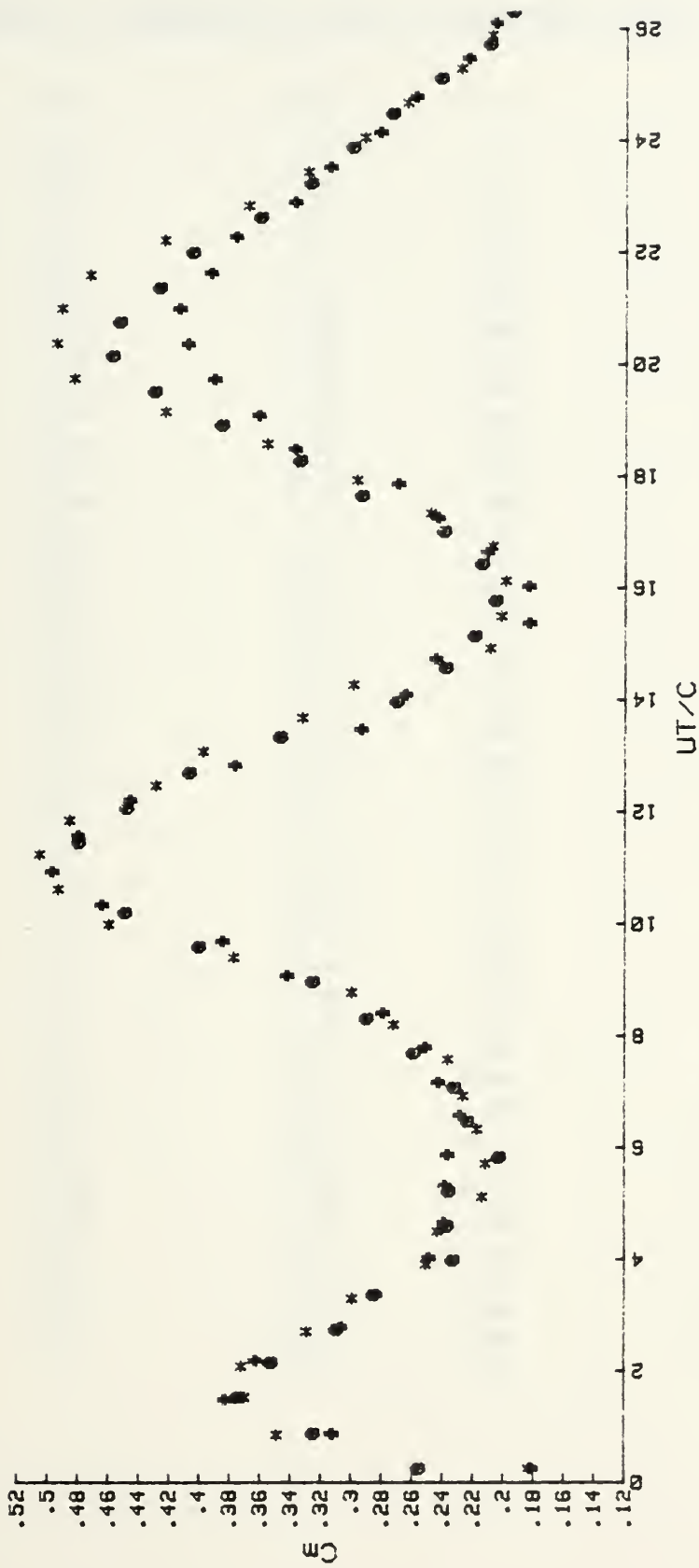


Figure 85. C_m vs. UT/C for the T-Shaped Body at -10° deg.

APPENDIX U: REPRESENTATIVE DATA FOR T-SHAPED BODY AT -15 DEGREES

<u>UT/C</u>	<u>Cd</u>	<u>UT/C</u>	<u>C1</u>	<u>UT/C</u>	<u>Cd</u>
1	.37	.13	.6	1.02	.49
1.84	.88	.35	.78	1.68	.52
2.28	1.1	.79	.27	2.33	.5
2.88	1.47	1.2	-.58	2.88	.43
3.5	1.84	1.8	-.31	3.49	.39
4.13	2	2.47	-.28	4.07	.38
4.76	1.92	3.08	-.38	4.71	.38
5.36	1.73	3.67	-.43	5.31	.34
5.98	1.74	4.33	-.59	5.91	.33
6.64	1.78	4.97	-.72	6.59	.31
7.25	1.85	5.56	-.79	7.13	.29
7.89	1.67	6.15	-.85	7.79	.3
8.49	1.69	6.77	-.86	8.38	.31
9.09	1.66	7.4	-.87	9.05	.32
9.77	1.56	8.01	-.79	9.61	.32
10.33	1.59	8.68	-.66	10.27	.34
10.97	1.64	9.24	-.48	10.85	.37
11.6	1.78	9.86	-.2	11.46	.41
12.24	1.87	10.49	.24	12.1	.45
12.85	1.92	11.11	.75	13.35	.5
13.48	1.89	11.72	1.23	12.73	.49
14.13	1.8	12.36	1.58	13.96	.49
14.72	1.87	12.97	1.72	14.57	.46
15.34	1.56	13.6	1.68	15.16	.42
15.97	1.44	14.19	1.49	15.78	.39
16.61	1.41	14.82	1.17	16.41	.35
17.21	1.4	15.43	.76	17	.31
17.85	1.41	16.05	.26	17.64	.29
18.44	1.44	16.63	-.29	18.23	.27
19.09	1.41	17.27	-.72	18.85	.26
19.7	1.49	17.89	-.95	19.5	.25
20.35	1.47	18.49	-.96	20.1	.28
20.97	1.38	19.1	-.76	20.71	.31
21.55	1.36	19.73	-.38	21.32	.35
22.2	1.34	20.34	.87	21.96	.4
22.86	1.33	20.97	.55	22.54	.45
23.46	1.35	21.55	1.01	23.2	.48
24.09	1.35	22.21	1.39	23.81	.5
24.7	1.32	22.79	1.63	24.4	.5
25.35	1.29	23.46	1.71	25.02	.48
25.92	1.22	24.05	1.68	25.64	.46
26.52	1.13	24.71	1.57	26.28	.41
27.2	1	25.28	1.38	26.89	.38



Figure 86. C_d vs. UT/C for the T-Shaped Body at -15° .

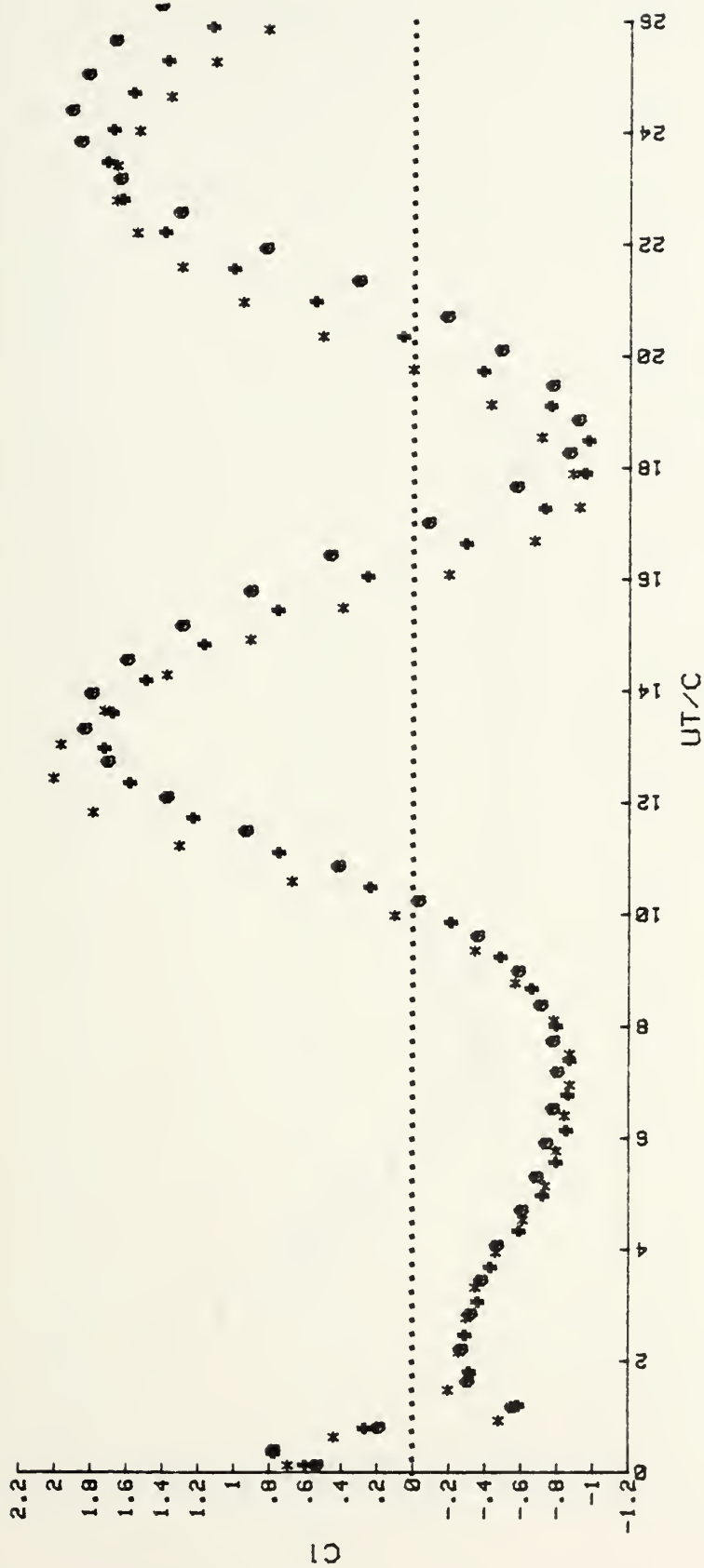


Figure 87. $C1$ vs. UT/C for the T-Shaped Body at -15° .

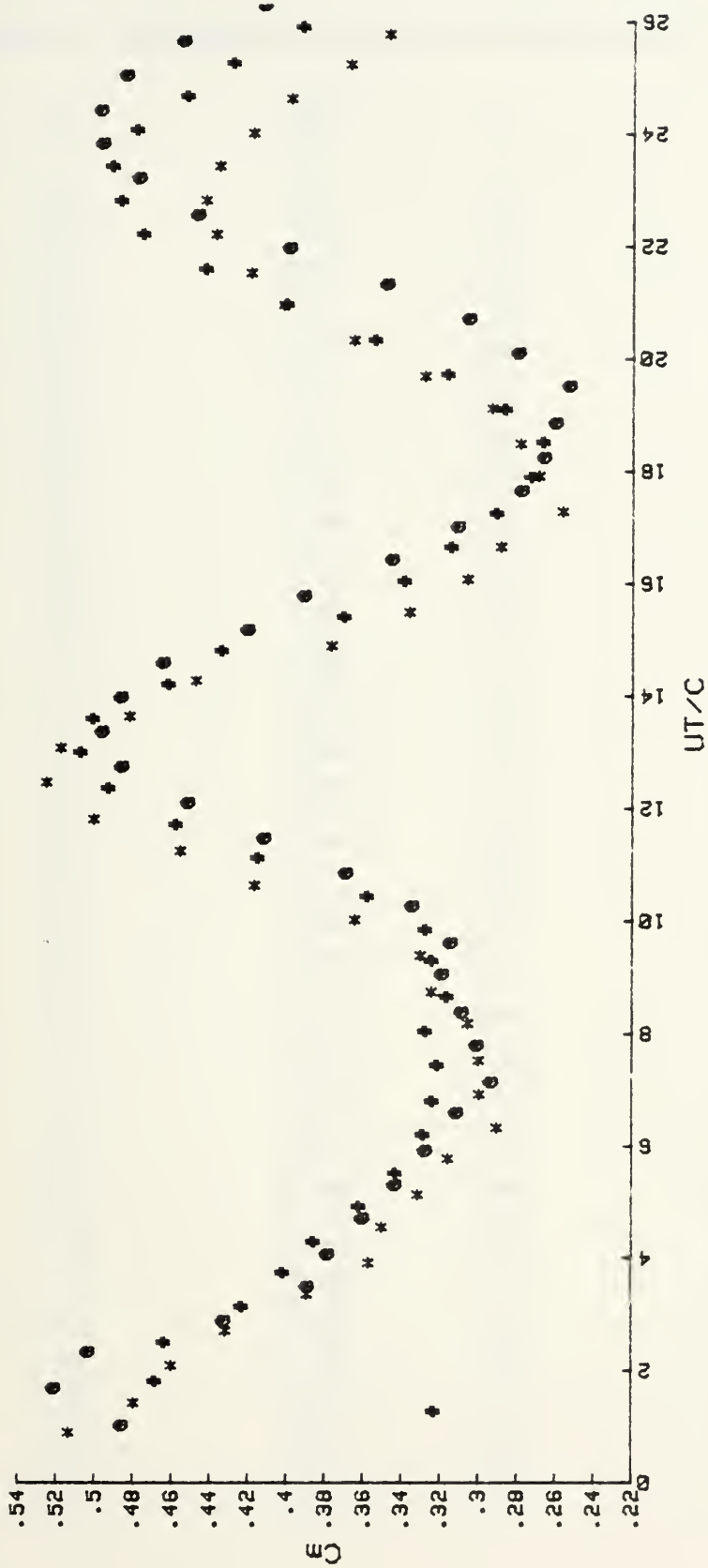


Figure 88. C_m vs. UT/C for the T-Shaped Body at -15° .

APPENDIX V: REPRESENTATIVE DATA FOR T-SHAPED BODY AT -20 DEGREES

<u>UT/C</u>	<u>Cd</u>	<u>UT/C</u>	<u>Cl</u>	<u>UT/C</u>	<u>Cn</u>
.39	.34	.12	.8	.39	.43
1.88	.66	.58	.13	1.85	.54
1.62	.96	1.23	-.17	1.81	.52
2.21	1.13	1.8	-.17	2.22	.46
2.76	1.34	2.4	-.19	2.82	.45
3.39	1.83	3	-.16	3.43	.44
3.96	1.91	3.58	-.18	4	.42
4.58	1.92	4.21	-.25	4.81	.4
5.17	1.75	4.8	-.28	5.22	.37
5.83	1.67	5.4	-.34	5.86	.38
6.42	1.73	6.83	-.36	6.44	.38
7.83	1.65	6.93	-.42	7.84	.36
7.65	1.6	7.25	-.47	7.54	.37
8.25	1.63	7.83	-.51	8.24	.36
8.91	1.63	8.41	-.54	8.86	.37
9.42	1.58	9.84	-.54	9.44	.37
10.87	1.43	9.64	-.5	10.1	.38
10.68	1.45	10.22	-.4	10.73	.39
11.29	1.45	10.83	-.2	11.33	.39
11.89	1.41	11.44	.05	11.96	.4
12.51	1.38	12.88	.31	12.5	.41
13.1	1.37	12.63	.53	13.13	.41
13.68	1.38	13.25	.74	13.71	.42
14.31	1.37	13.85	.92	14.35	.42
14.9	1.39	14.45	1.22	15	.41
15.53	1.42	15.05	1.01	15.52	.4
16.11	1.41	15.68	.94	16.16	.38
16.74	1.36	16.28	.77	16.77	.37
17.34	1.23	16.86	.57	17.35	.37
17.9	1.23	17.47	.34	17.98	.35
18.55	1.18	18.08	.15	18.58	.34
19.12	1.14	18.68	-.07	19.2	.33
19.75	1.13	19.28	-.27	19.79	.33
20.34	1.08	19.88	-.41	20.37	.33
20.94	1.16	20.49	-.47	21.83	.34
21.56	1.12	21.87	-.44	21.61	.34
22.16	1.12	21.67	-.35	22.19	.34
22.82	1.13	22.27	-.2	22.8	.35
23.38	1.12	22.88	0	23.41	.36
24.82	1.12	23.48	.2	24.83	.37
24.59	1.85	24.88	.38	24.63	.38
25.23	1.84	24.67	.57	25.24	.38
25.81	1.83	25.29	.75	25.82	.38
26.44	1.82	25.89	.84	26.45	.37
27.81	1.81	26.5	.88	27.85	.36
27.64	1.81	27.11	.82	27.65	.36
28.22	1	27.71	.73	28.23	.35

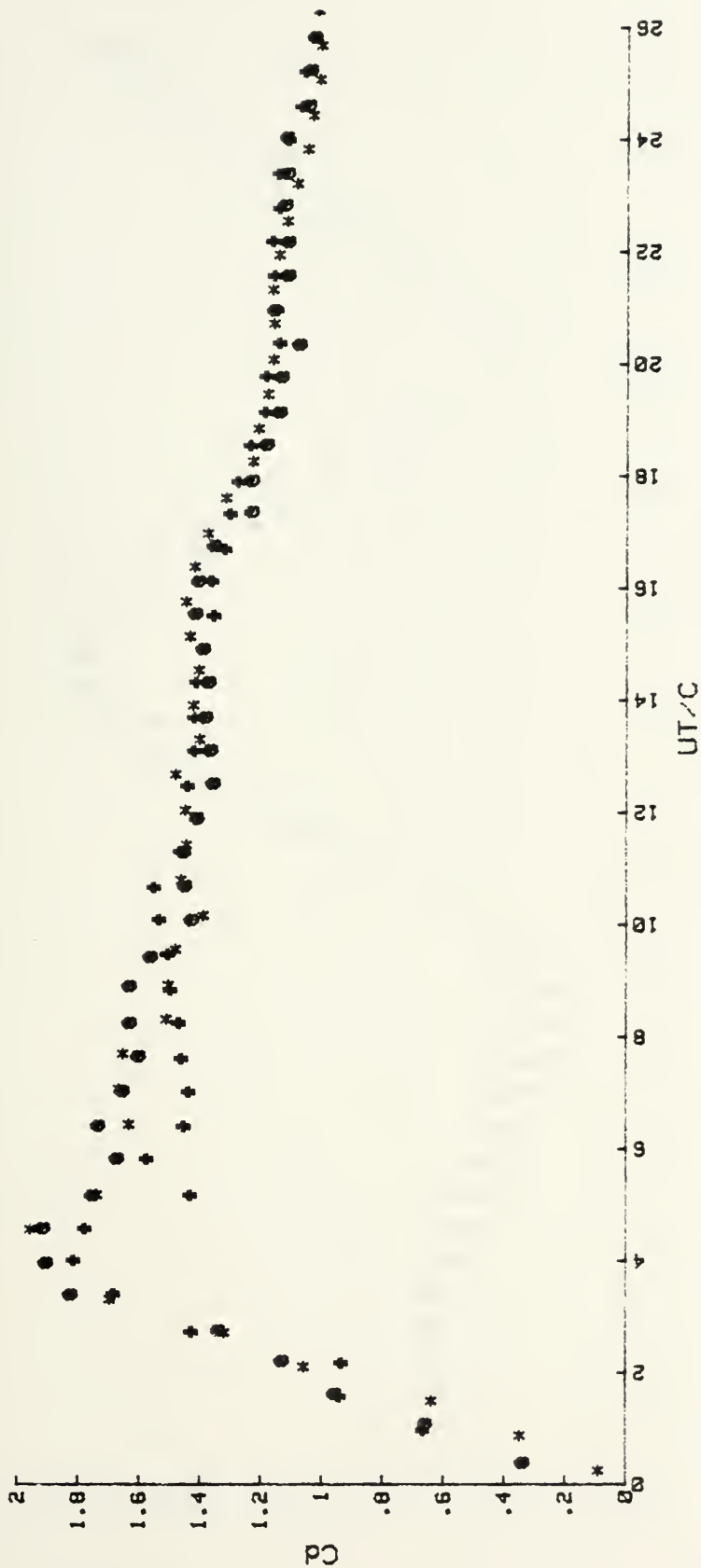


Figure 89. C_d vs. UT/C for the T-Shaped Body at -20° .

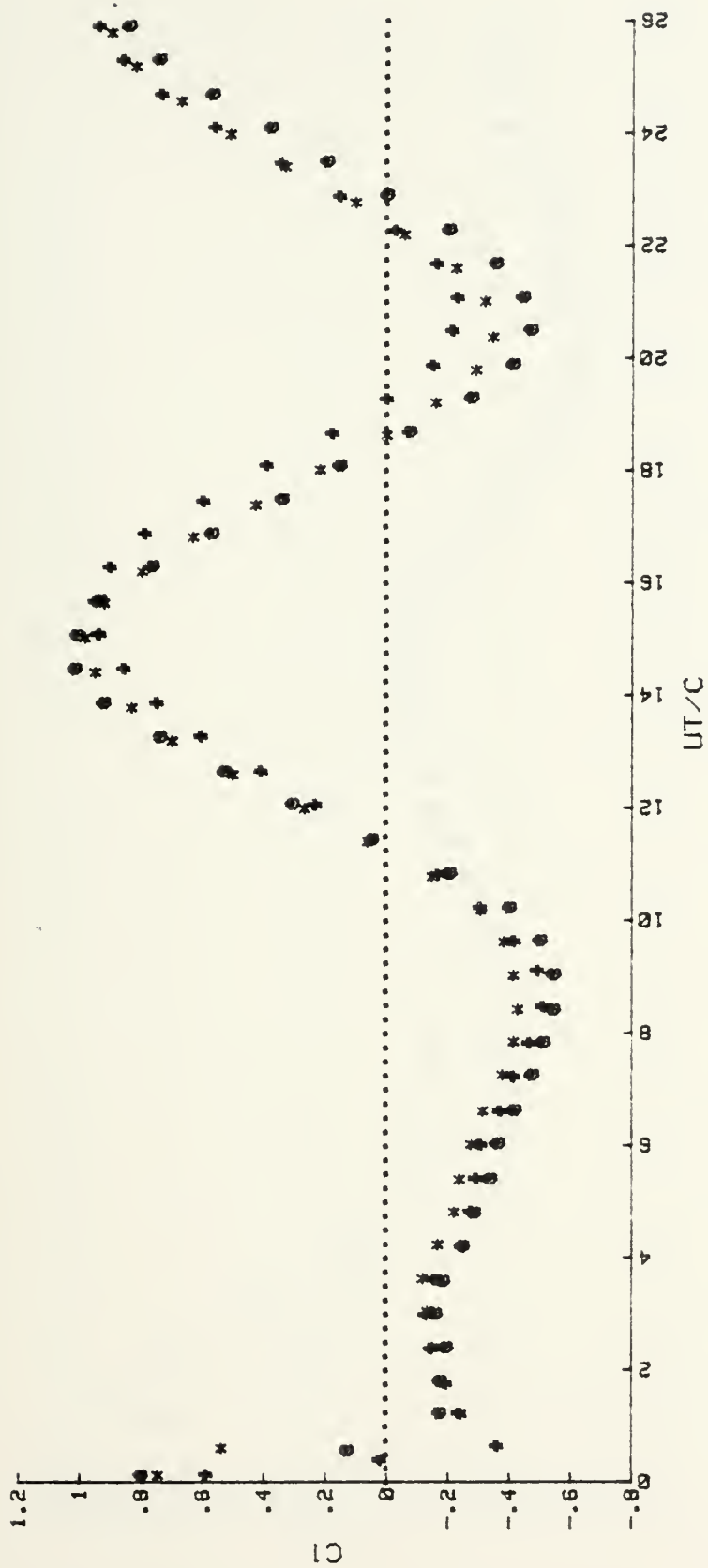


Figure 90. $C1$ vs. UT/C for the T-Shaped Body at -20° deg.

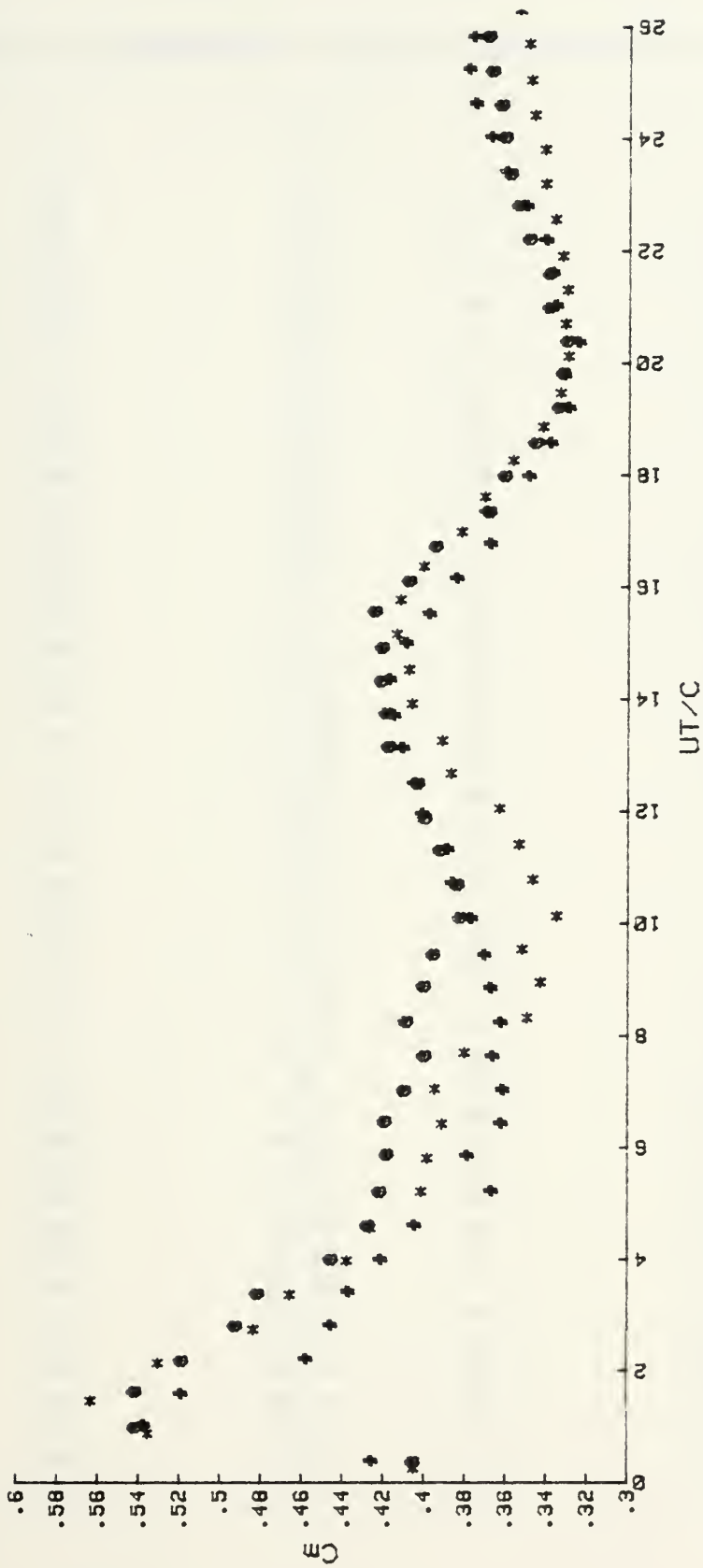


Figure 91. C_m vs. UT/C for the T-Shaped Body at -20° .

APPENDIX H: REPRESENTATIVE DATA FOR T-SHAPED BODY AT -25 DEGREES

<u>UT/C</u>	<u>Cd</u>	<u>UT/C</u>	<u>Ci</u>	<u>UT/C</u>	<u>Cm</u>
.62	.32	.13	1	1.16	.35
1.31	.43	.5	.59	1.77	.57
1.81	.92	.89	-.35	2.44	.81
2.49	1.18	1.75	-.14	3.03	.8
3.13	1.57	2.33	.83	3.6	.59
3.75	1.93	2.95	.17	4.25	.57
4.33	2.1	3.8	.25	4.89	.56
4.92	2.1	4.18	.31	5.46	.56
5.58	1.97	4.82	.33	6.03	.58
6.23	1.85	5.45	.34	6.7	.56
6.88	1.79	6.05	.39	7.25	.57
7.46	1.76	6.69	.43	7.89	.56
8.07	1.7	7.28	.5	8.52	.54
8.86	1.55	7.89	.54	9.17	.52
9.33	1.56	8.54	.57	9.79	.52
9.95	1.52	9.1	.64	10.42	.51
10.57	1.48	9.75	.69	11.05	.48
11.17	1.47	10.38	.72	11.65	.47
11.76	1.47	10.98	.67	12.21	.45
12.4	1.44	11.65	.6	12.84	.44
13.01	1.4	12.27	.53	13.43	.43
13.64	1.4	12.84	.46	14.07	.42
14.28	1.39	13.45	.32	14.73	.4
14.87	1.34	14.09	.14	15.43	.39
15.5	1.28	14.71	-.04	16	.38
16.2	1.26	15.34	-.2	16.59	.38
16.81	1.22	15.98	-.29	17.22	.38
17.4	1.2	16.57	-.36	17.78	.4
17.95	1.15	17.15	-.41	18.42	.41
18.65	1.11	17.78	-.34	18.98	.42
19.23	1.1	18.35	-.24	19.8	.44
19.89	1.08	19	-.09	20.25	.44
20.43	1.09	19.57	.06	20.87	.45
21.06	1.08	20.2	.21	21.49	.46
21.71	1.05	20.81	.39	22.08	.46
22.31	1.04	21.44	.53	22.72	.46
22.94	1.03	22.07	.67	23.32	.46
23.58	1.02	22.66	.74	23.96	.45
24.17	1.01	23.28	.77	24.6	.44
24.79	1	23.92	.74	25.18	.43
25.46	.98	24.5	.66	25.82	.41
26.09	.97	25.15	.55	26.42	.4
26.68	.95	25.74	.39	27.03	.39
27.27	.94	26.4	.28	27.62	.38
27.9	.92	27.02	.1	28.29	.37
28.52	.88	27.59	-.03	28.88	.36

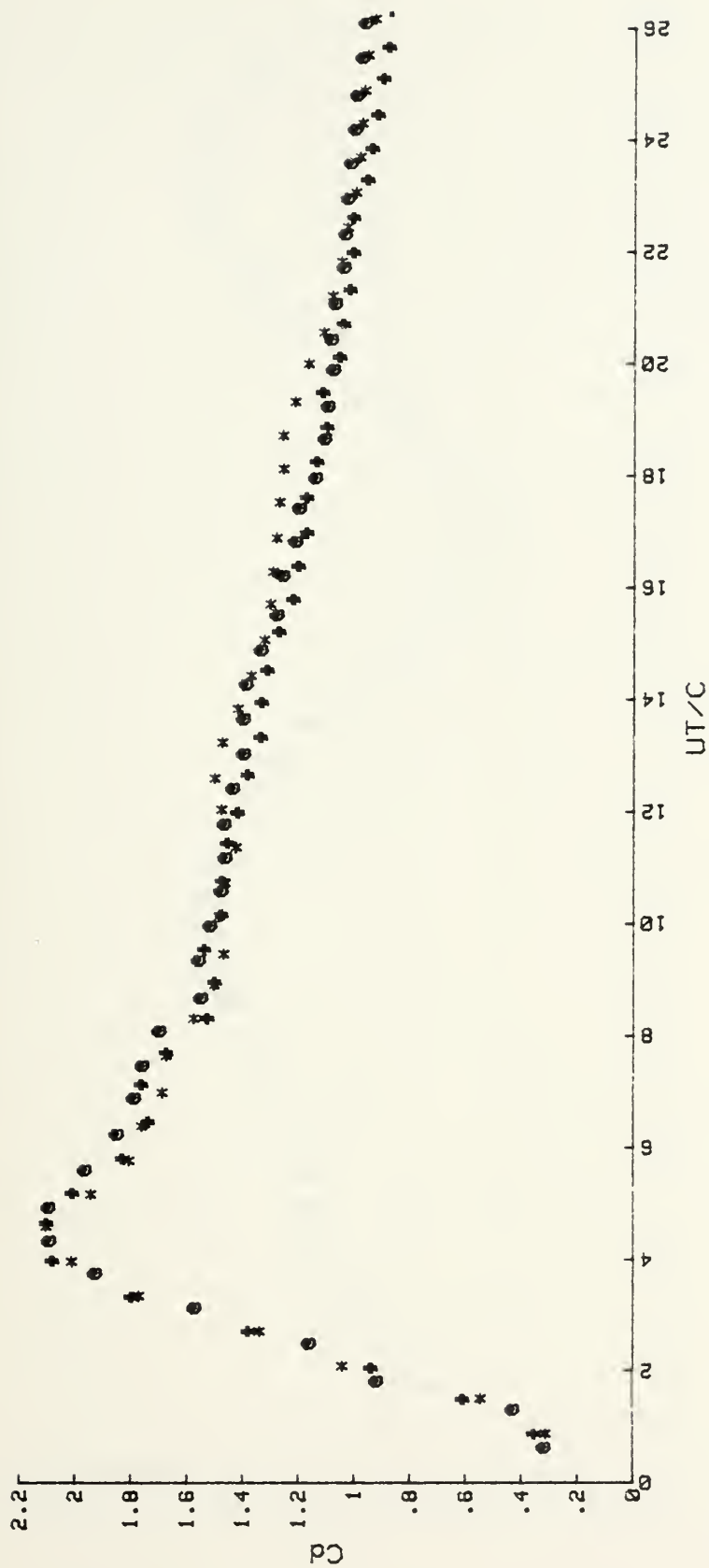


Figure 92. C_d vs. UT/C for the T-Shaped Body at -25° .

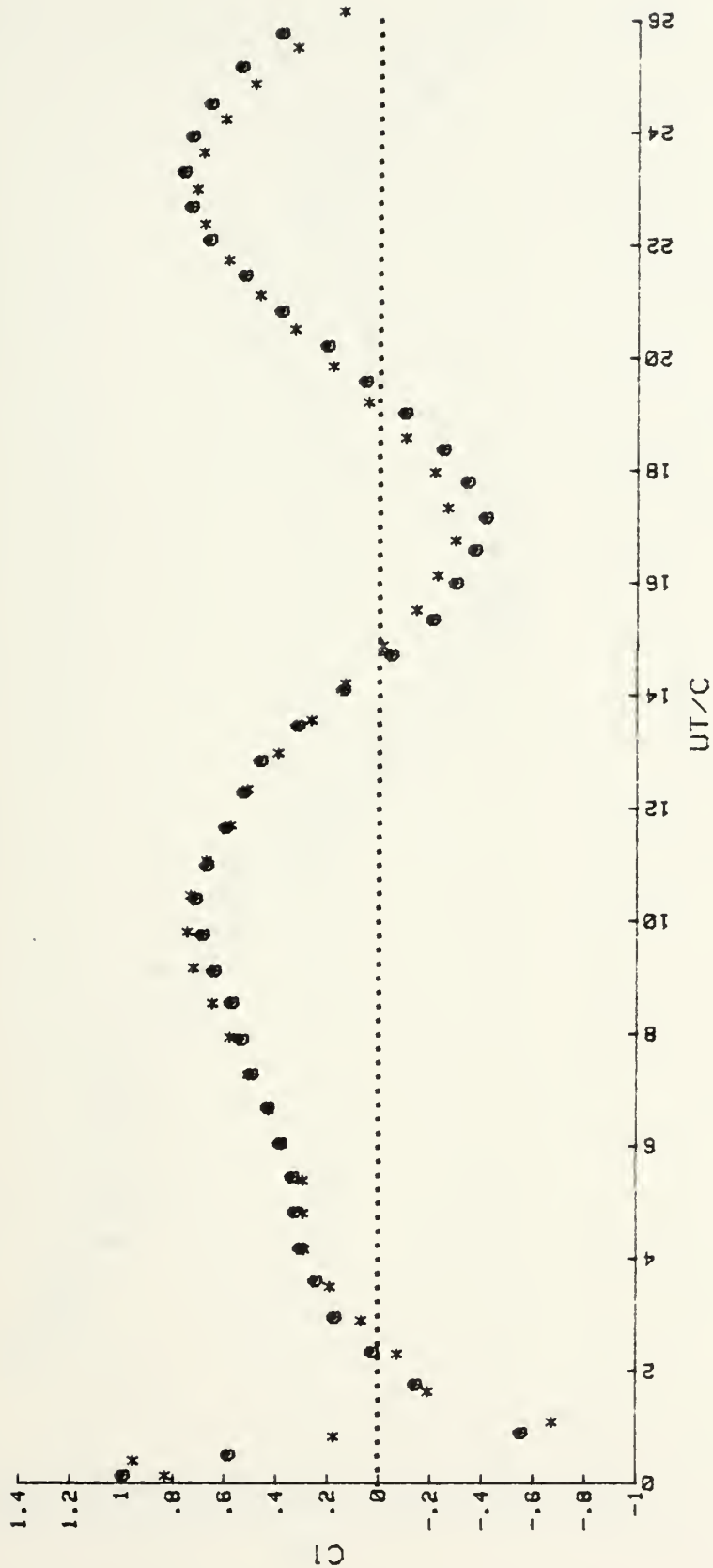


Figure 93. C1 vs. UT/C for the T-Shaped Body at -25 deg.

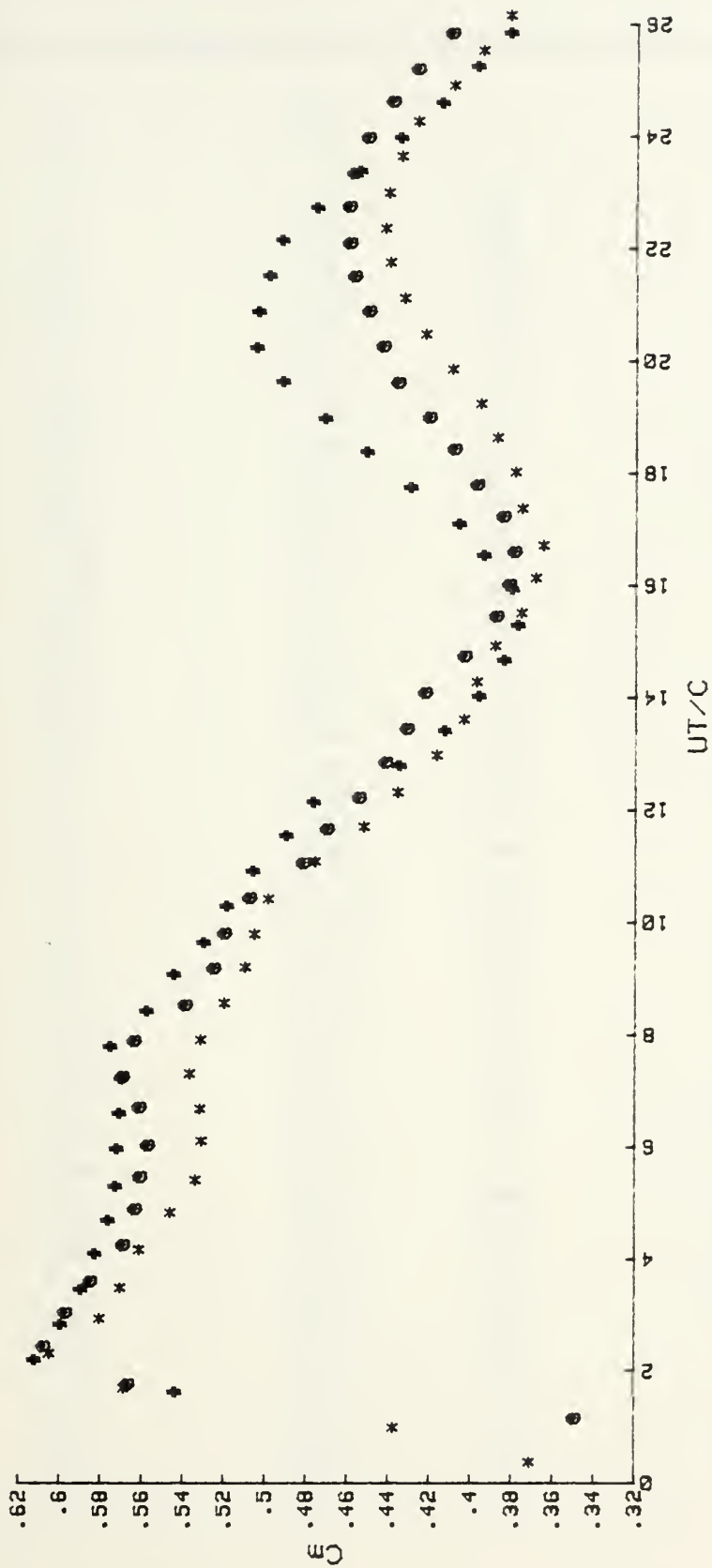


Figure 94. C_m vs. UT/C for the T-Shaped Body at -25° .

APPENDIX X: REPRESENTATIVE DATA FOR T-SHAPED BODY AT -30 DEGREES

<u>UT/C</u>	<u>Cd</u>	<u>UT/C</u>	<u>C1</u>	<u>UT/C</u>	<u>Cm</u>
.62	.19	.13	.84	.38	.28
1.24	.4	.38	.98	1.22	.42
1.89	.75	.75	.38	1.7	.66
2.47	.87	.98	-.23	2.27	.67
3.11	1.41	1.59	-.27	2.94	.63
3.72	1.75	2.21	-.21	3.55	.64
4.37	2	2.81	.11	4.11	.62
4.96	2.21	3.41	.28	4.7	.61
5.55	2.14	4.25	.47	5.32	.59
6.19	1.98	4.65	.6	5.99	.59
6.86	1.9	5.29	.67	6.63	.38
7.49	1.91	5.89	.75	7.13	.6
8.16	1.92	6.52	.83	7.75	.6
8.77	1.79	7.13	.95	8.37	.56
9.37	1.72	7.73	1.25	9	.55
10	1.66	8.4	1.22	9.68	.55
10.88	1.62	8.99	1.21	10.25	.54
11.31	1.61	9.57	.91	10.9	.51
11.87	1.62	10.22	.73	11.57	.47
12.45	1.59	10.81	.43	12.35	.43
13.12	1.54	11.44	.38	12.93	.41
13.71	1.47	12.25	-.24	13.5	.4
14.3	1.44	12.75	-.47	14.28	.38
14.89	1.46	13.38	-.64	14.7	.39
15.55	1.48	13.98	-.77	15.24	.4
16.21	1.5	14.58	-.74	15.8	.42
16.75	1.51	15.15	-.62	16.38	.44
17.29	1.47	15.73	-.42	16.94	.45
17.97	1.47	16.35	-.13	17.57	.48
18.61	1.44	16.95	.17	18.19	.5
19.2	1.43	17.6	.46	18.79	.52
19.77	1.41	18.17	.73	19.37	.53
20.36	1.39	18.77	.95	20.31	.53
21.21	1.36	19.38	1.1	20.63	.52
21.61	1.36	19.99	1.14	21.23	.51
22.23	1.37	20.6	1.29	21.86	.49
22.87	1.38	21.22	.95	22.49	.46
23.47	1.33	21.82	.73	23.12	.44
24.26	1.3	22.44	.49	23.75	.42
24.74	1.26	23.25	.23	24.38	.39
25.34	1.22	23.67	-.21	25	.38
25.96	1.18	24.31	-.23	25.65	.37
26.59	1.18	24.96	-.4	26.28	.36
27.19	1.13	25.57	-.48	26.88	.36
28.41	1.11	26.18	-.47	27.45	.37
29.27	1.12	26.78	-.43	28.25	.38

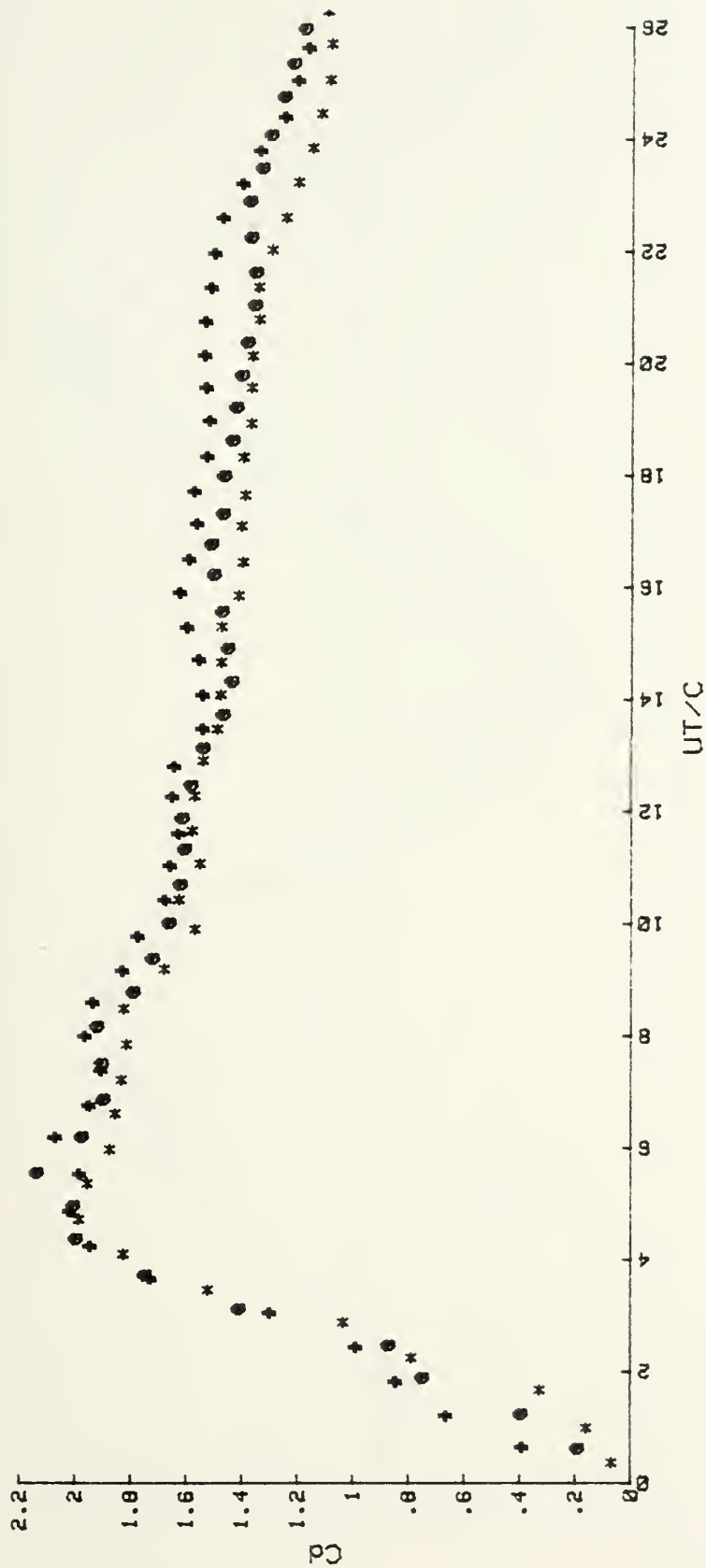


Figure 95. C_d vs. UT/C for the T-Shaped Body at -30° .

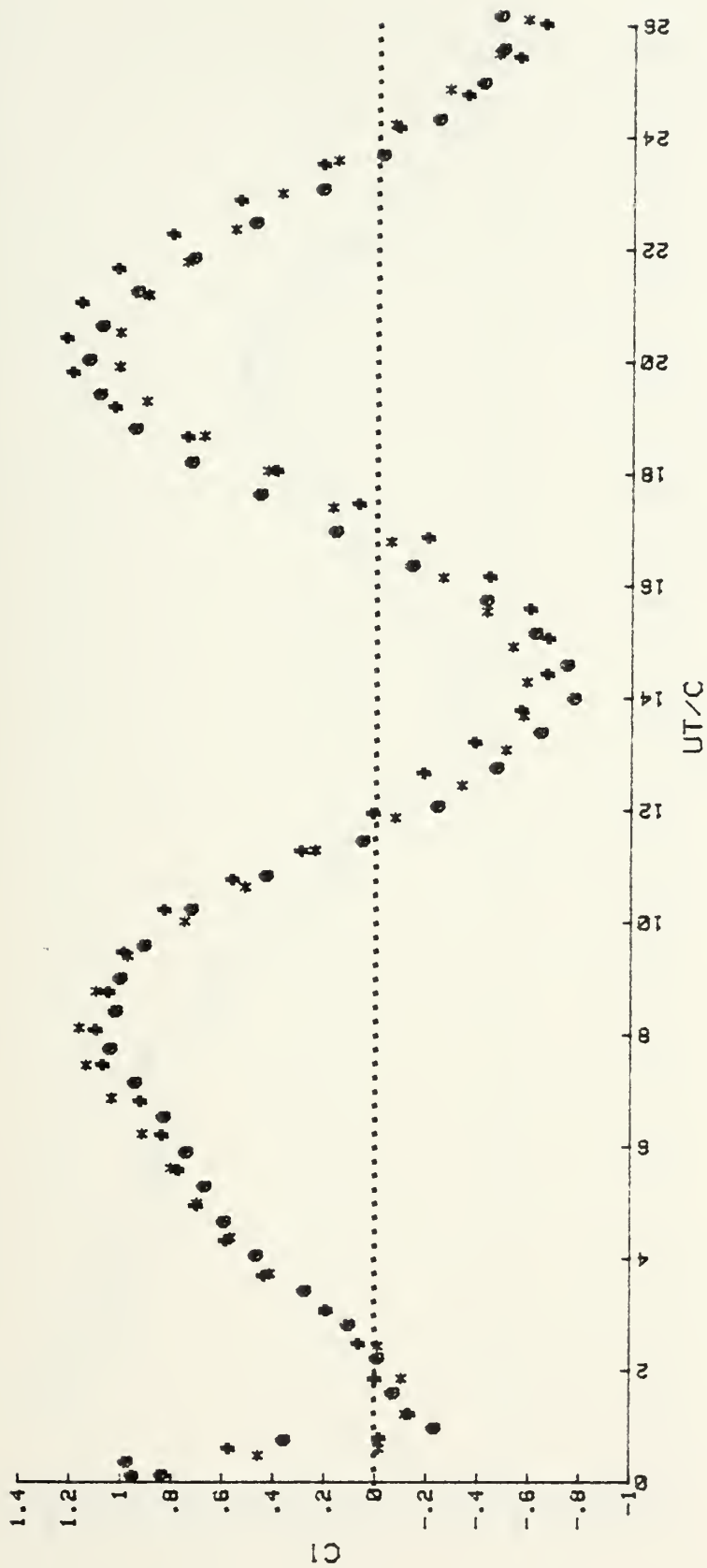


Figure 96. $C1$ vs. UT/C for the T-Shaped Body at -30° .

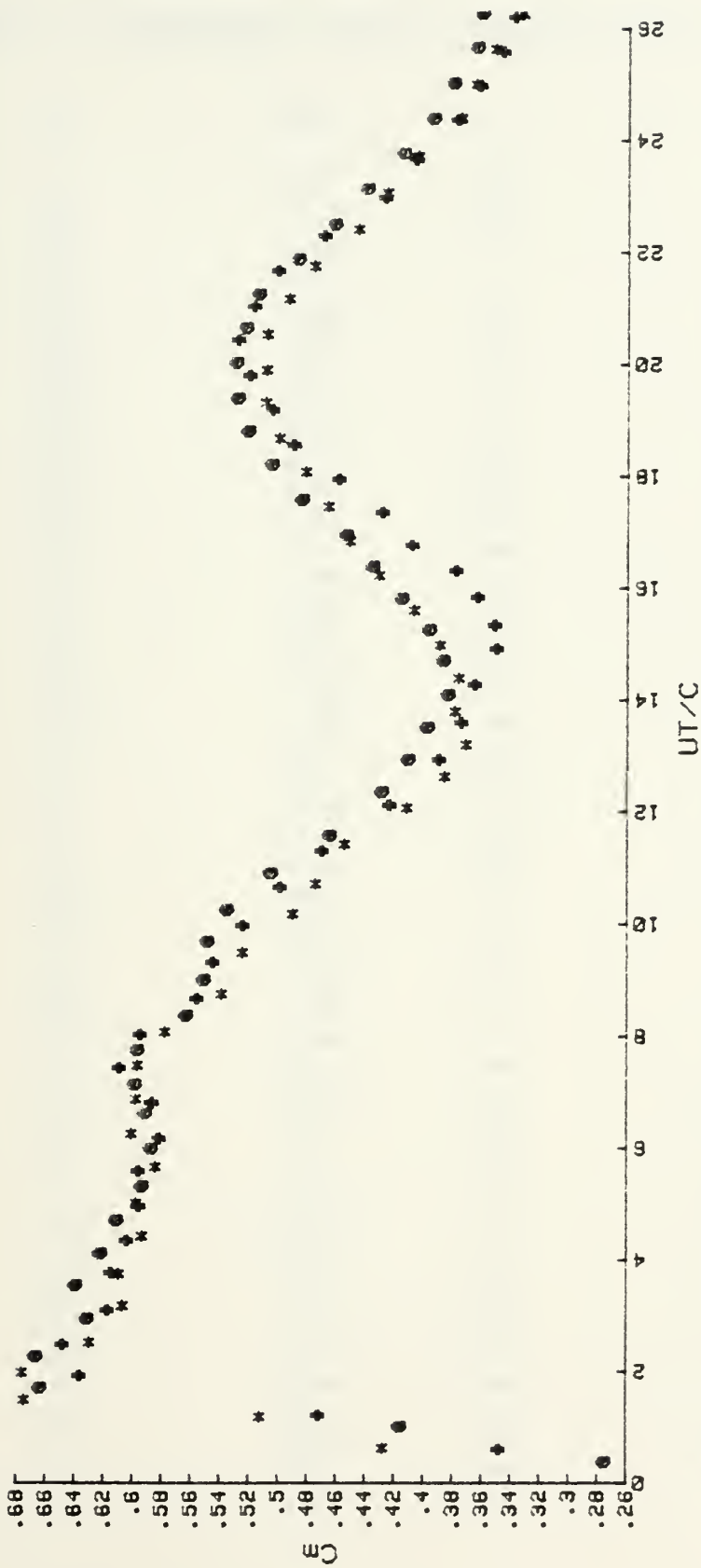


Figure 97. Cm vs. UT/C for the T-Shaped Body at -30 deg.

APPENDIX Y: REPRESENTATIVE DATA FOR T-SHAPED BODY AT -45 DEGREES

<u>UT/C</u>	<u>Cd</u>	<u>UT/C</u>	<u>Cl</u>	<u>UT/C</u>	<u>Cm</u>
.83	.2	.23	1.87	.73	.62
1.24	.34	.64	.53	1.44	.73
1.75	.55	1.12	-.18	1.97	.69
2.46	.88	1.82	.1	2.68	.89
3.28	1.17	2.44	.18	3.29	.88
3.71	1.39	3.28	.38	3.89	.89
4.33	1.62	3.68	.81	5.1	.71
5.84	1.86	4.3	.99	4.5	.7
5.75	2.25	4.93	1.4	5.73	.73
6.46	2.2	5.54	1.75	6.39	.73
7.21	2.28	6.13	1.95	7.23	.75
7.94	2.28	6.77	2.25	7.81	.74
8.77	2.35	7.37	2.28	8.25	.71
9.43	2.28	8	2.22	8.89	.67
9.89	2.3	8.62	1.81	9.53	.61
10.35	2.23	9.23	1.51	10.18	.56
10.92	2.1	9.86	1.29	10.91	.5
11.6	2.01	10.54	.54	11.88	.42
12.18	1.99	11.39	-.11	13.19	.34
12.72	2.26	11.95	-.66	12.54	.4
13.2	2.19	12.51	-1.15	13.7	.33
13.86	2.24	13.12	-1.38	14.34	.33
14.44	2.18	13.83	-1.4	14.93	.36
15	2.14	14.6	-1.33	15.42	.41
15.58	1.93	15.45	-1.28	15.94	.47
16.17	1.85	16.1	-.71	16.47	.55
16.72	1.82	16.37	-.12	17.23	.63
17.3	1.7	16.75	.58	17.65	.69
17.91	1.69	17.28	1.11	18.26	.72
18.55	1.68	17.89	1.51	18.88	.72
19.16	1.72	18.48	1.7	19.47	.69
19.78	1.8	19.12	1.68	20.1	.65
20.39	1.85	19.75	1.52	20.73	.58
21.03	1.82	20.35	1.29	21.39	.52
21.71	1.81	21	.98	22.16	.44
22.34	1.7	21.67	.53	22.8	.39
22.99	1.72	22.38	.21	23.45	.35
23.61	1.62	23.21	-.41	24.22	.31
24.31	1.67	23.55	-.72	24.63	.29
24.9	1.66	24.1	-.97	25.31	.28
25.5	1.68	24.71	-1.12	25.99	.28
26.23	1.63	25.28	-1.12	26.65	.28
26.82	1.53	25.94	-.98	27.22	.32
27.24	1.51	26.65	-.81	27.74	.37
27.8	1.45	27.35	-.59	28.33	.41
28.38	1.33	28	-.28	28.89	.44



Figure 98. C_d vs. UT/C for the T-Shaped Body at -45° .

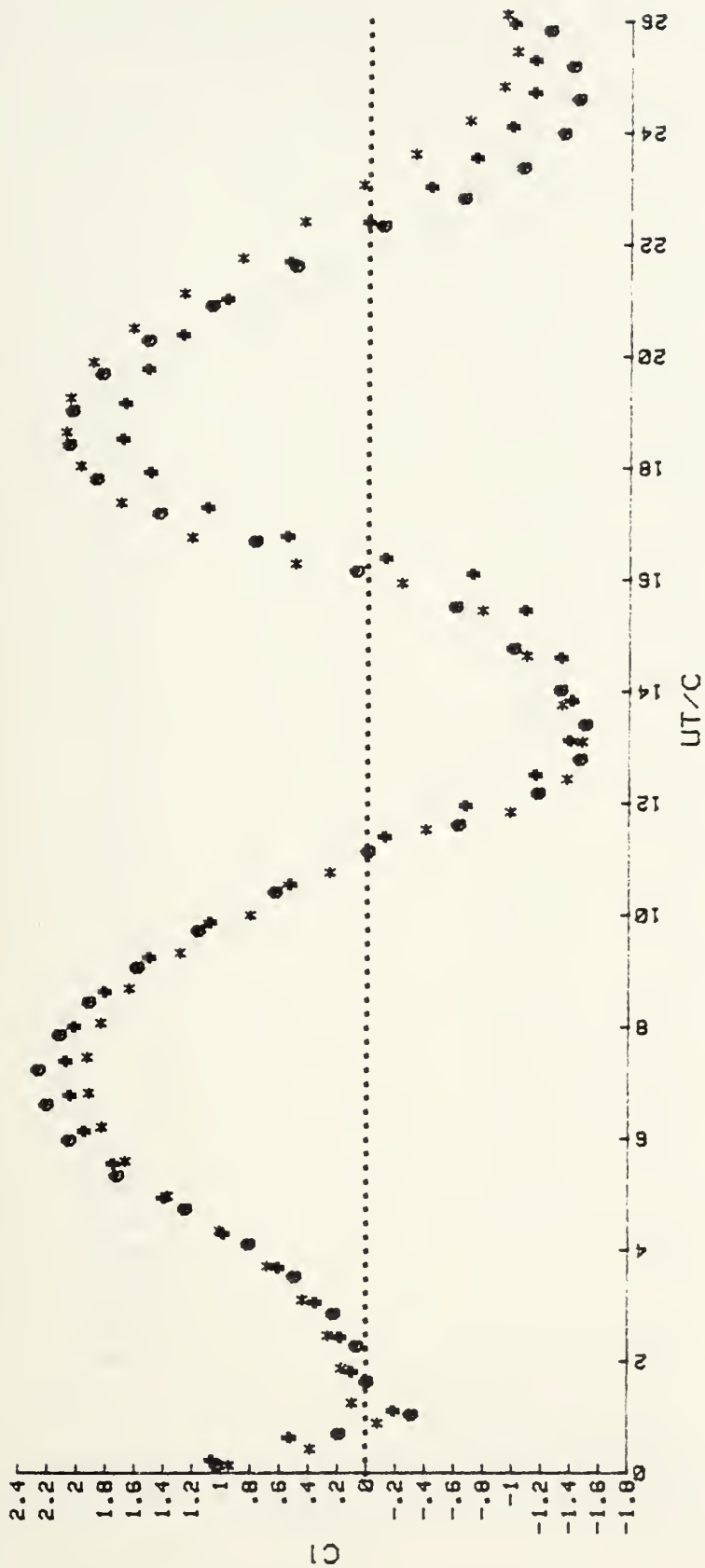


Figure 99. $C1$ vs. UT/C for the T-Shaped Body at -45° .

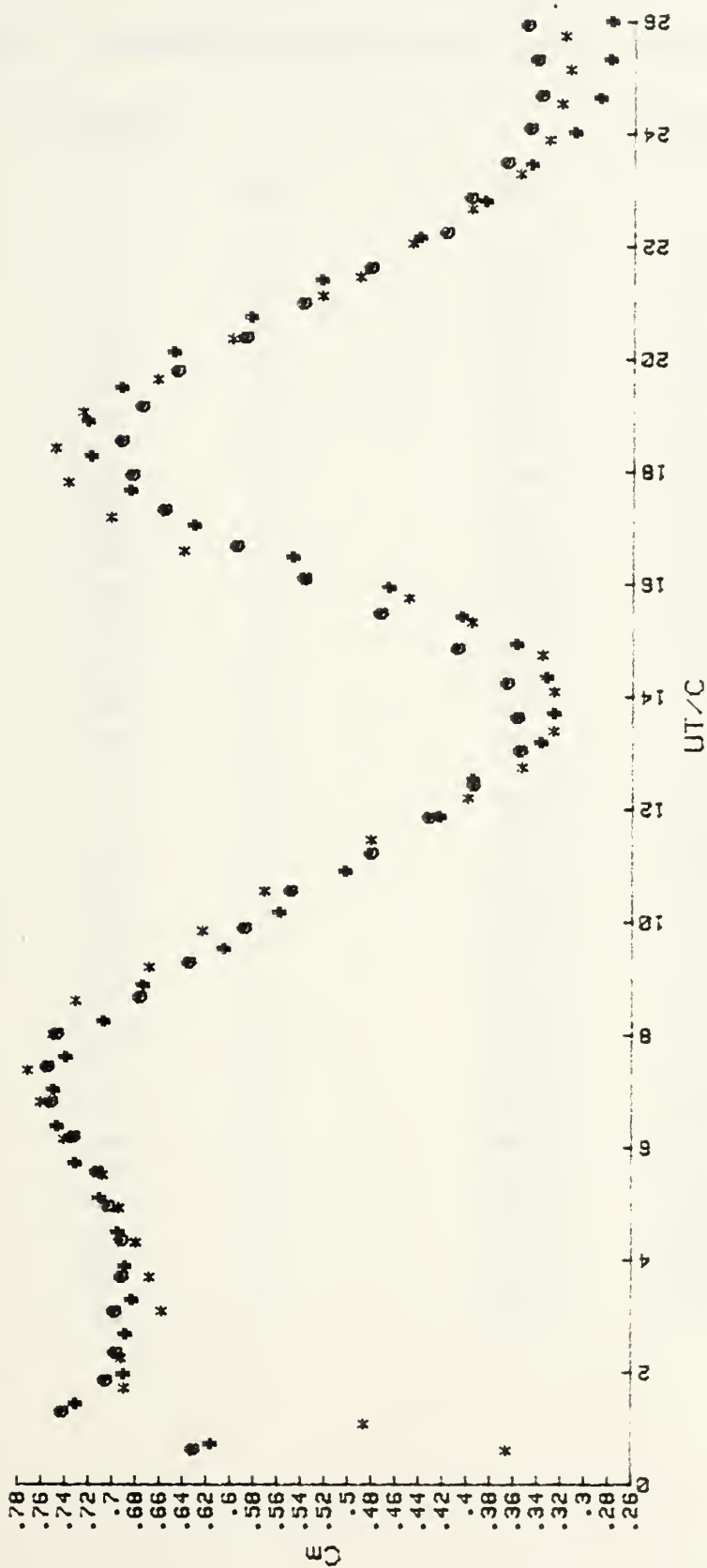


Figure 100. E_C vs. UT/C for the T-Shaped Body at -45° .

APPENDIX Z: REPRESENTATIVE DATA FOR FLAT PLATE AT 90 AND 85 DEGREES

<u>90 DEGREES</u>			<u>85 DEGREES</u>		
<u>UT/B</u>	<u>Cn</u>	<u>X/B</u>	<u>UT/B</u>	<u>Cn</u>	<u>X/B</u>
1.53	2.71	0	1.91	3.11	.066
2.27	3	0	2.64	2.86	.077
3.01	2.91	0	3.39	2.73	.081
3.76	2.72	0	4.13	2.69	.081
4.5	2.63	0	4.88	2.63	.086
5.24	2.51	0	5.6	2.65	.084
5.98	2.45	0	6.33	2.68	.086
6.73	2.43	0	7.08	2.73	.086
7.48	2.37	0	7.83	2.82	.084
8.23	2.34	0	8.57	2.86	.085
8.98	2.38	0	9.29	2.9	.081
9.73	2.29	0	10.04	2.91	.083
10.47	2.16	0	10.76	2.77	.083
11.2	2.19	0	11.52	2.76	.082
11.95	2.11	0	12.25	2.57	.084
12.7	2.08	0	12.99	2.49	.078
13.46	2.08	0	13.73	2.4	.074
14.21	2.14	0	14.47	2.43	.063
14.96	2.14	0	15.26	2.3	.058
15.71	2.14	0	16.05	2.3	.052
16.46	2.17	0	16.77	2.31	.047
17.22	2.23	0	17.47	2.29	.047
17.97	2.25	0	18.23	2.32	.045
18.71	2.27	0	18.96	2.36	.048
19.46	2.25	0	19.66	2.34	.047
20.2	2.23	0	20.38	2.36	.049
20.92	2.18	0	21.12	2.36	.05
21.66	2.18	0	21.87	2.43	.052
22.42	2.14	0	22.58	2.43	.057
23.18	2.11	0	23.32	2.42	.057
23.91	2.14	0	24.06	2.39	.062
24.65	2.07	0	24.8	2.37	.062
25.39	2.07	0	25.55	2.35	.063
26.14	2.01	0	26.27	2.3	.066
26.87	2.01	0	27.01	2.28	.064
27.61	1.93	0	27.75	2.23	.067
28.37	1.9	0	28.51	2.15	.068
29.14	1.89	0	29.26	2.14	.07

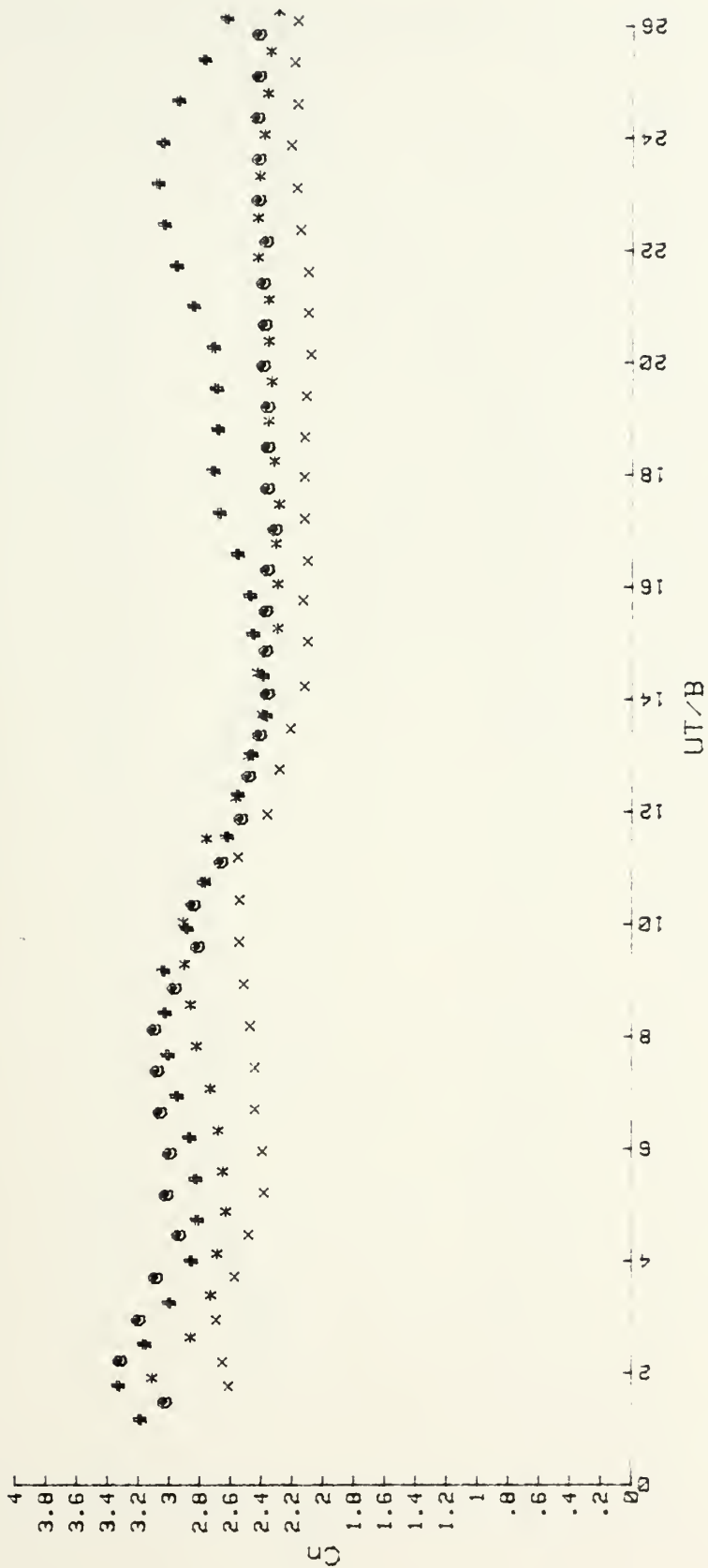


Figure 101. Cn vs. UT/B for the Flat Plate at 85 deg.



Figure 102. X/B vs. UT/B for the Flat Plate at 85° .

APPENDIX Aa: REPRESENTATIVE DATA FOR FLAT PLATE AT 80 AND 75 DEGREES

<u>80 DEGREES</u>			<u>75 DEGREES</u>		
<u>U/B</u>	<u>Cn</u>	<u>X/B</u>	<u>U/B</u>	<u>Cn</u>	<u>X/B</u>
1.17	3.26	.108	1.17	3.14	.224
1.9	3.4	.122	1.76	3.24	.171
2.94	3.14	.128	2.47	3.17	.157
3.38	3.04	.132	3.22	3.19	.153
4.13	3.06	.131	3.95	3.18	.14
4.86	3.17	.124	4.68	3.16	.127
5.6	3.18	.123	5.42	3.17	.111
6.32	3.2	.12	6.13	3.03	.1
7.07	3.29	.112	6.86	2.96	.09
7.8	3.25	.113	7.59	2.86	.083
8.56	2.99	.115	8.33	2.9	.037
9.31	2.81	.115	9.06	3.39	-.035
10.23	2.62	.091	9.8	3.96	-.066
10.77	2.91	.019	10.52	4.04	-.067
11.52	3.39	-.044	11.25	3.82	-.06
12.26	3.8	-.053	11.98	3.65	-.002
13.02	3.84	-.05	12.7	4.24	.12
13.79	3.75	-.041	13.43	4.95	.176
14.53	3.83	.03	14.17	5.35	.174
15.29	3.97	.101	14.89	5.4	.171
15.85	4.23	.144	15.62	5.19	.152
15.78	4.37	.156	16.34	4.86	.124
17.51	4.46	.156	17.07	4.41	.107
18.23	4.53	.15	17.81	3.78	.091
18.96	4.31	.15	18.52	3.71	.024
19.68	3.89	.135	19.26	3.91	-.044
20.4	3.5	.118	19.99	4.02	-.082
21.13	3.35	.064	20.72	4	-.096
21.84	3.3	-.002	21.45	3.86	-.099
22.6	3.44	-.035	22.18	3.64	-.079
23.31	3.47	-.052	22.92	3.34	-.049
24.05	3.46	-.051	23.66	3.12	-.019
24.78	3.38	-.05	24.38	2.96	.024
25.53	3.2	-.05	25.1	3.01	.063
26.27	2.93	-.038	25.83	3.1	.091
27.01	2.68	-.012	26.56	3.19	.096
27.74	2.65	.032	27.28	3.19	.096
28.47	2.7	.078	28.02	3.07	.1
29.21	2.74	.102	28.75	2.98	.096



Figure 103. C_n vs. UT/B for the Flat Plate at 80 deg.

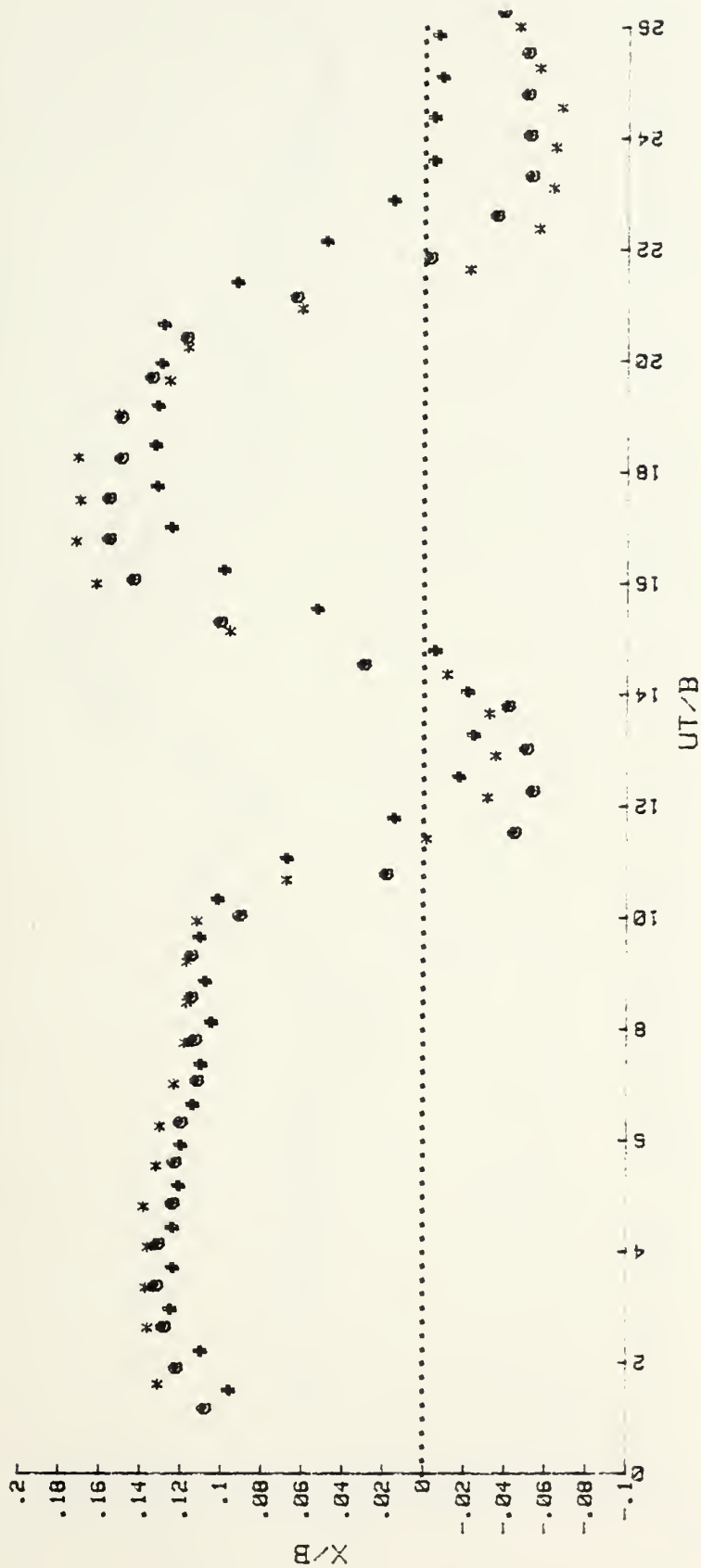


Figure 104. X/B vs. UT/B for the Flat Plate at 80 deg.

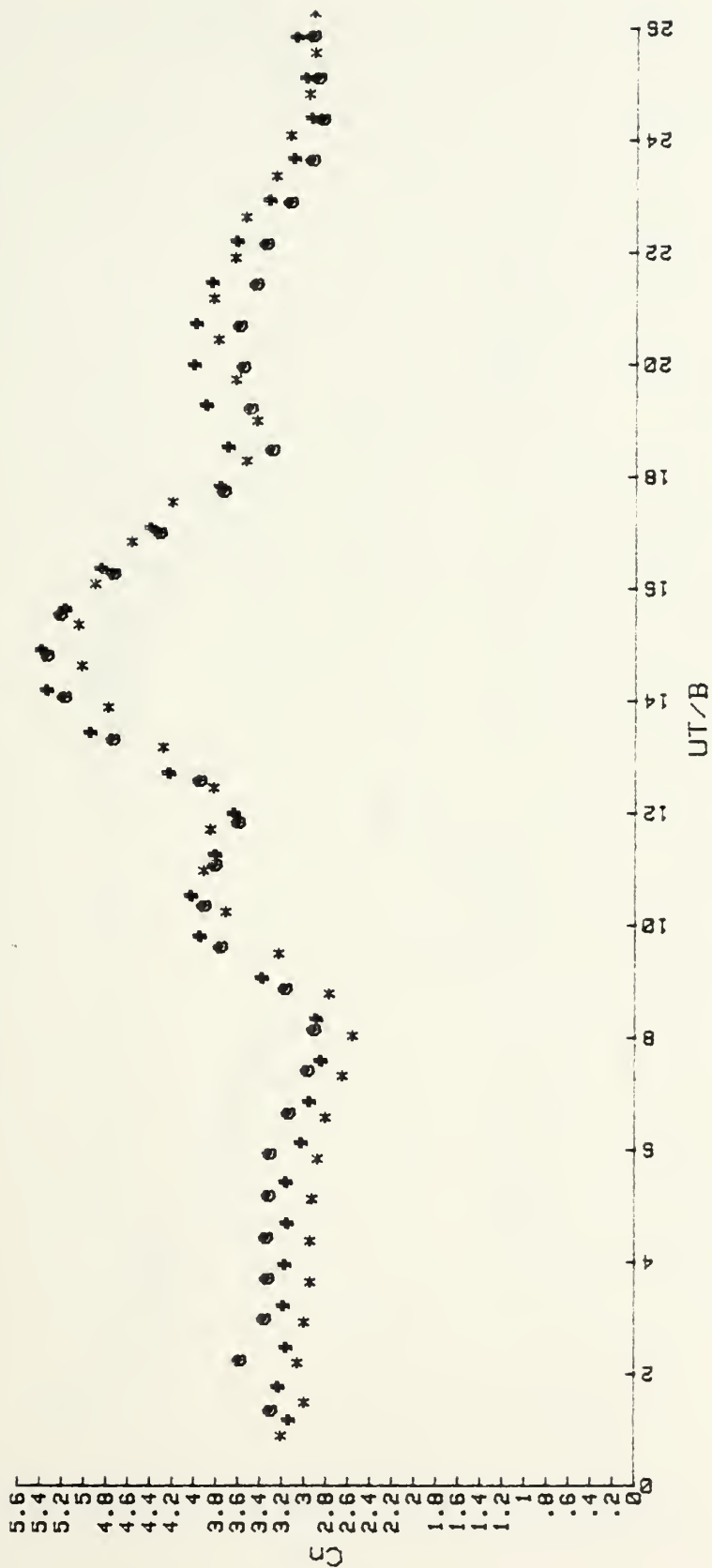


Figure 105. C_n vs. UT/B for the Flat Plate at 75 deg.

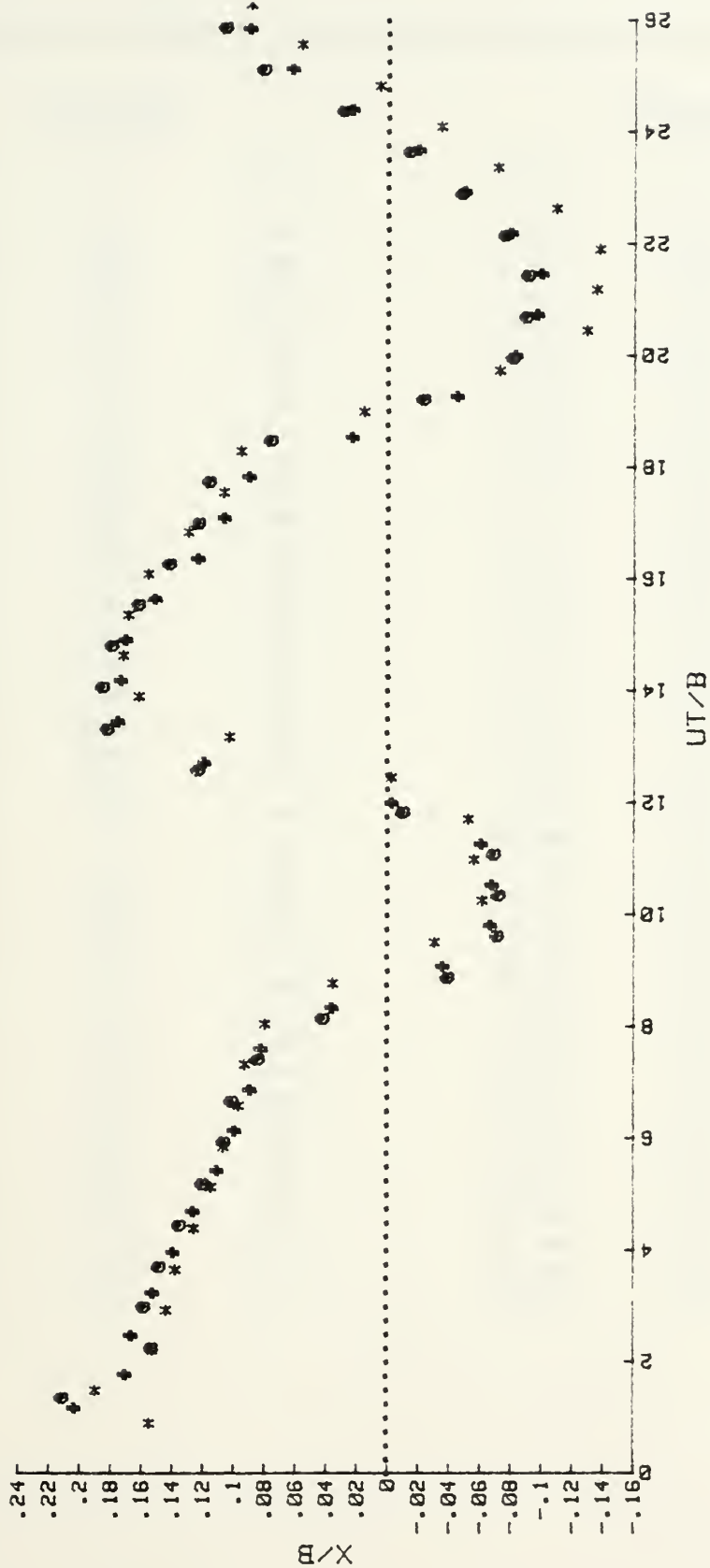


Figure 106. X/B vs. UT/B for the Flat Plate at 75 deg.

APPENDIX AB: REPRESENTATIVE DATA FOR FLAT PLATE AT 70 AND 65 DEGREES

<u>70 DEGREES</u>			<u>65 DEGREES</u>		
<u>UT/B</u>	<u>Cn</u>	<u>X/B</u>	<u>UT/B</u>	<u>Cn</u>	<u>X/B</u>
1.32	3.07	.228	1.32	2.86	.376
2.07	3.52	.202	2.07	3.43	.25
2.82	3.31	.214	2.81	3.5	.215
3.55	3.35	.203	3.54	3.42	.193
4.28	3.41	.181	4.28	3.38	.162
5.01	3.28	.167	5.01	3.21	.137
5.75	3.2	.15	5.76	2.95	.13
6.49	3	.147	6.49	2.65	.129
7.23	2.86	.136	7.25	2.76	.07
7.97	3.06	.077	7.97	3.33	-.027
8.72	3.63	-.004	8.71	3.59	-.066
9.45	3.82	-.03	9.44	3.62	-.064
10.18	3.75	-.031	10.18	3.47	-.043
10.92	3.51	-.03	10.92	3.54	.05
11.66	3.6	.037	11.67	4.08	.145
12.39	4.35	.138	12.4	4.71	.172
13.14	4.99	.163	13.14	4.99	.168
13.87	5.27	.162	13.87	5.02	.162
14.62	5.29	.139	14.61	4.9	.135
15.34	5.03	.156	15.34	4.5	.117
16.08	4.50	.145	16.08	3.83	.107
16.83	4	.14	16.82	3.7	.01
17.58	3.47	.125	17.55	3.79	-.092
18.3	3.69	.021	18.3	3.93	-.136
19.04	3.88	-.061	19.03	3.69	-.147
19.77	3.84	-.087	19.77	3.57	-.136
20.52	3.7	-.092	20.52	3.38	-.082
21.27	3.56	-.094	21.25	3.04	-.022
22	3.44	-.073	21.98	3.02	.057
22.73	3.15	-.027	22.72	3.02	.137
23.47	3.13	.031	23.46	3.2	.155
24.21	3.18	.094	24.21	3.32	.157
24.95	3.28	.121	24.95	3.42	.153
25.68	3.35	.127	25.68	3.37	.137
26.42	3.33	.129	26.42	3.24	.112
27.17	3.22	.131	27.15	3.13	.076
27.9	3.04	.135	27.89	2.98	.059
28.64	2.8	.141	28.62	2.75	.048

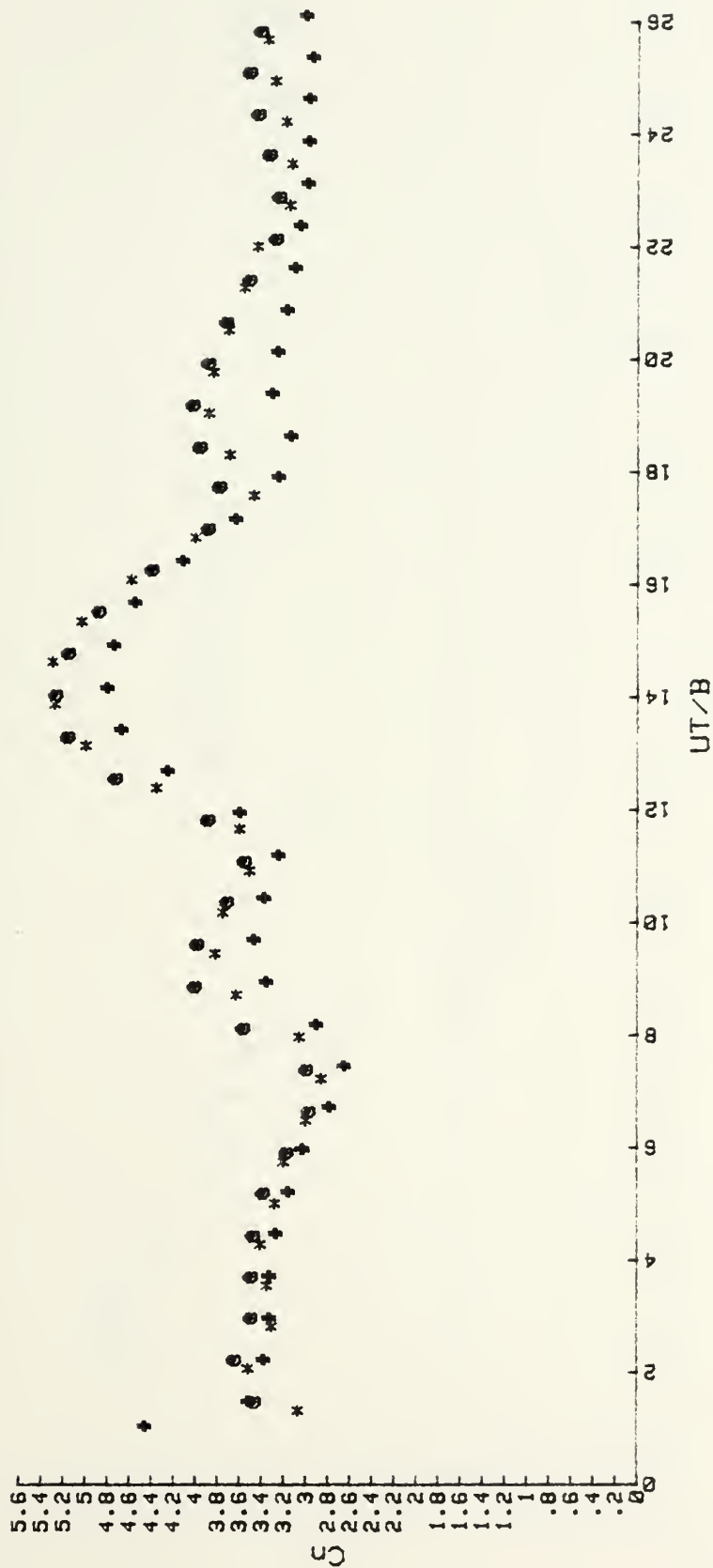


Figure 107. C_n vs. UT/B for the Flat Plate at 70° deg.



Figure 108. X/B vs. UT/B for the Flat Plate at 70 deg.

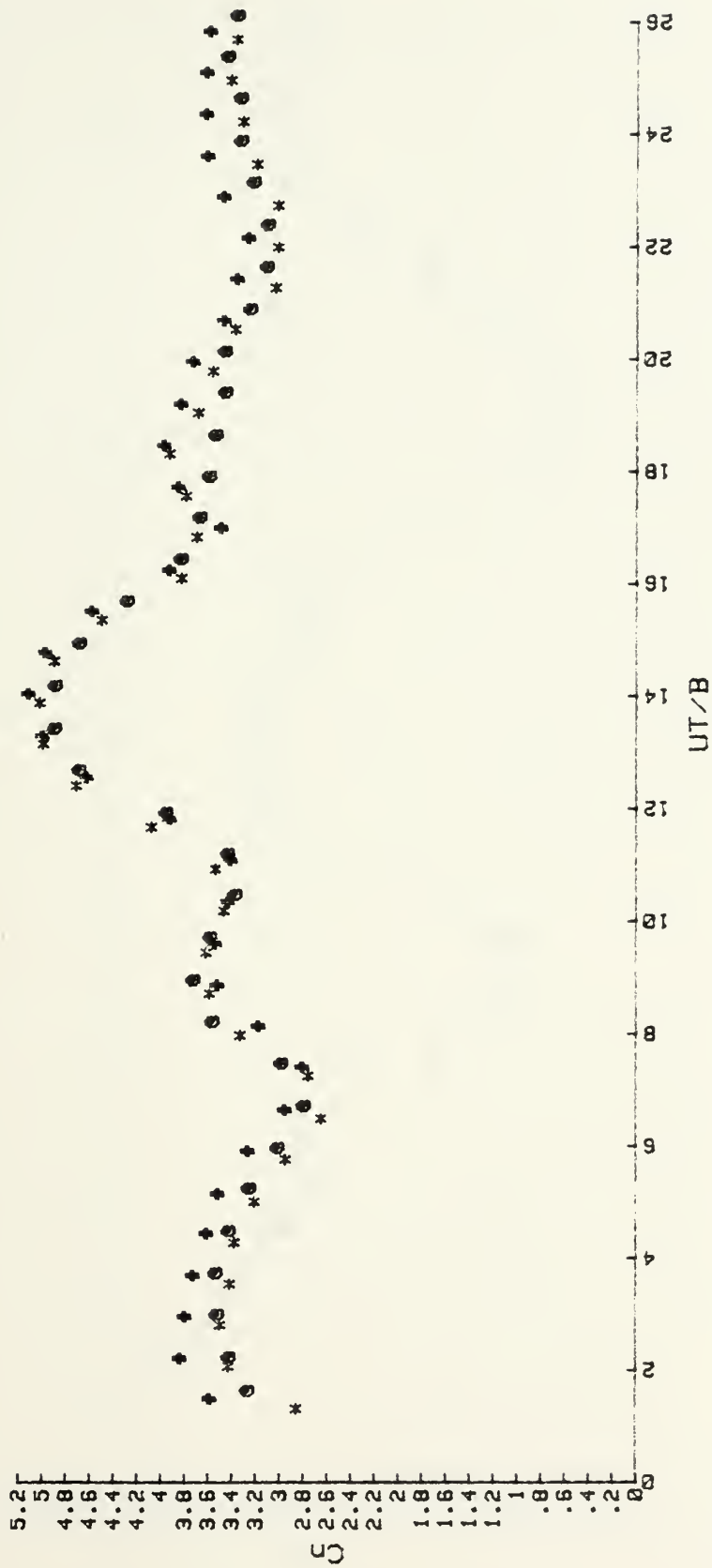


Figure 109. C_n vs. UT/B for the Flat Plate at 65 deg.

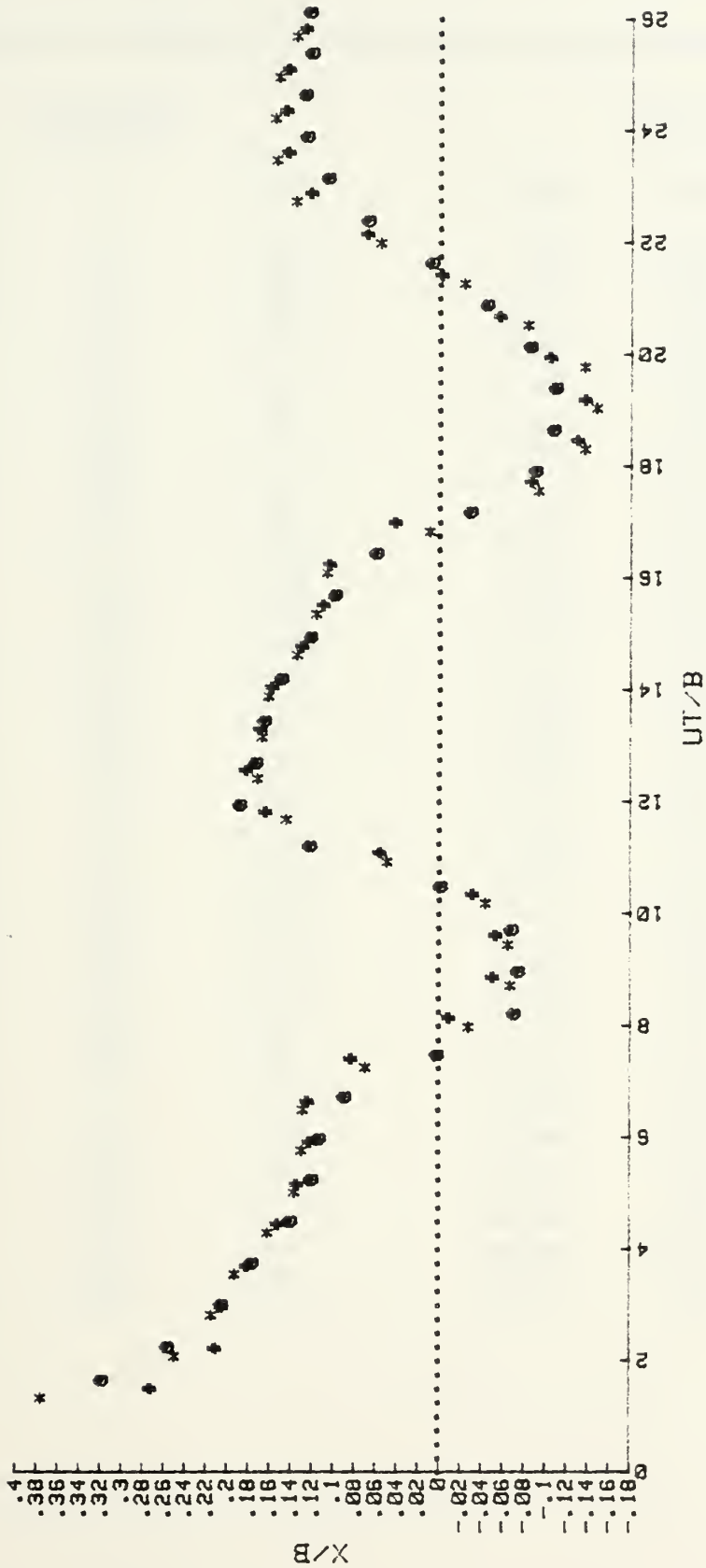


Figure 110. X/B vs. UT/B for the Flat Plate at 65 deg.

APPENDIX AC: REPRESENTATIVE DATA FOR FLAT PLATE AT 60 AND 55 DEGREES

<u>60 DEGREES</u>			<u>55 DEGREES</u>		
<u>UT/B</u>	<u>Cn</u>	<u>X/B</u>	<u>UT/B</u>	<u>Cn</u>	<u>X/B</u>
.74	2.9	.327	1.02	2.86	.387
1.46	3.4	.278	1.46	3.23	.337
2.19	3.43	.266	2.19	3.39	.298
2.91	3.43	.251	2.92	3.5	.265
3.64	3.47	.214	3.66	3.52	.223
4.37	3.45	.184	4.38	3.4	.186
5.1	3.15	.167	5.11	3.26	.156
5.82	2.95	.152	5.84	2.97	.155
6.57	2.65	.172	6.57	2.64	.156
7.31	2.69	.123	7.3	2.56	.103
8.04	2.98	.232	8.02	2.87	.201
8.76	3.17	-.216	8.75	3.25	-.234
9.49	3.16	-.215	9.49	2.97	-.23
10.23	3.08	-.221	10.23	2.89	.319
10.97	3.14	.286	10.95	2.99	.115
11.72	3.53	.168	11.67	3.4	.178
12.45	4.07	.174	12.39	3.96	.168
13.23	4.53	.158	13.12	4.28	.159
13.94	4.68	.15	13.85	4.42	.144
14.66	4.6	.129	14.57	4.38	.124
15.4	4.36	.115	15.31	4.29	.113
16.29	3.9	.281	16.05	3.77	.073
16.82	3.69	-.204	16.78	3.46	.23
17.54	3.49	-.259	17.51	3.28	.205
18.27	3.53	-.278	18.24	3.29	.201
19	3.37	-.279	18.96	2.97	.223
19.72	3.21	-.272	19.69	2.93	.216
20.44	3.29	-.223	20.41	2.81	.247
21.19	2.99	.251	21.15	2.74	.283
21.9	2.97	.128	21.88	2.82	.112
22.63	3.11	.135	22.62	2.87	.131
23.35	3.22	.136	23.34	2.95	.13
24.28	3.34	.134	24.26	3.23	.128
24.82	3.38	.133	24.81	3.24	.124
25.55	3.29	.132	25.53	2.92	.12
26.28	3.12	.134	26.26	2.73	.116
27	2.89	.132	26.98	2.51	.109
27.73	2.72	.123	27.71	2.32	.296

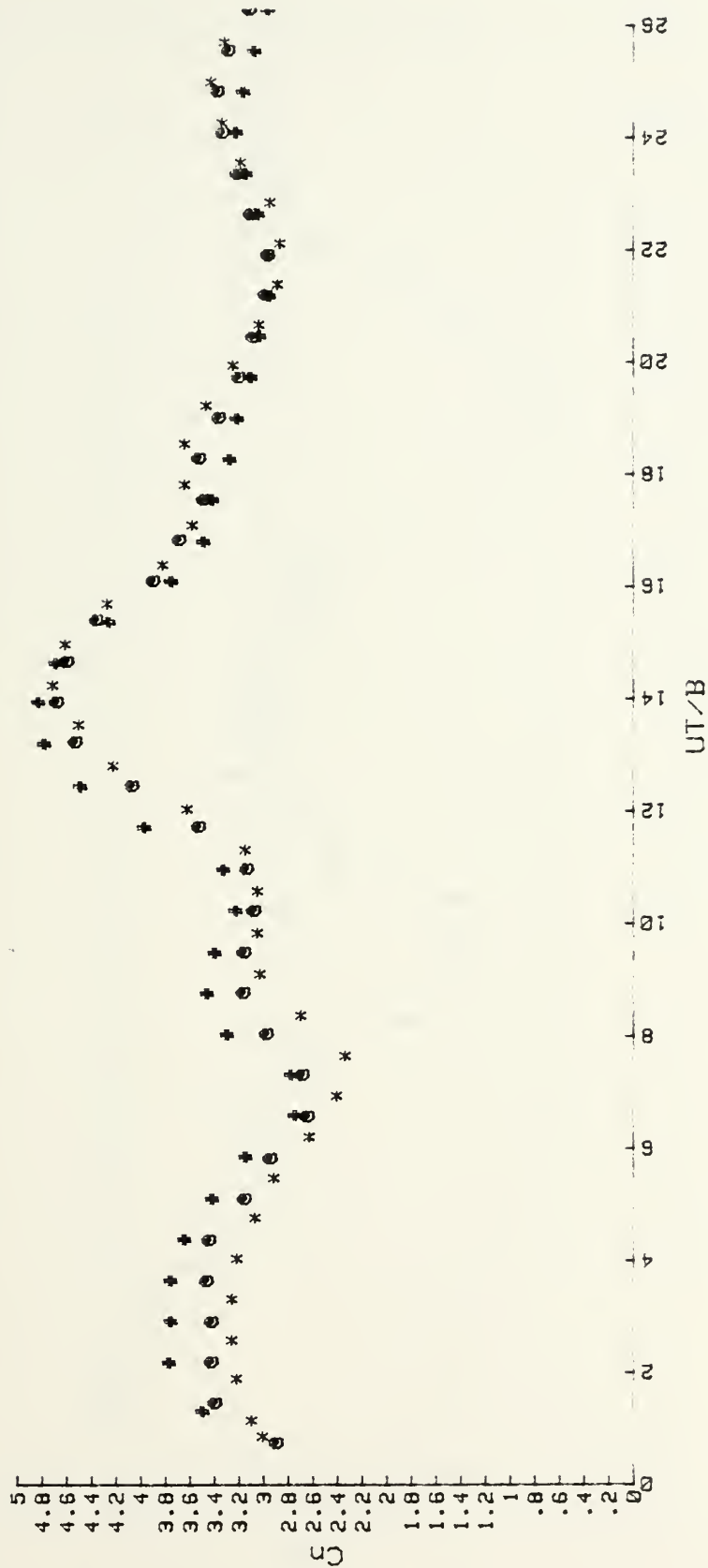


Figure 111. C_n vs. UT/B for the Flat Plate at 60° .

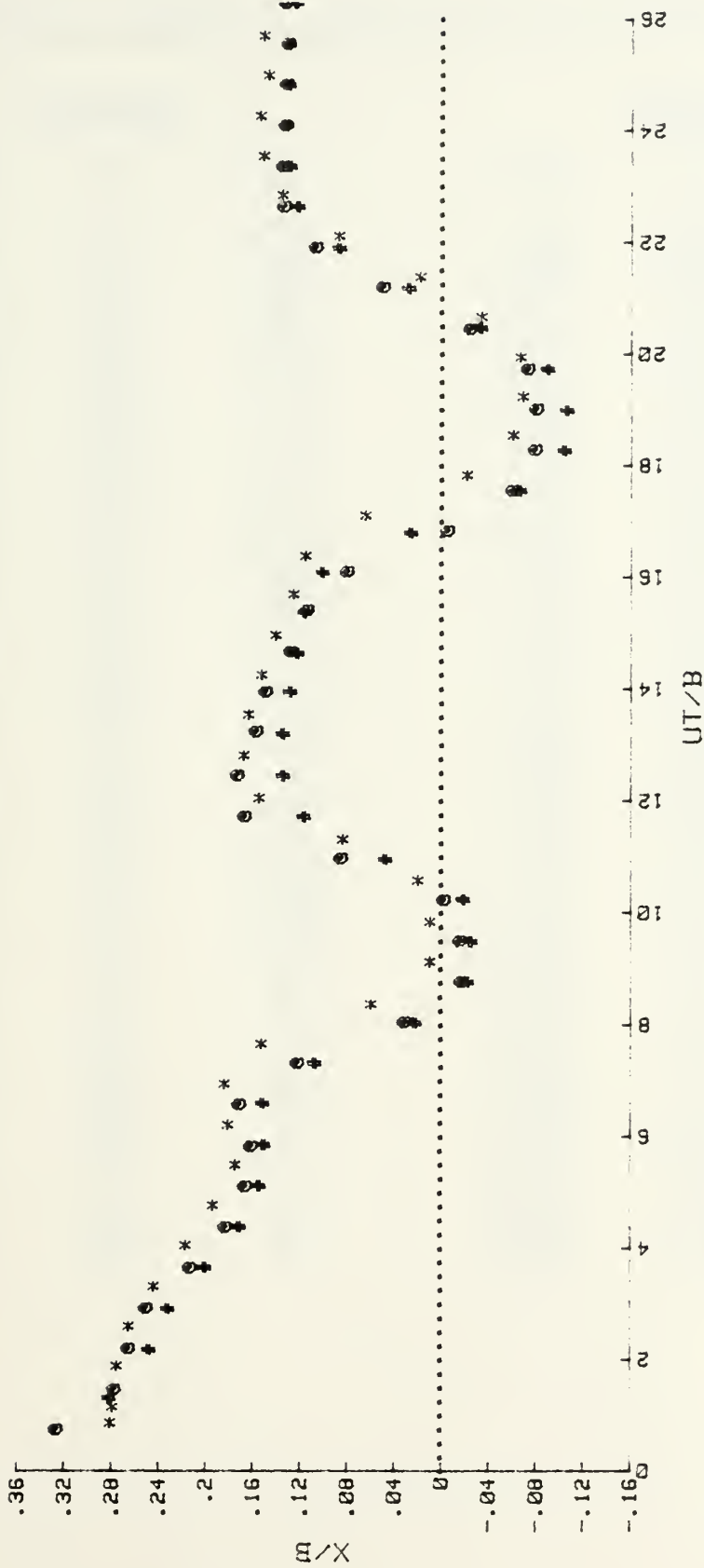


Figure 112. X/B vs. UT/B for the Flat Plate at 60 deg.

APPENDIX AD: REPRESENTATIVE DATA FOR FLAT PLATE AT 50 AND 45 DEGREES

<u>50 DEGREES</u>			<u>45 DEGREES</u>		
<u>UT/B</u>	<u>Cn</u>	<u>X/B</u>	<u>UT/B</u>	<u>Cn</u>	<u>X/B</u>
.89	2.77	.384	1.63	2.99	.419
1.49	3.47	.293	2.22	3.49	.32
2.23	3.63	.258	2.98	3.65	.287
2.98	3.66	.259	3.71	3.7	.241
3.74	3.62	.221	4.47	3.64	.203
4.46	3.53	.183	5.22	3.36	.17
5.22	3.32	.166	5.97	3.23	.158
5.97	2.97	.16	6.71	2.47	.183
6.72	2.43	.188	7.46	2.54	.137
7.46	2.32	.13	8.2	2.9	.04
8.2	2.75	.022	8.94	2.87	.01
8.95	2.81	-.011	9.69	2.69	.02
9.68	2.75	-.004	10.43	2.8	.081
10.45	2.81	.062	11.18	3.18	.138
11.2	3.18	.137	11.93	3.53	.149
11.95	3.63	.164	12.69	3.72	.146
12.69	3.93	.16	13.44	3.73	.144
13.45	4.09	.153	14.18	3.59	.129
14.18	4.1	.139	14.93	3.32	.117
14.91	3.86	.118	15.66	2.95	.097
15.68	3.48	.112	16.42	2.83	.068
16.43	2.99	.104	17.16	2.78	.038
17.17	2.85	.024	17.9	2.66	.035
17.92	2.91	-.026	18.64	2.59	.037
18.65	2.9	-.036	19.4	2.53	.054
19.41	2.77	-.022	20.15	2.55	.097
20.15	2.75	.03	20.89	2.72	.12
20.89	2.7	.103	21.64	2.91	.126
21.63	2.71	.144	22.37	2.98	.127
22.39	2.82	.151	23.14	2.91	.128
23.13	2.89	.153	23.88	2.76	.133
23.87	2.89	.151	24.63	2.62	.126
24.63	2.85	.15	25.37	2.45	.122
25.37	2.7	.148	26.13	2.25	.118
26.13	2.54	.131	26.87	2.13	.111
26.86	2.38	.122	27.62	2.03	.103
27.6	2.22	.109	28.35	1.99	.1

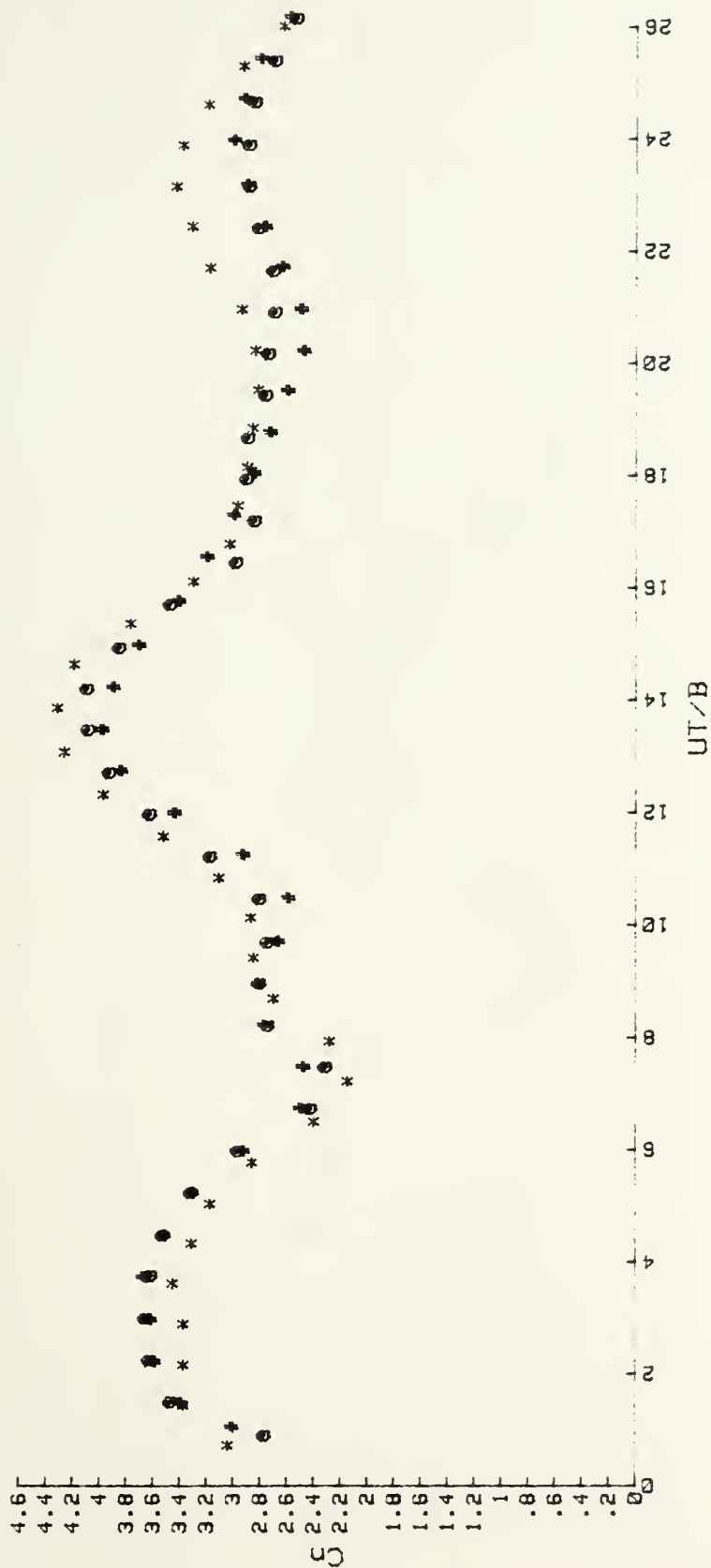


Figure 113. C_n vs. UT/B for the Flat Plate at 50 deg.

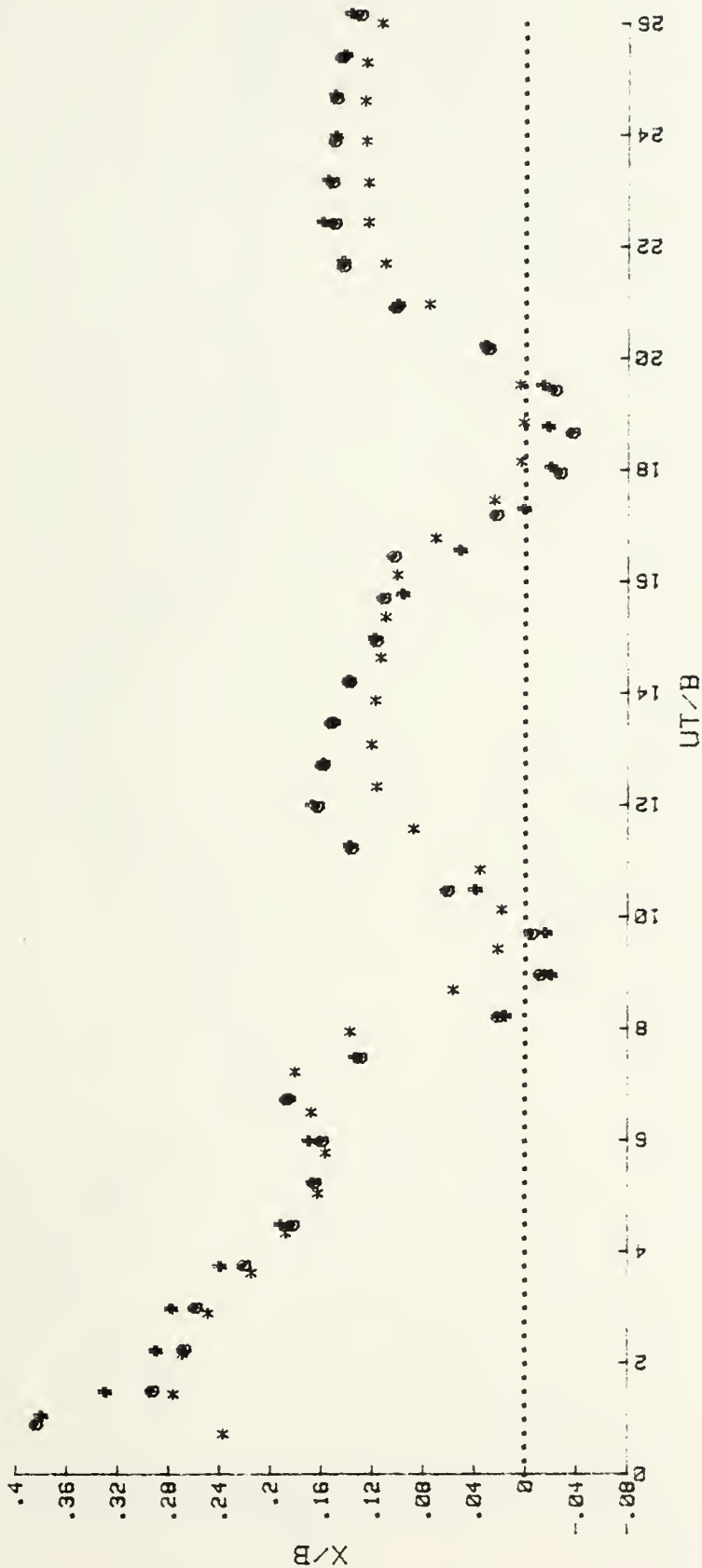


Figure 114. X/B vs. UT/B for the Flat Plate at 50° .

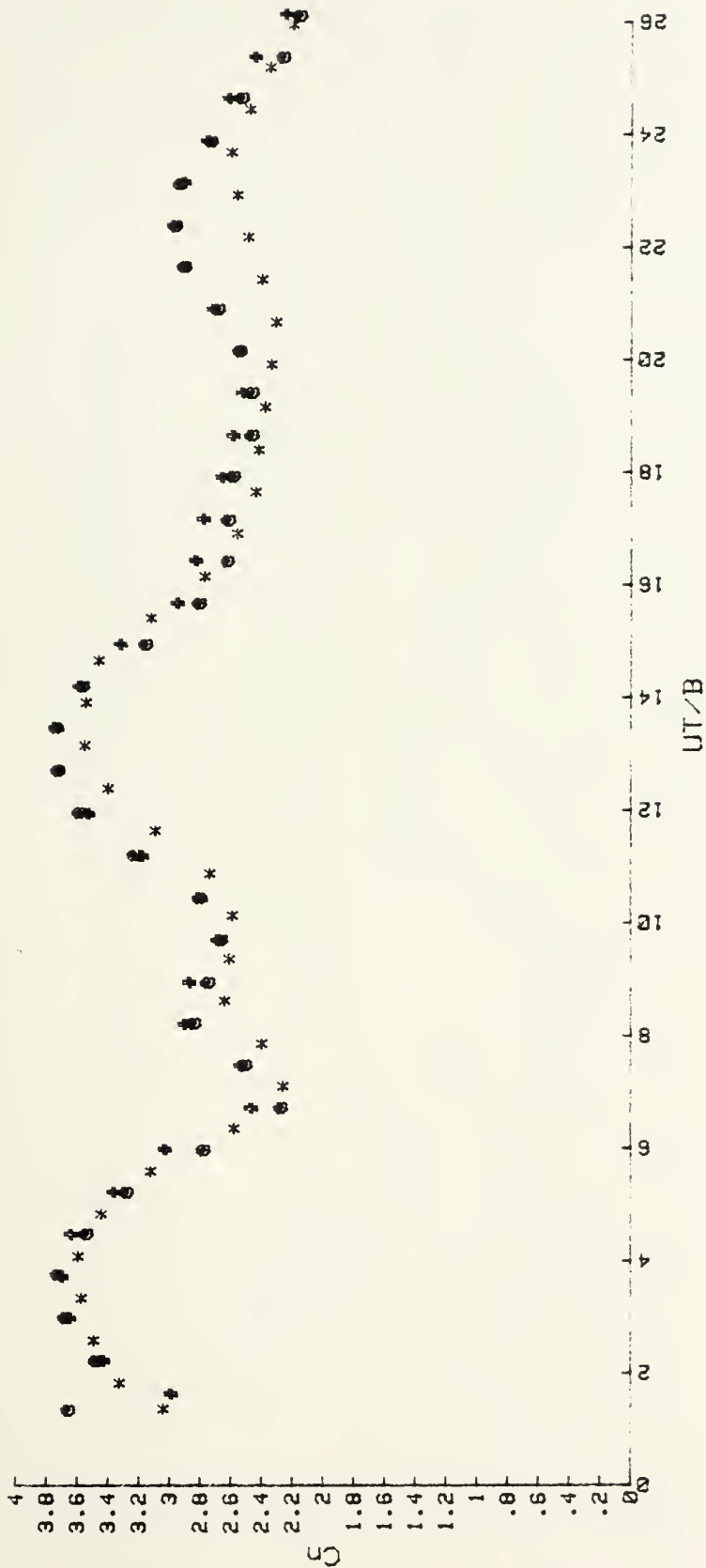


Figure 115. Cn vs. UT/B for the Flat Plate at 45 deg.

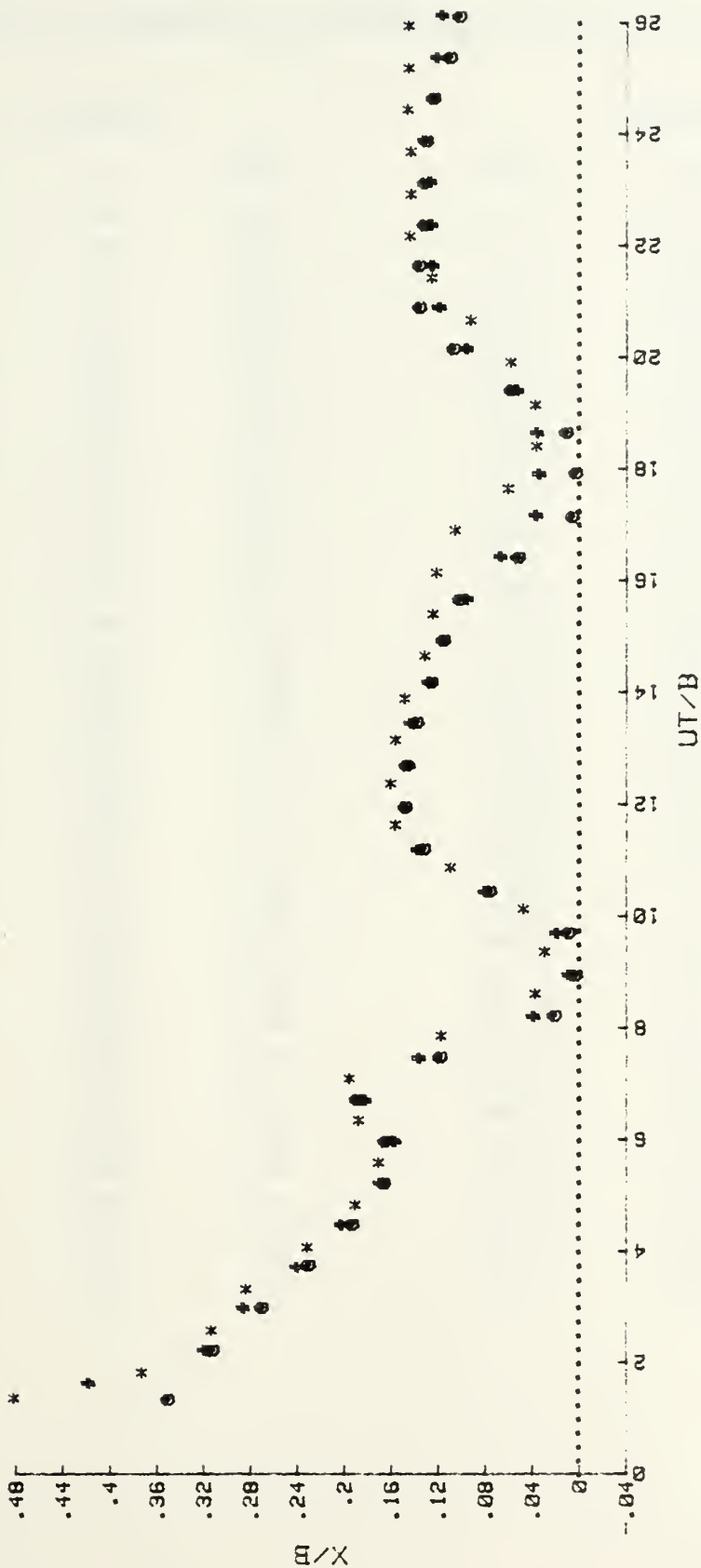


Figure 116. X/B vs. UT/B for the Flat Plate at 45 deg.

APPENDIX A: REPRESENTATIVE DATA FOR FLAT PLATE AT 40 AND 30 DEGREES

<u>40 DEGREES</u>			<u>30 DEGREES</u>		
<u>UT/B</u>	<u>Cn</u>	<u>X/B</u>	<u>UT/B</u>	<u>Cn</u>	<u>X/B</u>
1.05	2.79	.481	1.01	2.05	.375
1.79	3.26	.327	1.47	2.43	.327
2.54	3.4	.311	2.19	2.59	.302
3.27	3.42	.304	2.92	2.8	.293
4.05	3.61	.255	3.65	3.07	.27
4.81	3.52	.214	4.38	3.18	.26
5.52	3.28	.179	5.11	3.33	.231
6.29	2.83	.178	5.84	3.28	.197
7.03	2.3	.199	6.55	3.07	.177
7.77	2.33	.147	7.29	2.6	.181
8.52	2.6	.045	8.03	2.43	.186
9.24	2.59	.019	8.74	2.46	.162
10.01	2.54	.029	9.49	2.41	.153
10.75	2.7	.009	10.22	2.36	.164
11.51	3.05	.144	10.95	2.43	.169
12.25	3.21	.162	11.67	2.68	.169
12.99	3.33	.159	12.38	2.76	.169
13.74	3.33	.158	13.15	2.73	.171
14.48	3.17	.154	13.86	2.49	.181
15.22	2.88	.147	14.59	2.29	.182
15.99	2.63	.134	15.35	2.09	.187
16.73	2.36	.12	16.05	1.91	.185
17.49	2.21	.115	16.79	1.84	.193
18.23	2.17	.115	17.51	1.86	.193
18.97	2.14	.126	18.25	1.9	.192
19.72	2.23	.133	18.97	2.01	.192
20.45	2.29	.155	19.71	2.02	.198
21.22	2.43	.158	20.42	1.99	.195
21.96	2.5	.156	21.17	1.95	.196
22.7	2.52	.154	21.88	1.82	.207
23.47	2.43	.153	22.61	1.72	.219
24.22	2.27	.161	23.33	1.58	.233
24.96	2.19	.159	24.07	1.56	.236
25.69	2.00	.18	24.8	1.54	.24
26.46	2.01	.164	25.52	1.55	.239
27.19	2	.163	26.28	1.59	.233
27.97	1.96	.171	27	1.56	.242
28.66	1.96	.174	27.73	1.56	.243

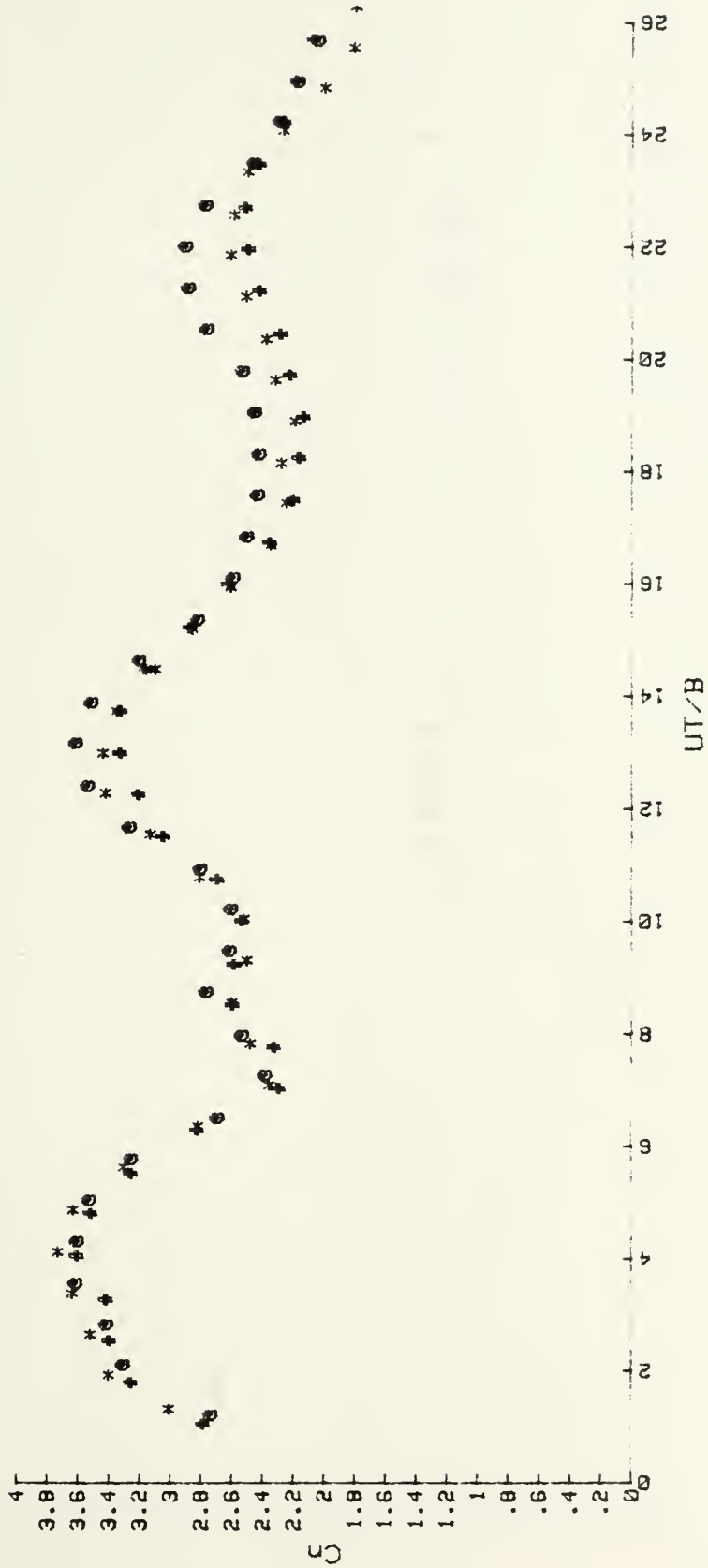


Figure 117. C_n vs. UT/B for the Flat Plate at 40 deg.

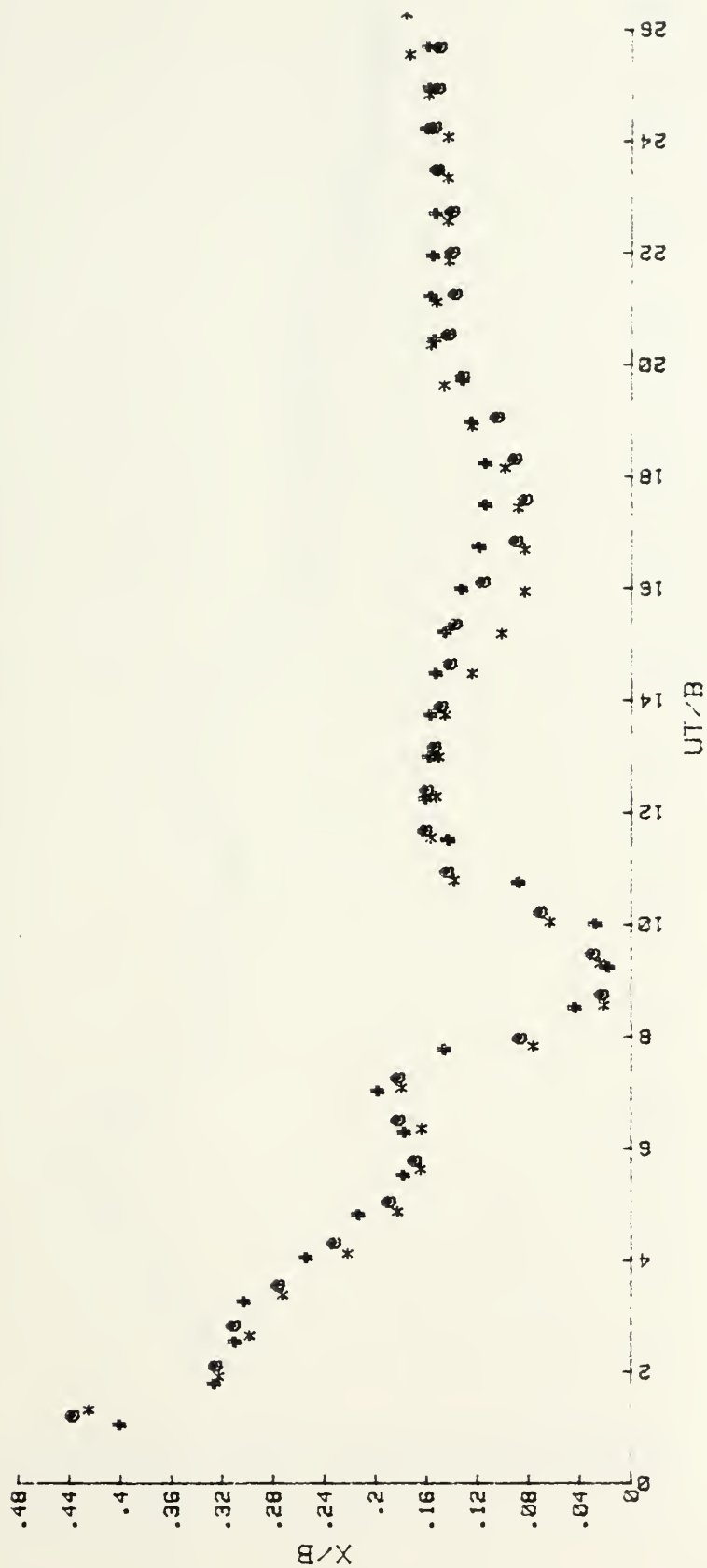


Figure 118. X/B vs. UT/B for the Flat Plate at 40 deg.

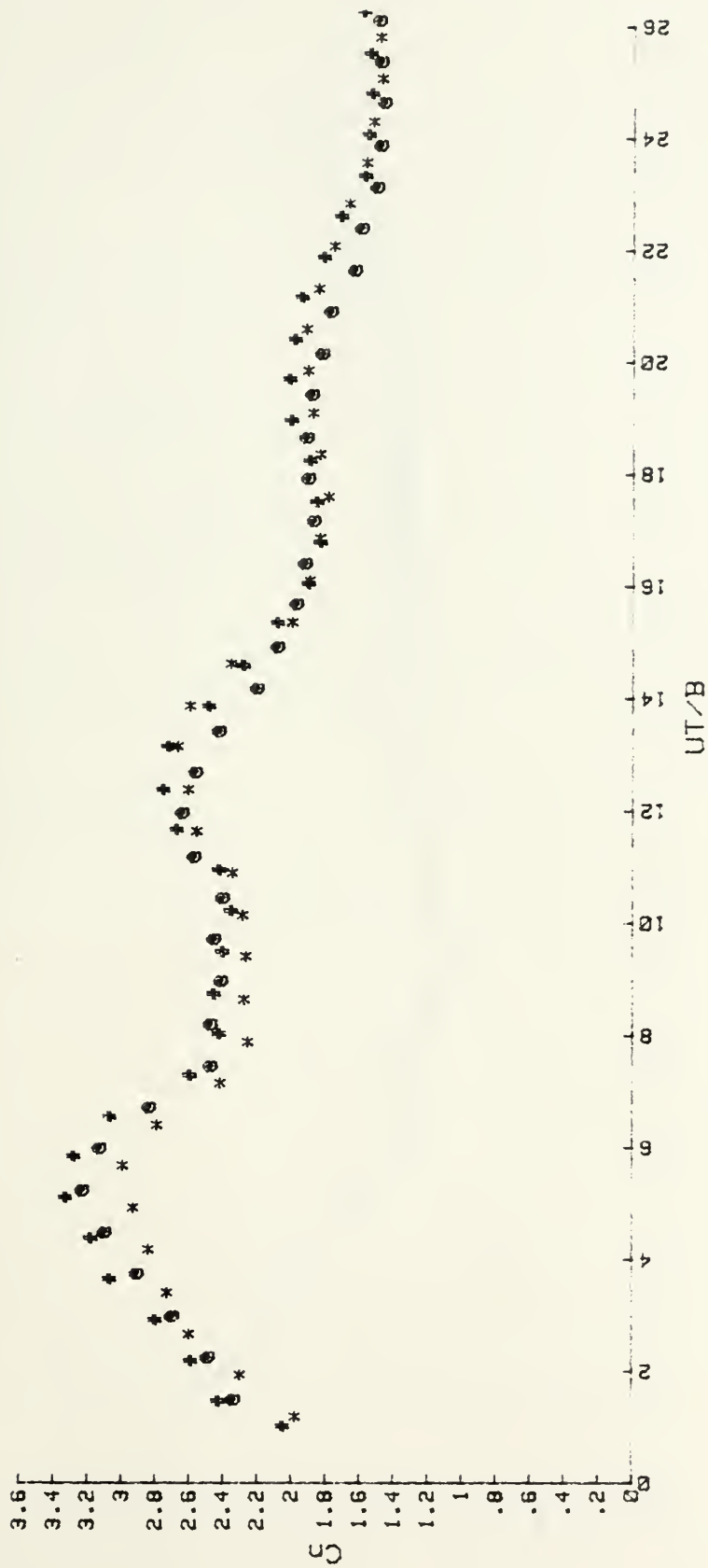


Figure 119. Cn vs. UT/B for the Flat Plate at 30 deg.

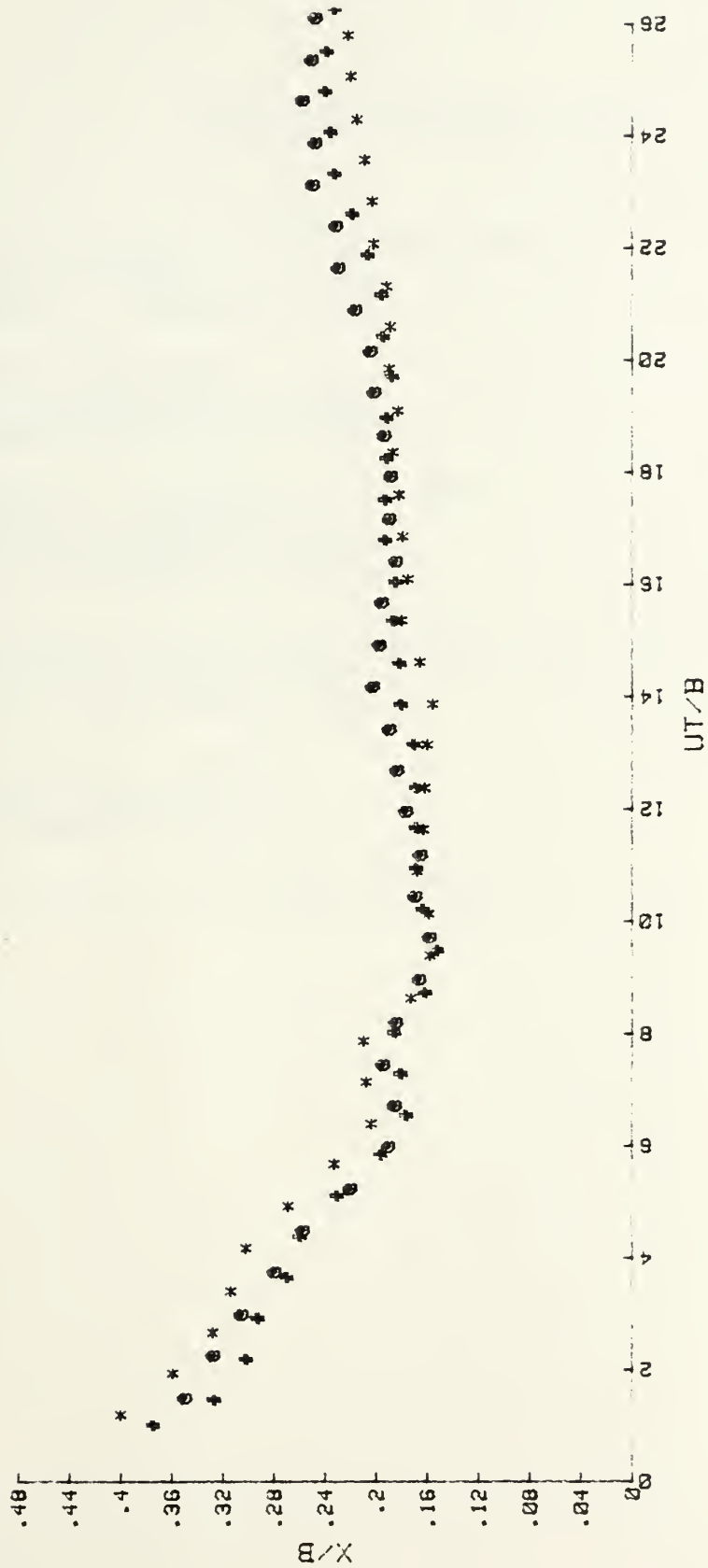


Figure 120. X/B vs. UT/B for the Flat Plate at 30 deg.

INITIAL DISTRIBUTION LIST

	No. Copies
1. Defense Technical Information Center Cameron Station Alexandria, Virginia 22314	2
2. Library, Code 0142 Naval Postgraduate School Monterey, California 93940	2
3. Professor T. Sarpkaya, Code 69S1 Mechanical Engineering Naval Postgraduate School Monterey, California 93940	5
4. Department of Mechanical Engineering, Code 69 Naval Postgraduate School Monterey, California 93940	2
5. LCDR Howard K. Kline Executive Officer USS OLDENDORF (DD-972) FPO San Francisco, California 96674	4

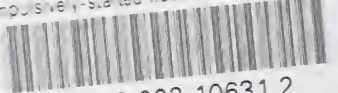
FROM MATERIAL

Thesis
K58375
c.1

192429

Kline

Impulsively-started
flow about submarine-
shaped bodies.

thesKob3
Impulsively-started flow about submarine

3 2768 002 10631 2
DUDLEY KNOX LIBRARY